

Dissertation zur Erlangung des Doktorgrades
der Fakultät für Chemie und Pharmazie
der Ludwig-Maximilians-Universität München

Design and synthesis of tubulin tyrosination probes for chemical proteomics

Dmytro Makarov

aus

Dnipro, Ukraine

2024

Erklärung

Diese Dissertation wurde im Sinne von § 7 der Promotionsordnung vom 28. November 2011 von Herrn *Dr. Pavel Kielkowski* betreut.

Eidesstattliche Versicherung

Diese Dissertation wurde eigenständig und ohne unerlaubte Hilfe erarbeitet.

München, 12.03.2024

Dmytro Makarov

Dissertation eingereicht am: 14.03.2024

1. Gutachter: Dr. Pavel Kielkowski

2. Gutachter: Prof. Dr. Thomas Carell

Mündliche Prüfung am: 18.04.2024

Publication List

Parts of this work that have already been published or presented at conferences:

Makarov, D.; Kielkowski, P. Chemical Proteomics Reveals Protein Tyrosination Extends Beyond the Alpha-Tubulins in Human Cells. *ChemBioChem* **2022**, 23 (23), e202200414. <https://doi.org/10.1002/cbic.202200414>.

Makarov, D.; Telek, A.; Becker, T.; Von Wrisberg, M.; Schneider, S.; Kielkowski, P. Clickable Report Tags for Identification of Modified Peptides by Mass Spectrometry. *J Mass Spectrom* **2022**, 57 (3), e4812. <https://doi.org/10.1002/jms.4812>.

Conference contributions

Poster “Derivatized tyrosine as a promising tool for chemical proteomic profiling of tubulin tyrosination”. EMBO | EMBL Symposium: Microtubules: from atoms to complex systems, 08-11 June 2022, EMBL Advanced Training Centre, Heidelberg, Germany.

Poster “Derivatized tyrosine as a promising tool for chemical proteomic profiling of tubulin tyrosination”. Nikolaus Symposium 2022, SFB1309, 05 December 2022, ICEM, LMU Munich.

Poster “Derivatized amino acids as a promising tool in chemical proteomic profiling exploiting biorthogonal reactions in studies of tubulin PTMs”. 56th European Symposium on Biological and Organic Chemistry (ESBOC), 19-21 May 2023, Gregynog Hall, Wales

Poster “Derivatized amino acids as a promising tool in chemical proteomic profiling exploiting biorthogonal reactions in studies of tubulin PTMs”. Nikolaus Symposium 2023, SFB1309, 04 December 2023, ICEM, LMU Munich.

Acknowledgment

I would like to extend my gratitude to my supervisor, Dr. Pavel Kielkowski, for his invaluable support throughout this journey. Your willingness to share knowledge and expertise has provided me with the unique opportunity to learn and master new concepts. Your understanding and the positive environment have made this experience truly enjoyable. I am profoundly thankful for your guidance and for believing in my potential. Your mentorship has been the foundation of my academic and personal development.

My sincere thanks go to Prof. Dr. Thomas Carell for kindly agreeing to evaluate this thesis as the second examiner.

I am also deeply grateful to the Deutsche Forschungsgemeinschaft (DFG) for their financial support of my research. The funding provided by DFG has been crucial in facilitating the progress and completion of this study.

I owe many thanks to the following people:

To Andreas Wiest, for his enlightening insights and valuable contributions that significantly enhanced my research.

To Tobias Becker, for sharing his invaluable expertise during the initial phase of my Ph.D., and for the meaningful discussions that followed.

To Haoyu Chen, for his loyal presence and generous help during challenging times, offering both professional and personal support.

To Ken Kögel, for the culinary delights and memorable gatherings that brought us all closer.

And a special acknowledgment to Özge Simsir, whose support and positive energy were beacons of light during my most challenging periods. Your encouragement was very helpful in my journey.

My sincere appreciation goes to my lab members, Manuel Hertwig, Rubaba Abanti, and Laura Hoffman, for their assistance and kindness. I wish all members of our research group the very best in their future endeavors.

I cannot express enough gratitude to my family for their support and love throughout this journey. Your encouragement, understanding, and belief in my abilities have been my greatest sources of strength and motivation.

Table of Contents

Summary.....	i
1. Introduction	1
1.1. The scope of post-translational modifications (PTMs)	1
1.2. Tubulin code.....	2
1.3. De-tyrosination/tyrosination cycle	5
1.4. Tubulin-tyrosine ligase (TTL).....	6
1.5. Tubulin carboxypeptidases (TCPs).....	7
1.6. De-tyrosination cycle in the context of neurodegenerative diseases	8
1.7. Methodologies for investigating de-tyrosination PTM.....	9
1.8. Chemical proteomics.....	10
1.9. Photo-reactive probes as a tool for probing protein-protein interactions	13
1.10. MS reporters	15
2. Aim of the thesis.....	17
3. Published work.....	19
3.1. Clickable report tags for identification of modified peptides by mass spectrometry ⁸⁵ ...	19
3.2. Chemical Proteomics Reveals Protein Tyrosination Extends Beyond the Alpha-Tubulins in Human Cells ⁸⁷	27
4. Unpublished work.....	35
4.1. Investigating Tubulin Dynamics Using Tyr-O-Alk Probes in TTL and SVBP Knockout Model Systems	35
4.2. Implementation of Tyr-O-Alk probe-based screening platform for identifying potential TTL inhibitors	37
Workflow description	37
Optimization of the protocol.....	38
4.3. Synthesis of photo reactive tyrosine probe	45
Design of photo reactive tyrosine	45
Optimizing conditions for the synthesis of aliphatic diazirines	48

The synthesis of the minimal alkyne diazirine linker	50
The synthesis of the tyrosine photo reactive probe.....	52
4.4. Decoding α -tubulin protein-protein interactions using photo-cleavable tyrosine probe .	54
Incorporation efficiency of the probe.....	54
Photo-crosslinking efficiency	55
Mass spectrometry analysis of photo-crosslinking experiments.....	57
Enrichment analysis of tubulins without UV treatment	58
Enrichment analysis of the samples after UV treatment.....	59
Repetition of the protocol.....	61
5. Bibliography	68
6. List of abbreviations	75
7. List of figures.....	77
8. Supplementary information.....	79
8.1. Supplementary information for “Clickable report tags for identification of modified peptides by mass spectrometry”	79
8.2. Supplementary information for “Chemical Proteomics Reveals Protein Tyrosination Extends Beyond the Alpha-Tubulins in Human Cells”	106
8.3. Experimental section: Investigating Tubulin Dynamics Using Tyr-O-Alk Probes in TTL and SVBP Knockout Model Systems	138
8.4. Experimental section: Implementation of Tyr-O-Alk probe-based screening platform for identifying potential TTL inhibitors.....	139
8.5. Experimental section: Synthesis of modified tyrosine probe simultaneously derivatized with terminal alkyne and photocleavable diazirine probe for the study of tubulin PPIs.....	141
Synthesis.....	141
Analytical section.....	148
8.6. Experimental section: Decoding α -tubulin protein-protein interactions using photo-cleavable tyrosine probe	155

Summary

DNA can be considered as a repository of genetic information, representing the framework from which life occurs. RNA, on the other hand, is a tool to decode this information, transmitting instructions and promoting the protein assembly. Proteins are, in turn, the executors of biological function, playing a variety of roles. They are responsible for interpreting signals, catalyzing biochemical reactions, promoting cellular trafficking, and maintaining cellular integrity.

Proteosynthesis is a highly energy-demanding process with limitations on the speed at which new proteins can be formed. To maintain an adequate response in fast-changing conditions and to efficiently modulate functions, organisms have evolved a sophisticated tool for orchestrating protein activity. Post-translational modifications (**PTMs**) provide a way to fine-tune the processes without expending the energy needs on new protein synthesis, ensuring dynamic and balanced response to environmental challenges.

Complex interplay and crosstalk of different PTMs challenge the scientific community and stimulate the discovery of new methods and protocols to study PTMs in living organisms while ensuring the physiological integrity and relevance of obtained data. The so-called tubulin code is a good representation of such complexity. The term refers to a plethora of modifications that occur at the C-terminal tails of tubulins and regulate complex mechanisms of microtubule assembly, trafficking along them, and supporting the integrity of different processes.

To unravel the tubulin code and explore its role in various physiological and pathological contexts, the objective was to establish an approach for studying one of its PTMs, de-tyrosination. De-tyrosination plays an important role in cell differentiation and maintaining cellular functionality. It is especially important for the health of neurons and cardiomyocytes, and its dysregulation causes major severe chronic conditions such as neurodegenerative disorders and cardiomyopathies.¹

The chemical approach to studying proteomics and PTM has proven to be effective.² As was demonstrated by Schumacher et al. 2017, TTL enzyme catalyzing the addition of tyrosine to the C-terminus of α -tubulin, has a broad substrate promiscuity.³ Derivatives of tyrosine were shown to incorporate into the structure of α -tubulin with different levels of efficiency. Among different tyrosine derivatives, *O*-propargyl-L-tyrosine was of great interest. Bearing the terminal alkyne, the molecule allows for further protein functionalization – an approach that has never been tested before.

To prove the concept of α -tubulin functionalization *in vivo*, the Tyr-*O*-Alk probe was synthesized and tested in a model cell line (**SH-SY5Y**). The probe was proven to be non-toxic for the cells and

could be supplemented at higher concentrations. The implementation of the click reaction allowed fluorescent labeling of the tubulin for cell imaging or gel-based analysis. The post-translational incorporation of the probe was demonstrated by various in-gel analyses. The probe incorporation was observed after inhibition of the ribosomal machinery with cycloheximide. Additionally, it was successfully outcompeted by natural tyrosine in competition assays. With an in-house developed SP2E protocol for enrichment analysis, we demonstrated that it was possible to evaluate the relative abundance of the tubulin between different conditions.² It was shown on neurogenin-inducible human-induced pluripotent stem cells (**iNGNs**) that the tyrosination rates decrease during the differentiation of pluripotent cells into neurons.⁴ This observation supports the fact of the cumulation of de-tyrosinated microtubules in mature neurons. Moreover, the probe facilitates the identification of specific α -tubulin isoforms, which has been problematic with immunochemistry approaches having cross-reactivity problems.

During the course of the study, a screening platform for the identification of TTL inhibitors was established for *in vivo* screening, which has significant advantages over *in vitro* assays. We identify several potential TTL inhibitor candidates for further evaluation with orthogonal approaches.

To further explore the possibility of the TTL enzymatic incorporation efficiency, the probe was functionalized with a diazirine photo-cleavable group to promote photo cross-labeling of the interaction proteins and pave the way for the analysis of protein-protein interactions (**PPIs**).

Rare or low-abundant PTMs become very challenging when it comes to their identification. Thus, to support the general vector of the PTM study in the Kielkowski group, a clickable report tag was developed, improving the identification rates during MS measurements and in-depth analysis.

The results of the study showed the potential of the approach and led the way for the exploration of other tubulin-related PTMs, thus covering the entire scope of the tubulin code.

1. Introduction

1.1. The scope of post-translational modifications (PTMs)

Post-translational modifications (**PTMs**) serve as a sophisticated mechanism through which the cell can modulate the function of proteins after translation. Unlike the fixed nature of DNA sequence, PTMs introduce a new dynamic regulatory layer, enabling rapid response to internal changes or external signals. Regulation of protein function is achieved through the incorporation or removal of specific molecular groups from its structure, altering their activity, stability, or localization.

The scope of all proteins within the cell is represented by the term “proteome” and potentially comprises millions of different proteoforms – various forms of proteins arising from a single gene. However, only approximately 20000 genes are responsible for encoding proteins.⁵ Through alternative splicing of the transcriptome, this number can expand to about 55000 alternatively translated protein variants.⁶ However, these numbers cannot explain the diversity of proteoforms found in humans. The extensive variety of proteoforms can be explained by PTMs that expand the functional repertoire of the genes, enhancing the complexity of the cell (see **Figure 1**). PTMs range from small modifications, such as an addition of a phosphate group, to the cleavage of peptide bonds or attachment of proteins like ubiquitin.^{7,8}

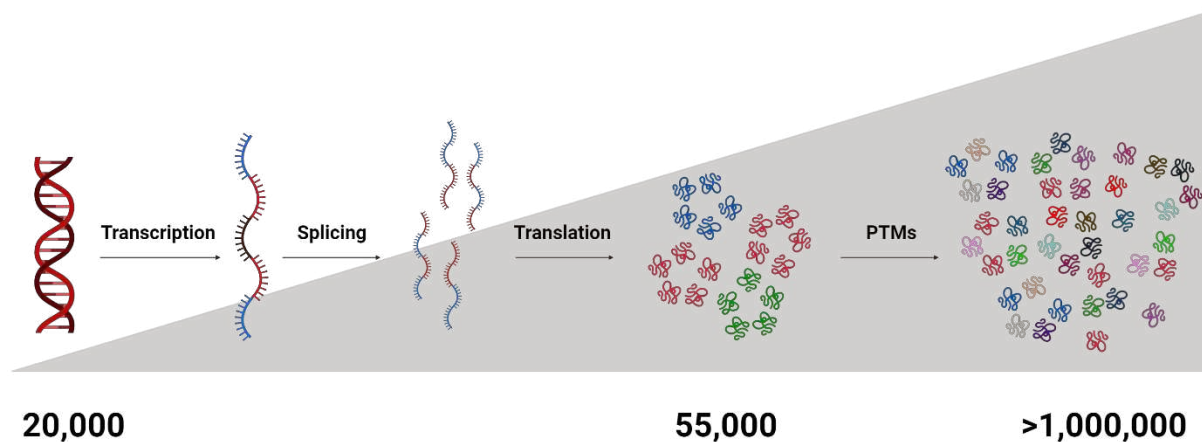


Figure 1. The diversity of proteoforms. Schematic representation of the diversity of proteins caused by PTMs. Created with [BioRender.com](https://www.biorender.com).

PTMs can cause conformational changes in proteins, altering their stability, activity, or interactions with other proteins. Phosphorylation can activate or inhibit enzyme activity, thus influencing

signaling pathways and cellular processes. For example, by phosphorylation of receptor tyrosine kinase (**RTK**), the cell can rapidly change the signaling cascade, allowing for responding to external stimuli such as growth factors or hormones.⁹

PTMs play a pivotal role in regulating metabolic pathways and genomic stability. As an example, histone acetylation can influence gene expression by changing the structure of chromatin, thus contributing to genomic control.¹⁰ Similarly, the modification of enzymes involved in metabolic pathways can rapidly adjust metabolic exchange in response to changing cellular energy demands.¹¹

PTMs can be attached to the structure of proteins in different ways. A regulated process of enzymatic modification requires a special writer protein for the attachment of PTMs and an eraser for its removal. Recognition of the specific PTMs is facilitated by reader enzymes, such as CLIP-170 which can “read” the sequence of the α -tubulin tail and specifically recognize the “-EEY” motif, thus controlling the dynamics of MTs enriched in tyrosinated α -tubulin.¹² Protein structure can be also modified non-enzymatically, e.g. due to oxidative stress.¹³

1.2. Tubulin code

The tubulin protein family includes several types of tubulins, highly conserved alpha (α -) tubulin and beta (β -) tubulin, and additional gamma (γ -), delta (Δ -) and epsilon (ϵ -) tubulin. The most abundant tubulin fraction is composed of α -, and β -tubulin, serving as building blocks for microtubules (**MTs**). γ -tubulin acts as a nucleation site for microtubule polymerization, acting in the formation of the microtubule-organizing center (**MTOC**).¹⁴ Both Δ -tubulin and ϵ -tubulin have been involved in maintaining the function of centrosomes and basal bodies.¹⁵

The focus of the thesis is on the microtubule’s building blocks, on α -, and β -tubulins. Tightly bound together, they create a heterodimer that serves as an elemental unit for the microtubule assembly. Dimers polymerize together through longitudinal interaction in a head-to-tail fashion to form a microtubule filament, protofilament.¹⁶ A combination of filaments, usually 13, bound together through lateral interactions, creates a hollow tubular structure called a microtubule.¹⁷ Head-to-tail organization of tubulin heterodimers induces polarity along the microtubule lattice, creating the plus-end (**+ end**) and minus-end (**- end**), navigating molecular transport along the microtubule, affecting the growth and shrinkage of the MTs differently at their poles (see **Figure 2**).¹⁶

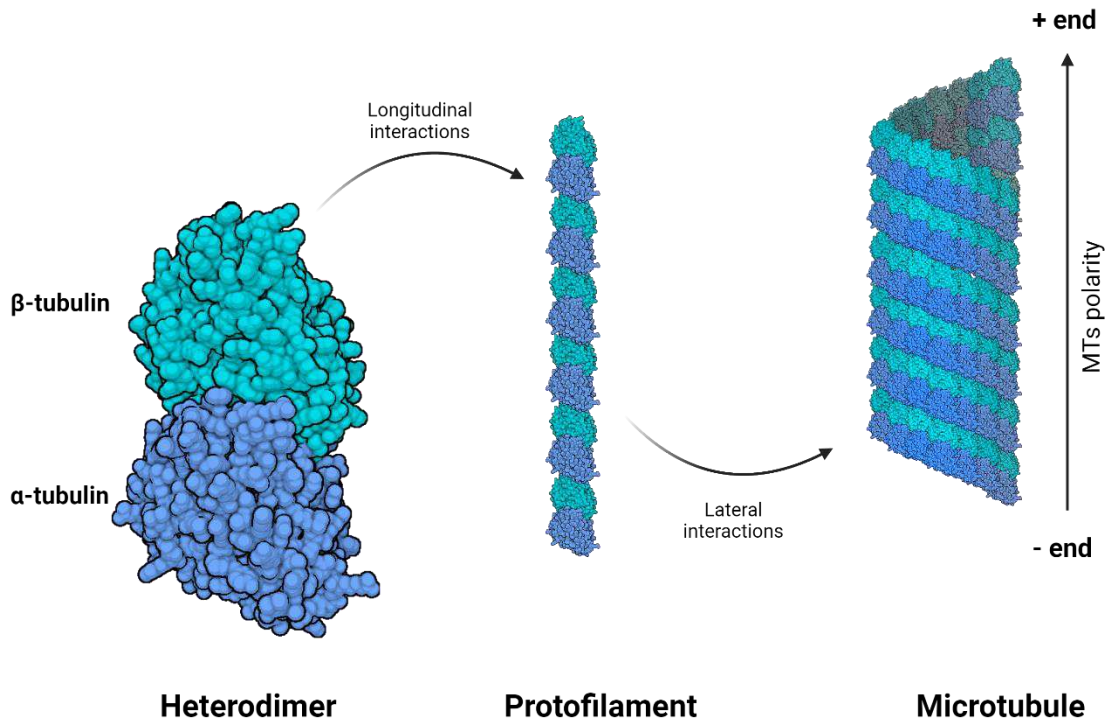


Figure 2. Building blocks of microtubules. Representation of tubulin dimer, protofilament and MTs. Created with [BioRender.com](https://www.biorender.com).

Structures of α -tubulin and β -tubulin are highly conserved, especially in the N-terminal domain. The structure of the protein can be divided into three parts: the N-terminal domain or nucleotide-binding domain, the intermediate domain, and the C-terminal region.¹⁸ The N-terminal and intermediate domains create a globular tubulin “body”, a genetically highly conserved part participating in the MTs assembly.

In humans, there are 8 α -, and 10 β -isotypes (see **Figure 3**).¹⁹ These isotypes, while highly conserved in their core regions, exhibit sequence variations primarily in their C-terminal region. Such variability is responsible for MTs' diverse functional specificity.

The C-terminal region points outside of the MTs lattice, providing an interface for microtubule-associated protein (**MAP**) binding. It consists of two antiparallel helices and an unstructured C-tail.¹⁸ The C-terminal tail (**CTT**) is the place of the highest sequence variability between isotypes and a region for the majority of PTMs to occur. These PTMs can influence the interaction of tubulin with MAPs, motor proteins, and other factors that regulate microtubule stability, dynamics, and interactions.¹⁹ Being very diverse, the C-terminal region is responsible for the functionality of microtubules and performing specific roles in cells.

The structural properties of microtubules are highly affected by the presence of distinct tubulin isotypes. The stability of MTs, their bending rigidity, and their response to depolymerizing agents can change upon the incorporation of different isotypes.^{20,21} Consequently, the arrangement of organelles and overall cellular architecture stability demonstrate isotype-specific behavior.²²

Another area where tubulin isotypes and distinct PTMs have a significant impact is intracellular transport, particularly in the context of motor proteins, such as kinesins and dyneins. Motor proteins demonstrate a directional preference for vesicle transport along the MTs because of their affinity for different PTMs.^{23,24}

Moreover, the role of tubulin isotypes extends to the regulation of cell division, influencing the assembly and stability of the mitotic spindle and affecting the segregation of chromosomes during mitosis. Errors in isoform composition or PTMs can lead to tumorigenesis.²⁵

As previously mentioned, the tubulin C-tail undergoes a range of PTMs. Different combinations of tubulin isoforms and their PTMs gave rise to the concept known as tubulin code (see **Figure 3**).²¹ The tubulin code refers to specific patterns that affect MTs' dynamics and interactions with "reader" proteins. These PTM-isoform patterns can be spatially separated depending on the cellular compartment or location on MTs. They can also exhibit temporal variability in response to specific stimuli. These spatial and temporal dimensions add another layer of complexity to the tubulin code, enabling dynamic regulation of MTs' function. Furthermore, the additional feature of the tubulin PTMs is the ability to cross-talking, allowing for fine-tuning of the cellular processes in fast-changing conditions.²⁶

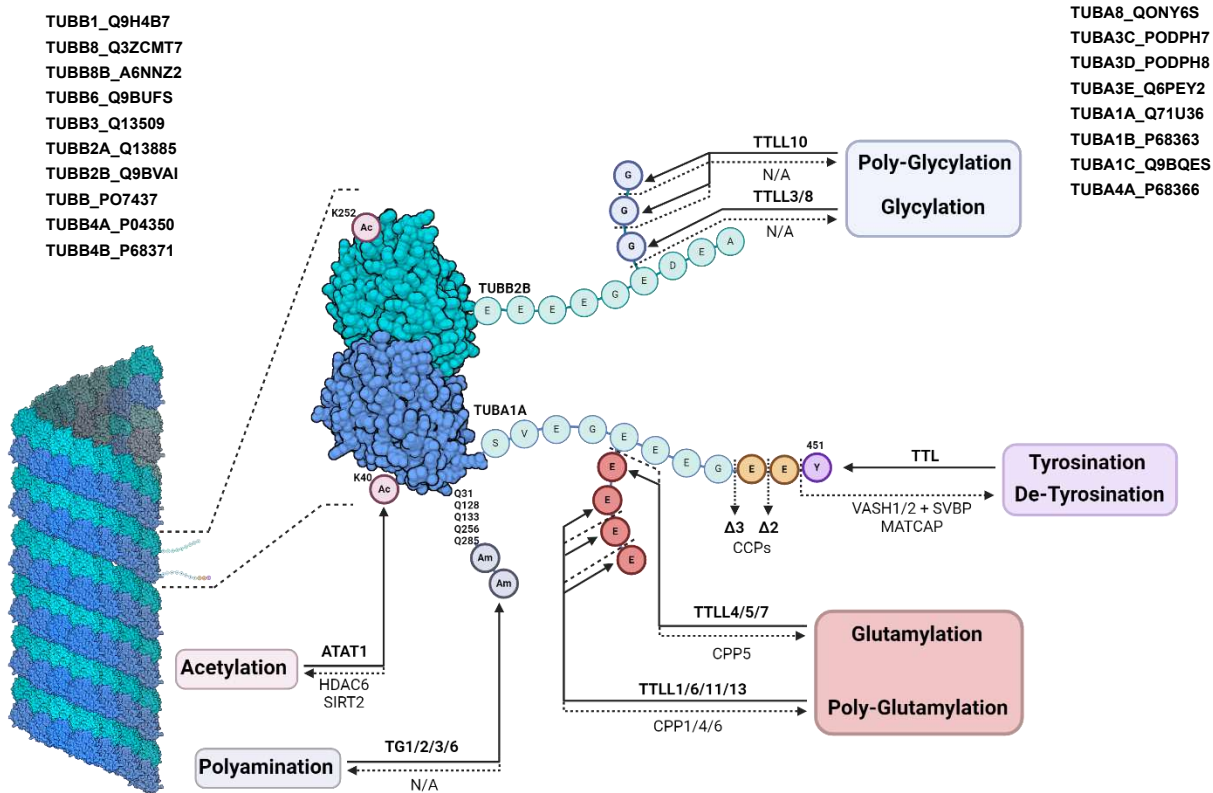


Figure 3. The Tubulin Code. Representation of the tubulin PTMs, their “writer” and “eraser” enzymes with positions on the amino acid sequence. Identification numbers of α - and β -tubulin isoforms are depicted on the figure. Created with [BioRender.com](https://www.biorender.com).

1.3. De-tyrosination/tyrosination cycle

Removal of the last tyrosine from the C-terminal of α -tubulins was known as the first tubulin PTM and was discovered in the year 1974.²⁷ Enzymatic removal of the amino acid is catalyzed by tubulin carboxy peptidases (**TCPs**). It was unknown which proteins act as TCPs and promote the cleavage. In the year 2017, two groups using different strategies revealed that vasohibins (**VASH1/2**) in synergy with small vasohibin-binding protein (**SVBP**) promote TCP activity.^{28,29} Later, in the year 2022, another de-tyrosinase, microtubule-associated tyrosine carboxypeptidase (**MATCAP**) was discovered, explaining the fact of remained de-tyrosinase activity upon SVBP-KO conditions.³⁰ In contrast to TCPs, an enzyme catalyzing the addition of tyrosine, tubulin tyrosine ligase (**TTL**) was purified from bovine brain tissues in 1977.³¹ TTL is part of a big protein family with a TTL-homology domain. TTL-like (**TLL**) enzymes catalyze the addition of glutamates or glycines into the structure of tubulin.³²

Tubulins are transcribed with the terminal tyrosine as the last amino acid. Only two isoforms are synthesized without tyrosine residue, TUBA4A ends with glutamate and TUBA8 contains phenylalanine instead of tyrosine.³³ Newly synthesized α -tubulin bearing tyrosine on its C-terminus enters the MTs polymerization-depolymerization cycle.

When incorporated into the structure of MTs, tyrosine can be cleaved by TCPs, giving rise to de-tyrosinated microtubules, which are considered to be a marker of stable microtubules.³⁴ However, de-tyrosination alone is not a reason for the stability of MTs.³⁵ On the other hand, de-tyrosinated tubulins can be further modified by cleavage of glutamate that follows the last tyrosine, resulting in $\Delta 2$ -tubulins. Such PTM is non-reversible, which reduces the amount of tubulin available for re-tyrosination and can be found only in very long-lived MTs.³⁶ In general, de-tyrosinated tubulin can be found in almost every type of MTs present in the cell, especially abundant in axons, where stable MTs promote polarity; also, in the axonemal region of cilia and flagella.³⁷ Additionally, higher amounts of de-tyrosinated tubulins are characteristics of differentiated cells, like neurons and cardiomyocytes, also playing an important role during neuro-, and cardiogenesis.^{1,38}

On the other hand, tyrosinated tubulin is a marker of labile or dynamic MTs and can be found in cycling cells, where it plays an important role in the fast rearrangement of the microtubular cytoskeleton by regulating the activity of depolymerizing motor mitotic centromere-associated kinesin (**MCAK**), which is important in the anaphase of chromosome segregation.^{39,40} In contrast to long-stable de-tyrosinated MTs with a half-time of 16 hours, tyrosinated MTs undergo fast turnover with a half-time of 3-5 minutes.¹⁷ Such behavior can be explained by the affinity of depolymerizing kinesin KIF2A to tyrosinated MTs, while having no activity towards de-tyrosinated MTs, further increasing their stability.⁴⁰ In addition to cycling cells, higher rates of tyrosinated tubulin are observed in the growth cone and in a distal end of an axon, where it plays an essential role in packing retrograde vesicles by recruiting end-binding protein CLIP-170 and p150Glued dynactin subunits (**DCTN1**).^{41,42} With the CAP-Gly domain, these proteins can specifically recognize the “-EEY” motif in the CTT of α -tubulin and a few other end-binding proteins (**EB1**, **EB2**) having the same motif in the C-terminus, and help to promote retrograde trafficking.⁴³ Furthermore, plus-end proteins promote microtubule-cell cortex interactions.⁴⁴

1.4. Tubulin-tyrosine ligase (TTL)

The PTM writer introducing tyrosination, TTL is a part of a broader **TTL** family, sharing the well-conserved catalytic domain, including polyglutamylases and polyglycylases.^{45,46} The structure of TTL is composed of three domains, N-domain, central and C-domain, creating a catalytic active site between the central and C-domain, engulfing an ATP molecule needed for the ligation.⁴⁷ Apart from ATP, Mg^{2+} ions as well as K^+ ions are needed for the enzymatic reaction.¹ Despite having a conserved catalytic domain, TTL promotes the ligation of tyrosine exclusively on the C-terminus of α -tubulin. Such specificity in recognition of α -tubulin's tail comes from different factors. First,

the positively charged region starting in the ATP-binding site and going to the N-terminal domain promotes interaction with the negatively charged tubulin's CTT, accompanying the last two glutamate residues into a catalytic pocket.⁴⁷ Moreover, the positioning of the tail is further enhanced by interactions between tubulin's Glu441, Glu449 and diverse TTL residues, which hold the tubulin tail in a specific position.⁴⁸ As a consequence of such anchoring, the length of the C-tail plays a crucial role, making it necessary to have the last two glutamates available for the ligation. Such specific interaction explains the inability of TTL to re-ligate tyrosine in $\Delta 2$ -tubulin, which lacks one of the glutamates.²¹ The length of the C-tail, specific interactions with the TTL docking site and the presence of two sequential glutamates are necessary for the re-tyrosination of the C-terminus, also explaining the TTL discrimination between α -, and β -tubulin and its inability to tyrosinate β -tubulin or any other protein.

TTL accepts only soluble, free tubulin fraction as a substrate for tyrosination. α -Tubulin incorporated into the structure of MTs doesn't undergo tyrosination.⁴⁷ Docking studies showed that the bent conformation of a free tubulin heterodimer is beneficial for the TTL-tubulin interaction and reactivity of the enzyme, whereas heterodimer incorporated into MTs is aligned into the straight line, causing clashes between enzyme and tubulin interface. Moreover, a substantial part of the binding region is blocked by lateral interactions between heterodimers in the structure of MTs.⁴⁸

To this date, no other protein tyrosinated by TTL has been identified, suggesting the exclusiveness of the tyrosination attachment into the α -tubulin structure.¹ On the other hand, TTL demonstrates high substrate flexibility, capable of incorporating tyrosine derivatives such as L-Dopa.⁴⁹ Further studies have shown the incorporation of 3-substituted tyrosine derivatives which were used for various labeling techniques.^{50,51} In the study by Schumacher et al. 2017, TTL's substrate promiscuity was further explored, uncovering broader range of substrates and revealing some patterns in it.³ The writer enzyme can largely incorporate amino acids bearing an aromatic group, as evidenced by the incorporation of tryptophan or fluorescence tags such as coumarin amino acid derivative and β -(1-azulenyl)-L-alanine. A particularly noteworthy achievement was the incorporation of a tyrosine derivatized with biotin via a short ethylene glycol linker at position 3, expanding potential applications by exploiting TTL's promiscuity in chemical proteomics.³

1.5. Tubulin carboxypeptidases (TCPs)

Tubulin carboxypeptidase is a general name for the family of enzymes disconnecting the last tyrosine residue from the α -tubulin sequence. Proteins processing de-tyrosination had not been discovered until the year 2017 when the protein complex of VASH1/2 and SVBP was discovered as the one promoting TCP reaction.²⁸ The vasohibins were known as a negative regulator of

angiogenesis, which was proven in different disease models such as cancer, arterial stenosis, and pulmonary diseases.⁵² Small vasohibin-binding protein is a chaperon-like protein providing the stabilization of the complex, thus indirectly promoting the de-tyrosination activity of VASH1/2. By treating the cell model with an irreversible inhibitor (apoY) while knocking-down the VASH1 or SVBP, the level of the de-tyrosinated fraction was decreased by 75%. Among different explanations of residual de-tyrosinated tubulins, an assumption of other proteins with TCP activity was made.²⁸ Indeed, an unstudied gene KIAA0895L was found as the strongest regulator of de-tyrosination levels in a haploid study, and was renamed as microtubule-associated tyrosine carboxypeptidase (MATCAP).³⁰ While vasohibins represent the cysteine proteases family, MATCAP binds Zn²⁺ ions inside the reactive center, thus belonging to gluzincin metalloproteases. Alongside different substrate recognition, different catalytic approaches create complementary machinery for the de-tyrosination. In contrast to a post-natal death of TTL-KO mice, simultaneous depletion of VASH1/2 and MATCAP led to reduced brain development and impaired behavior.^{30,53}

1.6. De-tyrosination cycle in the context of neurodegenerative diseases

De-tyrosination is an evolutionary very conserved PTM and has a huge impact on the functioning of the cell and human organism. In the experiment on TTL-KO mice, a poor establishment of mice cerebral cortex layers was identified, as well as underdeveloped connections between the neocortex and the thalamus, the main parts of the cortico-thalamus loop.⁵³ These abnormalities in development were lethal for the mice litter. Neuronal cells derived from the post-natal TTL-KO mice expressed abnormalities in the axonal formation.

Disruption of the tyrosination cycle can cause diverse pathological conditions and a detailed study of the PTM is highly beneficial for better understanding the context of neurodegenerative disorders and cancer.

Common for different types of neuropathies, abnormalities in the distribution of stable and dynamic microtubules can lead to impaired synaptic plasticity, resulting in brain degeneration. It is also crucial for axonal and dendritic trafficking since dysregulation affects motor proteins sensitive to tyrosinated MTs.

For example, behavioral tests with heterozygous mice with one inactive TTL allele showed a correlation with preclinical models of Alzheimer's disease in impairing short-term recognition memory. Post-mortem tissue analysis revealed that reduced TTL activity and de-tyrosinated tubulin cumulation affect the dendritic spine density, which is important for neuronal plasticity and dysregulated in many neurological disorders. On the other hand, re-tyrosination of tubulins by enhancing TTL expression protects synapses from amyloid- β -induced damage.⁵⁴

An imbalance in the ratio of tyrosinated and de-tyrosinated MTs plays a crucial role not only in the progression of neurodegenerative diseases but also in cardiomyopathies. An abnormal cumulation of de-tyrosinated tubulin was demonstrated in a cat model of pressure overload-induced right ventricular hypertrophy. The observation corroborates with the findings in the congestive heart failure model in rats. In human heart failure samples, elevated mRNA levels of VASH1, as opposed to VASH2, were identified shedding light on the correlation between de-tyrosination and heart failure conditions. By treating human-derived failing cardiomyocytes with a TCP inhibitor parthenolide, it was possible to restore significant contractile function.¹

Further investigating into the process of the de-tyrosination/tyrosination cycle could contribute to novel therapeutic targets in heart diseases.

1.7. Methodologies for investigating de-tyrosination PTM

To understand the functional dynamics of de-tyrosination PTM and interactions with associated proteins, as well as gain new insights about biological relevance *in vivo*, developing robust and sensitive tools is of the highest interest and value. Given the complexity of modifications introduced into C-tail by different PTMs and the number of isoforms present in the structure of MTs, it is crucial to develop protocols and tools for the distinctive identification and analysis of PTMs with a high degree of specificity and sensitivity. The primary challenge lies in the sequence similarity among different tubulin isoforms, challenged with all possible combinations of PTMs occurring in close proximity to each other. It means an approach should be designed in such a way to be able to discriminate between closely related modifications. For instance, an antibody against de-tyrosinated tubulin, without cross-reactivity towards tyrosinated or polyglutamylated tubulin is critical in understanding the tyrosination cycle and is already in use by the scientific community.⁵⁵ Also, it is essential to develop a tool capable of distinguishing the interplay between different PTMs occurring on the C-tail.

The study of de-tyrosination PTM started by using radioactive-labeled [¹⁴C]tyrosine, where its incorporation into the soluble fraction of α -tubulin was shown.⁴⁹ Nevertheless, special conditions and equipment are needed to establish experiments with radioactivity. An alternative approach to avoiding the use of radioactive material was in high demand.

After the successful integration of L-phenylalanine into the tubulin C-terminal, it became evident that TTL is capable of accepting substrates that are structurally similar to tyrosine to a certain degree.⁴⁹ Subsequent experiments explored different tyrosine derivatives for their ability to incorporate into the structure of tubulin C-terminus, for example, 3-iodotyrosine, revealing broader substrate tolerance of TTL.⁵⁶ Among other compounds that have been explored for the TTL's

substrate specificity were 3-substituted tyrosine derivatives such as 3-nitrotyrosine, 3-azidotyrosine, 3-formyltyrosine that was originally considered as potential inhibitors for TTL. Particularly noteworthy was the incorporation of formyl-tyrosine into the tubulin structure. It revealed the potential of the biorthogonal reactions by modifying incorporated formyl-tyrosine with coumarin hydrazine via hydrazone reaction.⁵¹ High substrate tolerance of TTL has significant implications, allowing for the derivatization of tubulin with various functional groups and study de-tyrosination PTM.

The ability of TTL to site-specifically incorporate modified tyrosine into the structure of tubulin has led to the development of the Tub-tag system approach as a protein ligation platform. It utilizes the ability of TTL to recognize the tubulin's CTT sequence and attach tyrosine derivative to its end.⁵⁷ Although the system exploited the specificity of TTL as a component of a ligation platform, it was evident from the study about the ability of TTL to incorporate 4-derivatized tyrosine – Tyr-O-Alk and use it as a handler in biorthogonal click reaction.

Another method allowing for the study of different PTMs on tubulin's CTT used an elegant approach of the split-intein technology for the ligation of the recombinant tubulin heterodimer with the synthetic CTT bearing tailored polyglutamylation modification. The study revealed the crosstalk between de-tyrosination and polyglutamylation, where long glutamate sidechains enhanced the activity of TCPs, promoting de-tyrosination PTM.²⁶

1.8. Chemical proteomics

Considering the amount of different biological processes acting within the cell, there is a need for specific tools to study the physiological or pathological status of a protein, analyze its distribution across cellular compartments or examine its specific interactions. The targeting and isolation of proteins of interest from a complex mixture require using a combination of various techniques for the isolation, separation and purification of the target protein, such as co-precipitation, immunoprecipitation, column chromatography, and gel-based separation methods. While these techniques are useful, they often lack physiological relevance.

To study proteins in their native environment with the possibility to target them directly for cell imaging or subsequent pull-down analyses, an interdisciplinary blend of chemistry and biology can offer a solution. Chemical proteomics is an approach of targeted protein labeling in their physiological context, using an active probe that has an affinity towards the protein of interest. The probe usually consists of a reactive group (reactive warhead) targeting the protein, a linker and a tag, providing the probe with additional functionality.⁵⁸ The interaction between the probe and the protein can result in covalent or non-covalent bond formation. Probes that form covalent bonds

with the proteins are referred to as activity-based probes (**ABPs**). If the reactive group of the probe facilitates a high-affinity non-covalent bonding interaction with the protein of interest, such probes are termed affinity-based probes (**AfBPs**).⁵⁹ To enhance the interaction strength between an AfBP and a protein, a photo-crosslinker may be installed into the structure of the probe near the affinity group. The photo-crosslink moiety is activated by light to form a covalent bond between the probe and the target protein.

Due to the advances in bioorthogonal chemistry, the reactive probe can be functionalized with a minimalist tag, consisting of a small functional group such as alkyne or azide. Thus, the probe doesn't significantly alter the structure of the studied protein, causing no perturbations of the protein's function. Moreover, it helps to overcome problems specific to high-molecular-weight molecules, such as solubility problems, poor cell membrane permeability and non-specific binding. Subsequently, by applying click chemistry, it is possible to functionalize modified peptides with bigger molecules. Such a two-step method is called the tag-then-capture approach.⁶⁰

Another approach to protein tagging is to use the cell's innate enzymatic machinery. A substrate bearing a bioorthogonal tag can be recognized by the writer enzyme and incorporated into the structure of the protein, making it an invaluable tool for the study of PTMs.⁶¹

The tagged protein then can be further functionalized with biotin or TAMRA fluorophore using the click chemistry approach. One of the most prevalent bioorthogonal reactions is a copper-catalyzed azide-alkyne cycloaddition reaction (**CuAAC**). However, conditions of the CuAAC reaction might lead to protein aggregation or side reactivity problems. Recent advances have improved the reaction efficiency. For example, using proper ligands such as trimethylammonium trifluoroacetate can reduce the required amount of toxic copper.⁶² Moreover, the formation of unspecific thiotriazole by-products responsible for the background binding can be suppressed by adjusting the reduction capacity of the reaction buffer.⁶³

Proteins functionalized with terminal alkyne can be further labeled with a fluorophore, such as Tamra-azide, allowing for imaging of the proteins in fixed cells or fluorescent detection of proteins after the separation of the lysates on SDS-Page coupled with subsequent immunochemical evaluation.

The functionalization with biotin in turn allows for pulling-down the proteins of interest by leveraging the biotin-avidin affinity. Recently reported methods that optimize the MS-sample preparation of enriched biotin-tagged proteins have demonstrated value to the scientific community, improving the isolation and analysis of biotinylated proteins and streamlining the whole process (see **Figure 4**).^{2,64}

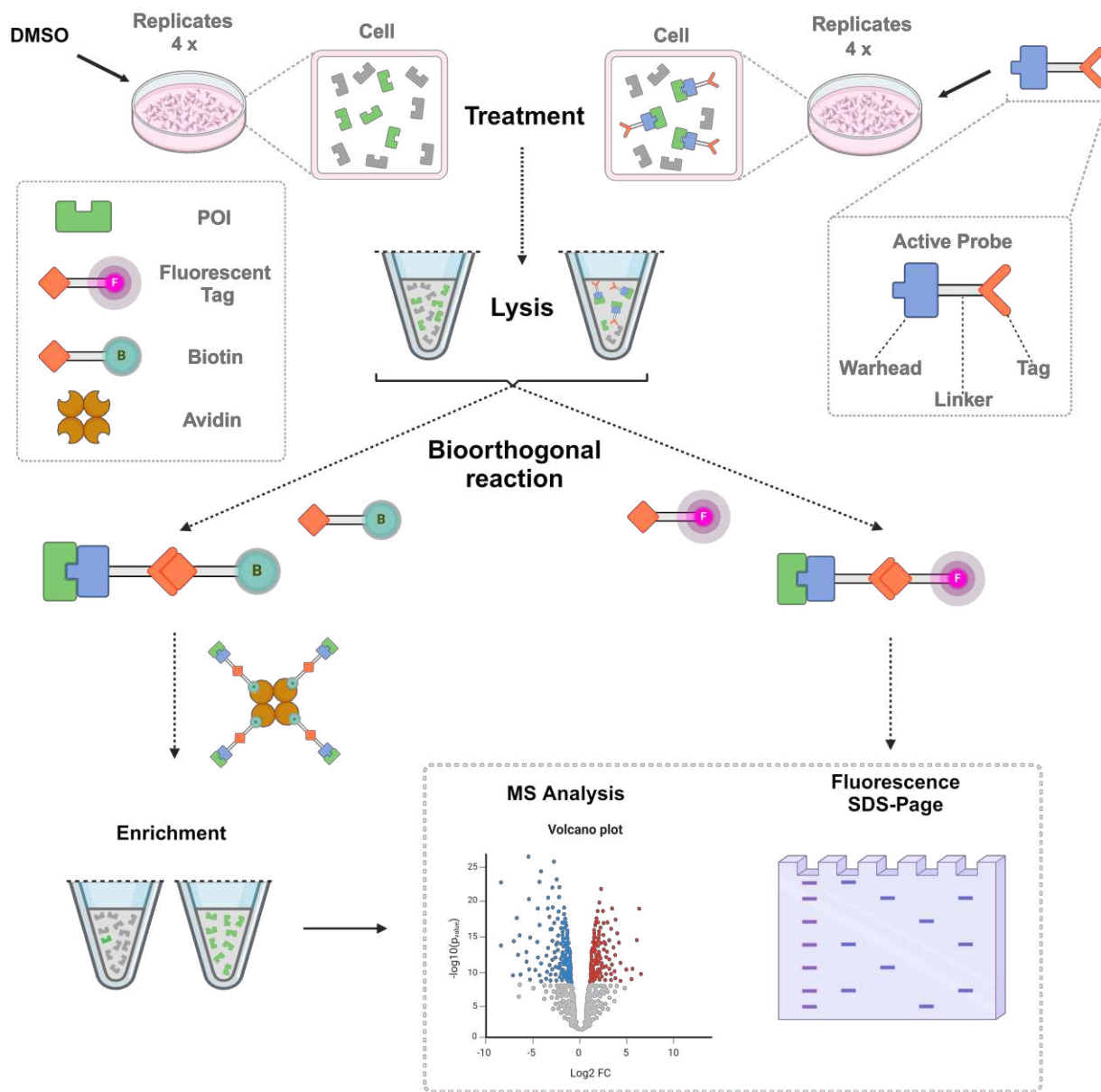


Figure 4. Chemical proteomics pipeline. *POI* – protein of interest. Created with [BioRender.com](https://www.biorender.com/).

The advancement in mass spectrometry techniques and computational analysis contributed even further to the chemical proteomics approach, enhancing the accuracy, robustness, and speed of the identification of even low-abundant proteins. Improved computational capabilities and algorithms for protein identification implemented alongside deep-learning functionality allowed for the deconvolution of extremely complex spectra. Software tools like DIA-Umpire and DIA-NN can predict the fragmentation patterns and retention values for the peptides and compare the *in-silico* created library with the actual experimental data.^{65,66} This, in turn, supported the implementation of more advanced data acquisition methods in mass spectrometry, facilitating the capture of data

even from low-abundant proteins. Unlike the data-dependent acquisition (**DDA**) method, the data-independent acquisition (**DIA**) offers broader coverage of the analyte. Instead of collecting information from the most abundant signals, the DIA method scans the entire mass range in small, consecutive isolation windows, gathering information from all detectable precursors. The DIA method does not overlook less abundant proteins because it does not rely on the precursors' intensities, ensuring a more complete dataset. It increases the protein coverage and reproducibility compared to DDA, making it a good choice for in-depth proteome analysis.⁶⁷

1.9. Photo-reactive probes as a tool for probing protein-protein interactions

Protein identification and the evaluation of the proteome offer a solid basis for studying protein functions. However, the investigation of protein interactions provides valuable insight into the mechanism of action and the dynamic nature of proteins. The study of protein-protein interactions (**PPI**) yields the formation of the complex map of protein interactions, which is known as interactome.⁶⁸ Among different methods of PPI analysis, such as affinity purification, mild immunoprecipitation techniques or chemical cross-linking, photo-affinity labeling (**PAL**) is particularly noteworthy. The PAL approach provides the tool for the spatio-selective cross-linking of the protein of interest (**POI**). In contrast to the chemical cross-linking approach, PAL overcomes the issue of excessive reactivity and formation of the secondary interactions that challenge the evaluation of interactome.⁶⁹ The targeted reactivity of PAL probes provides a strong tool for targeting PPIs with high specificity. Photoirradiation triggers the formation of the reactive species which react with proteins in close proximity, creating a covalent bond between the protein and its POI.⁷⁰ Functional groups used for PAL include benzophenone, aryl azide and diazine.⁷¹

The synthetic protocols for diazirines are indeed versatile.⁷² The canonical pathway for diazirines was established in the last century, involving the treatment of a ketone with liquid ammonia to generate an imine and followed by the addition of amination reagents like HOSA or chloramine to promote the intramolecular cyclization into diaziridine group.⁷³ Subsequently, diaziridine undergoes oxidation to yield diazine. Various oxidative reagents can be used to transform diaziridines into diazirines. Among them are freshly prepared silver(I) oxide and molecular iodine in the presence of Et₃N or Hünig's base or using DMSO/oxalyl chloride mixture (Swern oxidation) (see **Figure 5**).^{74,75}

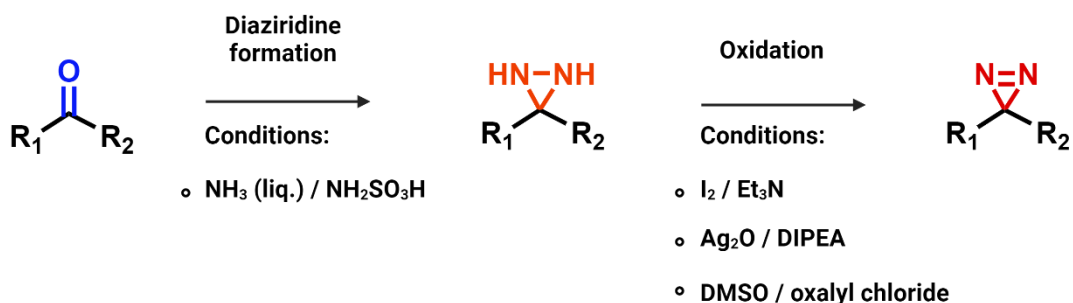


Figure 5. Approach into diazirines. Canonical two-step approach to diazirine synthesis. Created with [BioRender.com](https://www.biorender.com).

The canonical approach and its variations are known to be time-consuming and require changes in reaction conditions and/or isolation of intermediates.⁷³ Although there are different synthetic approaches to aliphatic diazirines, the main goal was to establish a robust protocol avoiding extreme conditions that require special equipment, such as running a reaction in liquid ammonia or using strong bases.^{76,77}

Over the years, attempts to develop alternative routes to diazirines have been made to overcome the problems. It was shown, for example, that a strong base such as *t*-BuOK can increase the rate of diazirine formation in a one-pot reaction condition.⁷⁷ Later, the protocol was further optimized to avoid using flammable *t*-BuOK, suggesting KOH as a substitute. Despite the slightly lower efficiency of KOH in comparison to *t*-BuOK, the benefits of using an easier-to-handle base compensate for the slightly lower yields. Unfortunately, the base-mediated one-pot synthesis requires a higher concentration of ammonia thus making less concentrated methanolic ammonia unsuitable for the reaction conditions we pursued.⁷⁷

Another one-pot synthesis of aliphatic diazirines from ketones in the presence of *t*-butyl hypochlorite was reported.⁷⁸ The protocol avoids using liquid ammonia as the amination source and suggests methanolic ammonia instead. The reaction runs in the presence of *t*-butyl hypochlorite which facilitates both the formation of diaziridine and its subsequent oxidation into diazirine. Preparation of *t*-BuOCl from the sodium hypochlorite is straightforward and the *t*-BuOCl solution can be stored in the fridge for a longer time. Compared to the classic approach the protocol provides a faster route to diazirines with much higher yields. The proposed mechanism suggests the formation of chloroetimine catalyzed by the first portion of *t*-BuOCl, which in turn reacts with free ammonia forming diaziridine. After removing unreacted ammonia from the reaction mixture, the second portion of the hypochlorite oxidates diaziridine into diazirine (see **Figure 6**).⁷⁸

One-pot reaction

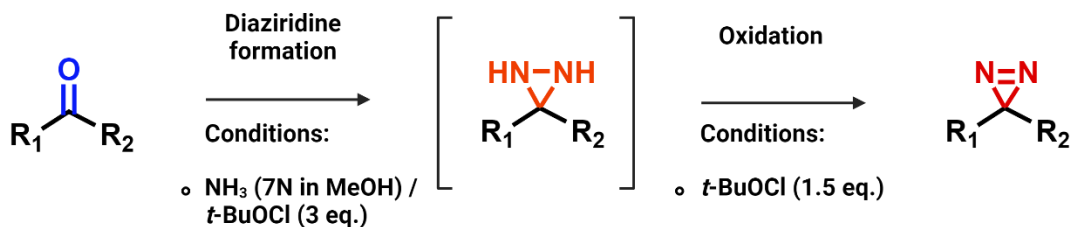


Figure 6. Approach into diazirines. One-pot synthesis of diazirines in the presence of tert-butyl hypochlorite. Created with [BioRender.com](https://www.biorender.com).

1.10. MS reporters

Chemical proteomics provides a comprehensive set of tools for protein identification, visualization and analysis. However, major complications emerge when it comes to quantification of the identified proteins. Different factors contribute to a bias in the signal intensity measured by MS and affect the reliability of protein quantification. For example, the ionization efficiency of the peptide depends on its sequence and is additionally affected by specific modifications and fragmentation patterns of the peptide ions.⁷⁹ Also, highly abundant proteins may mask the presence of low-abundant on a detector caused by its limited dynamic range.⁸⁰

The quantification problem might be overcome by sampling the analyte with the internal standard, differentiated from sample peptides by a mass shift, often achieved by labeling peptides with isotope-coded affinity tags (ICAT).⁸¹ The relative signal intensities between sample peptides and the internal standard represent their relative concentrations. However, the difference in the mass between tagged peptide pairs changes the physicochemical characteristics of the peptides, leading to different elution profiles, which is critical for accurate ion current integration.⁸² Moreover, the mass difference may affect the charge states of tagged pair peptides, potentially decreasing the reliability of the quantification.

The challenges in relative protein quantification were improved with the implementation of the isobaric tagging technique. Protein mixtures are functionalized with isobaric tags, meaning they are equal in mass but generate distinct diagnostic ion peaks upon MS/MS fragmentation. Pairs of analyzed peptides are co-eluted and give one signal in MS1 spectra upon ionization. Subsequent fragmentation of the selected MS1 ion releases diagnostic peaks enabling precise relative peptide quantification. Among them, for example, are tandem mass tags (TMT) and

isobaric tag for absolute and relative quantification (**iTRAQ**) (see **Figure 7**).^{82,83} All reagents allow for the multiplexing of samples, enabling simultaneous analysis of 4 to 16 samples depending on the tag.

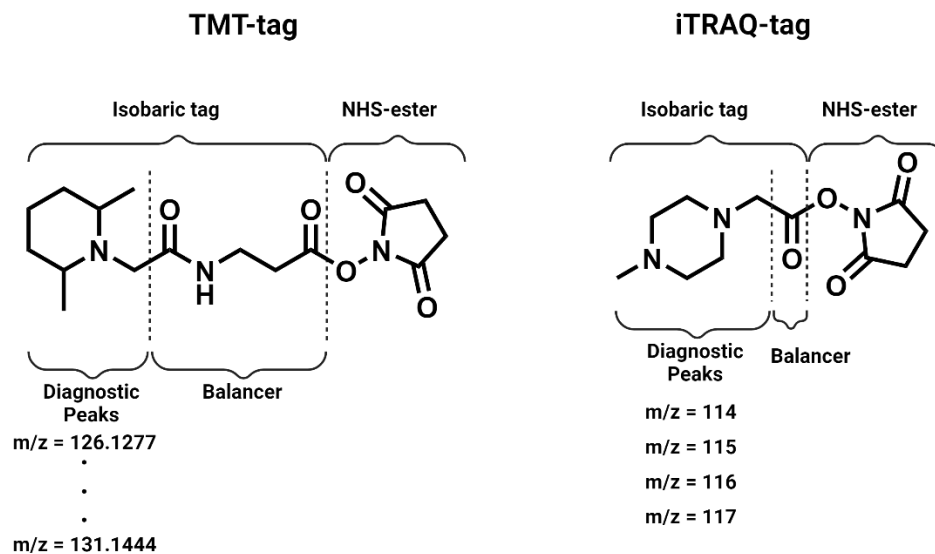


Figure 7. Isobaric tags. The structure of TMT and iTRAQ tags with diagnostic peaks. Created with [BioRender.com](https://www.biorender.com).

The quantification quality depends on the tag's ability for fragmentation, which in turn correlates with the intensity of the diagnostic peak. To improve the sensitivity of the quantification, one can improve the structure of the cleavable functional group. The introduction of the sulfoxide tag (**SOT**) attempted to address these issues.⁸⁴

2. Aim of the thesis

Post-translational modifications serve as a fine-tuning mechanism to maintain cellular homeostasis and provide the means of fast response to external signals or inner stimuli without the need for protein neosynthesis. Although different approaches have been developed to study proteomics, the scientific community still lacks the proper instrument to study PTMs in their native, physiological context, where the interplay of many cellular processes challenges *in vivo* analysis. There is a need for innovative tools and methodologies that can directly probe various PTMs within living cells to monitor their dynamics.

Central to the thesis research was an exploration of the tubulin code, with a particular focus on de-tyrosination/tyrosination PTM – a modification specific for α -tubulin, playing an important role in cell differentiation and its functioning.

The aim of the thesis was to develop a robust, high-throughput mass spectrometry-based proteoform analysis method enabling the *in vivo* characterization of tubulin de-tyrosination, helping to elucidate functional dynamics and principles of the modification.

The high promiscuity of the TTL enzyme which catalyzes the addition of tyrosine on the tubulin's C-terminal, facilitated the incorporation of the tyrosine derivatives into the α -tubulin structure. In this research, a novel tyrosine probe bearing an alkyne group was synthesized to monitor the tyrosination profiling in living cells. This approach aimed to validate the feasibility of enzymatical tubulin labeling with a modified amino acid, paving the way for the application of chemical proteomics tools.

Apart from validating the concept of studying the tubulin code employing the cell's enzymatic machinery, the thesis also aimed to provide examples of its applicability in related areas. The method of α -tubulin labeling with the probe demonstrated its potential in establishing a high-throughput pipeline for screening potential TTL inhibitors. The approach benefits from the use of living cells for screening, providing valuable insights into the toxicity, permeability, and effective concentration of potential inhibitors.

Attempts to map the interactors of tyrosinated α -tubulin were made. A bifunctional tyrosine probe with diazirine and alkyne functional groups was synthesized and shown to be successfully incorporated into the structure of α -tubulin. Diazirine functionality provides the cross-linking reactivity, while the alkyne group is used for the subsequent steps in the chemical proteomics pipeline and in-depth analysis.

Indeed, the success of the enzymatic labeling approach could pave the way for its application in studying other tubulin-related PTMs, such as polyglutamylation or polyglycylation, thereby

covering the scope of all tubulin code PTMs and expanding the toolkit available for their investigation.

3. Published work

3.1. Clickable report tags for identification of modified peptides by mass spectrometry⁸⁵

Makarov, D.; Telek, A.; Becker, T.; Von Wrisberg, M.; Schneider, S.; Kielkowski, P. Clickable Report Tags for Identification of Modified Peptides by Mass Spectrometry. *J Mass Spectrom* **2022**, 57 (3), e4812. <https://doi.org/10.1002/jms.4812>.

Prologue

The challenge in identifying low-abundant PTMs requires an efficient tool for improving the accuracy of the search algorithm in the identification and annotation of complex spectra generated by MS analysis. Alongside enrichment techniques resulting in the concentration of the protein of interest in the analyte, improvement can also be achieved in MS measurement and subsequent identification of the proteins by search engines. The current publication aimed to develop a complementary approach for the characterization and identification of rare PTMs by mass spectrometry, taking inspiration from the field of isobaric labeling.

To address this, clickable report tags were synthesized to functionalize rare PTMs, facilitating their detection. The structures of the two probes were inspired by TMT family tags and SOT.^{86,84} The tag is characterized by a functional group that yields characteristic ion peak upon fragmentation and contains an azide group allowing for the bioorthogonal reaction with the proteins functionalized with the terminal alkyne. The azide group in the structure of the probes is the major difference compared to canonical TMT and SOT probes. Instead of labeling reactive amines with the NHS-ester group, the newly synthesized tags allow for the targeted functionalization of the proteins labeled with terminal alkyne.

A set of experiments was conducted on the model protein (BSA) and in complex cell lysates, validating the effectiveness of the probes. Indeed, by fine-tuning search engines for the search of diagnostic ions generated by the clickable tags, improved identification rates were achieved. The publication provides comprehensive comparison data between two probes and evaluates their efficiency in protein identification as well as in PTM site identification.

Author contribution

Pavel Kielkowski conceived the study, assisted with MS measurements, and wrote the manuscript. Dmytro Makarov carried out the synthesis of the tags and participated in MS measurements. András Telek performed MS sample preparation and MS measurements. Tobias Becker carried out the affinity enrichment of AMP-DMP modified peptides. Marie-Kristin Von Wrisberg overexpressed the DrrA and Rab1b and performed *in vitro* AMPylation. All authors have revised the manuscript.

License

Copy of the open access publication based on the Creative Commons Attribution-NonCommercial License (CC BY-NC-ND 4.0), which allows the non-commercial reprint of the article.

Article available at:

<https://doi.org/10.1002/jms.4812>

License available at:

<https://creativecommons.org/licenses/by-nc/4.0/>

Supporting information is available in Supplementary Information (Chapter 8.1).

RESEARCH ARTICLE

Clickable report tags for identification of modified peptides by mass spectrometry

Dmytro Makarov¹  | András Telek^{1,2} | Tobias Becker¹ |
Marie-Kristin von Wrisberg¹  | Sabine Schneider¹  | Pavel Kielkowski¹ 

¹Department of Chemistry, LMU Munich, Munich, Germany

²Department of Applied Biotechnology, Budapest University of Technology and Economics, Budapest, Hungary

Correspondence

Pavel Kielkowski, Department of Chemistry, LMU Munich, Butenandtstr. 5-13, 81377 Munich, Germany.
Email: pavel.kielkowski@cup.lmu.de

Funding information

Deutsche Forschungsgemeinschaft, Grant/Award Number: SFB1309; Fonds der Chemischen Industrie

Abstract

The identification and quantification of modified peptides are critical for the functional characterization of post-translational protein modifications (PTMs) to elucidate their biological function. Nowadays, quantitative mass spectrometry coupled with various bioinformatic pipelines has been successfully used for the determination of a wide range of PTMs. However, direct characterization of low abundant protein PTMs in bottom-up proteomic workflow remains challenging. Here, we present the synthesis and evaluation of tandem mass spectrometry tags (TMT) which are introduced via click-chemistry into peptides bearing alkyne handles. The fragmentation properties of the two mass tags were validated and used for screening in a model system and analysis of AMPylated proteins. The presented tags provide a valuable tool for diagnostic peak generation to increase confidence in the identification of modified peptides and potentially for direct peptide-PTM quantification from various experimental conditions.

KEYWORDS

AMPylation, chemical proteomics, MS-tags, protein post-translational modifications, reporter ions

1 | INTRODUCTION

Post-translational protein modifications play a critical role in many cellular functions.¹ This creates numerous PTM proteins or so-called proteoforms, which largely exceed the number of encoded genes and generates an extraordinary diversity of protein properties.² However, techniques to confidently quantify and identify the site of modification are missing. This is, in particular, a challenging issue for low abundant and unstable PTMs such as AMPylation.³⁻⁸ Although the number of available linkers for enrichment complemented by various chemical proteomic approaches is quite large, there is a vacancy of the linker

that would yield a reporter ion upon MS/MS fragmentation and thus improve the site identification rates.⁹⁻¹¹ So far, isobaric labeling has been mainly used for protein quantification in bottom-up proteomics.¹² The large-scale employment of mass spectrometry-based proteomics has taken off. The isobaric strategies have allowed for the multiplication of the sample's measurement to minimize the measurement time while providing precise quantification of proteins prepared under different conditions. In parallel, chemical proteomic strategies have been utilized for the identification of PTM proteins using small compound PTM analogs containing an alkyne handle that allows the downstream enrichment of the modified proteins.¹³⁻¹⁸ It remained challenging to quantify and compare PTM stoichiometry between conditions because modified and unmodified peptides displayed

Dmytro Makarov and András Telek contributed equally.

This is an open access article under the terms of the Creative Commons Attribution-NonCommercial License, which permits use, distribution and reproduction in any medium, provided the original work is properly cited and is not used for commercial purposes.

© 2022 The Authors. *Journal of Mass Spectrometry* published by John Wiley & Sons Ltd.

different ionization properties. Furthermore, different total protein amounts, as well as shifted retention times during LC separation, contribute to the abovementioned problems.^{19,20} Here, we report the synthesis of two MS-tags conjugated to alkyne-modified proteins via click chemistry, which produce a reporter ion upon fragmentation in proof-of-concept experiments. The reporter ions are then used to improve the identification of the modified peptides by the search algorithms.

2 | RESULTS

Based on the structure of commercially available TMT-tag and the recently reported sulfoxide-containing MS-tag, we have designed and synthesized two novel MS-tags.^{21,22} The presented 2,6-dimethylpiperidine-based (DMP) and sulfoxide-containing (SOX) tags contain azido group for bioorthogonal Cu(I)-catalyzed azide-alkyne cycloaddition (CuAAC) with alkyne-modified peptides or proteins. Thus, the two new MS-tags enable selective labeling of modified peptides for MS analysis, in contrast to the original TMT-tag reagent bearing an *N*-hydroxysuccinimide ester (NHS) group to react with all available primary amines within the protein sample (Figure 1).¹⁸

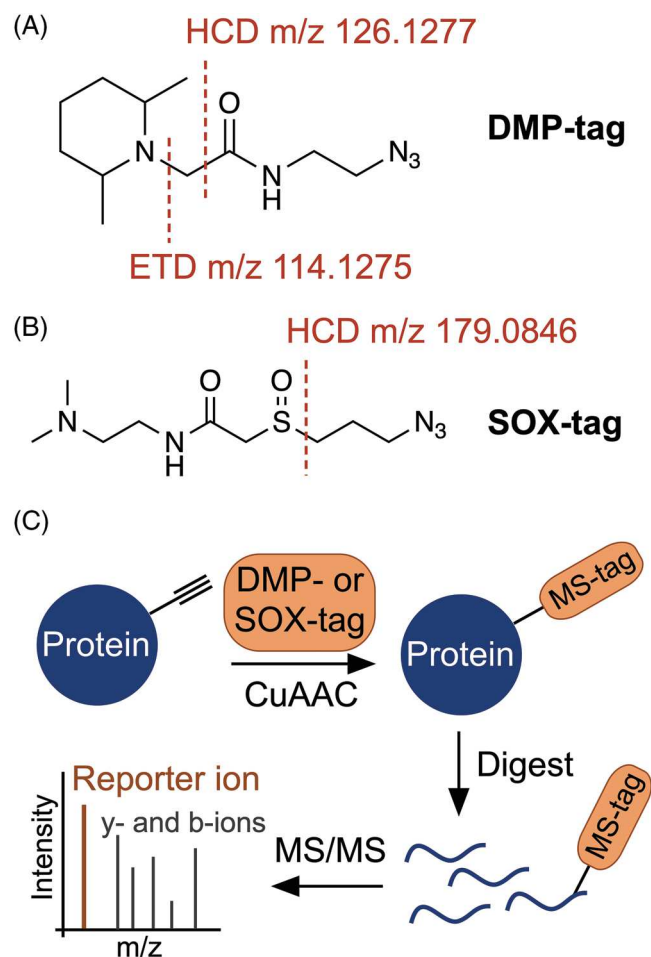


FIGURE 1 (A,B) Structure of the DMP- and SOX-tag with characteristic reporter ion masses. (C) Overall strategy to identify modified peptides in complex samples using the DMP- and SOX-tag

The study has been initiated by the synthesis of two new MS-tags (Figure 2). First, the DMP-tag containing 2,6-dimethylpiperidine was prepared from the carboxylic acid derivative **1** by HATU catalyzed amide coupling with 2-azidoethylamine, yielding after 3 days the desired DMP-tag at a 63% yield. Next, the synthesis of the sulfoxide-based tag was carried out in a total of five steps. In brief, the synthesis starts with nucleophilic substitution of ethyl bromoacetate with 3-mercaptopropanol, followed by activation of the hydroxyl group by tosylation (**2**) and subsequent conversion to azide **3** to equip the linker of the MS-tag with moiety suitable for click chemistry. Even though hydrolysis of the ester was a side reaction during nucleophilic substitution, obtained acid **3** was used in 1-ethyl-3-(3-dimethylaminopropyl) carbodiimide (EDC) and hydroxybenzotriazole (HOBT) catalyzed amide coupling giving compound **4**, which was oxidized by mCPBA to the final SOX-tag. Although all the steps provided moderate to good yields, the final oxidation showed a somewhat lower yield of 17% caused by side reactions and instability during purification. Both reagents DMP- and SOX-tags show good stability when stored as ready-to-use solutions in DMSO at -20°C .

To explore in detail the fragmentation properties of the DMP- and SOX-tags, we have established a model protein-PTM system in which the free thiol of the cysteine residue C58 of bovine serum albumin (BSA) was modified with the cysteine reactive probe IA-alkyne, which contains a terminal alkyne (Figure 3). The alkyne decorated BSA resembles the protein PTM isolated from cells treated with an alkyne-containing probe, which is common in chemical proteomic workflows that aim to map protein PTMs.^{15,18,23–25} The alkyne-modified BSA was further decorated with either DMP- or SOX-tag using the CuAAC. Next, the BSA was proteolytically cleaved by chymotrypsin, and the resulting peptide mixtures were desalted on

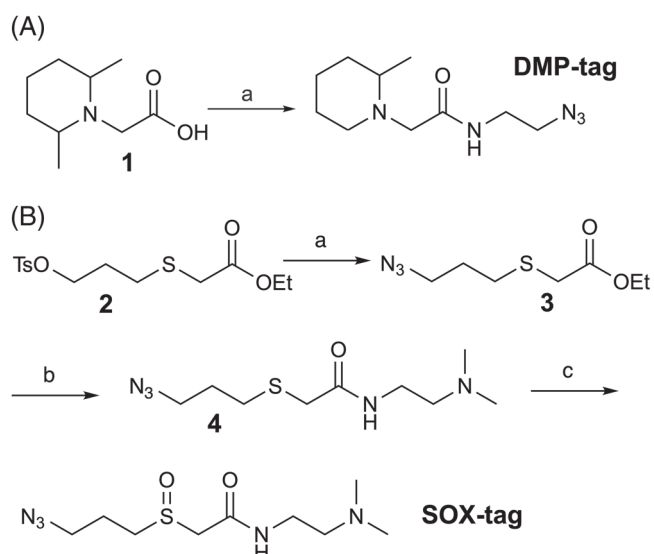


FIGURE 2 (A) Synthetic approach to DMP-tag (a) 2-azidoethan-1-amine, EDC, HOBT, DIPEA, DMF, r.t., 72 h, 63%. (B) Synthesis of the SOX-tag. (a) NaN_3 , EtOH, 95°C , 18 h, 60%. (b) N^1,N^1 -dimethylethane-1,2-diamine, EDC, HOBT, DIPEA, DCM, r.t., 18 h, 55%. (c) mCPBA, H_2O , r.t., 1.5 h, 17%

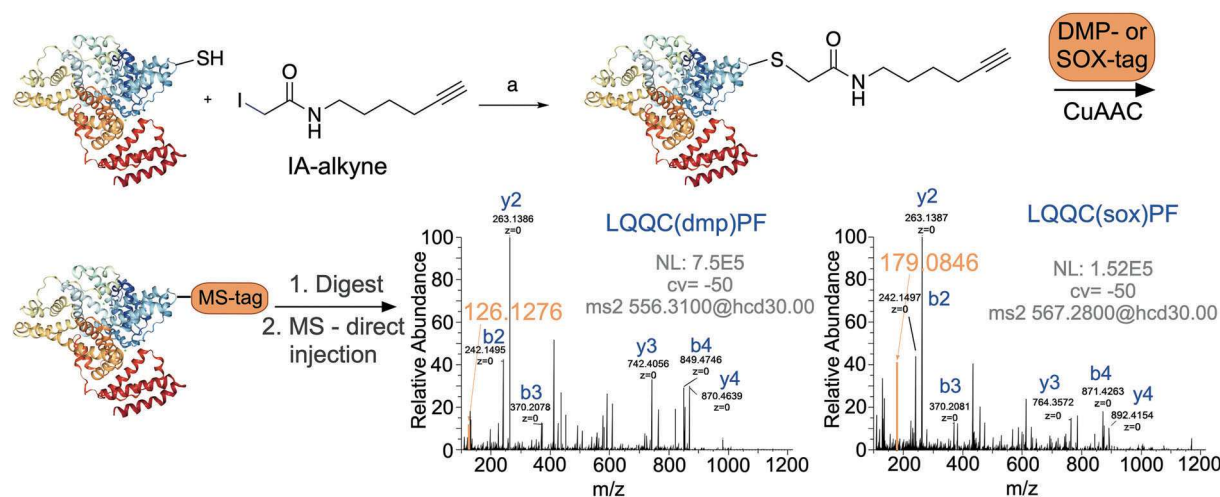


FIGURE 3 Proof-of-concept experiments with the BSA model system and the DMP- and SOX-tags

C18 columns and analyzed by direct injection into the Orbitrap Eclipse Tribrid mass spectrometer with high-field asymmetric waveform ion mobility spectrometry (FAIMS) introduced between the ion source and the Eclipse mass spectrometer.²⁶ We have started with an analysis of the DMP-tag modified BSA and the resulting DMP-tagged peptide LQQC (dmp)PF and its missed cleavage peptide LQQC (dmp) DEHVKLVNELTEF where dmp refers to the attached DMP-tag. Step-wise optimization of the FAIMS compensation voltage (CV) provided suitable conditions at -50 CV to acquire the MS1 spectra and select the target ions for the MS² experiment. To identify the suitable condition for the generation of the MS² spectra, with particular focus on the intensity of the reporter ion at 126.1277 m/z, resulting from the fragmentation of the DMP-tag, the higher-energy C-trap dissociation (HCD) energy has been gradually increased. Optimization has revealed that the most effective cleavage occurs at 30 V. A complementary set of experiments has been performed with the electron-transfer dissociation (ETD) fragmentation technique, showing a somewhat lower intensity of the corresponding reporter ion at 114.1275 m/z (Figure S1). In parallel, the fragmentation properties of the SOX-tag were assessed to show the anticipated reporter ion at 179.0846 m/z using HCD fragmentation. However, it surprisingly produced a complementary reporter ion at 131.1178 m/z as a major fragment upon ETD fragmentation (Figure S2). For both the DMP-tag and SOX-tag, better fragmentation was observed for species with higher charge peptide precursor ions. Measurement of the negative control, the BSA peptides, which were not modified with the DMP-tag or SOX-tag, but only with IA-alkyne, confirmed the specificity of all reporter ions (Figure S3).

Having characterized the fragmentation properties of the DMP- and SOX-tag in our model system, we have continued to test the possibility of using these MS-tags for the identification of modified peptides on the whole proteome level. For this, HeLa cells lysate was treated with IA-alkyne and further reacted with the DMP- or SOX-tag using click chemistry. Subsequently, the labeled proteome was acetone precipitated, trypsin digested and measured by LC-MS/MS using

the 2 h gradient with alternating FAIMS CV voltages between -50 and -70 V. The MS² has been acquired in the orbitrap, m/z range was adjusted to span from 110 to 1100 m/z and HCD fragmentation set to 30 V.²⁷ Next, MaxQuant searched the resulting spectra for the peptides modified with cysteine reactive probe and labeled with the DMP- or SOX-tag. The reporter ions were set up as diagnostic peaks. From the single run, MaxQuant identified an overall 10 802 peptides in the DMP-tag sample (Table S1). Among the total number of peptides, 3578 were modified with more than 99% of all MS² spectra containing the corresponding diagnostic peak of the DMP-tag (Figure 4A). In comparison, MSFragger search has found on average 18 673 peptides and 4783 modified peptides. SOX-label showed somewhat lower numbers with MaxQuant finding in total 14 601 peptides and 1992 modified peptides again with more than 99% containing the SOX-tag reporter ions, and again higher numbers resulted from the MSFragger search—17 380 peptides and 2916 modified peptides showing the efficiency of the offset search (Table S2). The average site identification probability for both tags with high-resolution MS² is over 99%. For comparison, the samples have been measured using the low-resolution ion trap MS² acquisition as well (Figure S4). This led to a significant increase in the total number of identified peptides but lower number of DMP-modified peptides (2325) and SOX-modified peptides (1550; both calculated with MaxQuant). This observation is in line with previously reported improvement of modified peptide identification rates by the high-resolution MS² spectra and demonstrates the feasibility of our approach compatible with a wide range of MS measurement setups.²⁸ Moreover, the identified DMP-modified peptides using the low-resolution MS² might contain interfering reporter ions at 126.0913 m/z from acetylated lysine.²⁹ Together, the application of the DMP- and SOX-tag with IA-alkyne in the proof-of-principle experiments show the high efficiency of the reporter ion release, which opens a way for relative quantification of modified peptides between various experimental conditions when used with isotopically labeled tags. However, the absolute quantification of modified peptides would need to be determined for each

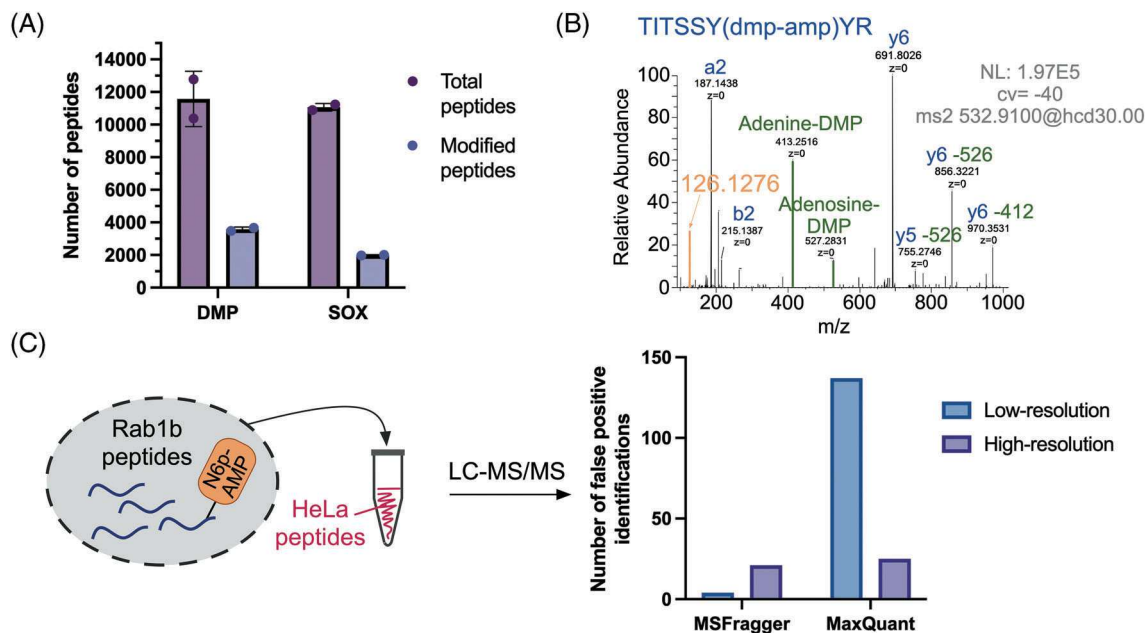


FIGURE 4 Analysis of cysteine DMP- and SOX-labeling on whole proteome level and Rab1b AMPylation with DMP-tag. (A) Total peptides and modified peptides found by MaxQuant in the DMP- and SOX-tag labeled cysteines using high-resolution MS² acquired in orbitrap. (B) Fragmentation properties of DMP-labeled AMPylated peptide from Rab1b. (C) Comparison of the MaxQuant and MSFragger search fidelity using the spiked in unnatural N⁶-propargyl AMPylated peptide from Rab1b

application because of its dependence on the used chemical proteomic probe, its metabolic incorporation rate or reactivity and CuAAC efficiency.

Encouraged by the results, we focused on our better performing DMP-tag to study protein AMPylation.³⁰ First, in an in vitro reaction of the well-described pair of AMP-transferase DrrA and its substrate Rab1b with ATP or N⁶-propargyl ATP the AMPylated Rab1b was prepared and characterized by intact protein MS (Figure S5 and S6).^{31,32} Both, wt and N⁶-propargyl modified proteins were then coupled with DMP-tag, reduced, alkylated and trypsinized. The resulting peptide mixture was analyzed by direct injection into the mass spectrometer. Of note, Rab1b is modified on Y77 with the tryptic peptide TITSSYYR, which makes the site identification in particular challenging because of six possible modification sites. The FAIMS compensation voltage optimization allowed us to select and enhance the intensity of the desired peptides for MS² experiments. The unmodified Rab1b peptide served as a control. Interestingly, the unmodified peptides were found only as double-charged peptides, whereas the AMPylated peptide was predominantly triple charged. The following fragmentation experiments corroborate previous reports and add additional insight on fragmentation properties.^{3,4,33} The fragmentation of the control AMPylated TITSSYYR peptide by HCD provided all characteristic ions and neutral losses. These were also paralleled in the analysis of the N⁶-propargyl AMP modified peptide. The measurement was repeated with the attached DMP-tag to explore the possibility to modulate fragmentation properties and improve the site identification rate of this unstable PTM. However, the DMP-AMP-peptide exhibits the same fragmentation properties, but as expected, it has yielded an

additional reporter ion at 126.1276 m/z with HCD and a low intensity 114.1275 m/z reporter ion when ETD was used (Figures 4B and S7). The artificial Rab1b DMP-AMP-peptides were spiked in the HeLa whole proteome tryptic digest and analyzed via LC-MS/MS. Indeed, it was possible to identify the desired DMP-AMP-peptide from the Rab1b by MaxQuant and MSFragger. Of note, the score was improved when the neutral losses were defined, but it led to the incorrect localization of the modification on the peptide (Table S3). This could be due to the fact that the modified Rab1b peptide contains six potentially modified sites out of eight amino acids in total. The MS² acquired in the ion trap resulted in false-positive identifications in both MaxQuant and MSFragger. The MaxQuant search was set up to search for unnatural modified peptides (with N⁶-propargyl AMP) but identified 137 modified peptides instead of one from Rab1b (Figure 4C). In comparison, the MSFragger search showed greater stringency by finding only four modified peptides, which were inherently incorrect but did not find the Rab1b peptide (Figure 4C). The high-resolution MS² acquired in the orbitrap has led to improvement of the MaxQuant search and in MSFragger to correct assignment of the modified Rab1b peptide (Figure 4C).

Our and others' previous attempts to search for AMPylated peptides in whole proteome tryptic digest proved to be challenging. In particular, Pieles et al have synthesized two adenosine analogs containing ¹⁵N and ¹³C stable isotopes, which were used for metabolic labeling of AMPylated proteins. Although it was possible to identify reporter ion clusters of labeled adenosines in in vitro activity assays, the search of the labeled peptides on a whole proteome has shown a rather low efficiency.⁴ Therefore, in our study, we have decided to

use a commercial DMP-specific antibody to enrich the DMP-modified peptides.³⁴ In principle, the main advantage compared to other approaches is the possibility of enriching and selectively eluting only the modified peptides without the necessity to use additional chemical or enzymatic cleavage of the linker used for the enrichment. The possibility of enriching DMP-modified peptides was first tested on a model system with an IA-alkyne probe coupled with the DMP-tag. The anti-DMP antibody was applied on the peptide level and resulted in a two-fold increase of the DMP-modified peptides in the sample comparison to DMP-modified peptides without enrichment (Figure 5 and Table S4). The same approach was then applied to pro-N6pA treated cell lysates, which resulted in the labeling of DMP-AMP-modified peptides. Even though we have identified numerous AMPylated peptides, there was no overlap with previously found AMPylated proteins using complementary methods.^{15,33} We hypothesize that this is mainly caused by challenging bioinformatic analysis, which has to deal with a complex mixture of ions after fragmentations. Although harnessing the potential of reporter ions and neutral losses presence might be a great advantage in future.

In summary, we have designed and synthesized two clickable MS-tags based on DMP- and SOX-moieties, which were evaluated using the single digested modified BSA protein and on whole proteome level with cysteine reactive IA-alkyne. Further on, we have applied the DMP-tag in the analysis of protein AMPylation and attempted enrichment of the AMPylated peptides using the DMP-specific antibody. This study extends the repertoire of available MS-linkers, opens the possibility to further develop isotopically labeled derivatives of DMP- and SOX-tags for quantification of PTM-peptides obtained from different cell types or stress conditions. Moreover, we have generated a high-quality MS spectra resource for optimization of the PTM search algorithms, which is freely available to the community.

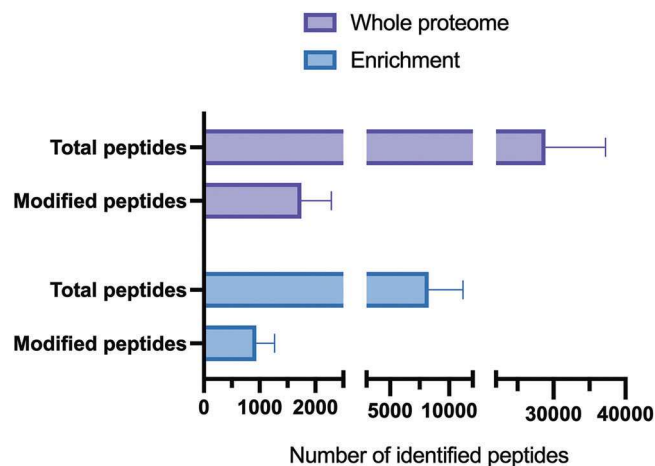


FIGURE 5 DMP-IA-alkyne-modified peptides identification rate in the whole proteome and after the enrichment using the DMP-specific antibody

ACKNOWLEDGMENTS

This research was supported by the Liebig fellowship from Fonds der Chemischen Industrie to P.K. and T.B., LMUexcellent Junior Fund to P.K. and Deutsche Forschungsgemeinschaft (DFG, German Research Foundation) – SFB 1309.

AUTHOR CONTRIBUTION

P.K. conceived the study, assisted with MS measurements, and wrote the manuscript. D.M. carried out the synthesis of the tags and participated in MS measurements. A.T. performed MS samples preparation and MS measurements. T.B. carried out the affinity enrichment of AMP-DMP modified peptides. M.-K.W. overexpressed the DrrA and Rab1b and performed in vitro AMPylation. All authors have revised the manuscript.

DATA AVAILABILITY STATEMENT

The data that support the findings of this study are available from the corresponding author upon reasonable request.

ORCID

Dmytro Makarov <https://orcid.org/0000-0001-9971-8570>

Marie-Kristin von Wrisberg <https://orcid.org/0000-0002-7100-4565>

Sabine Schneider <https://orcid.org/0000-0003-1054-8689>

Pavel Kielkowski <https://orcid.org/0000-0003-4910-6263>

REFERENCES

- Lin H, Caroll KS. Introduction: posttranslational protein modification. *Chem Rev.* 2018;118:887-888. doi:10.1021/acs.chemrev.7b00756
- Aebersold R, Agar JN, Amster IJ, et al. How many human proteoforms are there? *Nat Chem Biol.* 2018;14:206-214. doi:10.1038/nchembio.2576
- Li Y, Al-Eryani R, Yarbrough ML, Orth K, Ball HL. Characterization of AMPylation on threonine, serine, and tyrosine using mass spectrometry. *J Am Soc Mass Spectr.* 2011;22:752-761. doi:10.1007/s13361-011-0084-1
- Pieles K, Glatter T, Harms A, Schmidt A, Dehio C. An experimental strategy for the identification of AMPylation targets from complex protein samples. *Proteomics.* 2014;14:1048-1052. doi:10.1002/pmic.201300470
- Sanyal A, Dutta S, Camara A, et al. Alpha-synuclein is a target of Fic-mediated adenylation/AMPylation: possible implications for Parkinson's disease. *J Mol Biol.* 2019;431:2266-2282. doi:10.1016/j.jmb.2019.04.026
- Sanyal A, Chen AJ, Nakayasu ES, et al. A novel link between Fic (filamentation induced by cAMP)-mediated adenylation/AMPylation and the unfolded protein response. *J Biol Chem.* 2015;290:8482-8499. doi:10.1074/jbc.M114.618348
- Yu X, Woolery AR, Luong P, et al. Copper-catalyzed azide-alkyne cycloaddition (click chemistry)-based detection of global pathogen-host AMPylation on self-assembled human protein microarrays. *Mol Cell Proteomics.* 2014;13:3164-3176. doi:10.1074/mcp.M114.041103
- Preissler S, Rato C, Chen R, et al. AMPylation matches BiP activity to client protein load in the endoplasmic reticulum. *eLife.* 2015;4:e12621. doi:10.7554/eLife.12621

9. Zanon PRA, Lewald L, Hacker SM. Isotopically labeled desthiobiotin azide (isoDTB) tags enable global profiling of the bacterial cysteinome. *Angew Chem Int Ed*. 2020;132:2851-2858. doi:10.1002/anie.201912075
10. Speers AE, Cravatt BF. Activity based protein profiling (ABPP) and click chemistry (CC)-ABPP by MudPIT mass spectrometry. *Current Protocols in Chemical Biology*. 2009;1:29-41. doi:10.1002/9780470559277.ch090138
11. Wright MH, Clough B, Rackham MD, et al. Validation of N-myristoyltransferase as an antimalarial drug target using an integrated chemical biology approach. *Nat Chem*. 2014;6:112-121. doi:10.1038/nchem.1830
12. Rauniyar N, Yates JR III. Isobaric labeling-based relative quantification in shotgun proteomics. *J Proteome Res*. 2014;13:5293-5309. doi:10.1021/pr500880b
13. Martin BR, Wang C, Adibekian A, Tully SE, Cravatt BF. Global profiling of dynamic protein palmitoylation. *Nat Methods*. 2011;9:84-89. doi:10.1038/nmeth.1769
14. Storck EM, Morales-Sanfrutos J, Serwa RA, et al. Dual chemical probes enable quantitative system-wide analysis of protein prenylation and prenylation dynamics. *Nat Chem*. 2019;11:552-561. doi:10.1038/s41557-019-0237-6
15. Kielkowski P, Buchsbaum IY, Kirsch VC, et al. FICD activity and AMPylation remodeling modulate human neurogenesis. *Nat Commun*. 2020;11:517. doi:10.1038/s41467-019-14235-6
16. Kielkowski P, Buchsbaum IY, Becker T, Bach K, Cappello S, Sieber SA. A pronucleotide probe for live-cell imaging of protein AMPylation. *Chembiochem*. 2020;21:1285-1287. doi:10.1002/cbic.201900716
17. Chuh KN, Pratt MR. Chemical methods for the proteome-wide identification of posttranslationally modified proteins. *Curr Opin Chem Biol*. 2015;24:27-37. doi:10.1016/j.cbpa.2014.10.020
18. Parker CG, Pratt MR. Click chemistry in proteomic investigations. *Cell*. 2020;180:605-632. doi:10.1016/j.cell.2020.01.025
19. Olsen JV, Mann M. Status of large-scale analysis of post-translational modifications by mass spectrometry. *Mol Cell Proteomics*. 2013;12:3444-3452. doi:10.1074/mcp.o113.034181
20. Sharma K, D'Souza RCJ, Tyanova S, et al. Ultra-deep human phosphoproteome reveals a distinct regulatory nature of Tyr and Ser/Thr-based signaling. *Cell Rep*. 2014;8:1583-1594. doi:10.1016/j.celrep.2014.07.036
21. Stadlmeier M, Bogena J, Wallner M, Wühr M, Carell T. A sulfoxide-based isobaric labelling reagent for accurate quantitative mass spectrometry. *Angew Chem Int Ed*. 2018;57:2958-2962. doi:10.1002/anie.201708867
22. Li J, Vranken JGV, Vaites LP, et al. TMTpro reagents: a set of isobaric labeling mass tags enables simultaneous proteome-wide measurements across 16 samples. *Nat Methods*. 2020;17(4):399-404. doi:10.1038/s41592-020-0781-4
23. Grammel M, Hang HC. Chemical reporters for biological discovery. *Nat Chem Biol*. 2013;9:475-484. doi:10.1038/nchembio.1296
24. Backus KM, Correia BE, Lum KM, et al. Proteome-wide covalent ligand discovery in native biological systems. *Nature*. 2016;534(7608):570-574. doi:10.1038/nature18002
25. Heal WP, Tate EW. Getting a chemical handle on protein post-translational modification. *Org Biomol Chem*. 2010;8:731-738. doi:10.1039/b917894e
26. Bekker-Jensen DB, Martínez-Val A, Steigerwald S, et al. A compact quadrupole-orbitrap mass Spectrometer with FAIMS interface improves proteome coverage in short LC gradients*. *Mol Cell Proteomics*. 2020;19:716-729. doi:10.1074/mcp.tir119.001906
27. Wiśniewski JR, Zougman A, Nagaraj N, Mann M. Universal sample preparation method for proteome analysis. *Nat Methods*. 2009;6:359-362. doi:10.1038/nmeth.1322
28. Bakalarski CE, Haas W, Dephore NE, Gygi SP. The effects of mass accuracy, data acquisition speed, and search algorithm choice on peptide identification rates in phosphoproteomics. *Anal Bioanal Chem*. 2007;389:1409-1419. doi:10.1007/s00216-007-1563-x
29. Nakayasu ES, Wu S, Sydor MA, et al. A method to determine lysine acetylation stoichiometries. *Int J Proteom*. 2014;2014:730725. doi:10.1155/2014/730725
30. Sieber SA, Cappello S, Kielkowski P. From young to old: AMPylation hits the brain. *Cell Chem Biol*. 2020;27(7):773-779. doi:10.1016/j.chembiol.2020.05.009
31. Du J, von Wrisberg M-K, Gulen B, et al. Rab1-AMPylation by legionella DrrA is allosterically activated by Rab1. *Nat Commun*. 2021;12:460. doi:10.1038/s41467-020-20702-2
32. Müller MP, Peters H, Blümer J, Blankenfeldt W, Goody RS, Itzen A. The Legionella effector protein DrrA AMPylates the membrane traffic regulator Rab1b. *Science*. 2010;329:946-949. doi:10.1126/science.1192276
33. Broncel M, Serwa RA, Bunney TD, Katan M, Tate EW. Global profiling of huntingtin-associated protein E (HYPE)-mediated AMPylation through a chemical proteomic approach. *Mol Cell Proteomics*. 2016;15:715-725. doi:10.1074/mcp.O115.054429
34. Qu Z, Meng F, Bomgarden RD, et al. Proteomic quantification and site-mapping of S-nitrosylated proteins using isobaric iodoTMT reagents. *J Proteome Res*. 2014;13:3200-3211. doi:10.1021/pr401179v

SUPPORTING INFORMATION

Additional supporting information may be found in the online version of the article at the publisher's website.

How to cite this article: Makarov D, Telek A, Becker T, von Wrisberg M-K, Schneider S, Kielkowski P. Clickable report tags for identification of modified peptides by mass spectrometry. *J Mass Spectrom*. 2022;57(3):e4812. doi:10.1002/jms.4812

3.2. Chemical Proteomics Reveals Protein Tyrosination Extends Beyond the Alpha-Tubulins in Human Cells⁸⁷

Makarov, D.; Kielkowski, P. Chemical Proteomics Reveals Protein Tyrosination Extends Beyond the Alpha-Tubulins in Human Cells**. ChemBioChem 2022, 23 (23), e202200414. <https://doi.org/10.1002/cbic.202200414>.

Prologue

The publication describes the endeavor to create a chemical proteomics tool to study de-tyrosination/tyrosination PTM within its natural context. Implementing the promiscuity of TTL, the described chemical proteomics approach facilitates post-translational incorporation of modified tyrosine into α -tubulin structure. The focus on de-tyrosination PTM is justified by the importance of the PTM in neurodevelopment, neurodegenerative diseases and cardiomyopathies.¹ Its unique occurrence in α -tubulin makes it an ideal model PTM to prove the idea behind the study.

As was demonstrated in the study of Schumacher et. al. 2017, TTL can incorporate the Tyr-O-Alk probe into the structure of α -tubulin as the terminal amino acid *in vitro*.³ However, no attempt to evaluate all possibilities of the probe for studying tyrosination PTM *in vivo* was made.

The study provides the synthetic route to the probe – a natural tyrosine substituted with terminal alkyne at the para position. The alkyne functional group incorporation aimed to implement the chemical proteomics approaches. It facilitates click reaction with commercially available azide derivatives of fluorophores such as rhodamine-PEG₃-azide for imaging, biotin azide for the enrichment of modified α -tubulins or other tags like the trifunctional linker, bearing simultaneously biotin affinity group and fluorophore.

The neuroblastoma cell line (SH-SY5Y) was chosen as a model organism. The successful post-translational incorporation of the probe was proved by a series of biorthogonal experiments. After establishing the optimal concentration and treatment conditions, the probe was tested in the competition assay with natural tyrosine and tyrosine benzene-derivative. Competition assays simultaneously provided evidence of the enzymatic nature of the modification as well as TTL's capacities for the incorporation of complex tyrosine derivatives. Enzymatic incorporation was additionally proven by treating cells with a translation machinery inhibitor cycloheximide. The labeling of the analyzed tubulins was visible even after inhibiting ribosomes. Moreover, a centrifuge-based MTs polymerization/depolymerization protocol was applied to prove the incorporation of the probe-modified α -tubulin into the structure of MTs.

In-gel results were further corroborated by the MS approach. The SP2E enrichment protocol implemented for the quantitative analysis of modified α -tubulin revealed several-fold enrichment compared to the control set. The whole proteome analysis focusing on the identification of other proteins labeled with the probe did not observe any significant hits, additionally proving the enzymatic nature of the modification and its specificity for α -tubulin.

The approach was successfully implemented to study tyrosination profiles in the iNGNs cell line during neurodevelopment. The rates of tyrosination were decreasing with the differentiation of neurons, being in line with the fact of developing more stable (de-tyrosinated) microtubules for maintaining cell polarity.

Author contribution

The study was conceived in collaboration with Pavel Kielkowski. All experimental part was covered by the author of this thesis. The manuscript was written by Pavel Kielkowski.

License

Copy of the open access publication based on the Creative Commons Attribution-NonCommercial License (CC BY-NC-ND 4.0), which allows the non-commercial reprint of the article.

Article available at:

<https://doi.org/10.1002/cbic.202200414>

License available at:

<https://creativecommons.org/licenses/by-nc/4.0/>

Supporting information is available in Supplementary Information (Chapter 8.2).

VIP Very Important Paper

Chemical Proteomics Reveals Protein Tyrosination Extends Beyond the Alpha-Tubulins in Human Cells**

Dmytro Makarov^[a] and Pavel Kielkowski^{*[a]}

Tubulin detyrosination-tyrosination cycle regulates the stability of microtubules. With respect to α -tubulins, the tyrosination level is maintained by a single tubulin-tyrosine ligase (TTL). However, the precise dynamics and tubulin isoforms which undergo (de)tyrosination in neurons are unknown. Here, we exploit the substrate promiscuity of the TTL to introduce an *O*-propargyl-L-tyrosine to neuroblastoma cells and neurons. Mass spectrometry-based chemical proteomics in neuroblastoma cells using the *O*-propargyl-L-tyrosine probe revealed previously

discussed tyrosination of TUBA4A, MAPRE1, and other non-tubulin proteins. This finding was further corroborated in differentiating neurons. Together we present the method for tubulin tyrosination profiling in living cells. Our results show that detyrosination-tyrosination is not restricted to α -tubulins with coded C-terminal tyrosine and is thus involved in fine-tuning of the tubulin and non-tubulin proteins during neuronal differentiation.

Introduction

Microtubules (MTs) are composed of α - and β -tubulin heterodimers and are essential for function and stability of the cellular cytoskeleton. The defined MTs composition is critical for intracellular transport, mechanical resistance, mitosis and migration.^[1] Both α - and β -tubulin are encoded in the human genome in multiple isotypes, which have been observed to be tissue- and cell-type-specific.^[2] The heterogeneity of MTs is further extended by numerous post-translational modifications (PTMs) including acetylation, (poly)glutamylolation, (poly)glycylation, (poly)amination and tyrosination together called the tubulin code (Figure 1A).^[3] The majority of these PTMs are concentrated on the disordered tubulin C-terminus. In most of the α -tubulins, the encoded C-terminal amino acid is tyrosine, which can be cleaved by VASH-SVBP complex or most recently discovered MATCAP carboxypeptidase (Figure 1B).^[4] The terminal tyrosine is restored in translation independent manner by tubulin-tyrosine ligase. Regulation of the tyrosination statutes fine-tunes the stability of α - and β -tubulin heterodimer and MTs.^[5] The stable MTs induced by paclitaxel show an increased amount of detyrosinated α -tubulin, while

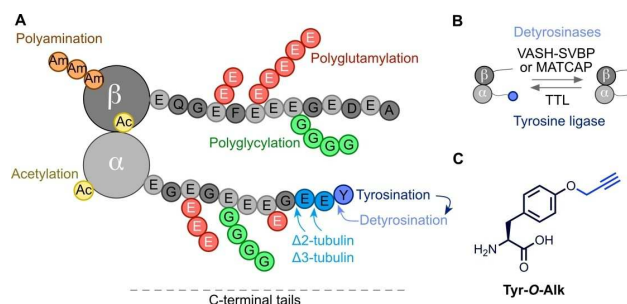


Figure 1. Microtubules detyrosination and tyrosination cycle. A) Tubulin code overview. B) Enzymes involved in detyrosination and tyrosination. C) Structure of the Tyr-O-Alk probe.

tubulin heterodimers and unstable MTs are characterized by tyrosinated α -tubulin.^[5] However, the tyrosinated tubulins are not required for MTs polymerization nor MTs detyrosination is sufficient for their stabilization. The physiological relevance was demonstrated on TTL knockout mice, which die perinatally and display dysregulated development of neuronal networks.^[6] The upregulated MTs detyrosination was linked to failing hearts in patients with ischemic cardiomyopathy.^[7] On the cellular level, MTs detyrosination is critical for directional transport of chromosomes and governance of interaction between MTs and microtubule-associated proteins (MAPs).^[7] Overall tubulin tyrosination was previously analyzed by cell pretreatment with cycloheximide (CHX) to block the protein synthesis and subsequent addition of tritiated tyrosine analogue to track the tyrosine incorporation by radioactivity.^[8] Tubulin C-terminus labelling can also be achieved by incorporation of non-natural tyrosine analogues, for example, 3-N₃-L-tyrosine or 3-formyltyrosine.^[8] The latter can subsequently react with 7-hydrazino-4-methyl coumarin to provide a fluorescent tag on labelled proteins in living cells. The tubulin (de)tyrosination status is usually identified by PTM-specific antibodies.^[8] However, these do not distinguish individual tubulin isotypes. On

[a] D. Makarov, Dr. P. Kielkowski
LMU München, Department of Chemistry
Institute for Chemical Epigenetics – Munich (ICEM)
Würmtalstrasse 201, 81375 Munich (Germany)
E-mail: pavel.kielkowski@cup.lmu.de

[**] A previous version of this manuscript has been deposited on a preprint server (<https://www.biorxiv.org/content/10.1101/2022.07.02.498566v1>).

Supporting information for this article is available on the WWW under <https://doi.org/10.1002/cbic.202200414>

This article is part of the Special Collection ChemBioTalents2022. Please see our homepage for more articles in the collection.

© 2022 The Authors. ChemBioChem published by Wiley-VCH GmbH. This is an open access article under the terms of the Creative Commons Attribution Non-Commercial NoDerivs License, which permits use and distribution in any medium, provided the original work is properly cited, the use is non-commercial and no modifications or adaptations are made.

the other hand, liquid chromatography (LC) with mass spectrometry (MS)-based detection of tyrosinated and detyrosinated peptide fragments is not feasible due to the very high complexity of C-terminal peptide PTMs.

Here, we report an MS-based chemical proteomics approach to decipher the composition of post-translationally tyrosinated proteins in living cells. The approach is based on the low substrate selectivity of the TTL. The TTL's active site was shown to be able to accommodate various tyrosine analogues.^[9] In contrast, modified tyrosines are poor substrates for translation machinery. Thus, avoiding unspecific labelling of bulk proteins.

Results and Discussion

To initiate the study, we designed and applied the *O*-propargyl-L-tyrosine (**Tyr-O-Alk**, Figure 1C), which was previously tested in *in vitro* tubulin C-terminus modification catalyzed by the TTL.^[9] The **Tyr-O-Alk** was synthesized in three steps from L-tyrosine (Figure S1). First, the cytotoxicity of the **Tyr-O-Alk** was evaluated on SH-SY5Y neuroblastoma cells to show no toxicity up to 2 mM final concentration of the probe in cell culture media (Figure S2). Second, a series of in-gel experiments were carried out to optimize the labelling efficiency and to test the probe's fidelity (Figure 2A). The **Tyr-O-Alk** treatment times of SH-SY5Y cells were optimized. To evaluate the extent of **Tyr-O-Alk** incorporation, the probe-treated cells were lysed and reacted under copper-catalyzed azide-alkyne cycloaddition (CuAAC) conditions with rhodamine-PEG₃-azide (TAMRA-N₃). The labelled proteins were separated using sodium dodecyl sulfate-polyacrylamide gel (SDS-PAGE) electrophoresis and rhodamine fluorescence was scanned. The successful protein labelling was observed already between 8 to 16 hours after the addition of the 300 μM **Tyr-O-Alk** into cell culture media but further increased for a total of two days (Figure 2B).

Interestingly, the strongest fluorescence band exhibiting time-dependent labelling was observed at around 50 kDa, suggesting the labelling of tubulins. In parallel, probe concentration was tested to reveal that already 200 μM final concentration provides bright fluorescent bands (Figure S3).

Next, to confirm the translation-independent incorporation of **Tyr-O-Alk** in proteins, the SH-SY5Y cells were pre-treated

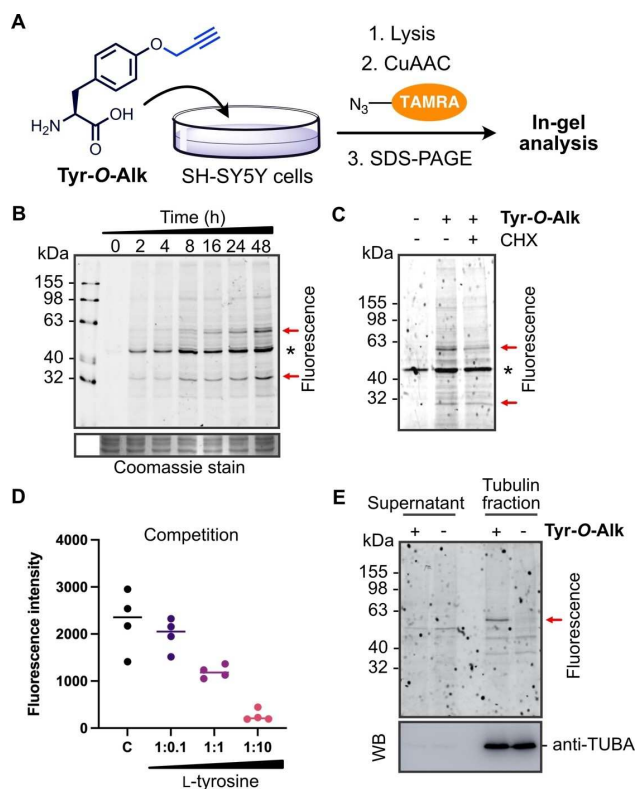


Figure 2. In-gel analysis of **Tyr-O-Alk** protein metabolic labelling in SH-SY5Y cells. A) The overall metabolic labelling strategy. B) Time-dependent labelling using the **Tyr-O-Alk** probe (300 μM). Cells were harvested at indicated time points after addition of the probe. C) The cells were pre-treated with CHX for 30 min before addition of the **Tyr-O-Alk** probe and incubation for 24 h. This excludes the incorporation of the probe via ribosomal translation machinery. D) The cells were treated with a constant final concentration of the **Tyr-O-Alk** probe and further supplemented with the increasing amount of L-tyrosine as indicated. E) In-gel fluorescence of the isolated tubulin fraction reveals a single specific band at around 55 kDa. Abbreviation: C : control, only **Tyr-O-Alk** probe treated cells. WB : Western blot. B), C) and E) The red arrows point to a fluorescent band stemming from estimated tubulin (~50 kDa) and MAPRE1 (~30 kDa) labelling. An asterisk marks unspecific TAMRA-N₃ labelling.

with CHX to block the protein synthesis before **Tyr-O-Alk** probe addition (Figure 2C). Indeed, we observed only a decrease in fluorescence intensity related to the decrease of total α-tubulin (Figure S4). This confirms the introduction of **Tyr-O-Alk** as protein PTM rather than via ribosomal protein synthesis. Furthermore, a competition experiment between the probe and natural tyrosine was performed to test the probe's fidelity. Indeed, the probe labelling was clearly diminished with an increasing amount of natural tyrosine (Figure 2D and Figure S5). Next, the tubulin fraction was isolated by taxol-induced depolymerization-polymerization of MTs from **Tyr-O-Alk** treated SH-SY5Y cells.^[8b,10] The single probe-specific fluorescent band was observed in the tubulin fraction, corroborating the fidelity of the probe (Figure 2E). Tubulin fraction isolation was tested by western blot using the anti-TUBA antibody. Finally, the turnover of the **Tyr-O-Alk** probe was examined by treatment of the SH-SY5Y cells with the probe, followed by cell culture media exchange without the probe. Surprisingly, we observed a rather



Pavel Kielkowski studied chemistry at University of Chemistry and Technology in Prague and continued with his PhD work on artificial nucleosides, nucleotides and nucleic acids with Prof. Michal Hocek at the IOCB in Prague and Charles University. In 2014, he joined the group of Prof. Stephan Sieber at the TUM, where he developed chemical proteomics approaches for analysis of protein AMPylation. Since 2019 he has been an independent research group leader at the LMU Munich. His laboratory focuses on chemical biology of protein post-translational modifications during neuronal differentiation and neurodegeneration.

slow replacement of incorporated propargyl tyrosine by natural tyrosine, only after 24 h, there was no observable band present (Figure S6). Together, these experiments support the efficient incorporation of **Tyr-O-Alk** in tubulins as PTM.

To decipher the composition of tubulin isoforms labelled by the **Tyr-O-Alk** probe, we continued with MS-based chemical proteomics. Recently, we have established an efficient chemical proteomics enrichment approach called SP2E.^[11] The SP2E workflow uses the carboxylate-modified magnetic beads to clean up the proteins after the click chemistry with biotin-N₃. During this process, the carboxylate-modified magnetic beads are aggregated together with proteins after addition of an organic solvent such as ethanol or acetonitrile.^[12] In the next step, the proteins are eluted from the carboxylate magnetic beads and transferred on streptavidin-coated magnetic beads. The biotin-labelled proteins are enriched and digested by trypsin. The resulting peptide mixtures corresponding to the enriched probe-modified proteins are collected and analyzed via LC-MS/MS. In parallel, the same procedure is carried out with control cells to be able to abstract the background, which is composed of non-specifically enriched proteins (Figure 3A). We have utilized the SP2E workflow to enrich **Tyr-O-Alk** labelled proteins from SH-SY5Y cells in quadruplicates using data-independent acquisition (DIA).^[13] Indeed, analysis of resulting MS spectra by DIA-NN^[13] via label-free quantification (LFQ)^[13] confirmed the significant enrichment of α -tubulin isoforms including TUBA1C and TUBA4A (Figure 3B). To gain more confidence in the identification of the highly similar tubulin isoforms, we have revised the peptides assigned to the tubulin isoforms together with corresponding MS2 spectra (Table S1). This analysis showed that at least 2 unique peptides were found for each α -tubulin isoform. The TUBA4A isoform does not

encode the C-terminal tyrosine resembling the de-tyrosinated tubulin when translated. However, TUBA4A was speculated to be possibly tyrosinated, which is now corroborated by our results. Surprisingly, several non-tubulin proteins were found to be significantly enriched as well. This group contains the microtubule-associated protein RP/EB family member 1 (MAPRE1 also called EB1) a marker of the microtubule plus-end, which regulates the dynamics of the microtubule cytoskeleton.^[14] MAPRE1 is involved in a mitotic spindle positioning and recruiting the CLIP170 to MTs (+)-end.^[14] Importantly, sequence analysis of this 30 kDa protein contains the α -tubulin-like C-terminus coding the terminal tyrosine adjacent to two glutamates (PQEEQEEY). This would suggest a potential de-tyrosination-tyrosination cycle, as discussed in the literature.^[15] The retrospective analysis of the in-gel fluorescence labelling shows clear time-dependent labelling of a protein at around 30 kDa (Figure 2B). Another microtubule-associated protein TUBGCP5 was significantly enriched based on the one unique peptide found in four probe-treated replicates but not in the controls suggesting TUBGCP5 modification by the probe. Some other non-tubulin proteins were significantly and consistently enriched (as well in the following experiments in iNGNs), such as MARCKS, DCTN3 and LSM6. From these, the MARCKS and DCTN3 are proteins with a role in cytoskeleton organization. Although it is assumed that the **Tyr-O-Alk** probe is incorporated into proteins and, in particular, in α -tubulin by TTL, it cannot be excluded that other proteins possess similar catalytic function. For example, He et al. described the tRNA synthetases to act as aminoacyl transferases modifying the lysine side chain amino group.^[16] In parallel, the **Tyr-O-Alk** probe-treated lysates were processed by SP3^[17] for whole proteome MS analysis to exclude the translation-dependent

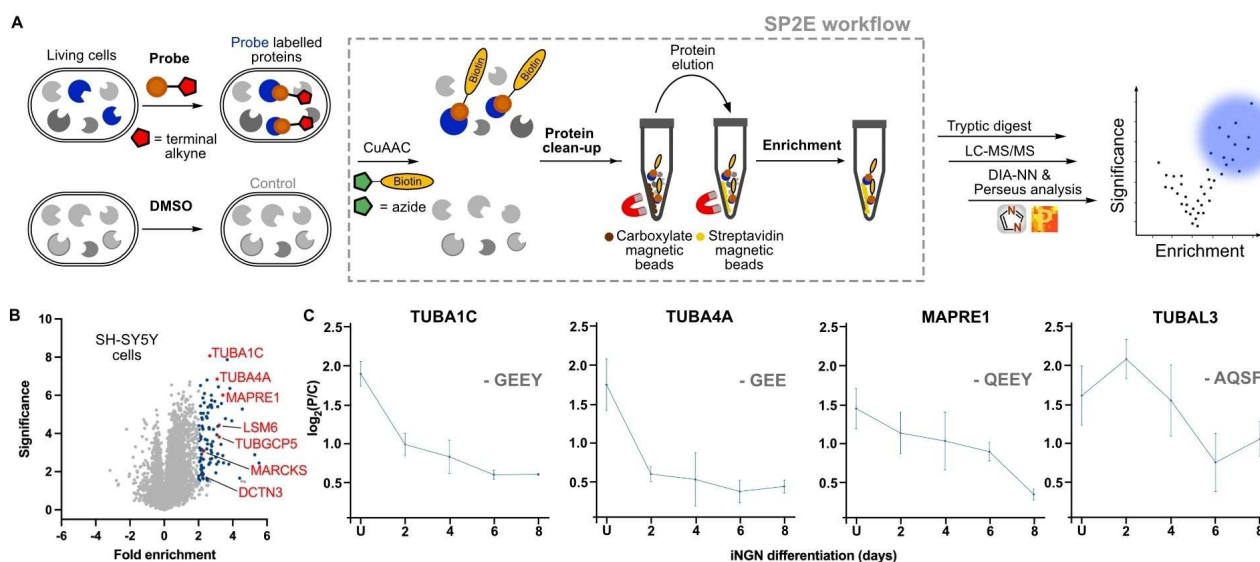


Figure 3. Mass spectrometry-based chemical proteomics of SH-SY5Y and iNGN cells uncovered the scope of protein tyrosination. A) Overview of MS-based chemical proteomics workflow using the SP2E. B) Volcano plot visualizing the enrichment of **Tyr-O-Alk** labelled proteins from SH-SY5Y cells; Blue dots are significantly enriched proteins with at least 4-fold enrichment. $n = 4$, fold enrichment ($\log_2(\text{Tyr-O-Alk}/\text{control})$), significance ($-\log_{10}(p\text{-value})$). C) Fold change of tyrosination on selected proteins during iNGNs neuronal differentiation showing tyrosination/de-tyrosination cycle of TUBA4A and MAPRE1. The isoform encoded C-terminal sequences are added for comparison. Points represent the mean of four replicates (C: control; P: **Tyr-O-Alk** probe treated) with standard error of the mean (SEM).

stochastic incorporation of the probe into a primary amino acid sequence of proteins. The resulting MS spectra were searched for the presence of peptides containing tyrosine with *O*-propargyl as variable modification. In both control and **Tyr-O-Alk** treated cells on average only 42.5 and 33 modified proteins were found from an average of 38606 and 37291 total peptides, respectively (Table S2 and Figure S7). Thus, suggesting the **Tyr-O-Alk** is not incorporated into proteins by ribosomal translation machinery but rather post-translationally. The direct identification of the C-terminal *O*-propargyl tyrosine on tubulins was unlikely as it is challenged by additional C-terminal PTMs exploding the number of possible combinations, which exceed the computational capacity. The whole proteome analysis also revealed that TUBA1C and TUBA4A were the only identified α -tubulins. With the established **Tyr-O-Alk** labelling and MS-based chemical proteomics workflow, we moved towards the application of the method to determine the dynamics of protein tyrosination during neuronal differentiation.

The neuronal cells are characterized by their strong polarization of the cell body containing dendrites, axons and synapses. The neuronal cytoskeleton is responsible for the maintenance of this polarization, it supports neuronal migration during cortex development and provides avenues for cellular trafficking.^[18] The composition of tubulin isoforms is known to play a role during neuronal differentiation. However, it was previously not possible to link the tubulin isoforms with the corresponding tyrosination status. We applied the **Tyr-O-Alk** probe to determine protein tyrosination status during neuronal differentiation of human induced pluripotent stem cells (hiPSCs). To streamline this process, we leveraged from fast (4 days) differentiation of hiPSCs engineered with doxycycline-inducible Neurogenin-1 and -2 cassette (iNGNs).^[19] To test the feasibility of our approach in iNGNs, they were treated with **Tyr-O-Alk** at four different time points during differentiation into mature neurons (Figure S8). Similar to SH-SY5Y cells, the fluorescent band at around 50 kDa was present, likely corresponding to the tubulins (Figure S8). In addition, we observed a clear change in fluorescence intensity of the 30 kDa band during iNGNs differentiation (Figure S8). Thus, we proceeded with the SP2E enrichment of **Tyr-O-Alk** labelled proteins using the trifunctional linker (containing 5/6-TAMRA-N₃-biotin moieties) instead of the biotin-N₃. In contrast to the previous MS experiments, enriched proteins were eluted from streptavidin magnetic beads using the SDS-PAGE loading buffer. Fluorescence imaging of the gel showed the labelling in a region around 30 kDa. The subsequent western blot of these enriched proteins and staining with the anti-MAPRE1 antibody showed the presence of MAPRE1 protein pool in probe-treated cells 2 days after doxycycline-induced neuronal differentiation (Figure S9). Next, the MS-based chemical proteomics was performed using the small-scale 96-well plate format SP2E workflow, starting with 100 μ g protein. In total, we have collected the cells at five time points during the iNGNs differentiation and maturation. We have observed a decrease in overall tubulin tyrosination on TUBA1C, TUBA4A and MAPRE1 during the neuronal differentiation (Figure 3C and Figure S10). Moreover, tubulin alpha chain-like 3 (TUBAL3) protein was

identified, showing a different pattern. Despite the high sequence similarity with α -tubulins (>75%), the TUBAL3C-terminus lacks the -EEY motive. Several other non-tubulin but cytoskeleton-associated proteins were significantly enriched suggesting their tyrosination including dynactin subunit 3 (DCTN3), alpha-tubulin N-acetyltransferase 1 (ATAT), MARCKS-related proteins MARCKS and MARCKSL1. Surprisingly, a cytosolic U6 snRNA-associated Sm-like protein Lsm6 (LSM6) was consistently enriched at all time points during the iNGNs differentiation (Figure S10). SP2E enrichment experiment in iNGNs was complemented by whole proteome analysis. This confirmed the identity of the neuronal cells and also aided estimation of the trends in tyrosination stoichiometry and thus dynamics. In general, there is a strong increase in total tubulin isoforms expression (Figure S11). The same trend was found for the MAPRE1 explaining the above-described observation using the western blot as the read-out. It was possible to detect MAPRE1 after enrichment with anti-MAPRE1 antibody only in two-day differentiated iNGNs, because of the sufficient absolute amount of tyrosinated MAPRE1 in the lysate. While the MAPRE1 tyrosination (fold enrichment) mildly decreases after two days, there is at the same time a dramatic increase in MAPRE1 protein expression (Figure 3C and Figures S11, S12). The tyrosination status of the proteins correlates well with the expression of the TTL, which is lower than that of carboxypeptidases responsible for tyrosine removal (VASH1 and MATCAP) (Figure S12). Apart from the enriched α -tubulin isoforms, the whole proteome analysis identified the protein group contacting TUBA1A, TUBA3C, TUBA3D and TUBA3E. Together, these experiments provide evidence of significant changes in tyrosination status during neuronal differentiation on tubulin and non-tubulin proteins.

To visualize the probe distribution and incorporation within the SH-SY5Y cells, the **Tyr-O-Alk** probe was used for fluorescence imaging (Figure 4A). Control or probe-treated cells were washed to remove excess of the probe, after fixation and permeabilization, they were incubated with TAMRA-N₃ under CuAAC conditions. The strong labelling in the probe-treated cells was observed, with a negligible background in control. Colocalization with TUBA and MAP2 showed partial overlap, which is in line with the fact that tyrosinated tubulins are mostly present in cells as dimers, which are not polymerized in microtubules.

Finally, we were interested in whether it is possible to further utilize the low substrate selectivity of TTL to introduce other functional groups in living cells. The selected *O*-(2-nitrobenzyl)-L-tyrosine (**ONBY**) was added together with **Tyr-O-Alk** to the cells in different ratios.

The final concentration of **Tyr-O-Alk** was kept constant. This setup resulted in the competition between the two unnatural tyrosines, which was then analyzed after CuAAC with TAMRA-N₃ and fluorescence scanning of the SDS-PAGE (Figure 4B and Figure S13). The MTs incorporated ONBY tubulin might be further used to probe the MTs' interactions with MAPs. The nitrobenzyl residue can be removed by UV-light irradiation, enabling modulation of the tyrosination function in the living cells.^[20]

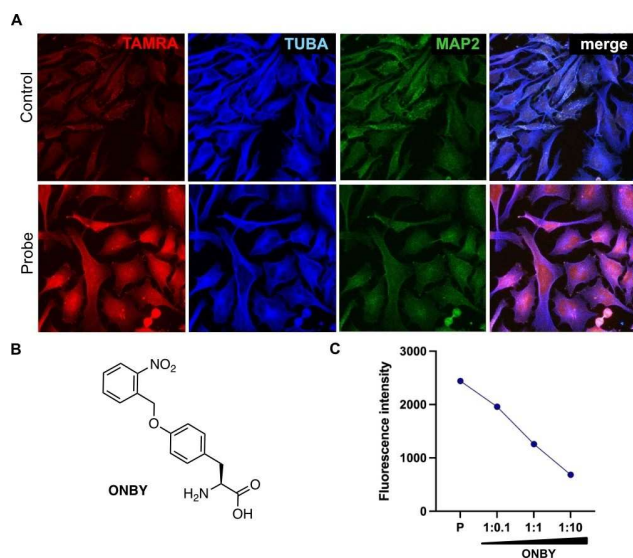


Figure 4. Fluorescence imaging and incorporation of sterically hindered tyrosine derivative. A) Fluorescence imaging of Tyr-O-Alk treated and control SH-SY5Y cells. B) ONBY structure. C) In-gel analysis of the competition experiment between Tyr-O-Alk and ONBY in SH-SY5Y cells. The fluorescence band at around 55 kDa was quantified. P – only Tyr-O-Alk treated cells.

Conclusion

A straightforward approach for chemical proteomic analysis of protein tyrosination in living cells based on the metabolic labelling using the Tyr-O-Alk probe was developed. Our method enables for the first time to profile tyrosinated tubulin isoforms during neuronal differentiation and strongly suggests that tyrosination is not restricted to α -tubulins. We have confirmed disputed tyrosination of microtubule-associated protein MAPRE1 and TUBA4A as well as on other non-tubulin proteins. Microtubules are critical for mechanical resistance of the cells and intracellular trafficking, the hallmarks of cancer research and neurodegeneration, respectively. Further research in this direction enabled by the reported strategy will be carried out in our laboratory to determine the pathophysiological relevance of protein tyrosination.

Experimental Section

Cell treatment and harvest. SH-SY5Y or iNGN cells were treated with the stock solution of Tyr-O-Alk ($\text{H}_2\text{O}:1\text{ M NaOH } 2:1$, 144 mM, sterile filtered), the final concentration in culture media was 0.3 mM. Unless otherwise stated, the cells were treated with the probe for 24 h. After the incubation, the medium was removed, and the cells were washed once with 5 mL of a phosphate-buffered saline solution (PBS). After removing PBS from a dish, cells were scraped with 1 mL of PBS, and transferred to a 1.5 mL tube. The cell suspension was centrifuged at 4 °C at 100 rcf to obtain the cell pellet.

Cell lysis. The cell pellet was reconstituted in 300 μL of a lysis buffer (1% NP40, 0.2% SDS in 25 mM HEPES, 7.5 pH) by sonication with an ultrasonic tip in 1 s on/1 s off cycles at 20% intensity for 10 s of

total time. The solution was clarified by centrifugation at 4 °C at 14000 rcf for 15 min.

Small-scale SP2E workflow. Lysates containing 100 μg of proteins were diluted to 19 μL with lysis buffer (1% NP40, 0.2% SDS in 25 mM HEPES, 7.5 pH). For each sample, 0.2 μL Biotin- N_3 (10 mM in DMSO), 0.2 μL of TCEP (100 mM in H_2O), and 0.125 μL TBTA (16.7 mM in DMSO) was added, vortexed, spun down, and supplemented with 0.4 μL of CuSO_4 (50 mM in H_2O) to initiate the reaction. The reaction mixture was incubated at r.t. while shaking at 450 rpm for 1.5 h. After completion of the click reaction, each sample was diluted with 60 μL of 8 M urea. A 1:1 mixture of hydrophobic and hydrophilic carboxylate-coated magnetic beads (100 μL) was washed three times with 100 μL MS-grade H_2O , and the reaction mixture was placed on the beads, diluted with 100 μL of absolute ethanol and vortexed. The suspension was incubated at r.t. while shaking at 950 rpm for 5 min. Afterward, the supernatant was discarded, and the beads were washed thrice with 150 μL of 80% ethanol in H_2O and once with 150 μL acetonitrile (LC-MS). Proteins were eluted separately by adding 60 μL of 0.2% SDS in PBS. For this, beads were resuspended and incubated for 5 min at 40 °C and 950 rpm. The supernatant was directly transferred onto 50 μL equilibrated streptavidin-coated magnetic beads (3 times prewashed with 100 μL 0.2% SDS in PBS). The elution step was repeated twice and the combined beads mixture was incubated at r.t. while shaking at 800 rpm for 1 h. The supernatant was discarded, and the beads were washed three times with 150 μL 1% NP-40 in PBS, twice with 150 μL 6 M Urea in H_2O , and twice with 500 μL MS-grade H_2O . After each round of washing, the beads were incubated at r.t. while shaking at 800 rpm for 1 min. The rinsed beads mixtures were resuspended in 50 μL 50 mM TEAB, and the proteins were digested overnight at 37 °C by adding 1.5 μL sequencing grade trypsin (0.5 mg/mL). The following day, the beads were washed twice with 20 μL of 50 mM TEAB buffer and twice with 20 μL 0.5% FA, and the wash fractions were collected and combined. The beads were incubated for 5 min at 40 °C and 600 rpm for each washing step. The combined washed fractions were acidified by adding 0.9 μL formic acid (FA) and transferred to MS vials.

MS acquisition and analysis. MS measurements were performed on an Orbitrap Eclipse Tribrid Mass Spectrometer (Thermo Fisher Scientific) coupled to an UltiMate 3000 Nano-HPLC (Thermo Fisher Scientific) via an EASY-Spray source (Thermo Fisher Scientific) and FAIMS interface (Thermo Fisher Scientific). First, peptides were loaded on an Acclaim PepMap 100 μ -precursor cartridge (5 μm , 100 \AA , 300 μm ID \times 5 mm, Thermo Fisher Scientific). Then, peptides were separated at 40 °C on a PicoTip emitter (noncoated, 15 cm, 75 μm ID, 8 μm tip, New Objective) that was *in-house* packed with Reprosil-Pur 120C18-AQ material (1.9 μm , 150 \AA , Dr. A. Maisch GmbH). The DIA duty cycle consisted of one MS1 scan followed by 30 MS2 scans with an isolation window of the 4 m/z range, overlapping with an adjacent window at the 2 m/z range. MS1 scan was conducted with Orbitrap at 60000 resolution power and a scan range of 200–1800 m/z with an adjusted RF lens at 30%. MS2 scans were conducted with Orbitrap at 30000 resolution power, RF lens was set to 30%. The precursor mass window was restricted to a 500–740 m/z range. HCD fragmentation was enabled as an activation method with a fixed collision energy of 35%. FAIMS was performed with one at 45 V compensation voltage (CV) for both MS1 and MS2 scans. Standalone DIA-NN software under version 1.8.1 was used for protein identification and quantification. First, a spectral library was predicted *in silico* by the software's deep learning-based spectra, RTs and IMs prediction using Uniprot *H. sapiens* decoyed FASTA (canonical and isoforms – May 2022). FASTA digest for library-free search/library generation option was enabled for this. Spectral library prediction was performed in 4 batches of

10 samples each to decrease the computational load. Second, all samples (40) were processed together without spectral library generation, with a match between runs (MBR) option and precursor FDR level set at 1%. DIA-NN search settings: Library generation was set to smart profiling, Quantification strategy - Robust LC. The mass accuracy the MS1 accuracy, and the scan window were set to 0 to allow the software to identify optimal conditions. The precursor m/z range was changed to 500–740 m/z to fit the measuring parameters. Carbamidomethylation was set as a fixed modification, oxidation of methionine and N-term acetylation were set as variable modifications. On the contrary, the small-scale samples of the 96-well plate were calculated without carbamidomethylation as a fixed modification. Statistical analysis of the DIA-NN result table "report.pg_matrix.csv" was done with Perseus 1.6.10.43.

Mass spectrometry-based proteomics data have been deposited at ProteomeXchange. The accession number is PXD037402.

Acknowledgements

This work was funded by Liebig fellowship (Fonds der chemischen Industrie) and LMUexcellent Junior Research Fund to P.K. We are grateful for generous support from SFB 1309 – 325871075 (Deutsche Forschungsgemeinschaft). Open Access funding enabled and organized by Projekt DEAL.

Conflict of Interest

The authors declare no conflict of interest.

Data Availability Statement

The data that support the findings of this study are openly available in ProteomeXchange at <https://www.ebi.ac.uk/pride/>, reference number PXD037402.

Keywords: chemical proteomics · microtubules · neuronal differentiation · protein modifications · tyrosination

- [1] a) C. P. Garnham, A. Roll-Mecak, *Cytoskeleton* **2012**, *69*, 442–463; b) P. W. Baas, A. N. Rao, A. J. Matamoros, L. Leo, *Cytoskeleton* **2016**, *73*, 442–460.
- [2] a) M. A. Tischfield, E. C. Engle, *Biosci. Rep.* **2010**, *30*, 319–330; b) T. J. Hausrat, J. Radwitz, F. L. Lombino, P. Breiden, M. Kneussel, *Dev. Neurobiol.* **2021**, *81*, 333–350.
- [3] a) C. Janke, M. M. Magiera, *Nat. Rev. Mol. Cell Biol.* **2020**, *21*, 307–326; b) J. Nieuwenhuis, T. R. Brummelkamp, *Trends Cell Biol.* **2018**, *29*, 80–92; c) A. Roll-Mecak, *Curr. Opin. Cell Biol.* **2019**, *56*, 102–108.
- [4] a) C. Aillaud, C. Bosc, L. Peris, A. Bosson, P. Heemeryck, J. V. Dijk, J. L. Friec, B. Boulan, F. Vossier, L. E. Sanman, S. Syed, N. Amara, Y. Couté, L. Lafanechère, E. Denarier, C. Delphin, L. Pelletier, S. Humbert, M. Boggy, A. Andrieux, K. Rogowski, M.-J. Moutin, *Science* **2017**, *358*, 1448–1453; b) C. Zhou, L. Yan, W. Zhang, Z. Liu, *Nat. Commun.* **2019**, *10*, 3212; c) L. Landskron, J. Bak, A. Adamopoulos, K. Kaplani, M. Moraiti, L. G. van den Hengel, J.-Y. Song, O. B. Bleijerveld, J. Nieuwenhuis, T. Heidebrecht, L. Henneman, M.-J. Moutin, M. Barisic, S. Taraviras, A. Perrakis, T. R. Brummelkamp, *Science* **2022**, *376*, eabn6020.

- [5] a) A. E. Prota, M. M. Magiera, M. Kuijpers, K. Bargsten, D. Frey, M. Wieser, R. Jaussi, C. C. Hoogenraad, R. A. Kammerer, C. Janke, M. O. Steinmetz, *J. Cell Biol.* **2013**, *200*, 259–270; b) C. A. Arce, J. A. Rodriguez, H. S. Barra, R. Caputto, *Eur. J. Biochem.* **1975**, *59*, 145–149.
- [6] C. Erck, L. Peris, A. Andrieux, C. Meissirel, A. D. Gruber, M. Vernet, A. Schweitzer, Y. Saoudi, H. Pointu, C. Bosc, P. A. Salin, D. Job, J. Wehland, *Proc. Natl. Acad. Sci. USA* **2005**, *102*, 7853–7858.
- [7] X. Yu, X. Chen, M. Amrute-Nayak, E. Allgeyer, A. Zhao, H. Chenoweth, M. Clement, J. Harrison, C. Doreth, G. Sirinakis, T. Krieg, H. Zhou, H. Huang, K. Tokuraku, D. S. Johnston, Z. Mallat, X. Li, *Nature* **2021**, *594*, 560–565.
- [8] a) H. S. Barra, C. A. Arce, J. A. Rodriguez, R. Caputto, *Biochem. Biophys. Res. Commun.* **1974**, *60*, 1384–1390; b) A. Banerjee, T. D. Panosian, K. Mukherjee, R. Ravindra, S. Gal, D. L. Sackett, S. Bane, *ACS Chem. Biol.* **2010**, *5*, 777–785; c) D. Schumacher, J. Helma, F. A. Mann, G. Pichler, F. Natale, E. Krause, M. C. Cardoso, C. P. R. Hackenberger, H. Leonhardt, *Angew. Chem. Int. Ed.* **2015**, *54*, 13787–13791; *Angew. Chem.* **2015**, *127*, 13992–13996; d) B. Eddé, J. Rossier, J.-P. L. Caer, E. Desbryères, F. Gros, P. Denoulet, *Science* **1990**, *247*, 83–85.
- [9] a) D. Schumacher, O. Lemke, J. Helma, L. Gerszonowicz, V. Waller, T. Stoschek, P. M. Durkin, N. Budisa, H. Leonhardt, B. G. Keller, C. P. R. Hackenberger, *Chem. Sci.* **2017**, *8*, 3471–3478; b) A. Banerjee, T. D. Panosian, K. Mukherjee, R. Ravindra, S. Gal, D. L. Sackett, S. Bane, *ACS Chem. Biol.* **2010**, *5*, 777–785; c) A. Rovini, G. Gauthier, R. Bergès, A. Kruczynski, D. Braguer, S. Honoré, *PLoS One* **2013**, *8*, e65694.
- [10] a) P. Verdier-Pinard, E. Pasquier, H. Xiao, B. Burd, C. Villard, D. Lafitte, L. M. Miller, R. H. Angeletti, S. B. Horwitz, D. Braguer, *Anal. Biochem.* **2009**, *384*, 197–206; b) V. Redeker, *Methods Cell Biol.* **2010**, *95*, 77–103.
- [11] T. Becker, A. Wiest, A. Telek, D. Bejko, A. Hoffmann-Röder, P. Kielkowski, *JACS Au* **2022**, *2*, 1712–1723.
- [12] C. S. Hughes, S. Moggridge, T. Müller, P. H. Sorensen, G. B. Morin, J. Krijgsveld, *Nat. Protoc.* **2019**, *14*, 68–85.
- [13] a) L. R. Heil, W. E. Fondrie, C. D. McGann, A. J. Federation, W. S. Noble, M. J. MacCoss, U. Keich, *J. Proteome Res.* **2021**, *21*, 1382–1391; b) Y. Kawashima, H. Nagai, R. Konno, M. Ishikawa, D. Nakajima, H. Sato, R. Nakamura, T. Furuyashiki, O. Ohara, *J. Proteome Res.* **2022**, *21*, 1418–1427; c) V. Demichev, C. B. Messner, S. I. Vernardis, K. S. Lilley, M. Ralser, *Nat. Methods* **2020**, *17*, 41–44.
- [14] a) P. Bieling, S. Kandels-Lewis, I. A. Telley, J. van Dijk, C. Janke, T. Surrey, *J. Cell Biol.* **2008**, *183*, 1223–1233; b) X. Song, F. Yang, X. Liu, P. Xia, W. Yin, Z. Wang, Y. Wang, X. Yuan, Z. Dou, K. Jiang, M. Ma, B. Hu, R. Zhang, C. Xu, Z. Zhang, K. Ruan, R. Tian, L. Li, T. Liu, D. L. Hill, J. Zang, X. Liu, J. Li, J. Cheng, X. Yao, *Nat. Chem. Biol.* **2021**, *17*, 1314–1323.
- [15] a) A. Rovini, G. Gauthier, R. Bergès, A. Kruczynski, D. Braguer, S. Honoré, *PLoS One* **2013**, *8*, e65694; b) A. Bosson, J.-M. Soleilhac, O. Valiron, D. Job, A. Andrieux, M.-J. Moutin, *PLoS One* **2012**, *7*, e33490.
- [16] X.-D. He, W. Gong, J.-N. Zhang, J. Nie, C.-F. Yao, F.-S. Guo, Y. Lin, X.-H. Wu, F. Li, J. Li, W.-C. Sun, E.-D. Wang, Y.-P. An, H.-R. Tang, G.-Q. Yan, P.-Y. Yang, Y. Wei, Y.-Z. Mao, P.-C. Lin, J.-Y. Zhao, Y. Xu, W. Xu, S.-M. Zhao, *Cell Metab.* **2018**, *27*, 151–166.e6.
- [17] C. S. Hughes, S. Foehr, D. A. Garfield, E. E. Furlong, L. M. Steinmetz, J. Krijgsveld, *Mol. Syst. Biol.* **2014**, *10*, 1–10.
- [18] a) M. A. Tischfield, E. C. Engle, *Biosci. Rep.* **2010**, *30*, 319–330; b) T. J. Hausrat, J. Radwitz, F. L. Lombino, P. Breiden, M. Kneussel, *Dev. Neurobiol.* **2021**, *81*, 333–350; c) P. Guedes-Dias, E. L. F. Holzbaur, *Science* **2019**, *366*, eaaw9997.
- [19] a) V. Busskamp, N. E. Lewis, P. Guye, A. H. Ng, S. L. Shipman, S. M. Byrne, N. E. Sanjana, J. Murn, Y. Li, S. Li, M. Stadler, R. Weiss, G. M. Church, *Mol. Syst. Biol.* **2014**, *10*, 760; b) E. Korytiaková, E. Kamińska, M. Müller, T. Carell, *Angew. Chem. Int. Ed.* **2021**, *60*, 16869–16873; c) T. Becker, C. Cappel, F. D. Matteo, G. Sossalla, E. Kamińska, F. Spada, S. Cappello, M. Damme, P. Kielkowski, *iScience* **2021**, *24*, 103521.
- [20] E. Arbely, J. Torres-Kolbus, A. Deiters, J. W. Chin, *J. Am. Chem. Soc.* **2012**, *134*, 11912–11915.

Manuscript received: July 21, 2022

Revised manuscript received: October 10, 2022

Accepted manuscript online: October 11, 2022

Version of record online: November 9, 2022

4. Unpublished work

4.1. Investigating Tubulin Dynamics Using Tyr-O-Alk Probes in TTL and SVBP Knockout Model Systems

To further investigate the potential of the Tyr-O-Alk probe, we performed tyrosination profiling in the TTL and SVBP-depleted mouse-derived embryonic fibroblast cells (**MEFs**). Since TTL catalyzes the addition of tyrosine and its derivatives on the C-terminal of α -tubulin and SVBP is an essential protein creating complex with VASH1 and VASH2 and promoting carboxypeptidase activity to detach tyrosine, the current model serves as a great tool to show the tyrosination profiling workflow applicability. By disrupting the de-tyrosination/tyrosination cycle, one could expect to observe decreased amounts of tyrosinated tubulin levels in TTL- and SVBP-depleted cells compared to control samples.

Cells were treated with the Tyr-O-Alk probe under standard conditions: namely, 24-hour incubation time and 0.3 mM final concentration of the probe in the medium. The cell lysates underwent click reaction with biotin-azide and were subjected to the SP2E protocol for enrichment analysis.

As expected, α -tubulin isoforms were among the top hits in WT cells (see **Figure 8**), whereas, in TTL-KO samples, tubulin isoforms fell below the cut-off lines (Fold Change (**FC**)>1, $p < 0.05$) (see **Figure 9a**). However, for SVBP-KO cells, the results of the t-test indicated p-values greater than 5%, suggesting that the differences observed between control samples and samples derived from SVBP-KO cells were not statistically significant (see **Figure 9b**).

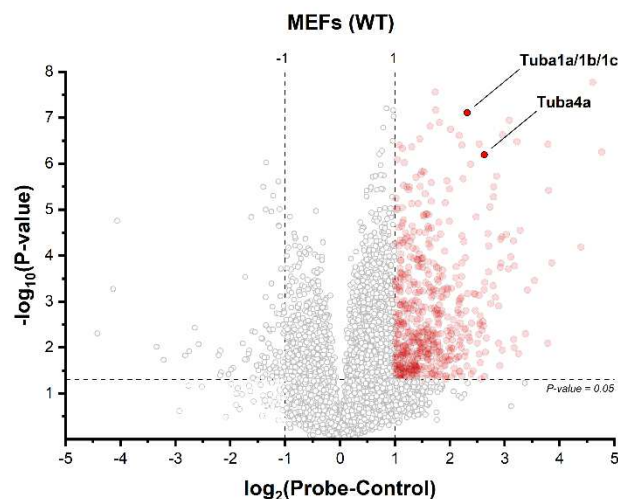


Figure 8. Volcano plot. Enrichment analysis of wild-type MEFs. Alpha-tubulins are among top hits.

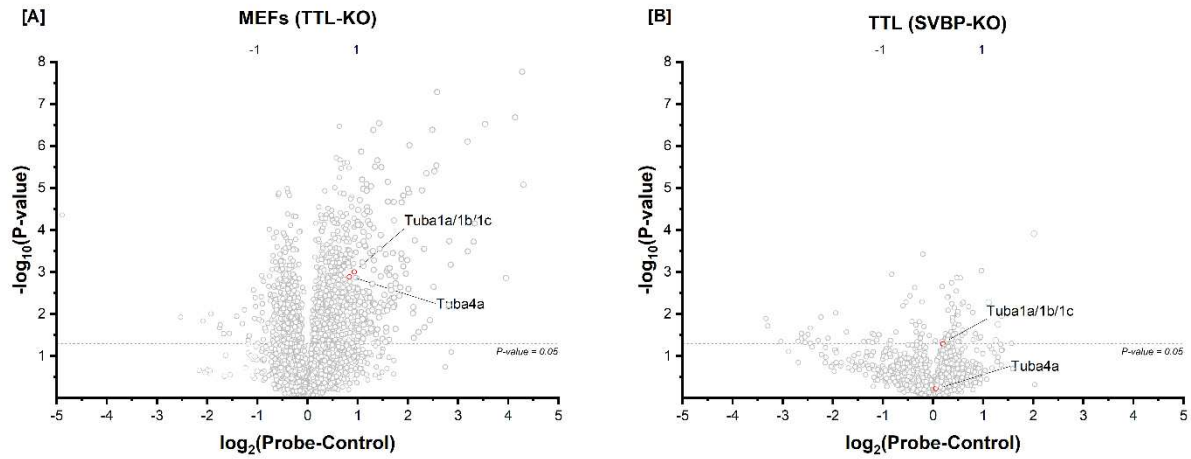


Figure 9 Volcano plot. Enrichment analysis of: a) TTL-KO MEFs, b) SVBP-KO MEFs

Results proved the probe incorporation into the tubulin's CTT in the WT cell line which corroborates the previous results obtained from SH-SY5Y neuroblastoma cells. In contrast to WT cells, tubulin isoforms were not enriched in TTL-KO and SVBP-KO cells, proving the probe is a substrate of the de-tyrosination/tyrosination cycle, and is dependent on the proper functioning of the cycle enzymes (TTL, VASH1/SVBP).

4.2. Implementation of Tyr-O-Alk probe-based screening platform for identifying potential TTL inhibitors

Workflow description

The tyrosine probe modified with the terminal alkyne functional group proved to be a suitable tool for the derivatization of α -tubulin's C-terminals in living cells.⁸⁷ The probe showed no toxicity for cells up to 2M concentrations. The probe was not incorporated into the structure of other proteins during translation, serving as the unique PTM specific for α -tubulins (see **Chapter 3.2**). That makes the probe suitable for studying the de-tyrosination/tyrosination cycle in living cells. Such specificity allowed us to establish a fast and robust workflow for the identification of potential inhibitors/activators of the de-tyrosination/tyrosination cycle *in vivo*.

The set of potential inhibitors was prepared by the group of Ioannis Kostakis at the Athens Institute. The primary screening of the selected compounds was done by the collaborative group through the measurement of the binding affinity of the compounds to the TTL enzyme *in vitro*. Initially, the binding affinity experiments were aimed at finding kinase inhibitors but unexpectedly identified a compound with a strong affinity to TTL. Subsequently, this initial compound served as a scaffold for the synthesizing of a series of related compounds to explore the structure-activity relationship (**SAR**) and improve the binding constant. The compounds with high affinity to TTL underwent the *in vivo* analysis using the Tyr-O-Alk probe-based platform.

The workflow of the Tyr-O-Alk platform could be represented in several steps. First, the neuroblastoma cell line (SH-SY5Y) was treated with the inhibitor candidate alongside the Tyr-O-Alk probe. Second, the cells were harvested to prepare the lysates. Third, the click reaction between Tamra-azide and the probe bearing a terminal alkyne was conducted to label the probe-functionalized α -tubulins. Finally, the separation of proteins on SDS-Page with subsequent fluorescence imaging was performed.

The intensity of the fluorescent band serves as a measure of the incorporation rate of the probe representing tyrosination levels following the treatment with the TTL inhibitor candidates. However, the change in the fluorescence signal solely cannot be interpreted because of TTL inhibition. The cellular environment involves a complex interplay of many processes, and the addition of compounds may disrupt pathways other than the de-tyrosination/tyrosination cycle, indirectly influencing the output signal. As an example, a compound may act as an inhibitor of MTs polymerization, causing indirect changes in the tyrosination cycle. On the other hand, the established workflow may dramatically decrease the scope of potential TTL inhibitor candidates and provide insights into cytotoxicity data.

Optimization of the protocol

The CEM198 compound was the first to be tested for TTL inhibition with the current protocol. Based on the previous MTT studies conducted by the collaborative group, the incubation time for the compound was set to 3 days. According to the studies, CEM198 was toxic in the low nanomolar range. Neuroblastoma cell line was used as a model system due to the higher incorporation efficiency of the Tyr-O-Alk probe compared, e.g. to HeLa. After the second day of incubation with the CEM198 compound, the Tyr-O-Alk probe was added to the medium and the cells were incubated for one more day to reach an overall incubation time of 3 days for CEM198. The first results showed no change in the fluorescent intensities of the bands (see **Figure 10**).

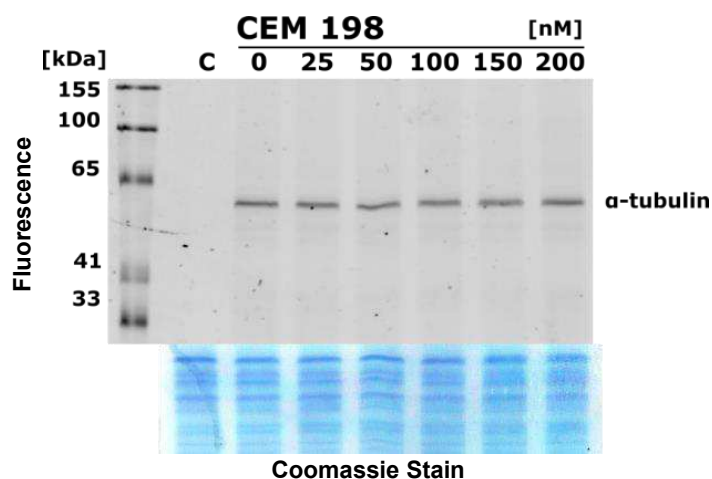


Figure 10. Fluorescent SDS-Gel with Coomassie staining as a loading control. CEM198. 3 days incubation time, nanomolar range. The band around 55 kDa represents α -tubulin functionalized with Tamra-azide dye.

During the next round of optimization, the concentration range for CEM198 was increased to 10 μ M at maximum. By increasing the concentration of the CEM198, a substantial decrement in fluorescence was visible. Although the protein concentration of the lysates was determined by Pierce BCA analysis to load equal amounts of protein mixture on a gel, staining of the gel with Coomassie solution showed a slight decrease in the protein load upon increased CEM198 concentration (see **Figure 11a**). After normalization of the fluorescent intensities with a Coomassie-stained gel signal, a 40% decrease in the fluorescence was observable already at a concentration of 2 μ M. Higher concentrations have led to an 80% decrease in fluorescence (see **Figure 11b**).

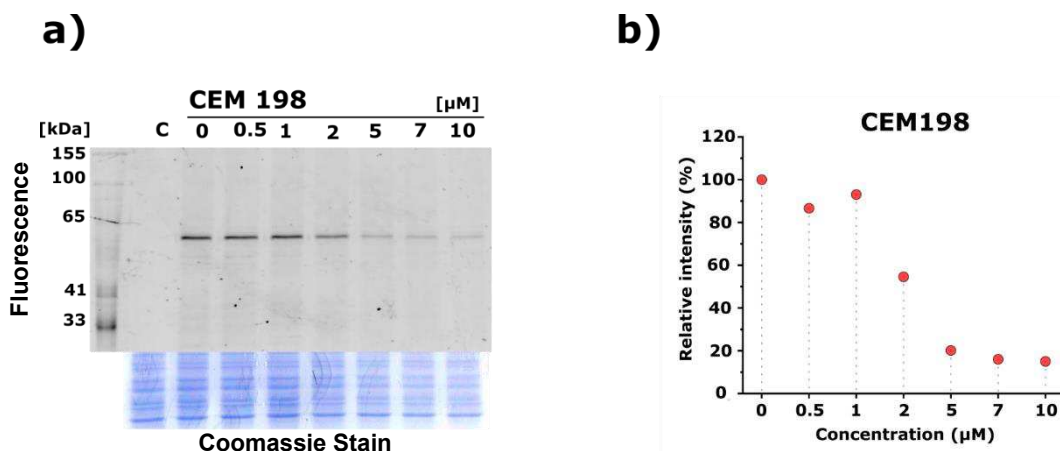


Figure 11. Fluorescent SDS-Gel with Coomassie staining and normalized intensities. (a) CEM198. 3 days incubation time, micromolar range. (b) Normalized intensities of the SDS-Page bands. Normalization was done towards Coomassie staining.

To understand the distribution of tubulin proteins across the concentration gradient, western blot analysis with anti- α -tubulin, tyrosinated, antibody was performed. The WB results showed a decrease in the abundance of the protein upon treatment with higher concentrations of the CEM198 compound. Subsequent staining with anti-GAPDH-rhodamine-linked antibody also showed a decrease in the abundance of the related protein (see **Figure 12a**). By the staining the membrane with anti-de-tyrosinated α -tubulin antibody, the diminishing of the signal was observed. Surprisingly, the signal of de-tyrosinated α -tubulin was gone at concentrations 5 μ M and higher (see **Figure 12b**).

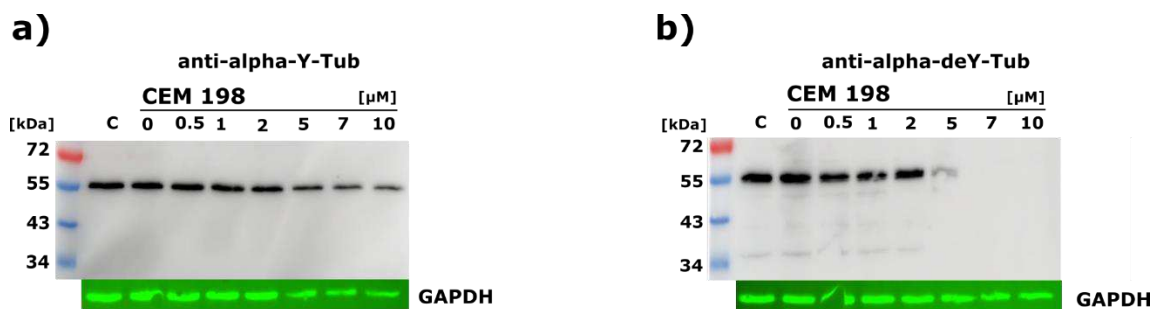


Figure 12. WB analysis with GAPDH control. CEM198. 3 days incubation time. (a) Staining with anti- α -tubulin, tyrosinated antibody. (b) Staining with anti- α -tubulin, de-tyrosinated antibody.

The second batch of the compounds (CEM353, CEM706, CEM670) was tested using the same protocol as for CEM198, maintaining a 3-day incubation time and with a concentration range of 10 μ M at maximum. The compound CEM353 did not show a substantial decrease in fluorescence signal upon treatment with concentrations up to 7 μ M. A slightly lower signal was observable at a concentration of 10 μ M (see **Figure 13**).

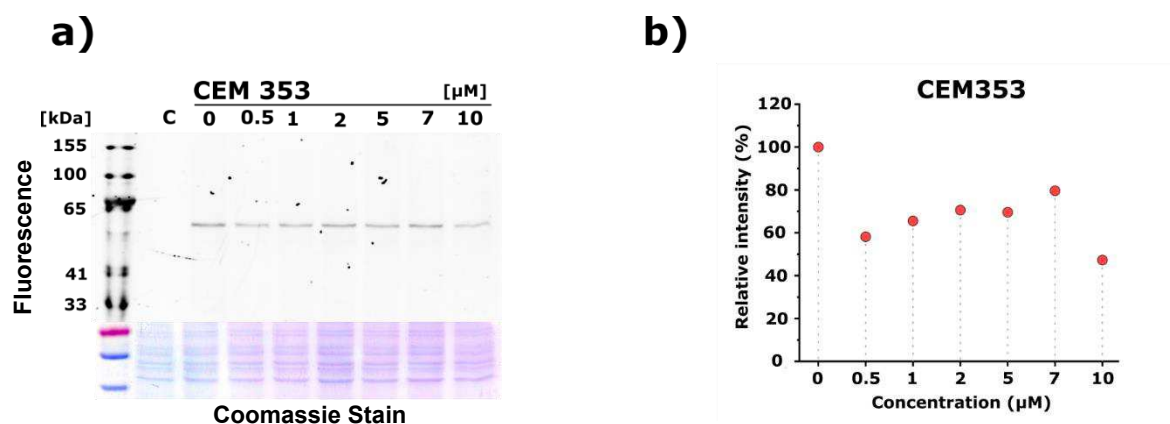


Figure 13. Fluorescent SDS-Gel with Coomassie staining and normalized intensities. (a) CEM 353. 3 days incubation time, micromolar range. (b) Normalized intensities of the SDS-Page bands. Normalization was done by Coomassie staining.

Upon cell treatment with the compound CEM670 at a final concentration of 10 μM, a slight decrease in fluorescence was visible, similar to what was seen with CEM353 (see **Figure 14**). However, this compound was rather toxic for the cells, leading to dosage-dependent cell death.

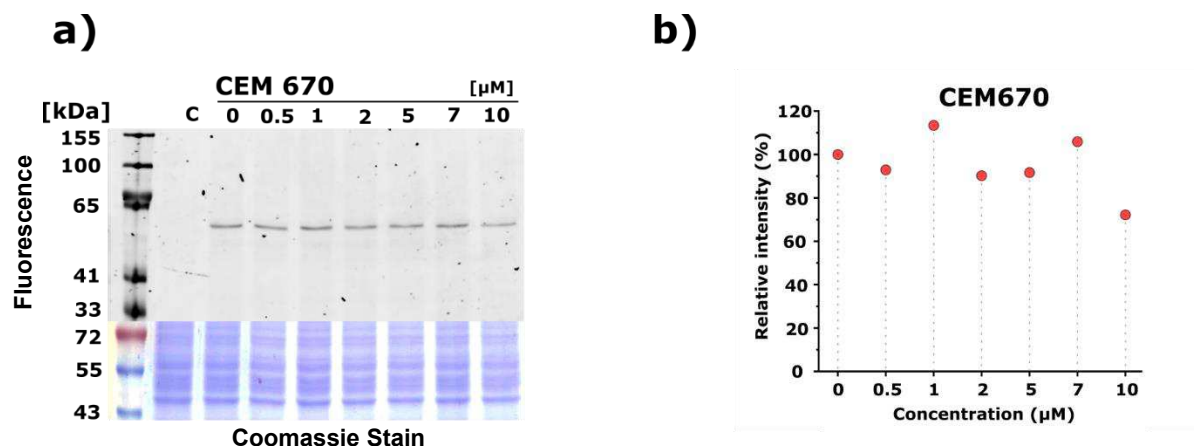


Figure 14. Fluorescent SDS-Gel with Coomassie staining and normalized intensities. (a) CEM 670. 3 days incubation time, micromolar range. (b) Normalized intensities of the SDS-Page bands. Normalization was done by Coomassie staining.

The compound CEM706 exhibited significant toxicity to the cells and was tolerated up to 2 μM concentration only. Upon treatment with higher concentrations, survival rates were dropped to zero and it was impossible to process the cell material. By normalization of the band intensities with Coomassie staining signal, the 40% decrease in intensity compared to cells treated with Tyr-O-Alk took place at a concentration of 2 μM (see **Figure 15**).

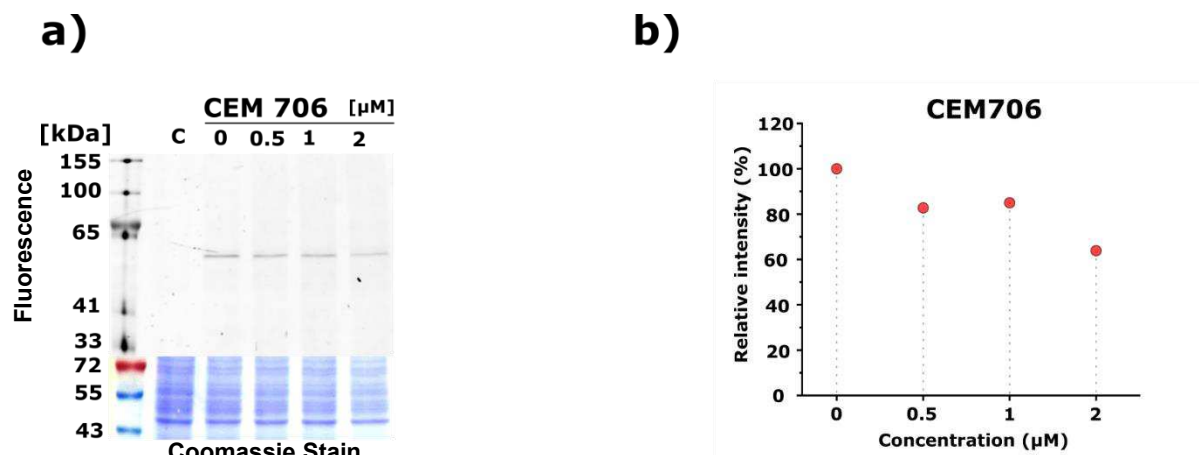


Figure 15. Fluorescent SDS-Gel with Coomassie staining and normalized intensities. (a) CEM 706. 3 days incubation time, micromolar range. (b) Normalized intensities of the SDS-Page bands. Normalization was done by Coomassie staining.

The fluorescence signal decreased to different extents upon the treatment with the CEM compounds (CEM198, CEM670, CEM706). However, the toxicity of the compounds remained as the main issue for the experimental procedure. The amount of viable cells ready for harvesting dropped by the increasing CEM concentrations. The cells' morphology was substantially changed compared to untreated cells. Even though the protein concentration in the lysates was measured, the staining of the gels with Coomassie dye revealed uneven loading of the samples. Most probably, the general protein composition was extensively changed upon treatment with the CEM compounds. To fully understand the underlying changes in proteome composition, the whole proteome analysis of the CEM-treated cells can be performed employing mass spectrometry. However, additional experiments exceed the scope of the current workflow. Because of toxicity problems, results obtained under described experimental conditions cannot be unambiguously interpreted.

Next, we hypothesized that if the CEM compounds were TTL inhibitors, the cells might not survive long enough due to impaired de-tyrosination/tyrosination cycle. Therefore, it was important to capture the exact time window before major changes in morphology or cell death take place, to determine if the TTL inhibition occurred. To meet the hypothesis, the protocol was changed in such a way that the incubation time of the TTL inhibitor was reduced to 24 hours and the incubation of the Tyr-O-Alk probe was left unchanged – 24 hours. This also allowed us to use extended concentration ranges of the CEM compounds.

With the new protocol in hand, the compounds CEM670 and CEM198 were tested in the concentration range up to 80 μM and 40 μM, accordingly and with an incubation time of 24 hours. The substantial decrease in the fluorescence was already visible at 30 μM concentration for CEM670, and at 20 μM concentration for CEM198 (see Figure 16a and 17a). Indeed,

by reducing the incubation time, it was possible to overcome the toxicity problem to some extent and acquire much more of the cell material compared to the previous 3-day incubation condition. However, the toxic effect on cells was still elevated and observable. For both compounds CEM670 and CEM198, WB analysis with anti- α -tubulin, tyrosinated antibody revealed a slight decrease in signal intensity at higher concentrations which can indirectly support TTL inhibition caused by the treatment with CEM compounds (see Figure 16b and 17b).

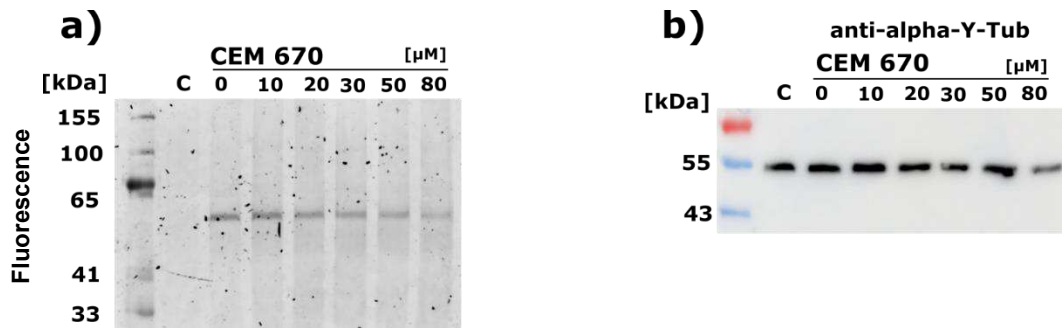


Figure 16. Fluorescent SDS-Gel and WB analysis. (a) CEM 670. 24-hour incubation time, maximum concentration at 80 μ M. (b) WB with anti- α -tubulin, tyrosinated.

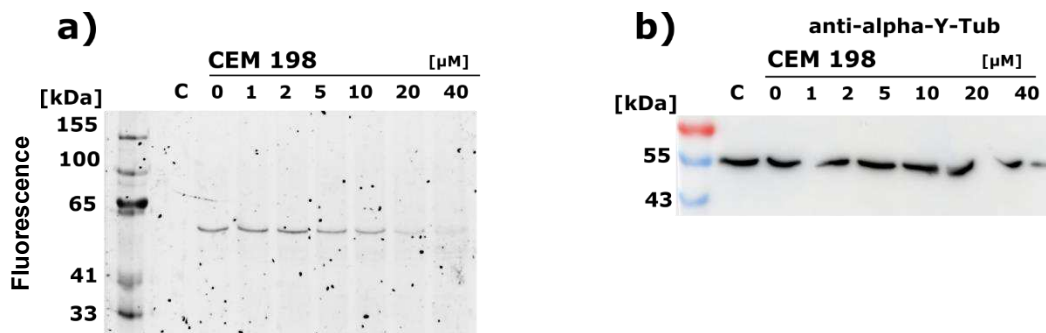


Figure 17. Fluorescent SDS-Gel and WB analysis. (a) CEM 198. 24-hour incubation time, maximum concentration at 80 μ M. (b) WB with anti- α -tubulin, tyrosinated.

Since the shortening of the incubation time for the CEM compounds brought substantial improvement in the quality of data, we decided to reduce the incubation times even further to 18 hours while increasing the concentration range of the CEM compound. The incubation of Tyr-O-Alk remained 24 hours.

To test new conditions, additional experiments were conducted with promising compounds that caused the decrease of the fluorescence signal (CEM198, CEM670), as well as with additional compounds that were obtained as a third batch from the collaborative group (CEM77, CEM373).

Under new conditions of reduced incubation times, it was possible to increase the concentration of the CEM198 compound to 120 μ M. As mentioned before, the treatment with CEM198 provoked a change in cell morphology as well as dose-dependent cell death. As visible from the fluorescent

gel, the tubulin signal was fading away upon increasing the concentration of the compound. Instead of using an anti- α -tyrosinated-tubulin antibody, WB with an anti- α -tubulin, de-tyrosinated, antibody was performed to capture the increased fraction of related protein proteoforms. Signals from the SDS-Page and WB bands were normalized to a signal of GAPDH. A substantial decrease in fluorescence was visible at a concentration of 20 μ M. While the fluorescence signal was diminishing, the de-tyrosinated tubulin fraction reached two times increase compared to the control sample at a concentration of 20 μ M. At higher concentrations, above 40 μ M, the fraction of de-tyrosinated tubulin was decreasing (see **Figure 18**).

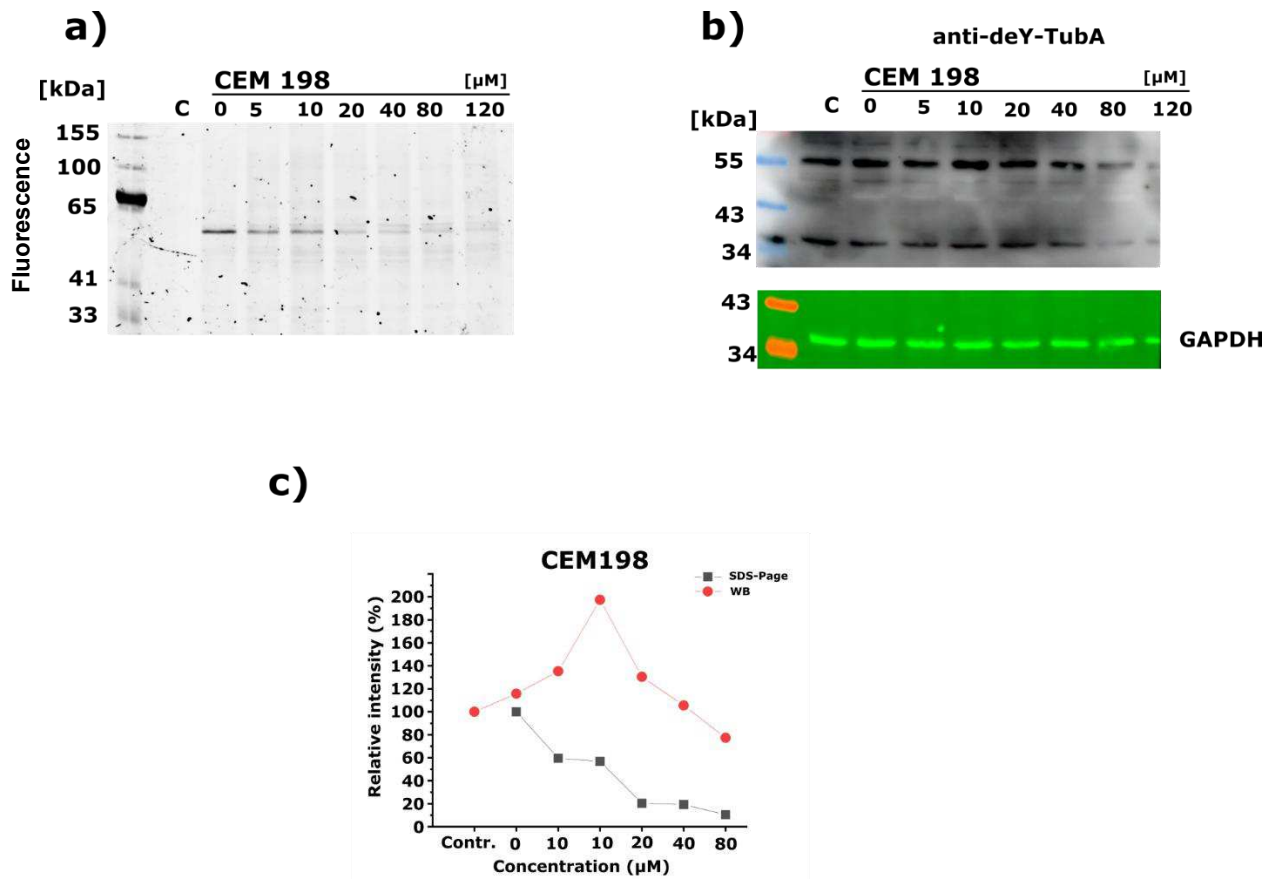


Figure 18. Fluorescent imaging of SDS-Page gel, WB analysis with results normalization. (a) CEM198. 18 hours incubation time. (b) WB with anti- α -tubulin, de-tyrosinated, and GAPDH signal as loading control. (c) Relative intensities of the signals normalized to GAPDH bands

The results for the compound CEM670 were almost the same as for CEM198. The fluorescence had a dose-dependent correlation and was not visible at the highest concentration of 200 μ M. The compound also changed the morphology of the cells and caused cell death in the same manner as CEM198. Staining with anti-tubulin, de-tyrosinated, antibody revealed almost the same amounts of the corresponding tubulin fraction among the samples treated with CEM670 up to a concentration of 40 μ M. At a concentration of 80 μ M, a spike in signal was observable that can

indicate the cumulation of the de-tyrosinated tubulin fraction in cells (see **Figure 19**). Due to artifacts on the membrane, it was not possible to evaluate the signal intensity for 120 μM and 200 μM concentrations.

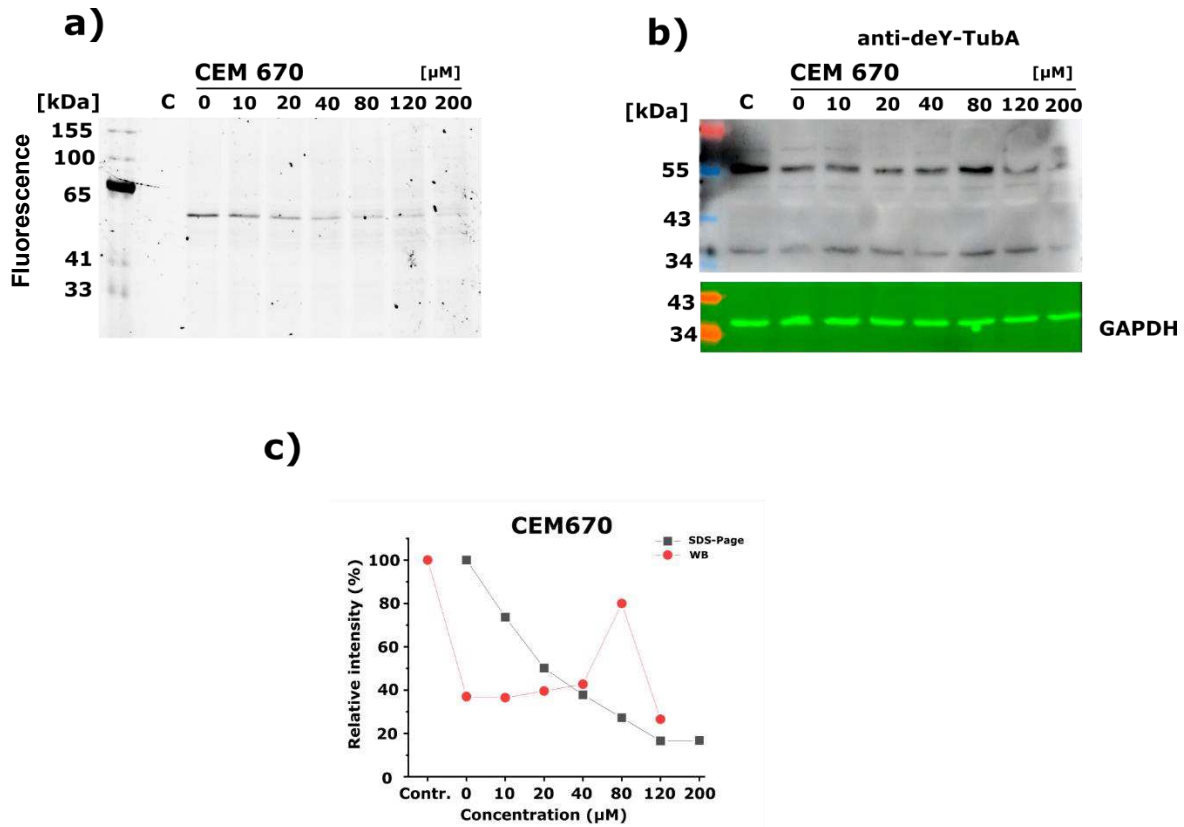


Figure 19. Fluorescent imaging of SDS-Page gel, WB analysis with results normalization. (a) CEM670. 18 hours incubation time. (b) WB with anti- α -tubulin, de-tyrosinated, and GAPDH signal as loading control. (c) Relative intensities of the signals normalized to GAPDH bands

Compounds CEM77 and CEM373 did not induce any change in the fluorescent signal (see **Figure 20**). Therefore, no further WB analysis was conducted.

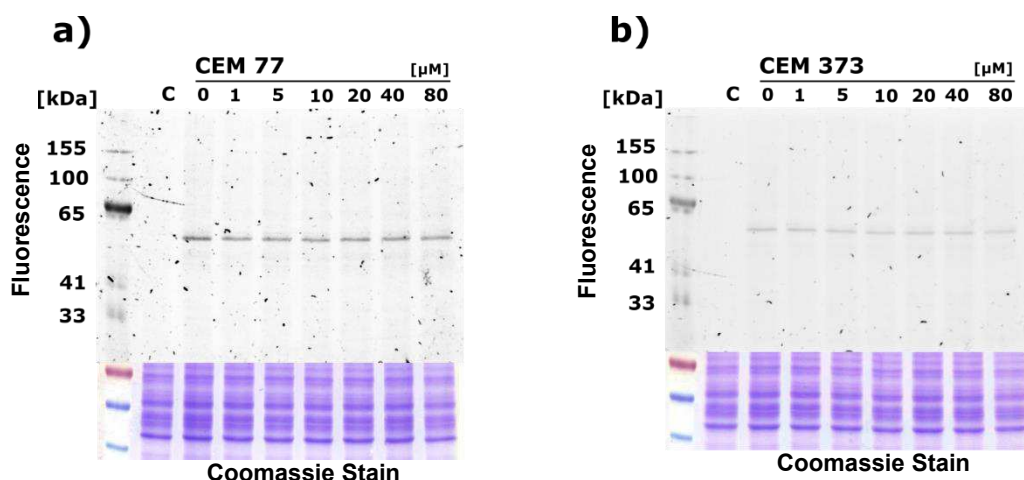


Figure 20. Fluorescent imaging of SDS-Page gel and Coomassie staining as loading control. 18 hours incubation time. (a) CEM77 and (b) CEM373

The initial data indeed showed a decrease in the incorporation rates of the Tyr-O-Alk probe, providing insight into the reactivity of the CEM compounds and raising the question about their potential inhibitory effect on TTL. However, the acquired data must be confirmed by running additional experiments with selected compounds to statistically validate their findings. SDS-Page and WB analysis should be performed in replicates to avoid misinterpretation of the data.

4.3. Synthesis of photo reactive tyrosine probe

Design of photo-reactive tyrosine

The final structure of the photo-reactive probe was chosen based on several considerations. First, the addition of another functional group on tyrosine should not disrupt the TTL-mediated incorporation of the probe into the α -tubulin structure. Despite TTL's broad substrate tolerance, we aimed to maintain a photoreactive group rather small and simple to prevent increasing the complexity of the final probe.⁵¹ Based on the previous publications, at least two positions for the functionalization of tyrosine can be distinguished – para- and ortho. The previous *in vitro* studies demonstrated that the incorporation efficiency of para-functionalized tyrosine into the structure of Tub-tag dropped compared to ortho-substituted derivatives, such as 3-nitrotyrosine, 3-formyltyrosine or 3,4-dihydroxyphenylalanine.³ However, it can be increased by elevating the probe's concentration in the reaction.⁵⁷ Since Tyr-O-Alk was proven as an efficient TTL substrate in our previous *in vivo* studies (see **Chapter 3.2**), a para position has been chosen for further functionalization with a photo-labile group.

Second, the photoreactive group must remain stable under different reaction conditions during the probe synthesis and cause minimal harm to proteins upon UV activation. Among different photoreactive groups such as benzophenone, aryl azide, trifluoromethyl phenyl diazirine, trifluoro

alkyl diazirine, the simplest alkyl diazirine was chosen due to its stability under different reaction conditions, small size, and straightforward synthesis.⁷¹ Photoactivation of alkyl diazirine occurs at 350-365 nm wavelength, causing less harm to proteins compared to aryl azide, which needs shorter wavelengths for its activation (254-400 nm – depending on the substituents).^{69,71,88}

However, we acknowledge the potential success of the ortho-functionalization with other already-mentioned PAL groups. The structures of alternative tyrosine derivatives substituted in ortho-position with different PAL groups are depicted in **Figure 21**.

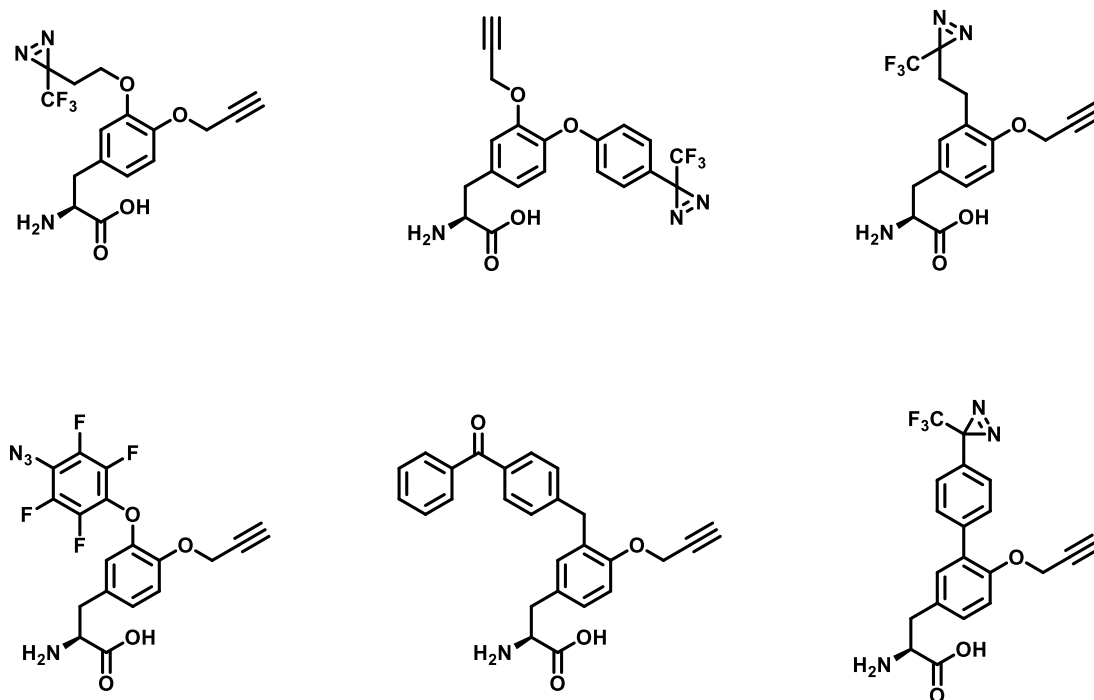


Figure 21. Structures of potential tyrosine cross-linking probes. Tyrosine scaffold with diverse PAL reactive groups attached in ortho-position that can be suitable as alternatives to Tyr-O-Diaz.

Knowing the position of the functionalization on the tyrosine and the photo-reactive group, we suggested the structure of the probe (**Tyr-O-Diaz**) for studying PPIs of α -tubulin (see **Figure 22**). Compared to the Tyr-O-Alk probe, the photo-reactive analog has a prolonged aliphatic linker bearing diazirine functional group and the terminal alkyne.

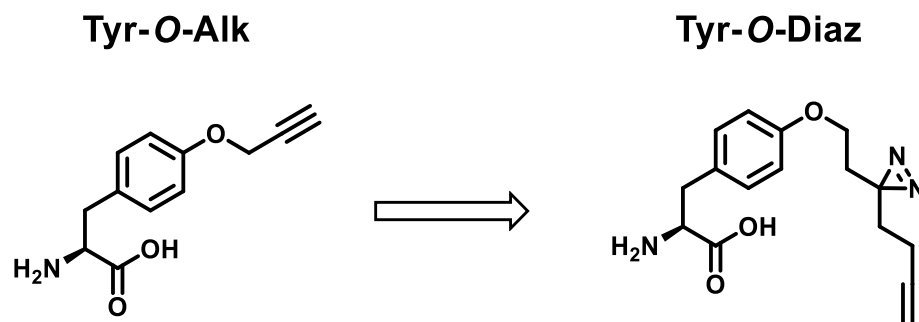


Figure 22. Two labeling probes. The comparison of Tyr-O-Alk probe with the photo-reactive probe bearing diazirine and terminal alkyne – Tyr-O-Diaz.

The so-called minimalist terminal alkyne-containing diazirine photo-crosslinker was chosen as the starting point for synthesizing the probe's structure.⁷⁶ Bearing simultaneously terminal alkyne for CuAAC and diazirine moiety for PAL, this linker could be installed into the para position of tyrosine. For this, it must be functionalized with a good leaving group to undergo nucleophilic substitution with tyrosine.

As a reference to the synthesis of a minimalist diazirine linker, the publication of Li, Z.; Hao et al., 2013 was used (see **Figure 23**).⁷⁶ Although the publication provides the established synthetic protocol, some modifications were implemented during the optimization process.

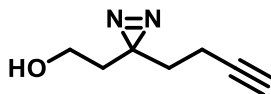


Figure 23. The structure of “minimalist” terminal alkyne-containing cross-linker.

The synthesis of Tyr-O-Diaz was divided into three parts: the synthesis of a diazirine linker bearing terminal alkyne and functionalized with a tosyl group, the synthesis of Boc-protected tyrosine *t*-butyl ester, and a coupling reaction between two fragments, followed by the formation of zwitterion ultimately yielding the desired compound. The retrosynthetic approach is depicted in **Figure 24**.

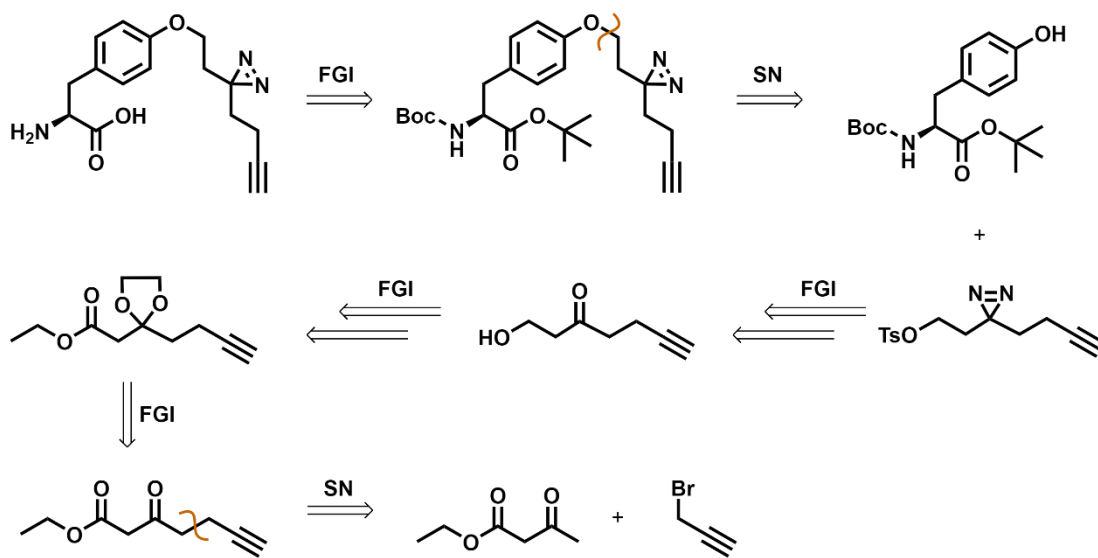
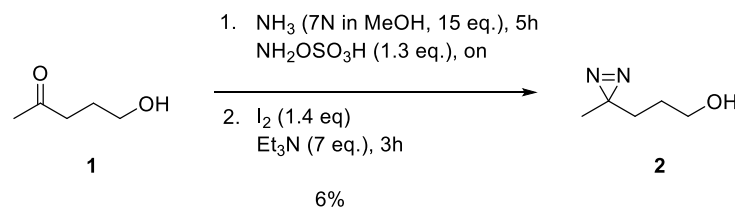


Figure 24. Retrosynthetic scheme. Retrosynthetic analysis of the tyrosine diazirine probe.

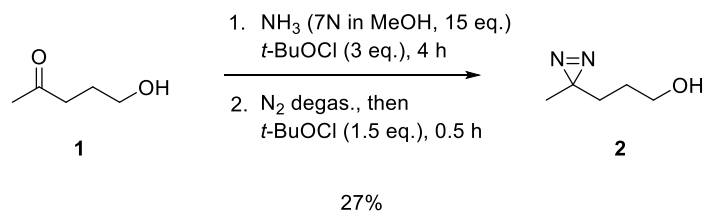
Optimizing conditions for the synthesis of aliphatic diazirines

To avoid using liquid ammonia, a solution of methanolic ammonia (7N NH₃ in MeOH) was used as an alternative reagent to promote the formation of an imine from a ketone.^{89,90} Also, affordable and cheap 5-hydroxypentan-2-one (**1**) was used as a model reagent instead of the valuable intermediate to test the reaction conditions. Unfortunately, low robustness of the protocol and low yields were observed after several attempts. The 3-(3-methyl-3H-diazirin-3-yl)propan-1-ol (**2**) reached a maximum of only 10% yield (see **Scheme 1**).



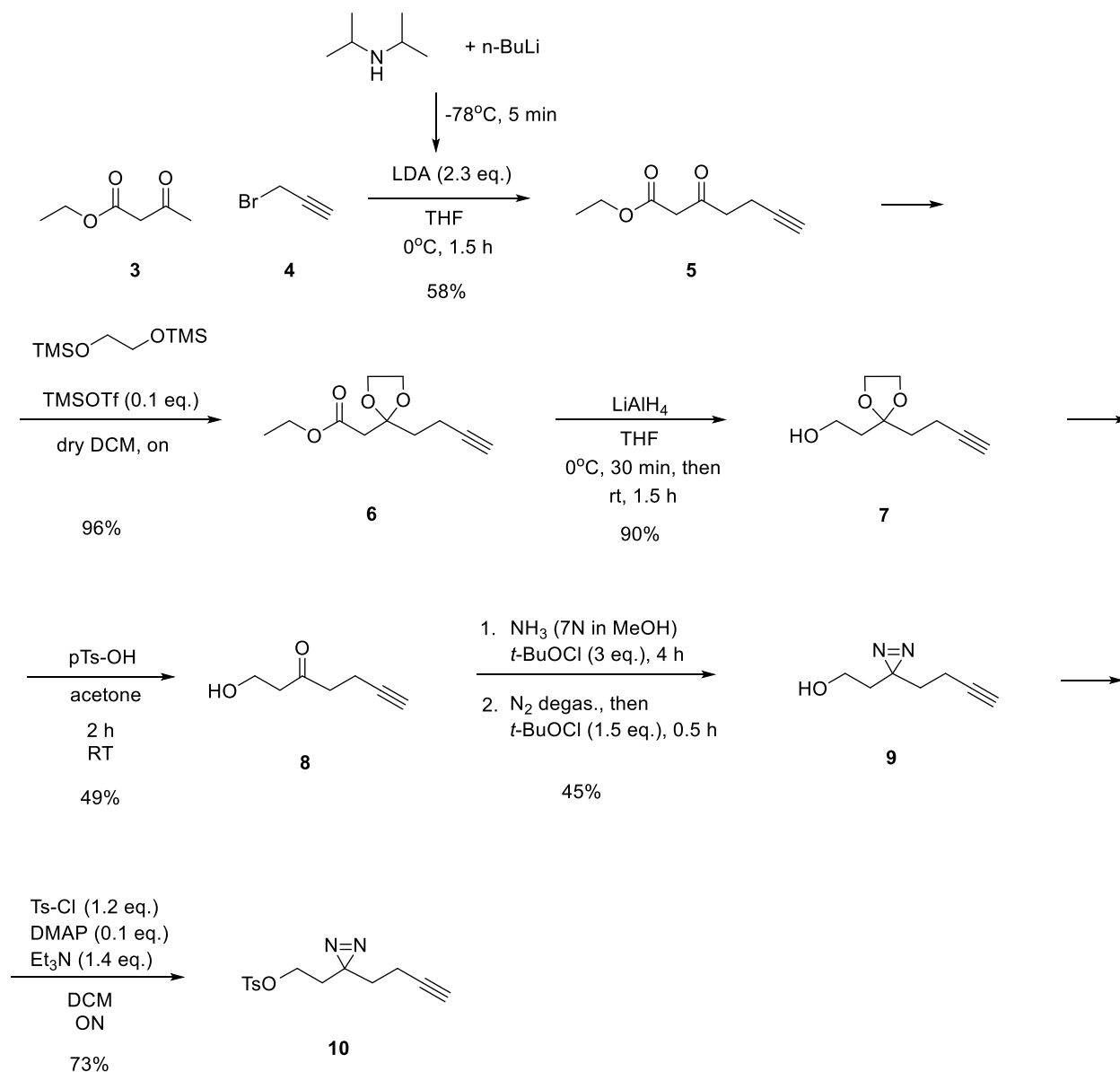
Scheme 1. Reaction scheme. Model diazirine synthesis using a standard two-step approach.

The alternative *t*-BuOCl-based protocol was at first tested on a model ketone **1**. After the first attempt, a 27% yield of model diazirine **2** was obtained. The robustness and feasibility of the protocol have met the expectations, and the protocol was chosen as a lead synthetic route for the synthesis of diazirines (see **Scheme 2**).



Scheme 2. Reaction scheme. Model diazirine synthesis using optimized one-pot two-step reaction conditions with $t\text{-BuOCl}$.

The synthesis of the minimal alkyne diazirine linker



Scheme 3. Reaction scheme. The synthesis of alkyne diazirine linker.

The first reaction was the attachment of the terminal alkyne to the backbone of the future linker. As the starting material, available and cost-effective ethyl acetoacetate (**3**) was used. Treatment with *in situ* generated LDA led to the formation of dianion, subsequently reacting with electrophilic propargyl bromide (**4**) to yield ethyl 3-oxohept-6-ynoate (**5**) in reasonable yield.

The second reaction was performed to form 1,3-dioxolan, serving as a protection group for the ketone group in a subsequent reduction reaction. Instead of the classic approach to ketone protection using ethylene glycol in the presence of mild *p*-toluenesulfonic acid (**Ts-OH**), the optimized Noyori condition was implemented to achieve higher yields and better

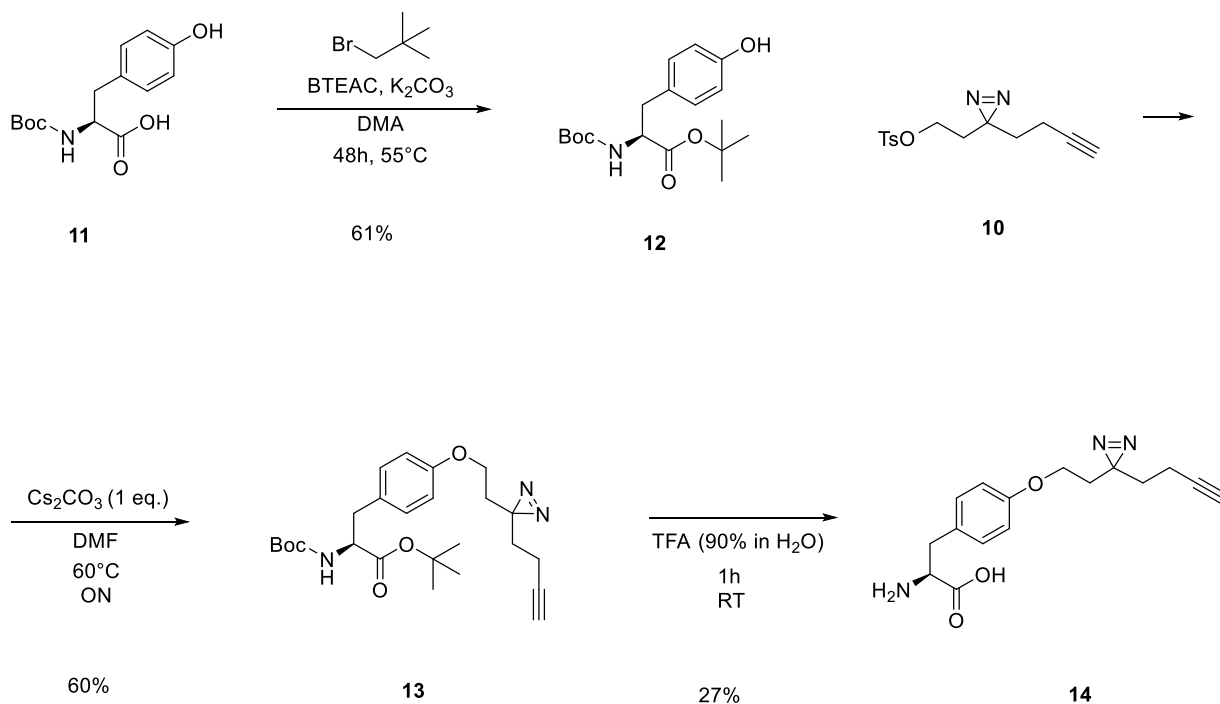
reproducibility.⁹¹ TMS-protected ethylene glycol reacted with keto ester **5** in the presence of a TMS-triflate catalyst in dry DCM, yielding ethyl 2-(2-(but-3-yn-1-yl)-1,3-dioxolan-2-yl)acetate (**6**). The next step in the synthesis was the reduction of ester **6** yielding 2-(2-(but-3-yn-1-yl)-1,3-dioxolan-2-yl)ethan-1-ol (**7**). The reaction yielded ketal **7** with an efficiency close to stoichiometric yield.

Reaction conditions for the deprotection of ketal **7** were optimized to increase the efficiency and yield of the reaction. Catalytic amounts of Ts-OH suggested by protocol did not catalyze the deprotection of ketal **7** even after prolonged times or elevated temperatures.⁷⁶ Moreover, by increasing the amounts of Ts-OH to 0.5-1 eq. of the starting compound, the formation of ether side product was observable. The same by-product was obtained when the reaction was heated to 50°C. Optimal conditions for the deprotection involved 0.25-0.35 eq. of Ts-OH in 10% water in acetone solution under room temperature (RT) for 16-24 hours. The final product 1-hydroxyhept-6-yn-3-one (**8**) was obtained in reasonable yield under optimized conditions. Ketone **8** is a volatile liquid and should not be dried under high vacuum conditions.

Following a one-pot two-reaction protocol, the diazirine formation from the deprotected ketone **8** was robust after several runs. Under inert conditions, propargyl-ketone **8** was dissolved in methanolic ammonia (7N NH₃ in MeOH), followed by the addition of *t*-BuOCl. The reaction proceeded at RT. for 4 hours to form diaziridine as an intermediate, which was not isolated. In the next step, unreacted ammonia should be removed from the reaction mixture by bubbling inert gas for 30 minutes through the solution. The ninhydrin test can help to prove the absence of the amines in the reaction mixture before the addition of the last portion of hypochlorite. The oxidation step was fast and took 30 minutes to complete. The protocol yielded 2-(3-(but-3-yn-1-yl)-3*H*-diazirin-3-yl)ethan-1-ol (**9**) in the range of 35 – 55% after several batches, proving the robustness and effectiveness of the approach.

The functionalization of the hydroxy group of diazirine **9** with tosyl was conducted in DCM with the addition of catalytic amounts of DMAP, tosyl chloride, and Et₃N. After overnight incubation, 2-(3-(but-3-yn-1-yl)-3*H*-diazirin-3-yl)ethyl 4-methylbenzenesulfonate (**10**) obtained in good yield (75%).

The synthesis of the tyrosine photo reactive probe



Scheme 4. Reaction scheme. Attachment of diazirine linker to tyrosine with subsequent simultaneous deprotection.

The reactant (*tert*-butoxycarbonyl)-L-tyrosine (**11**) was prepared using the standard synthetic protocol described in **Chapter 8.2**. Briefly, the reaction was conducted in a dioxane/water mixture with a ratio of 2:1 upon the addition of NaOH as a base while stirring for 3 hours at RT. The Boc-protected tyrosine **11** was obtained in almost stoichiometric yield.

The esterification reaction was done by following the procedure described by Chevallet et. al., 1993.^{92,93} The reaction was held in DMA with the addition of a phase transfer catalyst benzyl tri-ammonium chloride (**BTEAC**), excess of K_2CO_3 and excess *t*-BuBr for 48 hours at 55°C. The reaction yielded *tert*-butyl (*tert*-butoxycarbonyl)-L-tyrosinate (**12**) in good yield (see **Scheme 4**).

Substitution reaction between protected tyrosine **12** and tosylated diazirine **10** was conducted in DMF in the presence of Cs_2CO_3 as a base and DMAP as a catalyst. After stirring the reaction at 50°C for 16 hours, the desired *tert*-butyl (*S*)-3-(4-(2-(3-(but-3-yn-1-yl)-3*H*-diazirin-3-yl))-ethoxy)phenyl)-2-((*tert*-butoxycarbonyl)amino)propanoate (**13**) was obtained in reasonable yield.

The simultaneous cleavage of protection groups in Boc-protected *tert*-butyl tyrosine ester **13** was achieved by treating the starting compound with aq. TFA solution. Using a solution of 90% TFA in water, the formation of the desired product occurred fast. Unfortunately, a hydrolyzed by-product with $m/z = 289.3$ was observed as well. The optimal conditions to prevent the formation of

by-products were experimentally found and required treating of the starting compound with TFA in water solution in a concentration range of 30-50%. The purification of the final compound was carried out through reversed-phase chromatography on a C-18 column, using a gradient of 30-80% ACN/H₂O. The product was then concentrated by lyophilization. Photo-crosslinker (S)-2-amino-3-(4-(2-(3-(but-3-yn-1-yl)-3*H*-diazirin-3-yl)ethoxy)phenyl)propanoic acid (**14**) was obtained in moderate yield.

4.4. Decoding α -tubulin protein-protein interactions using photo-cleavable tyrosine probe

Incorporation efficiency of the probe

With the new photo-crosslinking probe in hand, we started a series of experiments to determine whether the probe was incorporated into the structure of α -tubulin in the same manner as the original Tyr-O-Alk probe. Subsequently to find suitable conditions for the UV irradiation to promote cross-linking in the cells.

The incorporation of the diazirine probe into the structure of α -tubulins was tested in the SH-SY5Y cell line, the same model organism used for studying tyrosination profiling with the Tyr-O-Alk probe. Cells were treated with the probe at a concentration of 0.3mM and incubation time was set to 24 hours. These conditions were utilized for the Tyr-O-Alk probe and proved effective for α -tubulin labeling. Also, they served as a reference point for comparing the two probes. After cell treatment with the Tyr-O-Diaz probe, SDS-Page fluorescence analysis revealed a band of 55 kDa which is characteristic of tubulins (see **Figure 25a**). Next, a direct comparison of the samples treated with two probes revealed bands of the same height on a fluorescence SDS-Page gel (see **Figure 25b**).

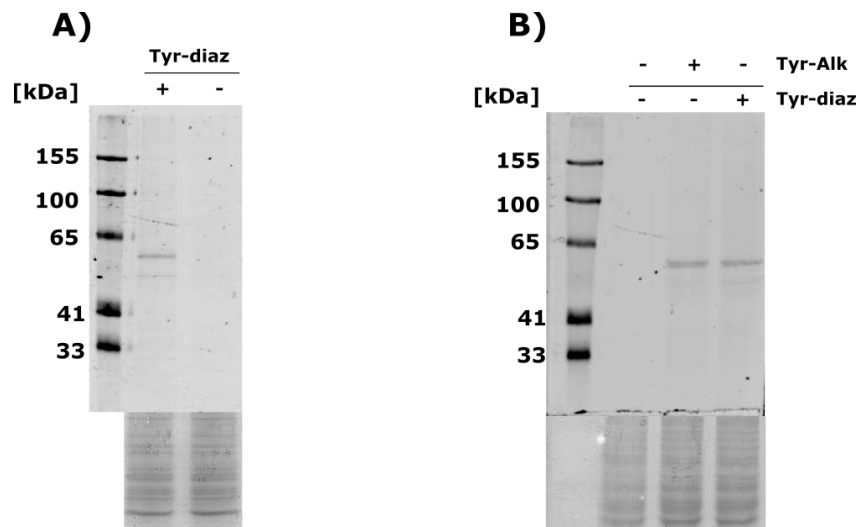


Figure 25. Fluorescent SDS-Page with Coomassie staining. (a) Fluorescent band of around 55 kDa upon treatment with Tyr-O-Diaz probe. (b) Comparison of Tyr-O-Alk and Tyr-diaz. Two bands of the same height represent successive incorporation of the Tyr-O-Diaz probe

Photo-crosslinking efficiency

Next, the cross-linking efficiency of the Tyr-O-Diaz probe was evaluated in SH-SY5Y cells. Cells treated with the probe were irradiated with a 365 nm diode for 5 min before harvesting. A substantial difference in overall fluorescence intensity was observed between UV-irradiated (**UV+**) and non-irradiated cells (**UV-**). Additionally, UV+ samples yielded more fluorescent bands on the gel compared to UV- samples (see **Figure 26**).

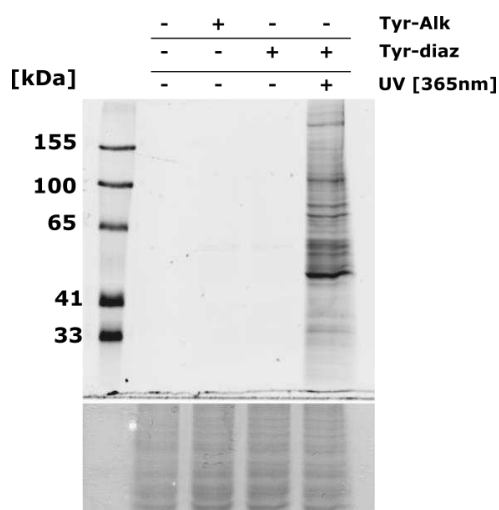


Figure 26. Fluorescent SDS-Page with Coomassie staining. Efficiency of Tyr-O-Diaz cross-linking. Cells were irradiated with 365 nm UV light for 5 min before harvesting.

Such strong labeling can be explained by the presence of the free probe in cells, forming cross-linkages with nearby proteins under diazine activation, and functionalizing them with terminal alkyne. These proteins subsequently react in a click reaction with a fluorophore, resulting in strong background fluorescence.

The obtained data provided strong evidence of the efficiency of the photo cross-linking probe and the efficacy of the irradiation conditions, shedding light on the background reactivity of the free probe. To eliminate or suppress unspecific cross-linkages, several approaches can be considered.

The first possible solution would be to inhibit or block the enzymatic incorporation of the probe. Without the incorporation of the probe into the protein structure, only the free probe undergoes a cross-linking reaction, labeling proteins nearby. Enriched proteins from TTL-depleted cells then serve as a background control set. Inhibition could be achieved by using a TTL inhibitor or using the genetically modified cell line with depleted TTL enzyme. Unfortunately, a lack of a proven TTL inhibitor creates a challenge, as only potential candidates have been published so far.⁹⁴

Second, the free probe could be washed away from the cells before UV irradiation, so only α -tubulin enzymatically labeled with diazirine can be present in the cells. To succeed with this approach, PTM turnover must be slower than the elimination of the probe from the cell compartments. As was shown in our previous experiments with the Tyr-O-Alk probe, the fluorescent band of interest was visible for up to 24 hours after the medium exchange (see **Figure 27**). This fact allowed for implementing the special treatment condition in the next round of experiments to overcome the unspecific cross-linking problem.

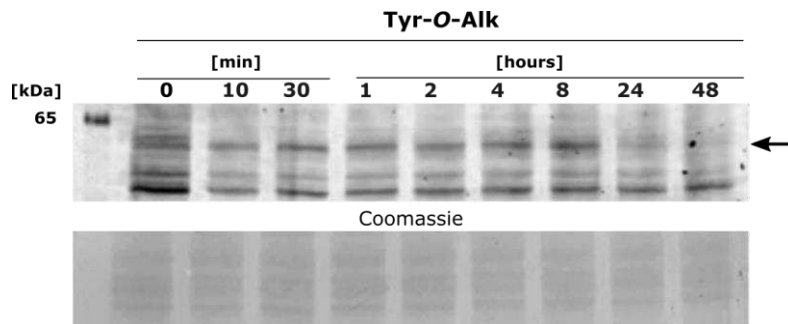


Figure 27. Fluorescent SDS-Page with Coomassie staining. Turnover of Tyr-O-Alk probe in SH-SY5Y cells. After one day of incubation, the medium was exchanged for a new one without the probe. Cells were harvested at different time points after exchange.

Mass spectrometry analysis of photo-crosslinking experiments

To identify proteins interacting with α -tubulin, enrichment using SP2E protocol followed by mass spectrometry analysis was performed. To address the background labeling problem, an additional condition was introduced into the experimental setup (see **Figure 28**). To capture unspecifically labeled proteins, cells were treated with the diazirine probe for 3 hours, allowing the probe to enter the cell without post-translational incorporation into the C-terminal of α -tubulins. On the other hand, the medium in the probe-treated cells was exchanged before the cross-linkage to decrease amounts of the free probe in cell compartments while keeping the modification on the tubulin C-terminal intact. Direct comparison of the enriched proteins between UV-treated probe and background control (**BG**) allows for subtracting unspecific cross-linking coming from BG-control samples.

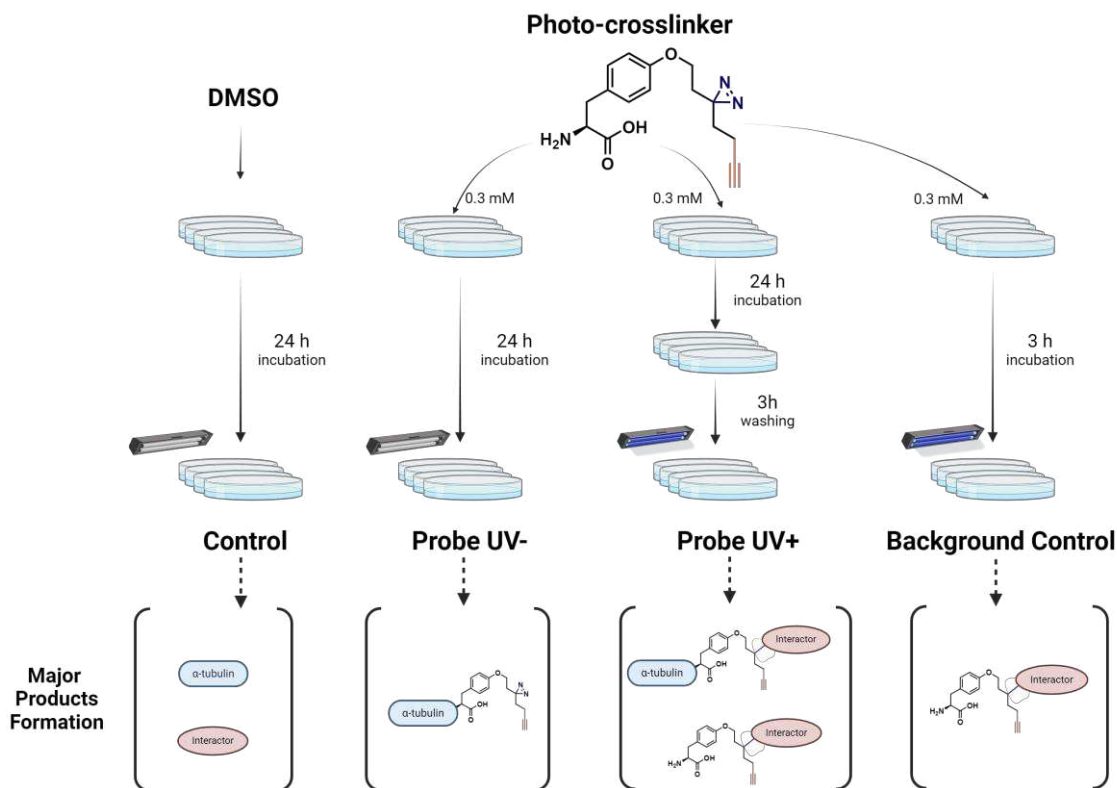


Figure 28. Experimental scheme. A set of control samples treated with the blank solution (negative-control), a set treated with Tyr-diaz probe without UV irradiation (probe UV-), a set treated with Tyr-diaz with UV irradiation (probe UV+), a set treated with Tyr-diaz probe for 3 hours (Background-control). Created with [BioRender.com](https://www.biorender.com/).

To capture the difference between conditions, principal component analysis (**PCA**) was performed on the dataset. The BG-control samples (treated with the probe only for the 3 hours) were clustering together, while samples from other experimental conditions tended to cumulate into one

broader cluster (see **Figure 29**). This suggests higher inconsistency in the data acquired from conditions other than BG-control.

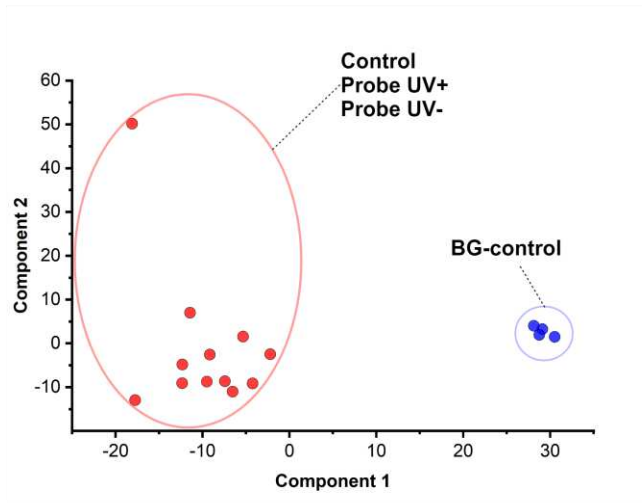


Figure 29. PCA plot. Clustering of the samples represents the differences/similarities between them. BG-control samples are represented in blue.

Enrichment analysis of tubulins without UV treatment

Initially, it was crucial to verify through mass spectrometry that the probe was indeed incorporated into the tubulin structure. To achieve this, we compared the abundance of the proteins between probe-treated samples without UV exposure and controls treated with a blank solution. α -Tubulin isoforms were among the top hits as indicated by the volcano plot (**VP**) (see **Figure 30a**). Although α -tubulins were above the cut-off lines (Fold Change (**FC**)>1, p -value<0.05), the difference between probe-treated and control samples was not substantial yet still statistically reliable. For example, by analyzing a previous experiment where cells were treated with the Tyr-O-Alk probe, the fold change enrichment was two orders higher (see **Figure 30b**). This observation may suggest reduced efficiency of TTL in incorporating tyrosine bearing additional functional group.

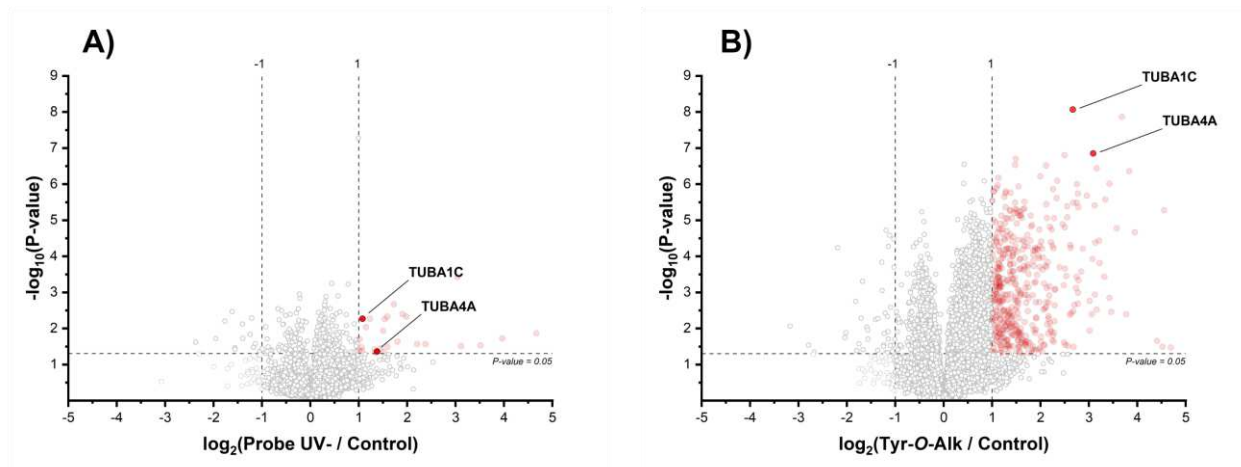


Figure 30. Volcano Plot. Fold enrichment analysis of samples treated with: A) Tyr-O-Diaz probe without UV and controls B) Tyr-O-Alk and controls.

Enrichment analysis of the samples after UV treatment

The protein composition of the samples subjected to UV exposure was the main interest of the project. The primary goal of the Tyr-O-Diaz probe was to reveal tubulin PPIs. To prove its efficiency, it was crucial to find known tubulin interactors, such as microtubule-associated proteins, and potentially to find unknown interactors.

Two sets of conditions were compared. The cells that were treated with Tyr-O-Diaz had no UV light exposure, and cells treated with Tyr-O-Diaz and UV irradiated. Unfortunately, volcano plot analysis was not informative, the distribution of the data points was rather even across the plot with slightly more accumulation on the left side, which could mean a downregulation of many proteins (see **Figure 31**). Tubulin isoforms (TUBA4A, TUBA1C) that usually stay among best hits, were downregulated on VP. Instead, proteins unrelated to tubulins were enriched, suggesting them to be either false positives or cross-linked with the free probe.

To understand if the enriched proteins from VP in **Figure 31** should be considered as nonspecific reactivity products, data from BG-control conditions were analyzed.

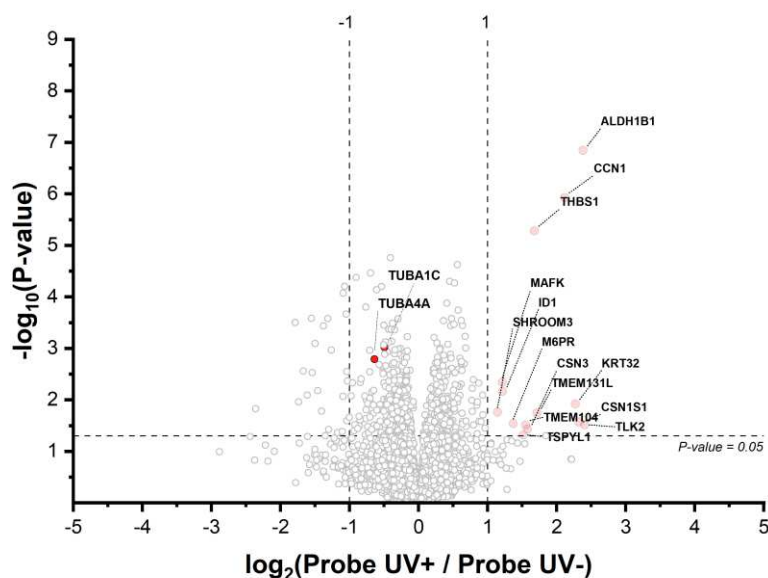


Figure 31. Volcano Plot. Fold enrichment analysis of diazirine-treated samples, where one sample was subjected to UV irradiation (Probe UV+) whilst the second one was not subjected to UV irradiation (Probe UV-). Tubulins were downregulated, in contrast to theory.

The difference in the protein composition between BG-control samples and samples treated with the probe and without UV irradiation (Probe UV-) was revealed by volcano plot analysis (see **Figure 32**). In total, 216 proteins were enriched when standard cut-off conditions were applied (FC>1, p-value<0.05). All these hits can be assumed as potential unspecifically cross-linked proteins since the incubation for the diazirine probe was too short for the incorporation into the tubulin structure. By running gene ontology (**GO**) terms analysis, many proteins were involved in protein folding processes, were a part of endoplasmic reticulum (**ER**) to Golgi vesicles or intermediate compartments, acting in lysosomes and ER (see **Experimental section 8.6, Table 1**). Tubulin isoforms were downregulated in the same manner as in the previous VP which was in line with the theoretical assumption that no incorporation of the probe can occur under shorter incubation time.

Unfortunately, only a set of 216 potential false positives was obtained from the first experiment, and no meaningful result could be acquired from the rest of the data. To confirm the obtained results, the same protocol was repeated.

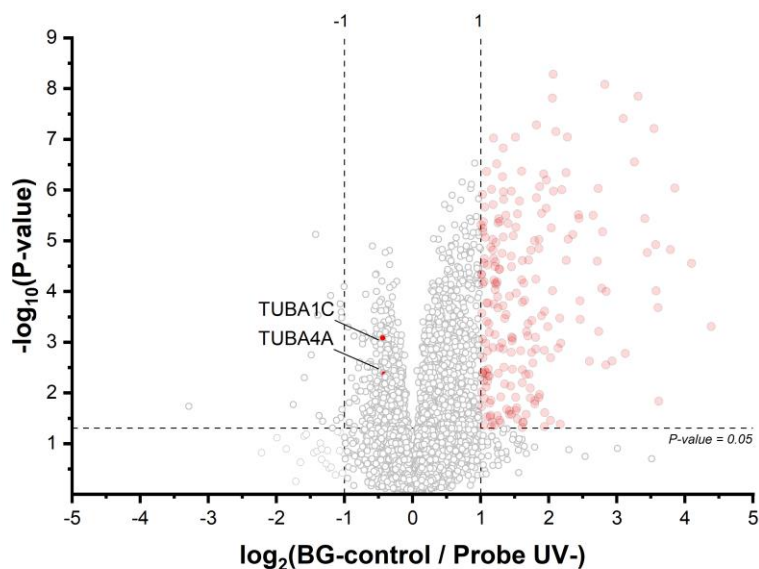


Figure 32. Volcano Plot. Fold enrichment analysis of proteins in BG-control samples compared to Probe UV- samples ($FC > 1$, $p\text{-value} < 0.05$). Enriched proteins (red) represent the background caused by free diazirine probe. Tubulins were downregulated, in contrast to theory.

Repetition of the protocol

As the first step, the quality and consistency of the data acquired from the second experiment were analyzed. From the clustering of the samples on the PCA plot, we can conclude the clear difference between sets of experimental conditions (see **Figure 33**). Three groups of clusters can be identified: the cluster of BG-controls (blue), Probe UV+ (green), and control with Probe UV- (red).

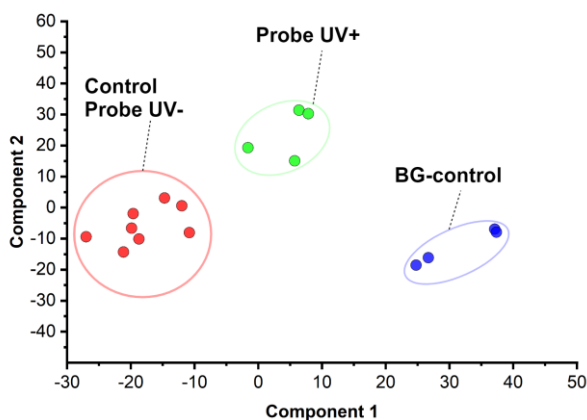


Figure 33. PCA plot. Clustering of the samples represents the difference/similarity between 16 samples acquired from the second experiment. Blue cluster represent the BG-control samples, green cluster represents UV irradiated, probe-treated samples, red cluster contains samples that were not UV irradiated, serving as controls.

The fold change analysis between probe-treated cells (Probe UV-) and control samples was made to prove the probe incorporation by showing the enrichment of tubulin family proteins. This time, TUBA1C and TUBA4A lie under cut-off lines, having an FC value of less than 1. Although the values were lower than expected ($FC[TUBA4A] = 0.30$, $FC[TUBA1C] = 0.47$), the t-test showed high confidence in the difference between the two sets of samples, confirming a slightly higher accumulation of α -tubulin fraction in probe-treated cells (Probe UV-) (see **Figure 34**).

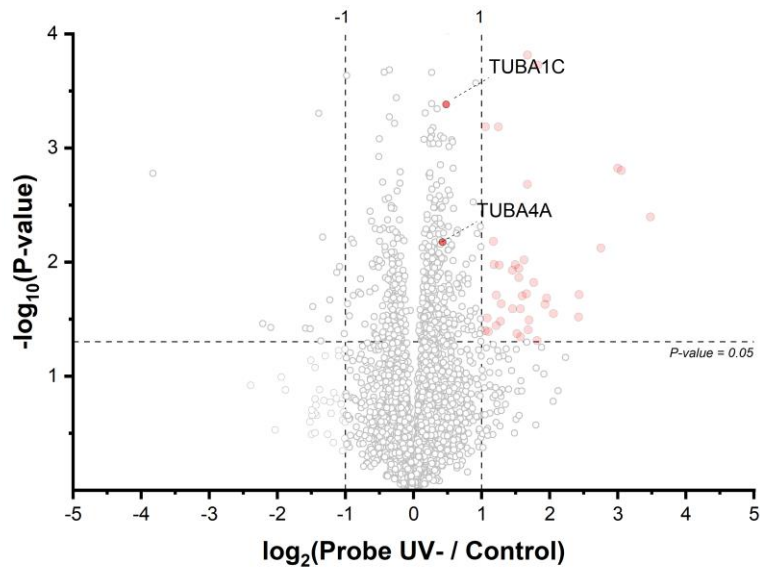


Figure 34. Volcano Plot. Fold enrichment analysis of probe-treated (Probe UV-) and control samples without UV irradiation. TUBA4A and TUBA1C fall under cut-off lines.

Next, BG-control samples were analyzed to reveal a set of unspecifically cross-linked proteins. For this, VP analysis was performed between BG-control samples and probe-treated (Probe UV-) samples. A set of 335 proteins were identified as enriched in BG-control (see **Figure 35**).

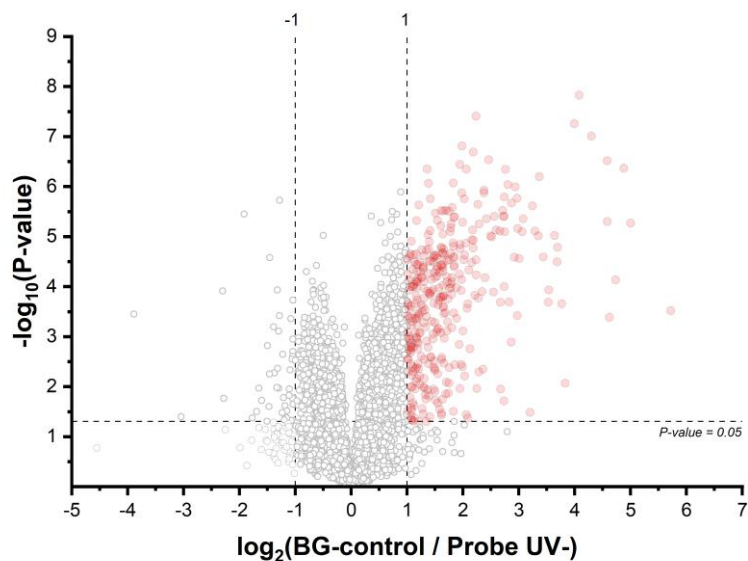


Figure 35. Volcano Plot. Fold enrichment analysis of BG-control and probe-treated (Probe UV-) samples. 335 potential background binder were identified (red).

By overlaying 335 potential false positive hits with the enriched proteins from the previous experiment (216 potential false positive proteins were found), 111 (24%) proteins were found to be common for two sets (see **Figure 36**). A high number of overlapping proteins increases the confidence of revealing actual false positives.

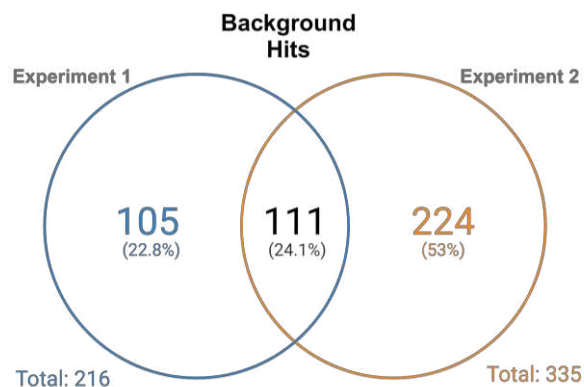


Figure 36. Venn diagram. Overlay representation between two experiments to identify background proteins. 111 common background proteins were identified after two experiments. Created with BioRender.com.

The VP analysis of UV-treated, probe-supplemented (Probe UV+) samples and samples without UV irradiation (Probe UV-) was aimed to identify the set of actual tubulin interactors together with false positives coming from unspecific cross-linking of proteins with the free probe. The standard cut-off lines (FC>1, p-value<0.05) were applied to determine the up-, and down-regulated proteins. Only 26 proteins (depicted in red) were enriched in the UV-irradiated samples (see **Figure 37**).

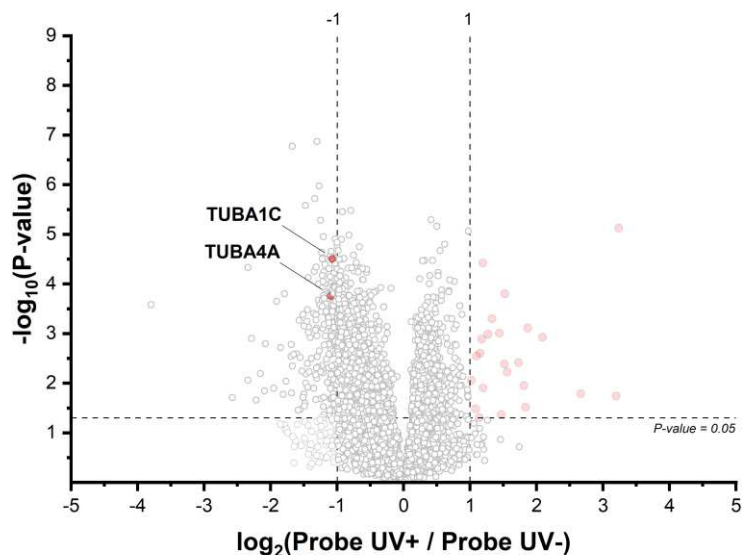


Figure 37. Volcano Plot. Fold enrichment analysis of UV-treated (Probe UV+) samples and samples without UV irradiation (Probe UV-). 26 proteins – upregulated, 204 proteins – downregulated. TUBA1C and TUBA1C are downregulated in contrast to theory.

A set of proteins enriched in UV-treated (Probe UV+) samples (26 enriched) was compared with a combined set of false positives (BG-control) from two experiments (see **Figure 38**). In total, 24 out of 26 proteins from the UV-treated (Probe UV+) samples were also found in the BG-control set of proteins. A substantial overlap between hits from both experiments indicates that these overlapping proteins are likely to be actual false positives.

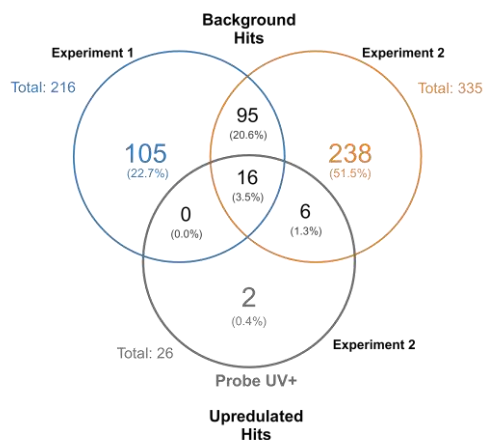


Figure 38. Venn diagram. Overlapping of background proteins from two experiments. Diagram represents the overlap of proteins from BG-control sets and upregulated proteins from UV-irradiated (Probe UV+) samples. Created with BioRender.com.

Surprisingly, α -tubulins were downregulated in the samples treated with UV light (Probe UV+), in contrast to our expectations (see **Figure 37**). The general shape of the volcano plot was skewed to the left side of the plot, suggesting a lot of the proteins were downregulated compared to the control conditions (Probe UV-). Thus, downregulated proteins were also carefully analyzed to find any correlation with microtubules and microtubule-associated proteins. 204 proteins were downregulated when strict conditions were applied ($FC < -1$, $p\text{-value} < 0.05$). Among downregulated proteins, proteins associated with microtubules, actin filaments, microtubule-associated proteins, cytoskeleton and mitotic spindle were found (see **Experimental section 8.6, Table 2**).

However, while applying strict cut-off lines to volcano plot, a bunch of potential hits are eliminated from the scope of enriched proteins, not capable of capturing subtle yet biologically meaningful changes. To address this problem, an approach described by Tusher et al. 2001, named significance analysis of microarrays (**SAM**) was implemented.⁹⁵ This approach provides a more comprehensive assessment of differential protein abundance by accounting for variations within and between experimental groups, ensuring that all meaningful changes are captured while maintaining precise statistical control. New cut-off lines representing FDR values were placed on VP instead of constant values (see **Figure 39**).

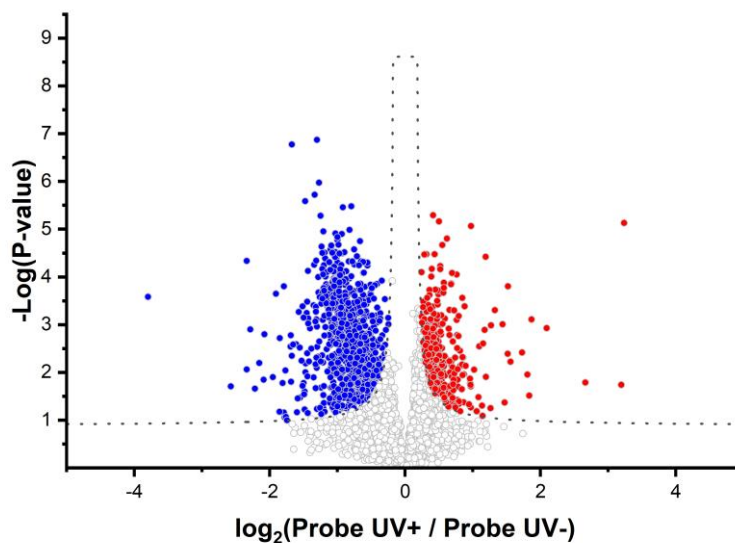


Figure 39. Volcano Plot. Fold enrichment analysis of UV-treated samples (Probe UV+). New cut-off lines that represent the adjusted FDR values ($FDR < 0.05$, $S_o = 0.1$) were applied.

With the SAM approach, 844 hits were identified as statistically significant downregulated proteins (depicted in blue in **Figure 39**). By analyzing these proteins, 47 proteins can be identified with microtubules GO term, 111 with microtubule cytoskeleton GO term, and 16 as microtubule-

24 previously annotated hits, 132 of which overlapped with the hits from background samples from the same experiment. Moreover, a significant overlap between background hits from the previous experiment was obtained – 58 hits, suggesting the partial success and robustness of the protocol in terms of identifying proteins cross-linked with the free diazirine probe (see **Figure 42**).

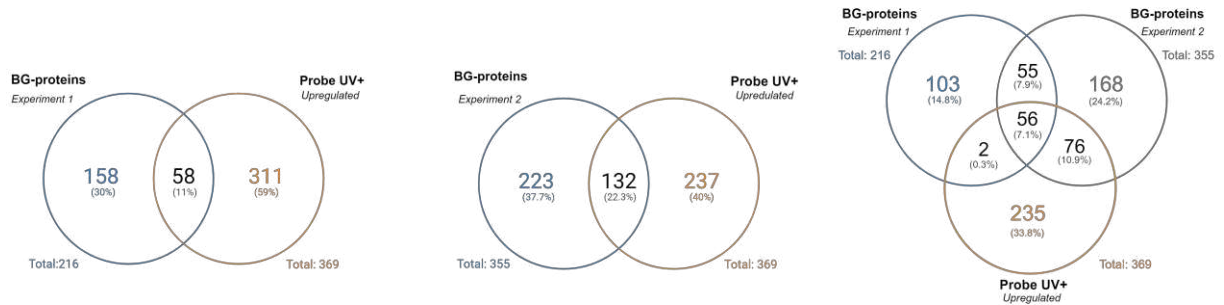


Figure 42. Venn Diagram. Venn diagram with overlapping proteins upregulated in UV-treated samples (Probe UV+) and background proteins (BG-proteins) while applying SEM approach cut-off lines. Created with BioRender.com.

By subtracting the set of potential background hits cumulated from both experiments, only 235 hits were left for the re-analysis. GO term analysis revealed that most hits were related to mitochondrial, ER, nucleus, Golgi, or membrane-associated proteins (see **Experimental section 8.6, Table 3**). Proteins associated with microtubules or cytoskeleton were not found.

The obtained results suggest that upon UV treatment and subsequent magnetic bead enrichment of the samples treated with the diazirine probe, only proteins marked as potential backgrounds were upregulated. On the other hand, microtubule-associated proteins that should be cross-coupled with functionalized α -tubulin were not found. Instead, a downregulation of the mentioned proteins took place. α -tubulin, β -tubulin as well as different MAPs and cytoskeleton-associated proteins were downregulated. A possible reason for such an issue may be the insufficient length of the diazirine probe's linker, causing the terminal alkyne to be blocked for the click reaction. It might cause the tubulin-interacting protein complex to be washed away during the magnetic bead enrichment.

5. Bibliography

- (1) Sanyal, C.; Pietsch, N.; Ramirez Rios, S.; Peris, L.; Carrier, L.; Moutin, M.-J. The Detyrosination/Re-Tyrosination Cycle of Tubulin and Its Role and Dysfunction in Neurons and Cardiomyocytes. *Semin. Cell Dev. Biol.* **2023**, *137*, 46–62. <https://doi.org/10.1016/j.semdb.2021.12.006>.
- (2) Becker, T.; Wiest, A.; Telek, A.; Bejko, D.; Hoffmann-Röder, A.; Kielkowski, P. Transforming Chemical Proteomics Enrichment into a High-Throughput Method Using an SP2E Workflow. *JACS Au* **2022**, *2* (7), 1712–1723. <https://doi.org/10.1021/jacsau.2c00284>.
- (3) Schumacher, D.; Lemke, O.; Helma, J.; Gerszonowicz, L.; Waller, V.; Stoschek, T.; Durkin, P. M.; Budisa, N.; Leonhardt, H.; Keller, B. G.; Hackenberger, C. P. R. Broad Substrate Tolerance of Tubulin Tyrosine Ligase Enables One-Step Site-Specific Enzymatic Protein Labeling. *Chem. Sci.* **2017**, *8* (5), 3471–3478. <https://doi.org/10.1039/C7SC00574A>.
- (4) Busskamp, V.; Lewis, N. E.; Guye, P.; Ng, A. H.; Shipman, S. L.; Byrne, S. M.; Sanjana, N. E.; Murn, J.; Li, Y.; Li, S.; Stadler, M.; Weiss, R.; Church, G. M. Rapid Neurogenesis through Transcriptional Activation in Human Stem Cells. *Mol. Syst. Biol.* **2014**, *10* (11), 760. <https://doi.org/10.15252/msb.20145508>.
- (5) Aebersold, R.; Agar, J. N.; Amster, I. J.; Baker, M. S.; Bertozzi, C. R.; Boja, E. S.; Costello, C. E.; Cravatt, B. F.; Fenselau, C.; Garcia, B. A.; Ge, Y.; Gunawardena, J.; Hendrickson, R. C.; Hergenrother, P. J.; Huber, C. G.; Ivanov, A. R.; Jensen, O. N.; Jewett, M. C.; Kelleher, N. L.; Kiessling, L. L.; Krogan, N. J.; Larsen, M. R.; Loo, J. A.; Ogorzalek Loo, R. R.; Lundberg, E.; MacCoss, M. J.; Mallick, P.; Mootha, V. K.; Mrksich, M.; Muir, T. W.; Patrie, S. M.; Pesavento, J. J.; Pitteri, S. J.; Rodriguez, H.; Saghatelian, A.; Sandoval, W.; Schlüter, H.; Sechi, S.; Slavoff, S. A.; Smith, L. M.; Snyder, M. P.; Thomas, P. M.; Uhlén, M.; Van Eyk, J. E.; Vidal, M.; Walt, D. R.; White, F. M.; Williams, E. R.; Wohlschläger, T.; Wysocki, V. H.; Yates, N. A.; Young, N. L.; Zhang, B. How Many Human Proteoforms Are There? *Nat. Chem. Biol.* **2018**, *14* (3), 206–214. <https://doi.org/10.1038/nchembio.2576>.
- (6) Khan, M. R.; Wellinger, R. J.; Laurent, B. Exploring the Alternative Splicing of Long Noncoding RNAs. *Trends Genet.* **2021**, *37* (8), 695–698. <https://doi.org/10.1016/j.tig.2021.03.010>.
- (7) Winter, D. L.; Iranmanesh, H.; Clark, D. S.; Glover, D. J. Design of Tunable Protein Interfaces Controlled by Post-Translational Modifications. *ACS Synth. Biol.* **2020**, *9* (8), 2132–2143. <https://doi.org/10.1021/acssynbio.0c00208>.
- (8) Kubatzky, K. F.; Gao, Y.; Yu, D. Post-Translational Modulation of Cell Signalling through Protein Succinylation. *Explor. Target. Anti-Tumor Ther.* **2023**, *4* (6), 1260–1285. <https://doi.org/10.37349/etat.2023.00196>.
- (9) Locascio, L. E.; Donoghue, D. J. KIDs Rule: Regulatory Phosphorylation of RTKs. *Trends Biochem. Sci.* **2013**, *38* (2), 75–84. <https://doi.org/10.1016/j.tibs.2012.12.001>.
- (10) Fuhrmann, J.; Clancy, K. W.; Thompson, P. R. Chemical Biology of Protein Arginine Modifications in Epigenetic Regulation. *Chem. Rev.* **2015**, *115* (11), 5413–5461. <https://doi.org/10.1021/acs.chemrev.5b00003>.
- (11) Anderson, K. A.; Hirschey, M. D. Mitochondrial Protein Acetylation Regulates Metabolism. *Essays Biochem.* **2012**, *52*, 23–35. <https://doi.org/10.1042/bse0520023>.
- (12) Chen, J.; Kholina, E.; Szyk, A.; Fedorov, V. A.; Kovalenko, I.; Gudimchuk, N.; Roll-Mecak, A. α -Tubulin Tail Modifications Regulate Microtubule Stability through Selective Effector Recruitment, Not Changes in Intrinsic Polymer Dynamics. *Dev. Cell* **2021**, *56* (14), 2016–2028.e4. <https://doi.org/10.1016/j.devcel.2021.05.005>.
- (13) Moellering, R. E.; Cravatt, B. F. Functional Lysine Modification by an Intrinsically Reactive Primary Glycolytic Metabolite. *Science* **2013**, *341* (6145), 549–553. <https://doi.org/10.1126/science.1238327>.
- (14) Raynaud-Messina, B.; Merdes, A. γ -Tubulin Complexes and Microtubule Organization. *Curr. Opin. Cell Biol.* **2007**, *19* (1), 24–30. <https://doi.org/10.1016/j.ceb.2006.12.008>.

- (15) Chang, P.; Stearns, T. δ -Tubulin and ϵ -Tubulin: Two New Human Centrosomal Tubulins Reveal New Aspects of Centrosome Structure and Function. *Nat. Cell Biol.* **2000**, *2* (1), 30–35. <https://doi.org/10.1038/71350>.
- (16) Gudimchuk, N. B.; McIntosh, J. R. Regulation of Microtubule Dynamics, Mechanics and Function through the Growing Tip. *Nat. Rev. Mol. Cell Biol.* **2021**, *22* (12), 777–795. <https://doi.org/10.1038/s41580-021-00399-x>.
- (17) Garnham, C. P.; Roll-Mecak, A. The Chemical Complexity of Cellular Microtubules: Tubulin Post-translational Modification Enzymes and Their Roles in Tuning Microtubule Functions. *Cytoskeleton* **2012**, *69* (7), 442–463. <https://doi.org/10.1002/cm.21027>.
- (18) Löwe, J.; Li, H.; Downing, K. H.; Nogales, E. Refined Structure of A β -Tubulin at 3.5 Å Resolution. *J. Mol. Biol.* **2001**, *313* (5), 1045–1057. <https://doi.org/10.1006/jmbi.2001.5077>.
- (19) Peng, N.; Nakamura, F. Microtubule-associated Proteins and Enzymes Modifying Tubulin. *Cytoskeleton* **2023**, *80* (3–4), 60–76. <https://doi.org/10.1002/cm.21748>.
- (20) Roll-Mecak, A. Intrinsically Disordered Tubulin Tails: Complex Tuners of Microtubule Functions? *Semin. Cell Dev. Biol.* **2015**, *37*, 11–19. <https://doi.org/10.1016/j.semcdb.2014.09.026>.
- (21) Janke, C.; Magiera, M. M. The Tubulin Code and Its Role in Controlling Microtubule Properties and Functions. *Nat. Rev. Mol. Cell Biol.* **2020**, *21* (6), 307–326. <https://doi.org/10.1038/s41580-020-0214-3>.
- (22) Vemu, A.; Atherton, J.; Spector, J. O.; Moores, C. A.; Roll-Mecak, A. Tubulin Isoform Composition Tunes Microtubule Dynamics. *Mol. Biol. Cell* **2017**, *28* (25), 3564–3572. <https://doi.org/10.1091/mbc.e17-02-0124>.
- (23) McKenney, R. J.; Huynh, W.; Vale, R. D.; Sirajuddin, M. Tyrosination of A-tubulin Controls the Initiation of Processive Dynein–Dynactin Motility. *EMBO J.* **2016**, *35* (11), 1175–1185. <https://doi.org/10.15252/embj.201593071>.
- (24) Sirajuddin, M.; Rice, L. M.; Vale, R. D. Regulation of Microtubule Motors by Tubulin Isoforms and Post-Translational Modifications. *Nat. Cell Biol.* **2014**, *16* (4), 335–344. <https://doi.org/10.1038/ncb2920>.
- (25) Lopes, D.; Maiato, H. The Tubulin Code in Mitosis and Cancer. *Cells* **2020**, *9* (11), 2356. <https://doi.org/10.3390/cells9112356>.
- (26) Ebberink, E.; Fernandes, S.; Hatzopoulos, G.; Agashe, N.; Chang, P.-H.; Guidotti, N.; Reichart, T. M.; Reymond, L.; Velluz, M.-C.; Schneider, F.; Pourroy, C.; Janke, C.; Gönczy, P.; Fierz, B.; Aumeier, C. Tubulin Engineering by Semi-Synthesis Reveals That Polyglutamylation Directs Detyrosination. *Nat. Chem.* **2023**, *15* (8), 1179–1187. <https://doi.org/10.1038/s41557-023-01228-8>.
- (27) Barra, H. S.; Arce, C. A.; Rodríguez, J. A.; Caputto, R. Some Common Properties of the Protein That Incorporates Tyrosine as a Single Unit and the Microtubule Proteins. *Biochem. Biophys. Res. Commun.* **1974**, *60* (4), 1384–1390. [https://doi.org/10.1016/0006-291X\(74\)90351-9](https://doi.org/10.1016/0006-291X(74)90351-9).
- (28) Aillaud, C.; Bosc, C.; Peris, L.; Bosson, A.; Heemeryck, P.; Van Dijk, J.; Le Fric, J.; Boulan, B.; Vossier, F.; Sanman, L. E.; Syed, S.; Amara, N.; Couté, Y.; Lafanechère, L.; Denarier, E.; Delphin, C.; Pelletier, L.; Humbert, S.; Bogoyo, M.; Andrieux, A.; Rogowski, K.; Moutin, M.-J. Vasohibins/SVBP Are Tubulin Carboxypeptidases (TCPs) That Regulate Neuron Differentiation. *Science* **2017**, *358* (6369), 1448–1453. <https://doi.org/10.1126/science.aao4165>.
- (29) Nieuwenhuis, J.; Adamopoulos, A.; Bleijerveld, O. B.; Mazouzi, A.; Stickel, E.; Celie, P.; Altelaar, M.; Knipscheer, P.; Perrakis, A.; Blomen, V. A.; Brummelkamp, T. R. Vasohibins Encode Tubulin Detyrosinating Activity. *Science* **2017**, *358* (6369), 1453–1456. <https://doi.org/10.1126/science.aao5676>.
- (30) Landskron, L.; Bak, J.; Adamopoulos, A.; Kaplani, K.; Moraiti, M.; Van Den Hengel, L. G.; Song, J.-Y.; Bleijerveld, O. B.; Nieuwenhuis, J.; Heidebrecht, T.; Henneman, L.; Moutin, M.-J.;

- Barisic, M.; Taraviras, S.; Perrakis, A.; Brummelkamp, T. R. Posttranslational Modification of Microtubules by the MATCAP Detyrosinase. *Science* **2022**, *376* (6595), eabn6020. <https://doi.org/10.1126/science.abn6020>.
- (31) Raybin, D.; Flavin, M. Enzyme Which Specifically Adds Tyrosine to the α Chain of Tubulin. *Biochemistry* **1977**, *16* (10), 2189–2194. <https://doi.org/10.1021/bi00629a023>.
- (32) Van Dijk, J.; Rogowski, K.; Miro, J.; Lacroix, B.; Eddé, B.; Janke, C. A Targeted Multienzyme Mechanism for Selective Microtubule Polyglutamylation. *Mol. Cell* **2007**, *26* (3), 437–448. <https://doi.org/10.1016/j.molcel.2007.04.012>.
- (33) Prassanawar, S. S.; Panda, D. Tubulin Heterogeneity Regulates Functions and Dynamics of Microtubules and Plays a Role in the Development of Drug Resistance in Cancer. *Biochem. J.* **2019**, *476* (9), 1359–1376. <https://doi.org/10.1042/BCJ20190123>.
- (34) Kreitzer, G.; Liao, G.; Gundersen, G. G. Detyrosination of Tubulin Regulates the Interaction of Intermediate Filaments with Microtubules In Vivo via a Kinesin-Dependent Mechanism. *Mol. Biol. Cell* **1999**, *10* (4), 1105–1118. <https://doi.org/10.1091/mbc.10.4.1105>.
- (35) Verhey, K. J.; Gaertig, J. The Tubulin Code. *Cell Cycle* **2007**, *6* (17), 2152–2160. <https://doi.org/10.4161/cc.6.17.4633>.
- (36) Rogowski, K.; Van Dijk, J.; Magiera, M. M.; Bosc, C.; Deloulme, J.-C.; Bosson, A.; Peris, L.; Gold, N. D.; Lacroix, B.; Grau, M. B.; Bec, N.; Larroque, C.; Desagher, S.; Holzer, M.; Andrieux, A.; Moutin, M.-J.; Janke, C. A Family of Protein-Deglutamylating Enzymes Associated with Neurodegeneration. *Cell* **2010**, *143* (4), 564–578. <https://doi.org/10.1016/j.cell.2010.10.014>.
- (37) Magiera, M. M.; Singh, P.; Gadadhar, S.; Janke, C. Tubulin Posttranslational Modifications and Emerging Links to Human Disease. *Cell* **2018**, *173* (6), 1323–1327. <https://doi.org/10.1016/j.cell.2018.05.018>.
- (38) Van Der Laan, S.; Lévêque, M. F.; Marcellin, G.; Vezenkov, L.; Lannay, Y.; Dubra, G.; Bompard, G.; Ovejero, S.; Urbach, S.; Burgess, A.; Amblard, M.; Sterkers, Y.; Bastien, P.; Rogowski, K. Evolutionary Divergence of Enzymatic Mechanisms for Tubulin Detyrosination. *Cell Rep.* **2019**, *29* (12), 4159–4171.e6. <https://doi.org/10.1016/j.celrep.2019.11.074>.
- (39) Janke, C.; Chloë Bulinski, J. Post-Translational Regulation of the Microtubule Cytoskeleton: Mechanisms and Functions. *Nat. Rev. Mol. Cell Biol.* **2011**, *12* (12), 773–786. <https://doi.org/10.1038/nrm3227>.
- (40) Peris, L.; Wagenbach, M.; Lafanechère, L.; Brocard, J.; Moore, A. T.; Kozielski, F.; Job, D.; Wordeman, L.; Andrieux, A. Motor-Dependent Microtubule Disassembly Driven by Tubulin Tyrosination. *J. Cell Biol.* **2009**, *185* (7), 1159–1166. <https://doi.org/10.1083/jcb.200902142>.
- (41) Zocchi, R.; Compagnucci, C.; Bertini, E.; Sferra, A. Deciphering the Tubulin Language: Molecular Determinants and Readout Mechanisms of the Tubulin Code in Neurons. *Int. J. Mol. Sci.* **2023**, *24* (3), 2781. <https://doi.org/10.3390/ijms24032781>.
- (42) Park, J. H.; Roll-Mecak, A. The Tubulin Code in Neuronal Polarity. *Curr. Opin. Neurobiol.* **2018**, *51*, 95–102. <https://doi.org/10.1016/j.conb.2018.03.001>.
- (43) Nirschl, J. J.; Magiera, M. M.; Lazarus, J. E.; Janke, C.; Holzbaur, E. L. F. α -Tubulin Tyrosination and CLIP-170 Phosphorylation Regulate the Initiation of Dynein-Driven Transport in Neurons. *Cell Rep.* **2016**, *14* (11), 2637–2652. <https://doi.org/10.1016/j.celrep.2016.02.046>.
- (44) Peris, L.; Thery, M.; Fauré, J.; Saoudi, Y.; Lafanechère, L.; Chilton, J. K.; Gordon-Weeks, P.; Galjart, N.; Bornens, M.; Wordeman, L.; Wehland, J.; Andrieux, A.; Job, D. Tubulin Tyrosination Is a Major Factor Affecting the Recruitment of CAP-Gly Proteins at Microtubule plus Ends. *J. Cell Biol.* **2006**, *174* (6), 839–849. <https://doi.org/10.1083/jcb.200512058>.
- (45) Janke, C.; Rogowski, K.; Wloga, D.; Regnard, C.; Kajava, A. V.; Strub, J.-M.; Temurak, N.; Van Dijk, J.; Boucher, D.; Van Dorsselaer, A.; Suryavanshi, S.; Gaertig, J.; Eddé, B. Tubulin Polyglutamylase Enzymes Are Members of the TTL Domain Protein Family. *Science* **2005**, *308* (5729), 1758–1762. <https://doi.org/10.1126/science.1113010>.

- (46) Ikegami, K.; Horigome, D.; Mukai, M.; Livnat, I.; MacGregor, G. R.; Setou, M. TTL10 Is a Protein Polyglycylase That Can Modify Nucleosome Assembly Protein 1. *FEBS Lett.* **2008**, *582* (7), 1129–1134. <https://doi.org/10.1016/j.febslet.2008.02.079>.
- (47) Szyk, A.; Deaconescu, A. M.; Piszczek, G.; Roll-Mecak, A. Tubulin Tyrosine Ligase Structure Reveals Adaptation of an Ancient Fold to Bind and Modify Tubulin. *Nat. Struct. Mol. Biol.* **2011**, *18* (11), 1250–1258. <https://doi.org/10.1038/nsmb.2148>.
- (48) Prota, A. E.; Magiera, M. M.; Kuijpers, M.; Bargsten, K.; Frey, D.; Wieser, M.; Jaussi, R.; Hoogenraad, C. C.; Kammerer, R. A.; Janke, C.; Steinmetz, M. O. Structural Basis of Tubulin Tyrosination by Tubulin Tyrosine Ligase. *J. Cell Biol.* **2013**, *200* (3), 259–270. <https://doi.org/10.1083/jcb.201211017>.
- (49) Arce, C. A.; Rodriguez, J. A.; Barra, H. S.; Caputto, R. Incorporation of L-Tyrosine, L-Phenylalanine and L-3,4-Dihydroxyphenylalanine as Single Units into Rat Brain Tubulin. *Eur. J. Biochem.* **1975**, *59* (1), 145–149. <https://doi.org/10.1111/j.1432-1033.1975.tb02435.x>.
- (50) Schumacher, D.; Helma, J.; Mann, F. A.; Pichler, G.; Natale, F.; Krause, E.; Cardoso, M. C.; Hackenberger, C. P. R.; Leonhardt, H. Versatile and Efficient Site-Specific Protein Functionalization by Tubulin Tyrosine Ligase. *Angew. Chem. Int. Ed.* **2015**, *54* (46), 13787–13791. <https://doi.org/10.1002/anie.201505456>.
- (51) Banerjee, A.; Panosian, T. D.; Mukherjee, K.; Ravindra, R.; Gal, S.; Sackett, D. L.; Bane, S. Site-Specific Orthogonal Labeling of the Carboxy Terminus of α -Tubulin. *ACS Chem. Biol.* **2010**, *5* (8), 777–785. <https://doi.org/10.1021/cb100060v>.
- (52) Sato, Y. The Vasohibin Family: A Novel Family for Angiogenesis Regulation. *J. Biochem. (Tokyo)* **2013**, *153* (1), 5–11. <https://doi.org/10.1093/jb/mvs128>.
- (53) Erck, C.; Peris, L.; Andrieux, A.; Meissirel, C.; Gruber, A. D.; Vernet, M.; Schweitzer, A.; Saoudi, Y.; Pointu, H.; Bosc, C.; Salin, P. A.; Job, D.; Wehland, J. A Vital Role of Tubulin-Tyrosine-Ligase for Neuronal Organization. *Proc. Natl. Acad. Sci.* **2005**, *102* (22), 7853–7858. <https://doi.org/10.1073/pnas.0409626102>.
- (54) Peris, L.; Parato, J.; Qu, X.; Soleilhac, J. M.; Lanté, F.; Kumar, A.; Pero, M. E.; Martínez-Hernández, J.; Corrao, C.; Falivelli, G.; Payet, F.; Gory-Fauré, S.; Bosc, C.; Blanca Ramirez, M.; Sproul, A.; Brocard, J.; Di Cara, B.; Delagrangé, P.; Buisson, A.; Goldberg, Y.; Moutin, M. J.; Bartolini, F.; Andrieux, A. Tubulin Tyrosination Regulates Synaptic Function and Is Disrupted in Alzheimer's Disease. *Brain* **2022**, *145* (7), 2486–2506. <https://doi.org/10.1093/brain/awab436>.
- (55) Lipka, J.; Kapitein, L. C.; Jaworski, J.; Hoogenraad, C. C. Microtubule-binding Protein Doublecortin-like Kinase 1 (DCLK1) Guides Kinesin-3-mediated Cargo Transport to Dendrites. *EMBO J.* **2016**, *35* (3), 302–318. <https://doi.org/10.15252/embj.201592929>.
- (56) Monasterio, O.; Nova, E.; López-Brauet, A.; Lagos, R. Tubulin-tyrosine Ligase Catalyzes Covalent Binding of 3-fluoro-tyrosine to Tubulin: Kinetic and [¹⁹F]NMR Studies. *FEBS Lett.* **1995**, *374* (2), 165–168. [https://doi.org/10.1016/0014-5793\(95\)01099-Z](https://doi.org/10.1016/0014-5793(95)01099-Z).
- (57) Stengl, A.; Gerlach, M.; Kasper, M.-A.; Hackenberger, C. P. R.; Leonhardt, H.; Schumacher, D.; Helma, J. TuPPL: Tub-Tag Mediated C-Terminal Protein–Protein-Ligation Using Complementary Click-Chemistry Handles. *Org. Biomol. Chem.* **2019**, *17* (20), 4964–4969. <https://doi.org/10.1039/C9OB00508K>.
- (58) Forrest, I.; Parker, C. G. Proteome-Wide Fragment-Based Ligand and Target Discovery. *Isr. J. Chem.* **2023**, *63* (3–4), e202200098. <https://doi.org/10.1002/ijch.202200098>.
- (59) Fang, H.; Peng, B.; Ong, S. Y.; Wu, Q.; Li, L.; Yao, S. Q. Recent Advances in Activity-Based Probes (ABPs) and Affinity-Based Probes (AFBPs) for Profiling of Enzymes. *Chem. Sci.* **2021**, *12* (24), 8288–8310. <https://doi.org/10.1039/D1SC01359A>.
- (60) Wright, M. H.; Sieber, S. A. Chemical Proteomics Approaches for Identifying the Cellular Targets of Natural Products. *Nat. Prod. Rep.* **2016**, *33* (5), 681–708. <https://doi.org/10.1039/C6NP00001K>.

- (61) Kielkowski, P.; Buchsbaum, I. Y.; Kirsch, V. C.; Bach, N. C.; Drukker, M.; Cappello, S.; Sieber, S. A. FICD Activity and AMPylation Remodelling Modulate Human Neurogenesis. *Nat. Commun.* **2020**, *11* (1), 517. <https://doi.org/10.1038/s41467-019-14235-6>.
- (62) Rudolf, G. C.; Sieber, S. A. Copper-Assisted Click Reactions for Activity-Based Proteomics: Fine-Tuned Ligands and Refined Conditions Extend the Scope of Application. *ChemBioChem* **2013**, *14* (18), 2447–2455. <https://doi.org/10.1002/cbic.201300551>.
- (63) Wiest, A.; Kielkowski, P. Cu-Catalyzed Azide–Alkyne–Thiol Reaction Forms Ubiquitous Background in Chemical Proteomic Studies. *J. Am. Chem. Soc.* **2024**, *146* (3), 2151–2159. <https://doi.org/10.1021/jacs.3c11780>.
- (64) Yan, T.; Desai, H. S.; Boatner, L. M.; Yen, S. L.; Cao, J.; Palafox, M. F.; Jami-Alahmadi, Y.; Backus, K. M. SP3-FAIMS Chemoproteomics for High-Coverage Profiling of the Human Cysteinome**. *ChemBioChem* **2021**, *22* (10), 1841–1851. <https://doi.org/10.1002/cbic.202000870>.
- (65) Tsou, C.-C.; Avtonomov, D.; Larsen, B.; Tucholska, M.; Choi, H.; Gingras, A.-C.; Nesvizhskii, A. I. DIA-Umpire: Comprehensive Computational Framework for Data-Independent Acquisition Proteomics. *Nat. Methods* **2015**, *12* (3), 258–264. <https://doi.org/10.1038/nmeth.3255>.
- (66) Demichev, V.; Messner, C. B.; Vernardis, S. I.; Lilley, K. S.; Ralser, M. DIA-NN: Neural Networks and Interference Correction Enable Deep Proteome Coverage in High Throughput. *Nat. Methods* **2020**, *17* (1), 41–44. <https://doi.org/10.1038/s41592-019-0638-x>.
- (67) Guo, J.; Huan, T. Comparison of Full-Scan, Data-Dependent, and Data-Independent Acquisition Modes in Liquid Chromatography–Mass Spectrometry Based Untargeted Metabolomics. *Anal. Chem.* **2020**, *92* (12), 8072–8080. <https://doi.org/10.1021/acs.analchem.9b05135>.
- (68) Luck, K.; Kim, D.-K.; Lambourne, L.; Spirohn, K.; Begg, B. E.; Bian, W.; Brignall, R.; Cafarelli, T.; Campos-Laborie, F. J.; Charlotiaux, B.; Choi, D.; Coté, A. G.; Daley, M.; Deimling, S.; Desbuleux, A.; Dricot, A.; Gebbia, M.; Hardy, M. F.; Kishore, N.; Knapp, J. J.; Kovács, I. A.; Lemmens, I.; Mee, M. W.; Mellor, J. C.; Pollis, C.; Pons, C.; Richardson, A. D.; Schlabach, S.; Teeking, B.; Yadav, A.; Babor, M.; Balcha, D.; Basha, O.; Bowman-Colin, C.; Chin, S.-F.; Choi, S. G.; Colabella, C.; Coppin, G.; D’Amata, C.; De Ridder, D.; De Rouck, S.; Duran-Frigola, M.; Ennajdaoui, H.; Goebels, F.; Goehring, L.; Gopal, A.; Haddad, G.; Hatchi, E.; Helmy, M.; Jacob, Y.; Kassa, Y.; Landini, S.; Li, R.; Van Lieshout, N.; MacWilliams, A.; Markey, D.; Paulson, J. N.; Rangarajan, S.; Rasla, J.; Rayhan, A.; Rolland, T.; San-Miguel, A.; Shen, Y.; Sheykhkarimli, D.; Sheynkman, G. M.; Simonovsky, E.; Taşan, M.; Tejada, A.; Tropepe, V.; Twizere, J.-C.; Wang, Y.; Weatheritt, R. J.; Weile, J.; Xia, Y.; Yang, X.; Yeger-Lotem, E.; Zhong, Q.; Aloy, P.; Bader, G. D.; De Las Rivas, J.; Gaudet, S.; Hao, T.; Rak, J.; Tavernier, J.; Hill, D. E.; Vidal, M.; Roth, F. P.; Calderwood, M. A. A Reference Map of the Human Binary Protein Interactome. *Nature* **2020**, *580* (7803), 402–408. <https://doi.org/10.1038/s41586-020-2188-x>.
- (69) Mishra, P. K.; Yoo, C.; Hong, E.; Rhee, H. W. Photo-crosslinking: An Emerging Chemical Tool for Investigating Molecular Networks in Live Cells. *ChemBioChem* **2020**, *21* (7), 924–932. <https://doi.org/10.1002/cbic.201900600>.
- (70) Seath, C. P.; Trowbridge, A. D.; Muir, T. W.; MacMillan, D. W. C. Reactive Intermediates for Interactome Mapping. *Chem. Soc. Rev.* **2021**, *50* (5), 2911–2926. <https://doi.org/10.1039/D0CS01366H>.
- (71) Murale, D. P.; Hong, S. C.; Haque, Md. M.; Lee, J.-S. Photo-Affinity Labeling (PAL) in Chemical Proteomics: A Handy Tool to Investigate Protein-Protein Interactions (PPIs). *Proteome Sci.* **2016**, *15* (1), 14. <https://doi.org/10.1186/s12953-017-0123-3>.
- (72) Tachrim, Z. P.; Wang, L.; Murai, Y.; Hashimoto, M. New Trends in Diaziridine Formation and Transformation (a Review). *Molecules* **2021**, *26* (15), 4496. <https://doi.org/10.3390/molecules26154496>.
- (73) Church, R. F. R.; Kende, A. S.; Weiss, M. J. Diazirines. I. Some Observations on the Scope of the Ammonia-Hydroxylamine-O-Sulfonic Acid Diaziridine Synthesis. The Preparation of

- Certain Steroid Diaziridines and Diazirines. *J. Am. Chem. Soc.* **1965**, *87* (12), 2665–2671. <https://doi.org/10.1021/ja01090a025>.
- (74) Hill, J. R.; Robertson, A. A. B. Fishing for Drug Targets: A Focus on Diazirine Photoaffinity Probe Synthesis. *J. Med. Chem.* **2018**, *61* (16), 6945–6963. <https://doi.org/10.1021/acs.jmedchem.7b01561>.
- (75) Richardson, S. K.; Ife, R. J. Swern Oxidation of Diaziridines to Diazirines. *J. Chem. Soc. Perkin 1* **1989**, No. 6, 1172. <https://doi.org/10.1039/p19890001172>.
- (76) Li, Z.; Hao, P.; Li, L.; Tan, C. Y. J.; Cheng, X.; Chen, G. Y. J.; Sze, S. K.; Shen, H.; Yao, S. Q. Design and Synthesis of Minimalist Terminal Alkyne-Containing Diazirine Photo-Crosslinkers and Their Incorporation into Kinase Inhibitors for Cell- and Tissue-Based Proteome Profiling. *Angew. Chem. Int. Ed.* **2013**, *52* (33), 8551–8556. <https://doi.org/10.1002/anie.201300683>.
- (77) Wang, L.; Tachrim, Z. P.; Kurokawa, N.; Ohashi, F.; Sakihama, Y.; Hashidoko, Y.; Hashimoto, M. Base-Mediated One-Pot Synthesis of Aliphatic Diazirines for Photoaffinity Labeling. *Molecules* **2017**, *22* (8), 1389. <https://doi.org/10.3390/molecules22081389>.
- (78) Ibert, Q.; Cauwel, M.; Glachet, T.; Tite, T.; Le Nahenec-Martel, P.; Lohier, J.; Renard, P.; Franck, X.; Reboul, V.; Sabot, C. One-Pot Synthesis of Diazirines and $^{15}\text{N}_2$ -Diazirines from Ketones, Aldehydes and Derivatives: Development and Mechanistic Insight. *Adv. Synth. Catal.* **2021**, *363* (18), 4390–4398. <https://doi.org/10.1002/adsc.202100679>.
- (79) Abdul-Khalek, N.; Wimmer, R.; Overgaard, M. T.; Gregersen Echers, S. Insight on Physicochemical Properties Governing Peptide MS1 Response in HPLC-ESI-MS/MS: A Deep Learning Approach. *Comput. Struct. Biotechnol. J.* **2023**, *21*, 3715–3727. <https://doi.org/10.1016/j.csbj.2023.07.027>.
- (80) Shuken, S. R. An Introduction to Mass Spectrometry-Based Proteomics. *J. Proteome Res.* **2023**, *22* (7), 2151–2171. <https://doi.org/10.1021/acs.jproteome.2c00838>.
- (81) Chan, J. C. Y.; Zhou, L.; Chan, E. C. Y. The Isotope-Coded Affinity Tag Method for Quantitative Protein Profile Comparison and Relative Quantitation of Cysteine Redox Modifications. *Curr. Protoc. Protein Sci.* **2015**, *82* (1). <https://doi.org/10.1002/0471140864.ps2302s82>.
- (82) Thompson, A.; Schäfer, J.; Kuhn, K.; Kienle, S.; Schwarz, J.; Schmidt, G.; Neumann, T.; Hamon, C. Tandem Mass Tags: A Novel Quantification Strategy for Comparative Analysis of Complex Protein Mixtures by MS/MS. *Anal. Chem.* **2003**, *75* (8), 1895–1904. <https://doi.org/10.1021/ac0262560>.
- (83) Ross, P. L.; Huang, Y. N.; Marchese, J. N.; Williamson, B.; Parker, K.; Hattan, S.; Khainovski, N.; Pillai, S.; Dey, S.; Daniels, S.; Purkayastha, S.; Juhasz, P.; Martin, S.; Bartlett-Jones, M.; He, F.; Jacobson, A.; Pappin, D. J. Multiplexed Protein Quantitation in *Saccharomyces Cerevisiae* Using Amine-Reactive Isobaric Tagging Reagents. *Mol. Cell. Proteomics* **2004**, *3* (12), 1154–1169. <https://doi.org/10.1074/mcp.M400129-MCP200>.
- (84) Stadlmeier, M.; Bogena, J.; Wallner, M.; Wühr, M.; Carell, T. Ein Auf Sulfoxid Basierendes, Isobares Derivatisierungsreagens Für Die Präzise Quantitative Massenspektrometrie. *Angew. Chem.* **2018**, *130* (11), 3008–3013. <https://doi.org/10.1002/ange.201708867>.
- (85) Makarov, D.; Telek, A.; Becker, T.; Von Wisberg, M.; Schneider, S.; Kielkowski, P. Clickable Report Tags for Identification of Modified Peptides by Mass Spectrometry. *J. Mass Spectrom.* **2022**, *57* (3), e4812. <https://doi.org/10.1002/jms.4812>.
- (86) Rauniyar, N.; Yates, J. R. Isobaric Labeling-Based Relative Quantification in Shotgun Proteomics. *J. Proteome Res.* **2014**, *13* (12), 5293–5309. <https://doi.org/10.1021/pr500880b>.
- (87) Makarov, D.; Kielkowski, P. Chemical Proteomics Reveals Protein Tyrosination Extends Beyond the Alpha-Tubulins in Human Cells**. *ChemBioChem* **2022**, *23* (23), e202200414. <https://doi.org/10.1002/cbic.202200414>.
- (88) MacKinnon, A. L.; Taunton, J. Target Identification by Diazirine Photo-Cross-Linking and Click Chemistry. *Curr. Protoc. Chem. Biol.* **2009**, *1* (1), 55–73. <https://doi.org/10.1002/9780470559277.ch090167>.

- (89) Shi, W.; Nacev, B. A.; Aftab, B. T.; Head, S.; Rudin, C. M.; Liu, J. O. Itraconazole Side Chain Analogues: Structure–Activity Relationship Studies for Inhibition of Endothelial Cell Proliferation, Vascular Endothelial Growth Factor Receptor 2 (VEGFR2) Glycosylation, and Hedgehog Signaling. *J. Med. Chem.* **2011**, *54* (20), 7363–7374. <https://doi.org/10.1021/jm200944b>.
- (90) Ahad, A. M.; Jensen, S. M.; Jewett, J. C. A Traceless Staudinger Reagent To Deliver Diazirines. *Org. Lett.* **2013**, *15* (19), 5060–5063. <https://doi.org/10.1021/ol402404n>.
- (91) Dooms, C.; Laurent, P.; Daloze, D.; Pasteels, J.; Nedved, O.; Braekman, J. Synthesis and Absolute Configuration of Hyperaspine, an Alkaloid of the Ladybird *Hyperaspis Campestris*. *Eur. J. Org. Chem.* **2005**, *2005* (7), 1378–1383. <https://doi.org/10.1002/ejoc.200400804>.
- (92) Topley, A. C.; Isoni, V.; Logothetis, T. A.; Wynn, D.; Wadsworth, H.; Gibson, A. M. R.; Khan, I.; Wells, N. J.; Perrio, C.; Brown, R. C. D. A Resin-Linker-Vector Approach to Radiopharmaceuticals Containing ¹⁸F: Application in the Synthesis of O-(2-[¹⁸F]-Fluoroethyl)-L-tyrosine. *Chem. – Eur. J.* **2013**, *19* (5), 1720–1725. <https://doi.org/10.1002/chem.201202474>.
- (93) Chevallet, P.; Garrouste, P.; Malawska, B.; Martinez, J. Facile Synthesis of Tert-Butyl Ester of N-Protected Amino Acids with Tert-Butyl Bromide. *Tetrahedron Lett.* **1993**, *34* (46), 7409–7412. [https://doi.org/10.1016/S0040-4039\(00\)60139-9](https://doi.org/10.1016/S0040-4039(00)60139-9).
- (94) Dal Piaz, F.; Vassallo, A.; Lepore, L.; Tosco, A.; Bader, A.; De Tommasi, N. Sesterterpenes as Tubulin Tyrosine Ligase Inhibitors. First Insight of Structure–Activity Relationships and Discovery of New Lead. *J. Med. Chem.* **2009**, *52* (12), 3814–3828. <https://doi.org/10.1021/jm801637f>.
- (95) Tusher, V. G.; Tibshirani, R.; Chu, G. Significance Analysis of Microarrays Applied to the Ionizing Radiation Response. *Proc. Natl. Acad. Sci.* **2001**, *98* (9), 5116–5121. <https://doi.org/10.1073/pnas.091062498>.
- (96) Szklarczyk, D.; Gable, A. L.; Lyon, D.; Junge, A.; Wyder, S.; Huerta-Cepas, J.; Simonovic, M.; Doncheva, N. T.; Morris, J. H.; Bork, P.; Jensen, L. J.; Mering, C. von. STRING V11: Protein–Protein Association Networks with Increased Coverage, Supporting Functional Discovery in Genome-Wide Experimental Datasets. *Nucleic Acids Res.* **2019**, *47* (D1), D607–D613. <https://doi.org/10.1093/nar/gky1131>.
- (97) Istvan Lazar Jr., PhD; Istvan Lazar Sr., PhD, CSc. GelAnalyzer 19.1. www.gelanalyzer.com.
- (98) Pepin, R.; Shaffer, C. J.; Tureček, F. Position-tunable Diazirine Tags for Peptide–Peptide Ion Cross-linking in the Gas Phase. *J. Mass Spectrom.* **2017**, *52* (8), 557–560. <https://doi.org/10.1002/jms.3960>.
- (99) Hayakawa, K.; Yodo, M.; Ohsuki, S.; Kanematsu, K. Novel Bicycloannulation via Tandem Vinylolation and Intramolecular Diels–Alder Reaction of Five-Membered Heterocycles: A New Approach to Construction of Psoralen and Azapsoralen. *J. Am. Chem. Soc.* **1984**, *106* (22), 6735–6740. <https://doi.org/10.1021/ja00334a044>.

6. List of abbreviations

ABPs	Activity-based Probes
AfBPs	Affinity-based Probes
BTEAC	Benzyl tri-ammonium chloride
BG	Background Control
CTT	C-terminal Tail
CuAAC	Copper-catalyzed Azide-alkyne Cycloaddition Reaction
DCTN1	p150Glued Dynactin Subunits 1
DDA	Data-dependent Acquisition
DIA	Data-independent Acquisition
EB1/2	End-binding Proteins 1/2
ER	Endoplasmic Reticulum
FC	Fold Change
GO	Gene Ontology
ICAT	Isotope Coded Affinity Tags
iNGNs	Induced Pluripotent Stem Cell-Derived Neural Cells
iTRAQ	Isobaric Tags for Relative and Absolute Quantitation
KO	Knock-out
MAP	Microtubule-associated Protein
MATCAP	Microtubule-associated Tyrosine Carboxypeptidase
MCAK	Mitotic Centromere-associated Kinesin
MEFs	Mouse-derived Embryonic Fibroblast Cells
MTs	Microtubules
MTOC	Microtubule-organizing Center
PAL	Photo-affinity Labeling
PCA	Principal Component Analysis
POI	Protein of Interest
PPI	Protein-protein Interaction

PTMs	Post-translational Modifications
RTK	Receptor Tyrosine Kinase
SAR	Structure-activity Relationship
SAM	Significance Analysis of Microarrays
SH-SY5Y	Human Neuroblastoma Cell Line
SOT	Sulfoxide Tag
TCPs	Tubulin Carboxy Peptidases
TMT	Tandem Mass Tag
TTL	Tubulin-tyrosine Ligase
TTLL	Tubulin Tyrosine Ligase-like
Ts-OH	para-Toluenesulfonic acid
Tyr-O-Diaz	(S)-2-amino-3-(4-(2-(3-(but-3-yn-1-yl)-3 <i>H</i> -diazirin-3-yl)ethoxy)phenyl)propanoic acid
VP	Volcano Plot
VASH1/2	Vasohibins 1/2
WT	Wild-type

7. List of figures

Figure 1. The diversity of proteoforms.	1
Figure 2. Building blocks of microtubules.	3
Figure 3. The Tubulin Code.	5
Figure 4. Chemical proteomics pipeline.	12
Figure 5. Approach into diazirines.	14
Figure 6. Approach into diazirines.	15
Figure 7. Isobaric tags.	16
Figure 8. Volcano plot.	35
Figure 10. Fluorescent SDS-Gel with Coomassie staining as a loading control.	38
Figure 11. Fluorescent SDS-Gel with Coomassie staining and normalized intensities.	39
Figure 12. WB analysis with GAPDH control.	39
Figure 13. Fluorescent SDS-Gel with Coomassie staining and normalized intensities.	40
Figure 14. Fluorescent SDS-Gel with Coomassie staining and normalized intensities.	40
Figure 15. Fluorescent SDS-Gel with Coomassie staining and normalized intensities.	41
Figure 16. Fluorescent SDS-Gel and WB analysis.	42
Figure 17. Fluorescent SDS-Gel and WB analysis.	42
Figure 18. Fluorescent imaging of SDS-Page gel, WB analysis with normalization. (a)....	43
Figure 19. Fluorescent imaging of SDS-Page gel, WB analysis with normalization.	44
Figure 20. Fluorescent imaging of SDS-Page gel and Coomassie staining.	45
Figure 21. Structures of potential tyrosine cross-linking probes.	46
Figure 22. Two labeling probes.	47
Figure 23. The structure of “minimalist” terminal alkyne-containing cross-linker.	47
Figure 24. Retrosynthetic scheme.	48
Figure 25. Fluorescent SDS-Page with Coomassie staining.	54
Figure 26. Fluorescent SDS-Page with Coomassie staining.	55
Figure 27. Fluorescent SDS-Page with Coomassie staining.	56
Figure 28. Experimental scheme.	57
Figure 29. PCA plot.	58
Figure 30. Volcano Plot.	59
Figure 31. Volcano Plot.	60
Figure 32. Volcano Plot.	61
Figure 33. PCA plot.	61
Figure 34. Volcano Plot.	62

Figure 35. Volcano Plot..... 63
Figure 36. Venn diagram..... 63
Figure 37. Volcano Plot..... 64
Figure 38. Venn diagram..... 64
Figure 39. Volcano Plot..... 65
Figure 40. Venn diagram..... 66
Figure 41. STRING interaction map..... 66
Figure 42. Venn Diagram..... 67

8. Supplementary information

8.1. Supplementary information for “Clickable report tags for identification of modified peptides by mass spectrometry”

Makarov, D.; Telek, A.; Becker, T.; Von Wrisberg, M.; Schneider, S.; Kielkowski, P. Clickable Report Tags for Identification of Modified Peptides by Mass Spectrometry. *J Mass Spectrom* **2022**, 57 (3), e4812. <https://doi.org/10.1002/jms.4812>.

Supplementary Information.

Clickable report tags for identification of modified peptides by mass spectrometry.

Dmytro Makarov^{1*}, András Telek^{1,2*}, Tobias Becker¹, Marie-Kristin von Wrisberg¹, Sabine Schneider¹, Pavel Kielkowski^{1*}

¹ LMU Munich, Department of Chemistry, Butenandtstr. 5-13, 81377, Munich, Germany.

² current address: Budapest University of Technology and Economics, Department of Applied Biotechnology, Szent Gellért sq. 4, 1111, Budapest, Hungary.

* These authors contributed equally.

* Correspondence to pavel.kielkowski@cup.lmu.de

Table of content:

Supplementary Figures and Tables	2
Supplementary Methods	6
Synthesis of small compounds	6
Biochemistry and Proteomics	11
NMR and MS Spectra of Small Compounds	15

Supplementary Figures

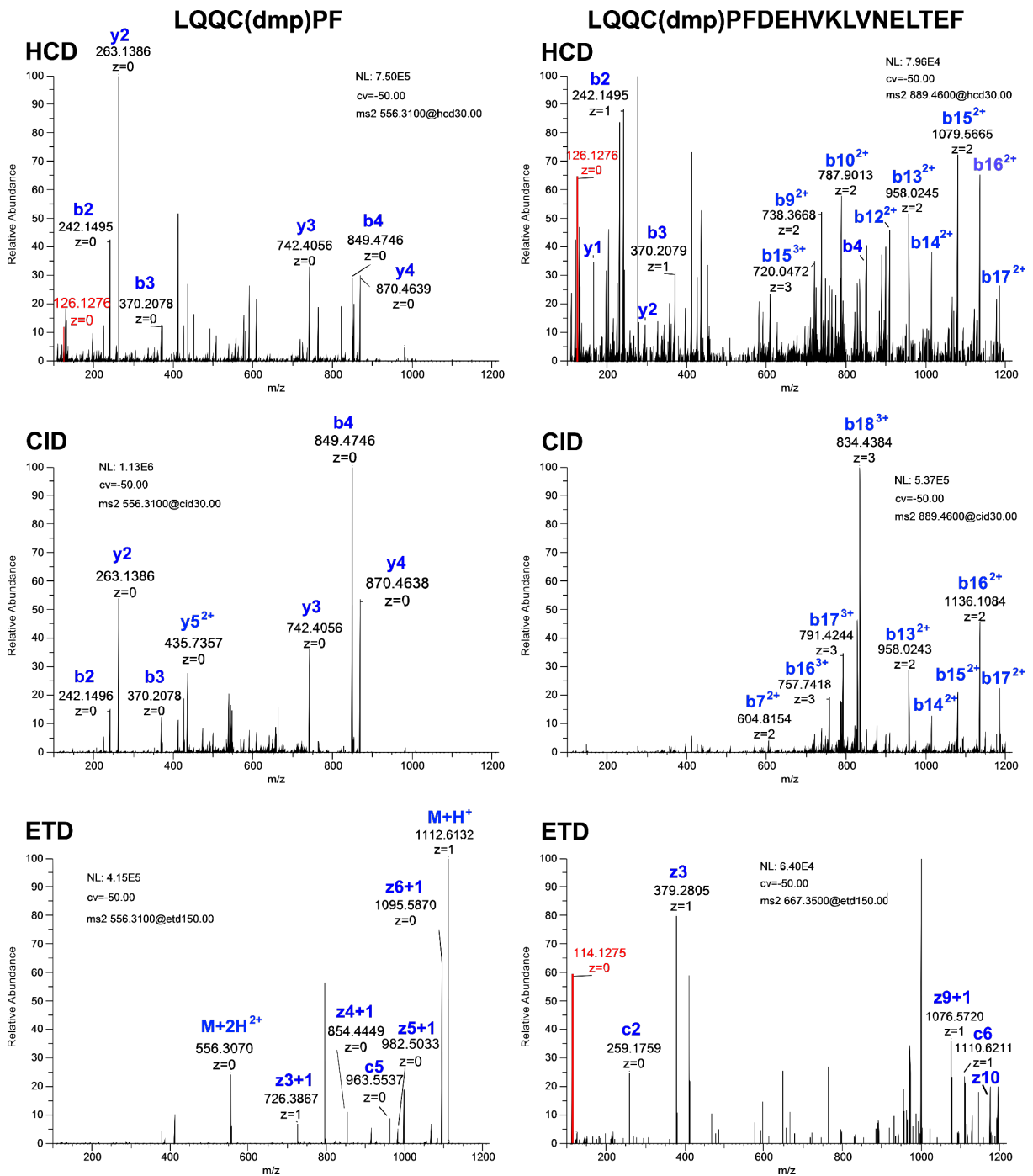


Figure S1: Fragmentation and reporter ion release from BSA peptide resulting from chymotrypsin digest labelled with DMP-tag.

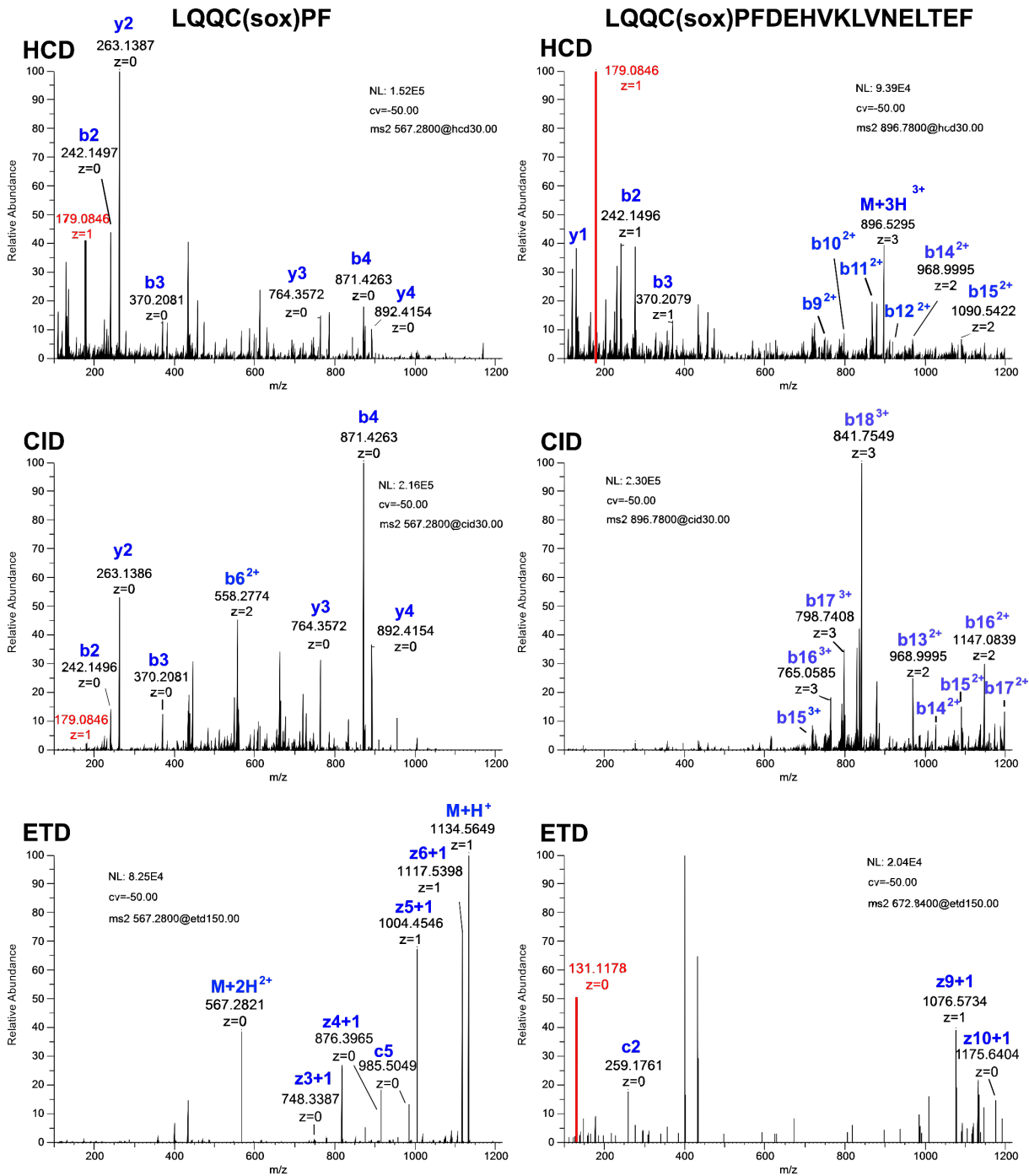


Figure S2: Fragmentation and reporter ion release from BSA peptide resulting from chymotrypsin digest labelled with SOX-tag.

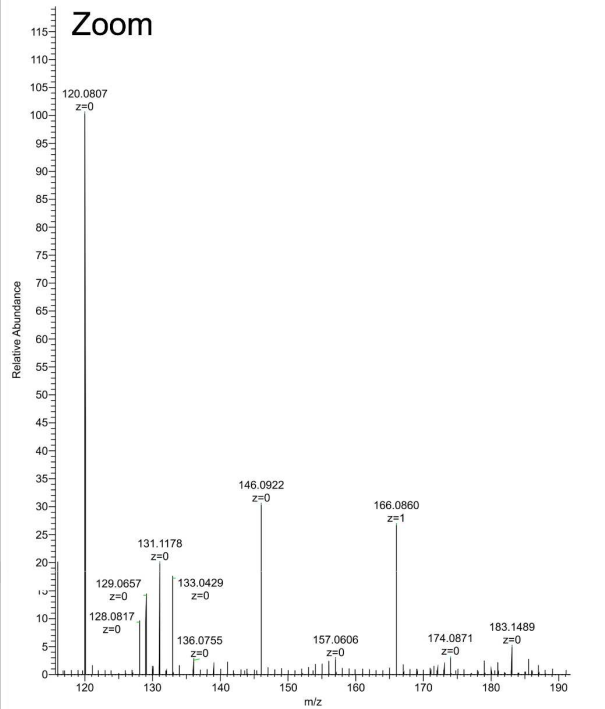
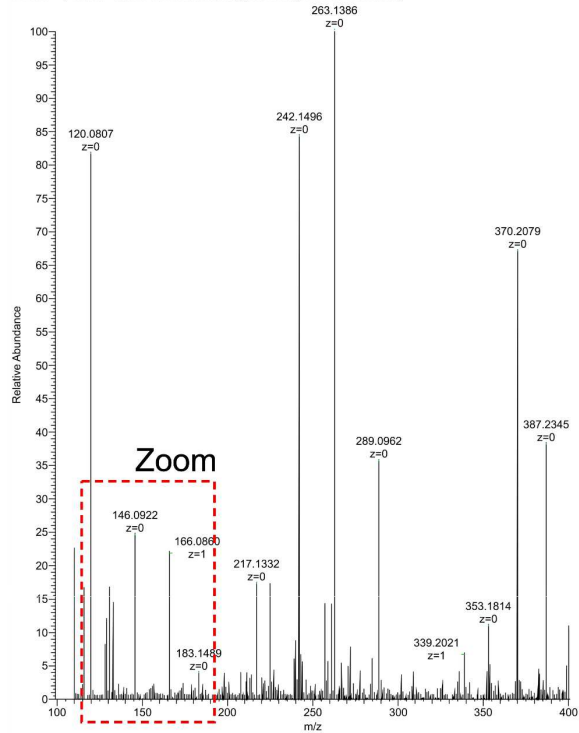


Figure S3: Control fragmentation experiment of BSA peptide showing absence of detectable peaks, which would overlap with DMP- or SOX-reporter ions.

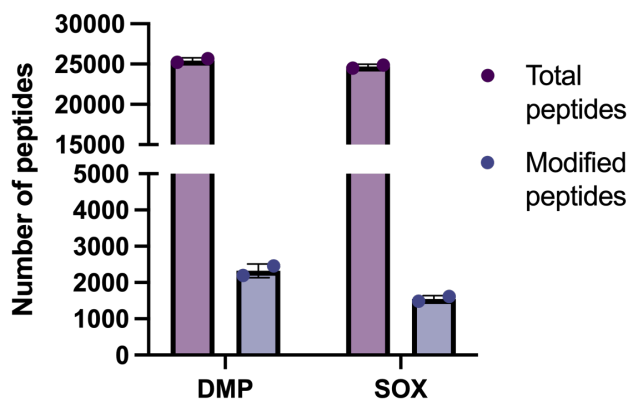


Figure S4: Total peptides and modified peptides found by MaxQuant in the DMP- and SOX-tag labelled cysteines using low-resolution MS2 acquired in ion trap.

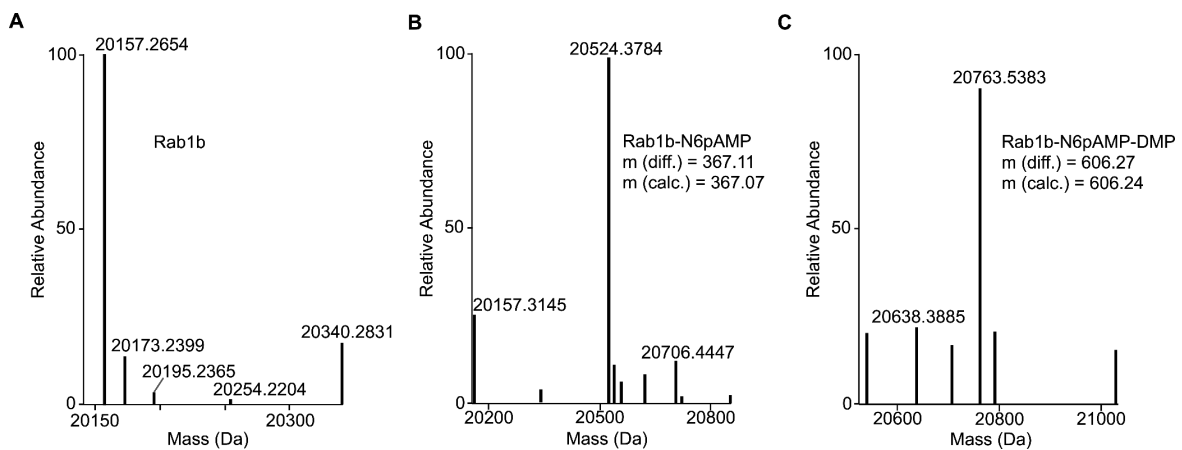


Figure S5: Deconvoluted intact protein MS spectra of **A**) Rab1b, **B**) N6pAMPylated Rab1b and **C**) N6pAMPylated Rab1b with DMP-tag.

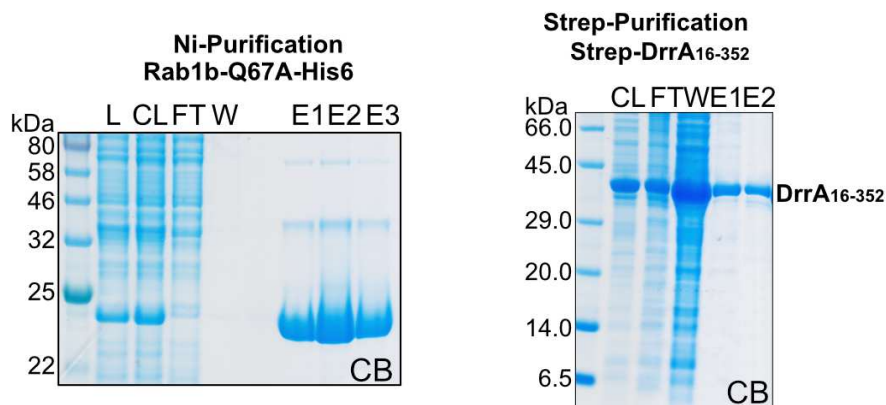


Figure S6: Rab1b and DrrA purification.

20210225_AT15_Rab1b_AMPTMT_digested-40cv_etd150 #1 RT: 0.00 AV: 1 NL: 7.14E3
 T: FTMS + p ESI cv=-40.00 Full ms2 532.9100@etd150.00 [100.0000-1000.0000]

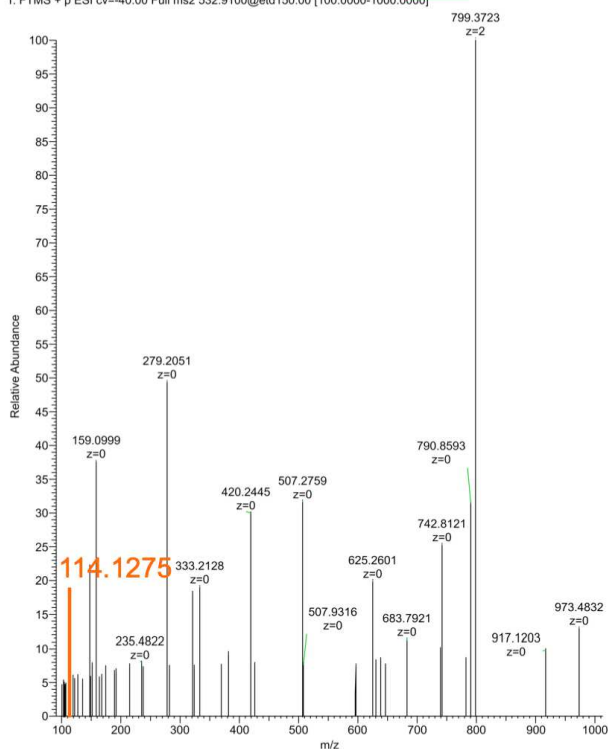


Figure S7: ETD fragmentation of AMPylated TITSSYYR peptide decorated with the DMP-tag yielding the 114.1275 reporter ion.

Table S3: Andromeda scores of modified Rab1b peptides with and without including neutral loss containing peptide fragments in the search. When these fragments were included, the modification was falsely assigned to the T3 of the peptide in case of the highest scoring PSMs.

Peptide	Score without neutral losses	Score with neutral losses
TITSSY(N6pAMP)YR	92.19	101.65
TITSSY(AMP-DMP)YR	75.18	103.55

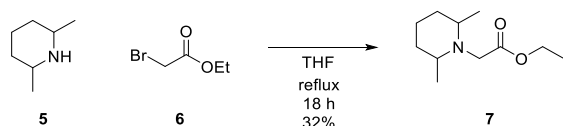
Supplementary Methods

Synthesis of small compounds

General Information

Unless noted otherwise, all reactions were performed using oven-dried glassware under an atmosphere of argon. Molsieve-dried solvents were used from *Sigma Aldrich* and chemicals were bought from *Sigma Aldrich*, *TCl*, *abcr*, *Roth* and *Carbosynth*. Reaction controls were performed using TLC-Plates from *Merck* (Merck 60 F²⁵⁴), flash column chromatography purifications were performed on *Merck Geduran Si 60* (40–63 μ M). Visualization of the TLC plates was achieved through UV-absorption or through staining with *Potassium permanganate stain*. NMR spectra were recorded in deuterated solvents on *Varian VXR400S*, *Varian Inova 400*, *Bruker AMX 600*, *Bruker Ascend 400* or *Bruker Avance III HD*. HR-ESI-MS spectra were obtained from a *Thermo Finnigan LTQ FT-ICR*. For MS-experiments, only highest grade solvents and reagents were used. The mass spectrometry proteomics data are available upon request.

Synthesis of *N*-(2-azidoethyl)-2-(2,6-dimethylpiperidin-1-yl)-acetamide:



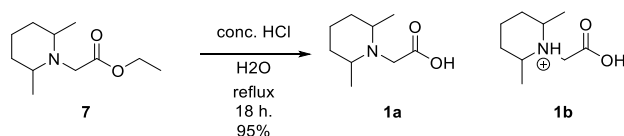
Ethyl 2-(2,6-dimethylpiperidin-1-yl)acetate (**7**) [33]

2,6-Dimethylpiperidine (**5**) (1.19 mL, 8.83 mmol) and ethyl 2-bromoacetate (**6**) (0.98 mL, 8.83 mmol) were dissolved in THF (15 mL) and the RM was stirred overnight under reflux. The solvent was evaporated and the residue was dissolved in H₂O (20 mL). The mixture was adjusted to pH 12 with 1M NaOH solution so a suspension was formed. The suspension was then extracted with EtOAc (3 \times 15 mL). The combined organic phase was dried over anhydrous Mg₂SO₄ and evaporated *in vacuo*. The residue was dissolved in hexane (15 mL) and solids were formed. The solids were filtered off and the solvent was evaporated. The residue was purified by column chromatography using 50% EtOAc in hexane. Product **7** was obtained as a yellowish liquid (0.56 g, 32%).

¹H NMR (400 MHz, Chloroform-*d*) δ 4.14 (q, J = 7.1 Hz, 2H), 3.56 (s, 2H), 2.86 – 2.78 (m, 2H), 1.70 – 1.62 (m, 1H), 1.60 – 1.53 (m, 2H), 1.44 – 1.32 (m, 1H), 1.26 (t, J = 7.1 Hz, 5H), 1.10 (d, J = 6.3 Hz, 6H).
¹³C NMR (101 MHz, CDCl₃) δ 207.20, 68.12, 54.79, 31.09, 30.48, 25.74, 23.01, 19.42.

MS(ESI⁺): m/z (%): 200.25 (100) [M+H]⁺.

2-(2,6-Dimethylpiperidin-1-yl)acetic acid (**1**)



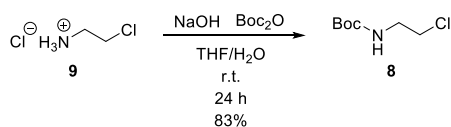
Ethyl 2-(2,6-dimethylpiperidin-1-yl)acetate **7** (0.55 g, 2.76 mmol) was dissolved in H₂O (5.50 mL) and concentrated HCl (0.55 mL) was added to the RM. The mixture was heated overnight to reflux. After being cooled to ambient temperature, the RM was extracted with Et₂O (3 \times 10 mL). The combined organic phase was dried over anhydrous Mg₂SO₄ and concentrated *in vacuo*. Products **1a** and **1b** were obtained as a mixture of protonated and non-protonated molecules in a 1:2 ratio and as an off-white solid (0.45 g, 95%).

Compound **1a** and **1b**. ¹H NMR (400 MHz, Methanol-*d*₄) δ 4.22 (s, 1H, [-CH₂-CO (**1a**)]), 4.00 (s, 2H, [-CH₂-CO (**1b**)]), 3.63 – 3.52 (m, 3H, [-CH-CH₃ (**1a** + **1b**)]), 1.99 – 1.51 (m, 9H, [-CH₂-CH₂-CH₂-(**1a** + **1b**)]), 1.40 (d, J = 6.4 Hz, 3H, [-CH₃-CH (**1a**)]), 1.28 (d, J = 6.6 Hz, 6H, [-CH₃-CH-(**1b**)]).

¹³C NMR (101 MHz, MeOD) δ 170.29, 63.77, 63.07, 42.72, 32.85, 26.52, 23.48, 23.19, 18.59, 17.17.

MS(ESI⁺): m/z (%): 172.22 (100) [M+H]⁺.

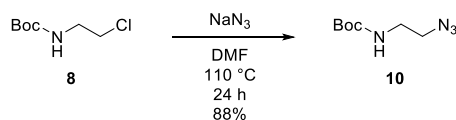
tert-Butyl (2-chloroethyl)carbamate (8)[34]



2-Chloroethan-1-amine hydrochloride (**9**) (2.00 g, 17.24 mmol) was suspended in THF (25 mL) and a solution of NaOH (0.83 g, 20.69 mmol) was added to H₂O (20 mL). The RM was cooled on an ice bath before a solution of Boc₂O (4.52 g, 20.69 mmol) in THF (30 mL) was added dropwise over 40 min. The RM was stirred for 24 h at r.t. THF was evaporated *in vacuo*. The aqueous phase was diluted with H₂O (30 mL) and extracted with EtOAc (3 × 25 mL). The combined organic layer was dried over anhydrous Mg₂SO₄ and concentrated *in vacuo*. Purification of the product was carried out by column chromatography using a mixture of EtOAc in hexane (0 – 25%). Product **8** was obtained as a transparent viscous liquid (2.58 g, 83%). NMR data were in agreement with the literature.[34]

¹H NMR (400 MHz, Chloroform-*d*) δ 4.99 (s, 1H), 3.58 (t, *J* = 5.7 Hz, 2H), 3.45 (q, *J* = 5.8 Hz, 2H), 1.43 (s, 9H).

tert-Butyl (2-azidoethyl)carbamate (10)

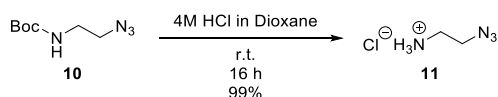


Carbamate **8** (2.58 g, 14.36 mmol) was dissolved in DMF (45 mL). NaN₃ (3.73 g, 57.43 mmol) was added to the mixture. The resulting suspension was stirred for 24 h at 115°C. The solvent was removed *in vacuo* and the residue was dissolved in H₂O (100 mL). The aqueous phase was extracted with EtOAc (3 × 50 mL). The combined organic phase was dried over anhydrous Mg₂SO₄ and concentrated *in vacuo*. Product **10** was obtained as a yellow viscous liquid (2.35 g, 88%). NMR data were in agreement with the literature.[35]

¹H NMR (400 MHz, Chloroform-*d*) δ 4.86 (s, 1H), 3.40 (t, *J* = 5.6 Hz, 2H), 3.29 (q, *J* = 5.8 Hz, 2H), 1.44 (s, 9H).

MS(ESI⁺): *m/z* (%): 187.22 (30) [M+H]⁺, 373.29 (25) [2M+H]⁺.

2-Azidoethan-1-amine hydrochloride (11)

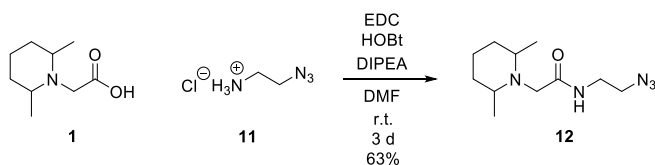


Carbamate **10** (1.15 g, 6.18 mmol) was added to the solution of 4M HCl in Dioxane (4.20 mL). The resulting mixture was stirred overnight at r.t. A suspension was formed and the solvent was removed *in vacuo*. Product **11** was obtained as a yellow solid after drying it under a high vacuum (0.75 g, 99%). NMR data were in agreement with the literature.[36]

¹H NMR (400 MHz, Deuterium Oxide) δ 3.72 – 3.65 (m, 2H), 3.17 – 3.11 (m, 2H).

MS(ESI⁺): *m/z* (%): 128.24 (100) [M+ACN+H]⁺.

N-(2-azidoethyl)-2-(2,6-dimethylpiperidin-1-yl)acetamide (12)



Acid **1** (1.13 g, 0.76 mmol), HOBt (0.18 g, 1.14 mmol), EDC.HCl (0.22 g, 1.14 mmol) and DIPEA (0.60 mL, 3.42 mmol) were dissolved in anhydrous DMF (15 mL) under inert atmosphere. The RM was stirred for 3 h at r.t. before the solution changed color. The mixture of azide **11** (0.14 g, 1.14 mmol) with

DIPEA (0.20 mL, 1.14 mmol) in anhydrous DMF (5 mL) was added to the RM. The RM was stirred under an inert atmosphere for 72 h at r.t. DMF was evaporated *in vacuo* and the residue was dissolved in DCM. The mixture was washed with H₂O (2 × 15 mL) and brine (1 × 15 mL). The organic phase was dried over anhydrous Mg₂SO₄ and the solvent was removed *in vacuo*. The product was purified by column chromatography using 5% MeOH in DCM as eluent. Product **12** was obtained as a yellow liquid (0.12 g, 63%).

¹H NMR (400 MHz, Chloroform-*d*) δ 7.87 (s, 1H), 3.44 (s, 4H), 3.08 (s, 2H), 2.49 – 2.41 (m, 2H), 1.61 – 1.54 (m, 2H), 1.42 – 1.17 (m, 4H), 1.02 (d, *J* = 6.2 Hz, 6H).

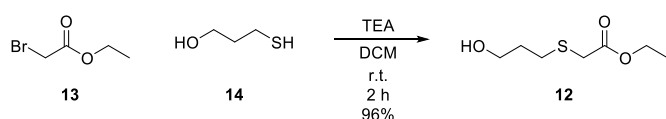
¹³C NMR (101 MHz, CDCl₃) δ 174.02, 58.95, 51.38, 50.92, 38.35, 24.33, 21.50.

MS(ESI⁺): *m/z* (%): 240.25 (100) [M+H]⁺.

HR-MS(ESI⁺): calculated for C₁₁H₂₂N₅O⁺ 240.18244, found 240.18196.

Synthesis of 2-((3-azidopropyl)sulfinyl)-*N*-(2-(dimethylamino)ethyl)acetamide:

Ethyl 2-((3-hydroxypropyl)thio)acetate (**12**) [37]



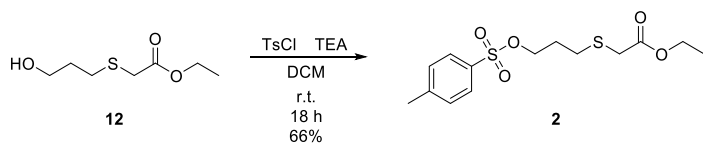
In a round bottom flask, ethyl 2-bromoacetate (**13**) (2.57 mL, 23.22 mmol) and triethylamine (4.85 mL, 34.83 mmol) were dissolved in DCM (20 mL). 3-Mercaptopropan-1-ol (**14**) (2.00 mL, 23.22 mmol) was added dropwise to the RM and the solution was stirred for 2 h at r.t. After completion of the reaction, the solution was washed with H₂O (1 × 15 mL), 1M HCl (1 × 15 mL) and with a saturated solution of NaHCO₃ (1 × 15 mL). The organic phase was collected and dried over anhydrous Mg₂SO₄, the solvent was evaporated *in vacuo*. Product **12** was obtained without purification as a yellow viscous liquid (3.98 g, 96%).

¹H NMR (400 MHz, Chloroform-*d*) δ 4.18 (q, *J* = 7.2 Hz, 2H), 3.78 – 3.71 (m, 2H), 3.22 (s, 2H), 2.75 (t, *J* = 7.1 Hz, 2H), 1.89 – 1.81 (m, 2H), 1.28 (t, *J* = 7.1 Hz, 3H).

¹³C NMR (101 MHz, CDCl₃) δ 207.23, 73.18, 72.42, 26.51, 21.52, 20.92, 10.39.

MS (ESI⁺): *m/z* (%): 179.24 (100) [M+H]⁺.

Ethyl 2-((3-(tosyloxy)propyl)thio) acetate (**2**) [TSAI, C.-S.; HUNG, T.-C.; CHUANG Hong-Yang. ANTIBODY-DRUG CONJUGATES. WO2018090045, 2018.]



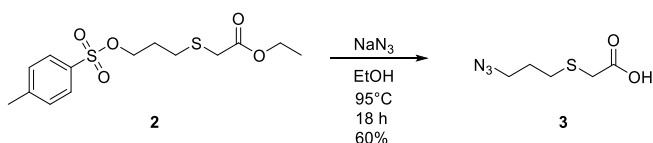
Ethyl thioacetate **12** (3.95 g, 22.16 mmol), *p*-Toluene sulfonyl chloride (6.34 g, 33.24 mmol) and TEA (6.17 mL, 44.32 mmol) were mixed in DCM (20 mL). The resulting RM was stirred overnight at r.t. After that, the mixture was washed with concentrated NaHCO₃ (1 × 20 mL), H₂O (2 × 15 mL) and brine (1 × 15 mL). The solvent was evaporated *in vacuo*. The product was purified by column chromatography using 50% EtOAc in hexane. Product **2** was obtained as a yellow liquid (4.88 g, 66%).

¹H NMR (400 MHz, Chloroform-*d*) δ 7.79 (d, *J* = 8.3 Hz, 2H), 7.35 (d, *J* = 7.7 Hz, 2H), 4.20 – 4.10 (m, 4H), 3.14 (s, 2H), 2.66 (t, *J* = 7.1 Hz, 2H), 2.45 (s, 3H), 1.95 (p, *J* = 6.6 Hz, 2H), 1.27 (t, *J* = 7.2 Hz, 3H).

¹³C NMR (101 MHz, CDCl₃) δ 175.41, 145.08, 132.80, 130.03, 127.98, 68.61, 61.58, 33.36, 28.56, 28.24, 21.74, 14.21.

MS (ESI⁺): *m/z* (%): 228.17 (100) [M+3ACN+2H]²⁺.

2-((3-azidopropyl)thio)acetic acid (**3**)



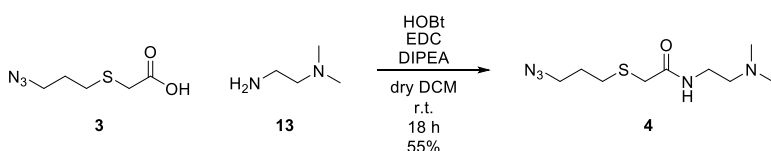
The suspension of tosylated ethyl thioacetate **2** (4.80 g, 14.44 mmol) and NaN₃ (2.82 g, 43.43 mmol) in EtOH (20 mL) was stirred overnight at 95°C. After the reaction was complete, the solids were filtered off and EtOH was evaporated *in vacuo*. The residue was diluted with H₂O (10 mL) and the mixture was acidified with 1M HCl to pH 2. The product was extracted with EtOAc (3 × 15 mL). The organic phase was subsequently washed with H₂O (3 × 10 mL), brine (1 × 10 mL) and dried over anhydrous Mg₂SO₄. The solvent was evaporated *in vacuo*. The product was purified by column chromatography using 10% EtOAc in hexane. Product **3** was obtained as a yellow liquid (1.51 g, 60%).

¹H NMR (400 MHz, Chloroform-*d*) δ 3.43 (t, *J* = 6.6 Hz, 2H), 3.26 (s, 2H), 2.76 (t, *J* = 7.1 Hz, 2H), 1.89 (p, *J* = 6.8 Hz, 2H).

¹³C NMR (101 MHz, CDCl₃) δ 175.16, 49.87, 33.34, 29.74, 28.11.

MS (ESI⁺): *m/z* (%): 176.24 (100) [M+H]⁺.

2-((3-Azidopropyl)thio)-*N*-(2-(dimethylamino)ethyl)acetamide (**4**)



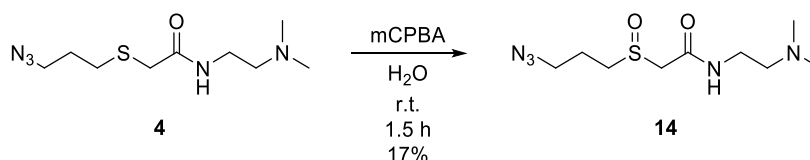
HOBT (1.74 g, 12.84 mmol) and EDC hydrochloride (2.46 g, 12.84 mmol) were dissolved in dry DCM (5 mL) under an inert atmosphere and the mixture was cooled down to 0°C on an ice bath. A mixture of azide **3** (1.50 g, 8.56 mmol) in dry DCM (7 mL) was added dropwise to the RM. After 15 min of stirring, a solution of *N*¹,*N*¹-dimethylethane-1,2-diamine (**13**) (1.49 mL, 13.70 mmol) and DIPEA (5.97 mL, 34.24 mmol) was added dropwise to the mixture. The RM was removed from the ice bath and stirred overnight at r.t. The RM was washed with conc. NaHCO₃ solution (1 × 10 mL) and H₂O (2 × 10 mL). The organic phase was dried over anhydrous Mg₂SO₄ and the solvent was evaporated *in vacuo*. The purification of the product was made by column chromatography using 70% EtOAc in hexane as a first eluent to elute polar impurities and using 10% MeOH in DCM with the addition of 0.5% of TEA as a second to elute the desired product. Product **4** was obtained as a transparent liquid (1.15 g, 55%).

¹H NMR (400 MHz, Chloroform-*d*) δ 7.14 (s, 1H), 3.41 (t, *J* = 6.6 Hz, 2H), 3.38 – 3.33 (m, 2H), 3.21 (s, 2H), 2.64 (t, *J* = 7.1 Hz, 2H), 2.43 (t, *J* = 6.0 Hz, 2H), 2.24 (s, 6H), 1.87 (p, *J* = 6.8 Hz, 2H).

¹³C NMR (101 MHz, CDCl₃) δ 168.82, 57.87, 50.04, 45.25, 37.16, 36.16, 31.08, 29.98, 28.41.

MS (ESI⁺): *m/z* (%): 246.21 (100) [M+H]⁺.

2-((3-Azidopropyl)sulfinyl)-*N*-(2-(dimethylamino)ethyl)acetamide (**14**) [21]



Acetamide **4** (0.116 g, 0.470 mmol) was dissolved in distilled H₂O (3 mL) and acidified with 1M HCl to pH 2. mCPBA (0.080 g, 0.470 mmol) was added to the flask and the reaction mixture was stirred for 1.5 h at r.t. The completion of the reaction was monitored by LC-MS. The aqueous phase was washed with DCM (3 × 3 mL). The crude product was obtained by removing water *in vacuo*. The purification of the desired compound was made by semi-preparative HPLC. Product **14** was obtained as a yellowish viscous liquid (0.021 g, 17%).

¹H NMR (400 MHz, Methanol-*d*₄) δ 7.77 (dd, *J* = 39.1, 8.1 Hz, 1H), 7.49 – 7.38 (m, 1H), 3.79 (dd, *J* = 110.2, 13.4 Hz, 2H), 3.53 (t, *J* = 6.5 Hz, 2H), 3.21 (q, *J* = 7.3 Hz, 2H), 3.11 – 3.02 (m, 2H), 2.94 (s, 6H), 2.08 – 2.00 (m, 2H), 1.31 (t, *J* = 7.3 Hz, 2H).

^{13}C NMR (101 MHz, MeOD) δ 164.84, 57.55, 49.82, 48.64, 44.03, 36.87, 22.10, 15.88, 15.69.
MS (ESI⁺): m/z (%): 262.24 (100) [M+H]⁺.
HR-MS(ESI⁺): calculated for C₉H₂₀N₅S 262.13377, found 262.13327

Biochemistry and proteomics.

Expression and Purification of Rab1b.

Competent *E. coli* NEB 10-beta cells were transformed with pBAD_Rab1b₃₋₁₇₄-Q67A-His6 plasmid. The transformation was directly inoculated into 50 mL non-AI medium (Hammill *et al.*, 2007) containing ampicillin (100 µg/mL) and incubated overnight at 37 °C, 200 rpm. The pre-culture was diluted to an OD₆₀₀ between 0.04 – 0.07 in 500 mL AI medium (Hammill *et al.*, 2007) supplemented with ampicillin (100 µg/mL). The cells were cultivated at 37 °C, 200 rpm for 12 hours at 37 °C, 200 rpm.

The obtained cell pellets were resuspended in His-wash buffer containing 50 mM HEPES pH 8.0, 500 mM LiCl, 20 mM imidazole, 2 mM β-mercaptoethanol, 1 mM MgCl₂, 0.01 mM GTP supplemented with 0.1 mg/mL DNase I (AppliChem) and one cOmplete™ ULTRA EDTA-free protease inhibitor tablet (Roche). High pressure cell lysis was performed using the Emulsiflex C5 homogenizer (Avestin). The cell lysate was centrifuged (18,000 rpm, 1 h, 4 °C) and the cleared lysate was incubated together with 1 mL Ni-NTA slurry (Jena Bioscience) for 1 h at 4 °C slightly shaking. The beads were transferred to a gravity flow column and washed with His-wash buffer before eluting the proteins in 1 mL fractions using His-wash buffer supplemented with 500 mM imidazole pH 8.0. The fractions containing the protein were pooled, concentrated and rebuffed in storage buffer (20 mM HEPES pH 8.0, 150 mM NaCl, 5 mM MgCl₂, 2 mM DTT and 0.01 mM GTP) with Amicon® Ultra-4 10K NMWL centrifugal filter units (Millipore). Purified proteins were analyzed by 15 % SDS PAGE and stored at -80 °C. Protein concentration was determined using NanoPhotometer® N60 (Implen GmbH).

Expression and Purification of DrrA.

Competent *E. coli* NEB 10-beta cells were transformed with pBAD-RSF1031K-StrepII-TEV-DrrA₁₆₋₃₅₂ and directly inoculated into 50 mL non-AI medium (Hammill *et al.*, 2007) containing kanamycin (50 µg/mL). Next day the pre-culture was diluted to an OD₆₀₀ between 0.04 – 0.07 in 500 mL AI medium (Hammill *et al.*, 2007) supplemented with kanamycin (50 µg/mL) and incubated for 16 hours at 37 °C, 200 rpm.

The obtained cell pellet was thoroughly resuspended in 30 mL of Strep-wash buffer containing 100 mM Tris pH 8.0, 150 mM NaCl, 1 mM EDTA and supplemented with 0.1 mg/mL DNase I (AppliChem) and one cOmplete™ ULTRA EDTA-free protease inhibitor tablets (Roche). The cells were lysed using an Emulsiflex C5 high pressure homogenizer (Avestin). Cell debris was removed by centrifugation (18,000 rpm, 45 min, 4 °C) and the cleared lysate was applied to an ÄKTA Pure FPLC system (Cytiva, former GE Healthcare) equipped with a 1 mL StrepTrap HP column (Cytiva). The column was washed with Strep-wash buffer and eluted in 1 mL fractions with Strep-wash buffer supplemented with 50 mM biotin. The fractions containing the protein were pooled together, concentrated and rebuffed (20 mM HEPES pH 8.0, 150 mM NaCl, 2 mM DTT, and 5 mM MgCl₂) using Amicon® Ultra-4 10K NMWL centrifugal filter units (Millipore). Purified proteins were analyzed by 15 % SDS PAGE and stored at -80 °C. Protein concentration was determined using NanoPhotometer® N60 (Implen GmbH).

In vitro AMPylation of Rab1b.

Purified Rab1b₃₋₁₇₄ was mixed with DrrA₁₆₋₃₅₂ in a 50:1 Rab1b:DrrA ratio in AMPylation buffer (20 mM HEPES pH 8.0, 150 mM NaCl, 1 mM DTT, 1 mM MgCl₂, 0.01 mM GTP) supplemented with an 2.5-fold excess of ATP compared to the Rab1b. Samples were incubated at 25 °C for 3 hours at 200 rpm and AMPylated Rab1b was purified via size exclusion chromatography using a superdex 75 10/300 GL column and SEC buffer (20 mM HEPES pH 8.0, 150 mM NaCl, 1 mM DTT, 1 mM MgCl₂, 0.01 mM GTP).

Cysteine labelling on BSA and click chemistry.

To a 1.6 mg/mL BSA solution in 20 mM Hepes pH=7.5 or 50 mM ABC buffer was added IAA-alkyne to a final concentration of 10 mM. The mixture was incubated for 1h at 60°C. Excess IAA-alkyne was removed by buffer exchange on a 50k cutoff Amicon® Ultra Centrifugal Filter. The solution was transferred to a new reaction tube and the click reaction was performed with 2 mM DMP-N₃ or SOX-N₃, 4 mM TCEP, 4 mM CuSO₄ and 0.4 mM TBTA.

Peptide preparation from purified proteins.

If proteins contained disulphide bridges (e.g. BSA) those were reduced and the free cysteines alkylated by 5 mM TCEP and 20 mM CAA by incubation for 5 minutes at 95°C, 550 rpm. Trypsin digestion was performed in 20 mM Hepes pH=7.5 buffer with 1:200 trypsin to protein ratio by incubation for 16 h at 37°C, 550 rpm. Chymotrypsin digestion was carried out with 1:100 chymotrypsin to protein ratio in 50 mM ABC buffer containing 2mM CaCl₂ by incubation for 16 h at 25°C, 550 rpm. The samples were acidified by the addition of FA to 0.5%. The peptides were desalted on SepPak C18 50 mg cartridges (Waters) using vacuum manifold with final elution into 300 µL 0.5% FA, 80% ACN in water.

HeLa proteome preparation.

HeLa cells were cultivated in high glucose Dulbeccos's Modified Eagle's Medium (DMEM) supplemented with 10% fetal bovine serum (FBS) and 2 mM L-glutamine. Cells were grown at 37 °C and 5% CO₂. Cells were seeded into 15 cm diameter dishes and grown to 90-100% confluency. The medium was removed, the cells were washed with PBS and the scrapped into 1 mL PBS and centrifuged. The pellets were lysed in 600 µL 20 mM Hepes pH=7.5, 1% NP40, 0.2% SDS by sonication and the lysates were centrifuged. 2 µL samples were diluted 100x and used for determining protein concentration by BCA assay (carried out as recommended by the supplier). To the lysates 4x volume of acetone was added, and the proteins were let precipitate for 2 h or overnight at -20 °C. Precipitated proteins were pelletized by centrifuging for at 4 °C at 4000g. The pellet was washed with cold methanol and redissolved in X-buffer (3.9 M urea, 1.1 M thiourea in 20 mM Hepes pH=7.5). Proteins were reduced by incubating with 1 mM DTT at 37 °C for 45 min, then alkylated by IAA 5.5 mM IAA at 25 °C for 30 min in the dark. The excess IAA was quenched with 4 M DTT at 25 °C for 30 min. To this solution 3x volume of 50 mM TEAB buffer (pH=8) was added, and the proteins were digested by trypsin. The samples were acidified by the addition of FA to 0.5%. The peptides were desalted on SepPak C18 50 mg cartridges (Waters) using vacuum manifold with final elution into 750 µL 0.5% FA, 80% ACN in water and dried in SpeedVac (Thermo Scientific).

Cysteine labelling, click chemistry and DMP-enrichment. 1 mg HeLa cell lysate per sample was diluted to 2 mg/mL protein concentration with 0.2% SDS in PBS. IAA-alkyne (or DMSO for controls) was added to the samples to 1 mM final concentration and the mixture was incubated for 1 h at 25°C 550 rpm. Thereafter, DMP-N₃ / SOX-N₃ was added to 2 mM final concentration together with 2 mM TCEP, 2 mM CuSO₄ and 0.2 mM TBTA. The mixture was incubated for 1.5 h at 25°C at 550 rpm. The proteins were precipitated by addition of 4x volume of acetone and incubation for 2 h at -20°C. Peptides were prepared from the labelled proteome as described in HeLa proteome preparation above.

Spike-in sample preparation.

Peptides prepared from purified proteins were dried in SpeedVac (Thermo Scientific) and reconstituted in 1% FA in water. 25 ng/µl digested HeLa proteome standard was prepared in 1% FA in water. To this solution the prepared peptide solution was mixed to yield a 20 ng/µl theoretical concentration of the spiked-in peptides. From these samples 8 µl was injected in every LC/MS/MS measurement.

Intact protein measurements.

The 10 mM (10 pmol/µl) desalted protein solutions were injected into the Orbitrap Eclipse Tribrid mass spectrometer by the microinjection source. For injection 10 µl/min sample flow was applied, for data acquisition the flow was lowered to 2-4 µl/min. The measurements were carried out in Standard Pressure Mode (8 mtorr) with ion transfer tube temperature set to 320 °C. The full MS scans were acquired on the orbitrap with 120k FWHM (at 200 *m/z*) resolution applying 5 microscans. The AGC target was set to 2e5 allowing maximal ion injection time of 100 ms. FAIMS CV was scanned from -70 to 30 V in 2 V steps to find the optimal setting for each protein. The CV where the most intense protein peaks could be detected were selected for measurement.

Peptide measurements with direct injection.

The desalted 10 mM peptide solutions (calculated from the initial protein concentration assuming 100% peptide recovery) were injected into the Orbitrap Eclipse Tribrid mass spectrometer by the microinjection

source. The measurements were carried out in Standard Pressure Mode (8 mtorr) with ion transfer tube temperature set to 320 °C. The full MS scans were acquired on the orbitrap with 60k FWHM (at 200 m/z) resolution applying 5 microscans. The AGC target was set to $2e5$ allowing maximal ion injection time of 100 ms. FAIMS CV was scanned from -80 to -30 V in 2 V steps to find the optimal setting for the peptide of interest. The CV where the peak of the desired peptide was the most intense was selected for measurement. For MS2 fragmentation the peptide ion of interest was selected on the quadrupole (with a 1.5 m/z window) in all available charge states. Fragmentation parameters were varied systematically, CID energy between 5-50%, HCD energy between 10-40%, ETD reaction time between 2-150 ms.

Standard LC/MS/MS method.

The default LC/MS/MS analysis was performed on the Orbitrap Eclipse Tribrid mass spectrometer (Thermo Fisher Scientific) coupled to an UltiMate3000 Nano-HPLC (Thermo Fisher Scientific) via a NanoFlex source (Thermo Fisher Scientific) and FAIMS interface (Thermo Fisher Scientific). First, peptides were loaded on an Acclaim PepMap 100 μ -precolumn cartridge (5 μ m, 100 Å, 300 μ m ID \times 5 mm, Thermo Fisher Scientific). Then, peptides were separated at 40 °C on a PicoTip emitter (noncoated, 15 cm, 75 μ m ID, 8 μ m tip, New Objective) that was in house packed with Reprosil-Pur 120 C18-AQ material (1.9 μ m, 150 Å, Dr. Maisch GmbH). The gradient was run from 4-35.2% acetonitrile supplemented with 0.1% formic acid during a 150 min method (0-5 min at 4%, 5-6 min to 7%, 7-105 min to 24.8%, 105-126 min to 35.2%, 126-140 at 80%, 140-150 min at 4%) at a flow rate of 300 nL/min. Unless otherwise stated, this LC method was used in all LC/MS/MS analyses. FAIMS was performed with two alternating CVs including -50 V and -70 V with cycle times of 1.7 and 1.3 s respectively. The Orbitrap Eclipse Tribrid Mass Spectrometer was operated in data dependent MS2 mode with following settings: Polarity: positive; MS1 resolution: 240k; MS1 AGC target: standard; MS1 maximum injection time: 50 ms, MS1 scan range: m/z 375-1500; MS2 ion trap scan rate: rapid; MS2 AGC target: standard; MS2 maximum injection time: 35 ms; MS2 isolation window: m/z 1.2; HCD stepped normalized collision energy: 30%; intensity threshold: $1.0e4$ counts; included charge states: 2-6; dynamic exclusion: 60 s; MS2 scan range: m/z 120-1200. The high-resolution MS2 was acquired in orbitrap with 15k resolution.

Data analysis.

To analyse the acquired MS data with MaxQuant the .raw files were split by FAIMS-MzXML-generator (GitHub) to separate the information acquired using different FAIMS CVs. For most analyses the MaxQuant version 1.6.15.0 was used. The spectra were searched against the *in silico* digested Uniprot database for Homo sapiens (taxon identifier: 9606). False discovery rate (FDR) was determined by using a decoy database and set to 1% as thresholds for both peptide-spectrum match and protein levels. In these analyses the focus was on identifications, so no quantification was performed. Carbamidomethylation (+57.0215) was set up as fixed modification except for cysteine labelling experiments, where it was set up as variable modification. Protein N-terminal acetylation (+42.0106) and methionine oxidation (+15.9949) were always included as variable modifications. Other modifications were included in the search depending on the sample. The reverse and potential contaminant identifications as well as identifications from control samples were filtered out. For all the analyses MSFragger version 3.2 was used together with Philosopher 3.4.13 integrated into the graphical user interface FragPipe v15.0. The modification search was performed both in the conventional way (modification of the *in silico* digested peptides and matching to the altered fragmentation spectrum) and with mass offset search (allowing for certain precursor mass shifts for peptide spectrum matching). To achieve this, the mass of the modifications were supplied both as a variable modification on certain amino acids and as mass offsets restricted to the same amino acids. For the mass offset search, the labile modification mode was used, where the diagnostic fragment masses were defined. This search mode was only activated if the diagnostic ion intensity exceeded the relative intensity threshold of 10%. In AMPylation searches Y-ion mass of 79.9663 was also provided corresponding to the neutral loss off the adenosine fragment from the intact peptide. Validation of the identifications was performed by the TransProteomic Pipeline tools PeptideProphet and ProteinProphet.

DMP-enrichment.

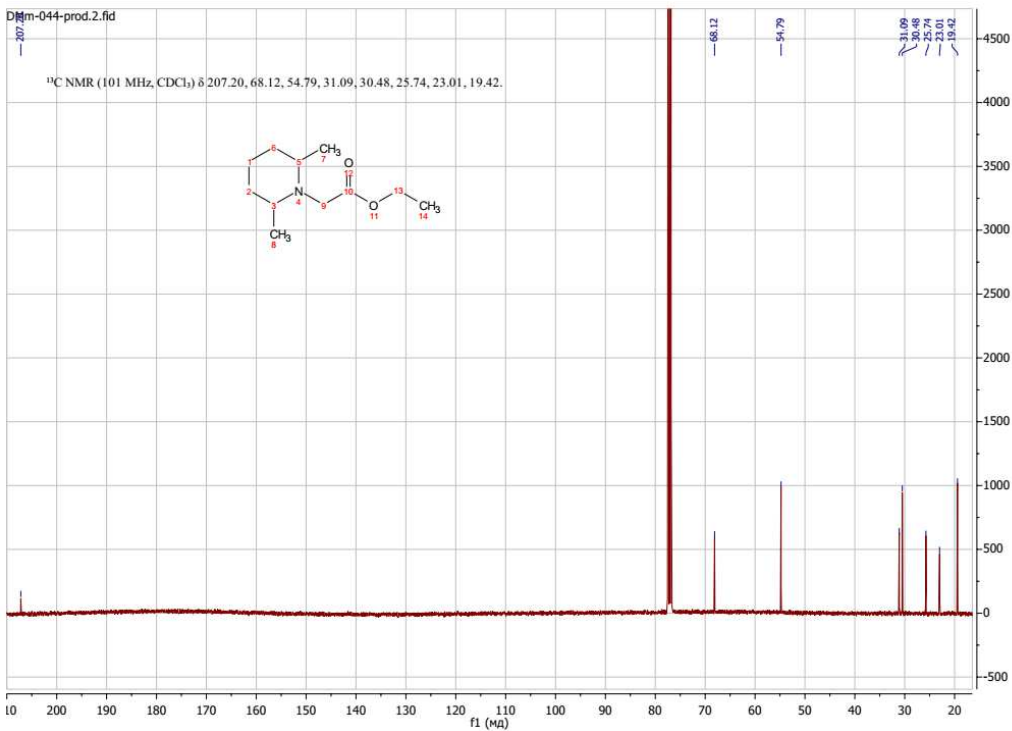
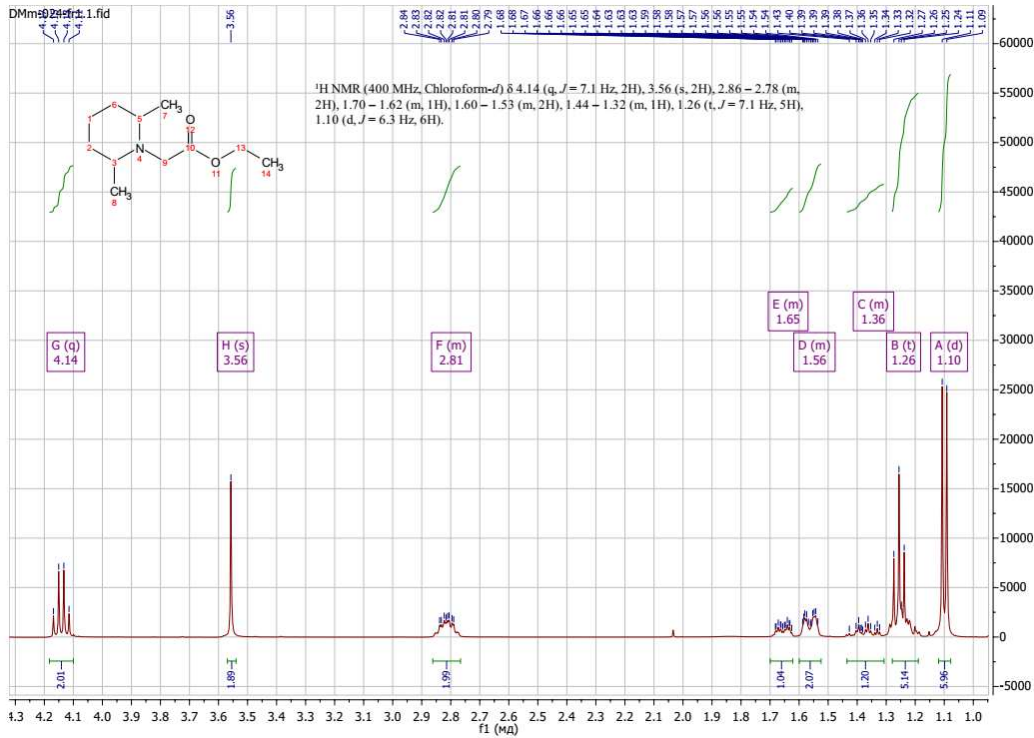
1 mg HeLa cell lysate per sample was diluted to 2 mg/mL protein concentration with 0.2% SDS in PBS. IAA-alkyne was added to the samples to 1 mM final concentration and the mixture was incubated for 1 h at 25°C. Thereafter, DMP-N3 was added to 2 mM final concentration together with 2 mM TCEP, 2 mM CuSO₄ and 0.2 mM TBTA. The mixture was incubated for 1.5 h at 25°C. The proteins were precipitated by the addition of 4× volume of acetone and incubation for 2 h or overnight at -20°C. Peptides were prepared from the labelled proteome as described in HeLa proteome preparation above. Dried peptides were redissolved in IP buffer (50 mM Tris HCl pH=8, 250 mM NaCl) to a final theoretical peptide concentration of 2 mg/mL. 2 µL of these solutions were taken for full proteome measurements. The rest was loaded on 100 µL equilibrated anti-TMT resin (Thermo Fisher Scientific) and incubated for 16 h at 4°C. The supernatant was removed, and the beads were washed with 2×500 µL 2M urea in IP buffer, 2×500 µL 0.05% SDS in IP buffer, 2×500 µL IP buffer and 2×500 µL water. The captured peptides were eluted by 3×500 µL TMT elution buffer (Thermo Fisher Scientific). The eluate was desalted on SepPak C18 50 mg cartridges (Waters) as described above, and dried in SpeedVac (Thermo Scientific). Peptides were reconstituted in 25 µL 1% FA in water for MS measurement.

Data availability.

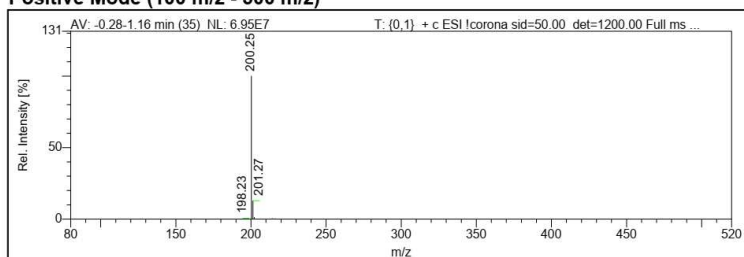
Mass spectrometry-based proteomics data have been deposited at ProteomeXchange and are publicly available as of the date of publication. The accession number is PXD030608.

NMR and MS Spectra of Small Compounds.

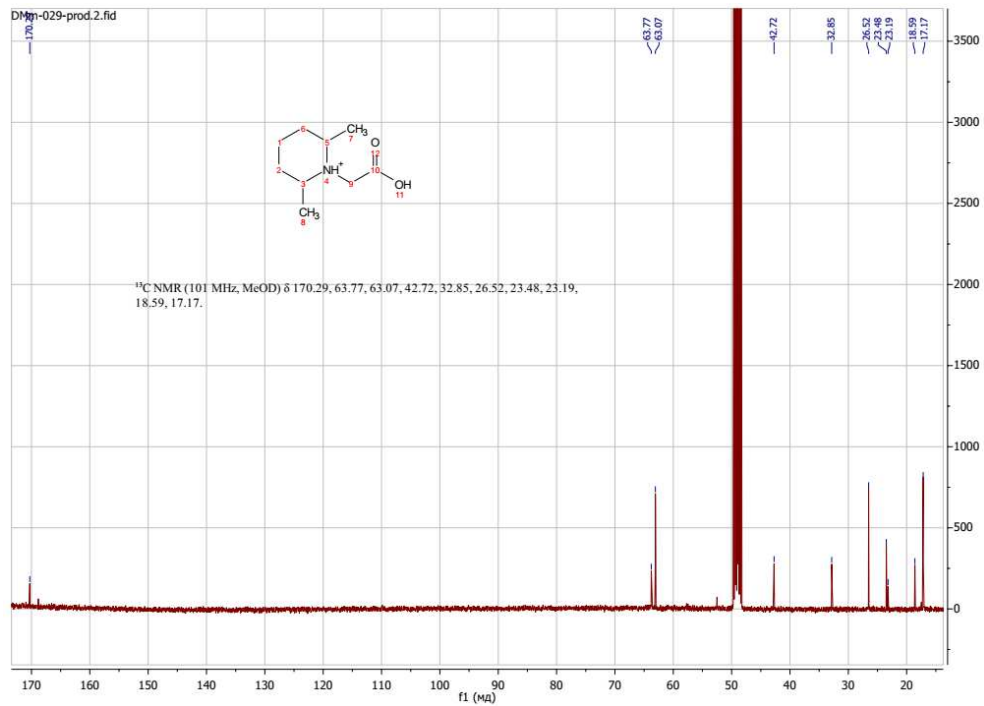
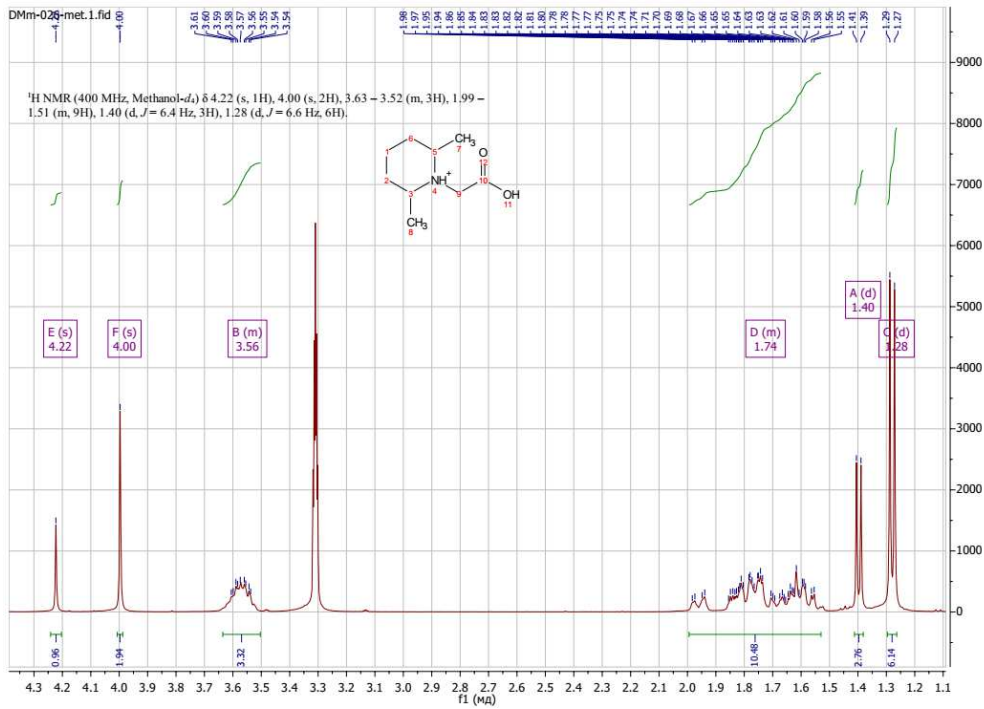
Ethyl 2-(2,6-dimethylpiperidin-1-yl)acetate (7)



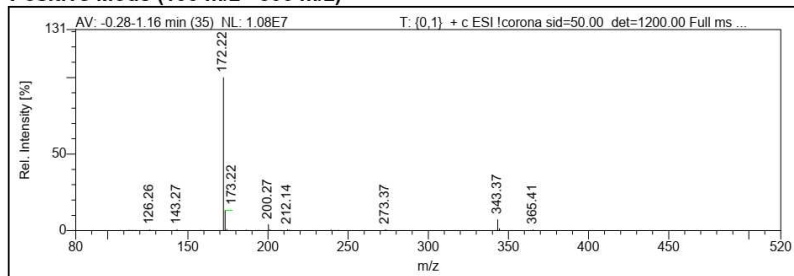
Positive Mode (100 m/z - 500 m/z)



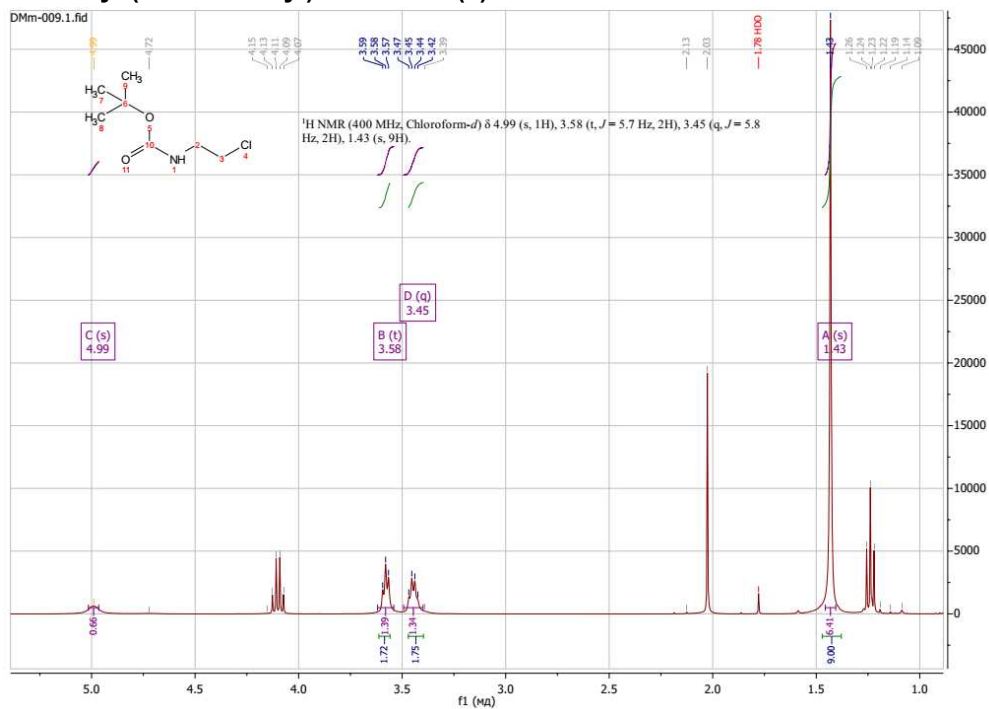
2-(2,6-Dimethylpiperidin-1-yl)acetic acid (1)



Positive Mode (100 m/z - 500 m/z)



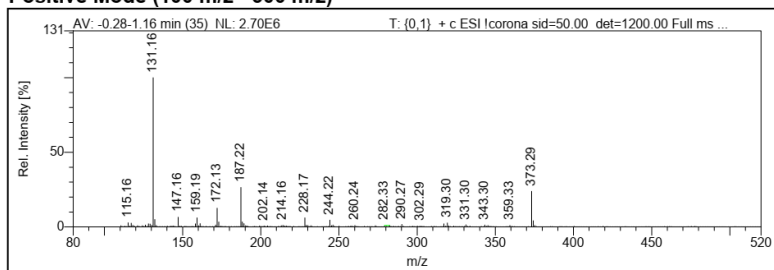
tert-Butyl (2-chloroethyl)carbamate (8)



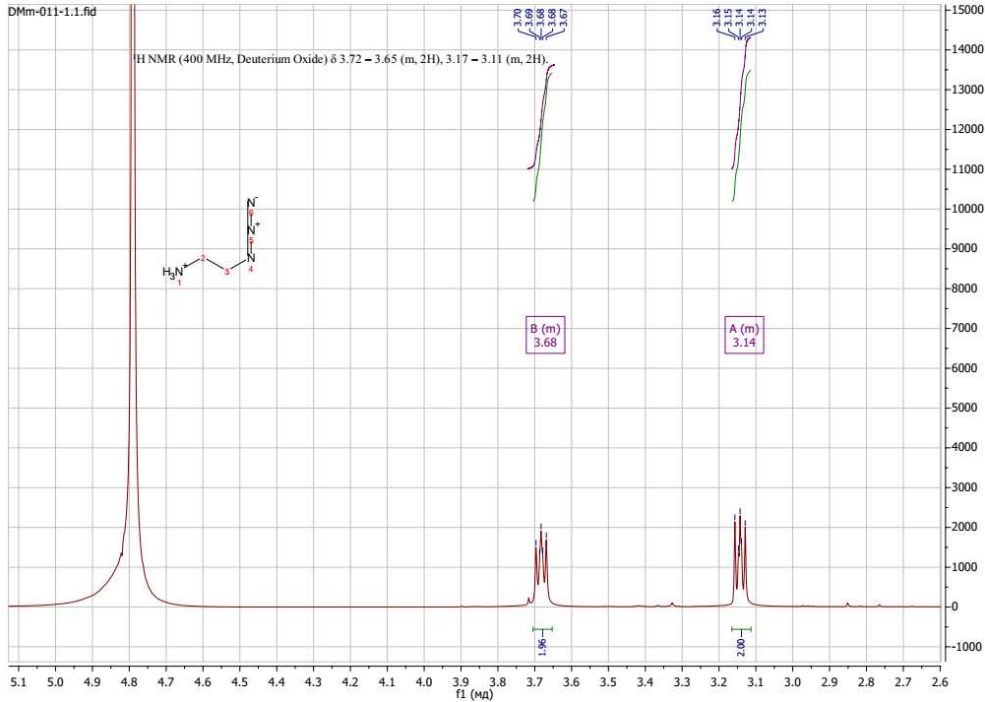
tert-Butyl (2-azidoethyl)carbamate (10)



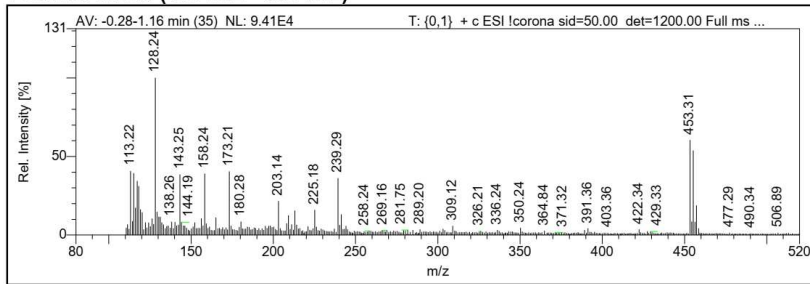
Positive Mode (100 m/z - 500 m/z)



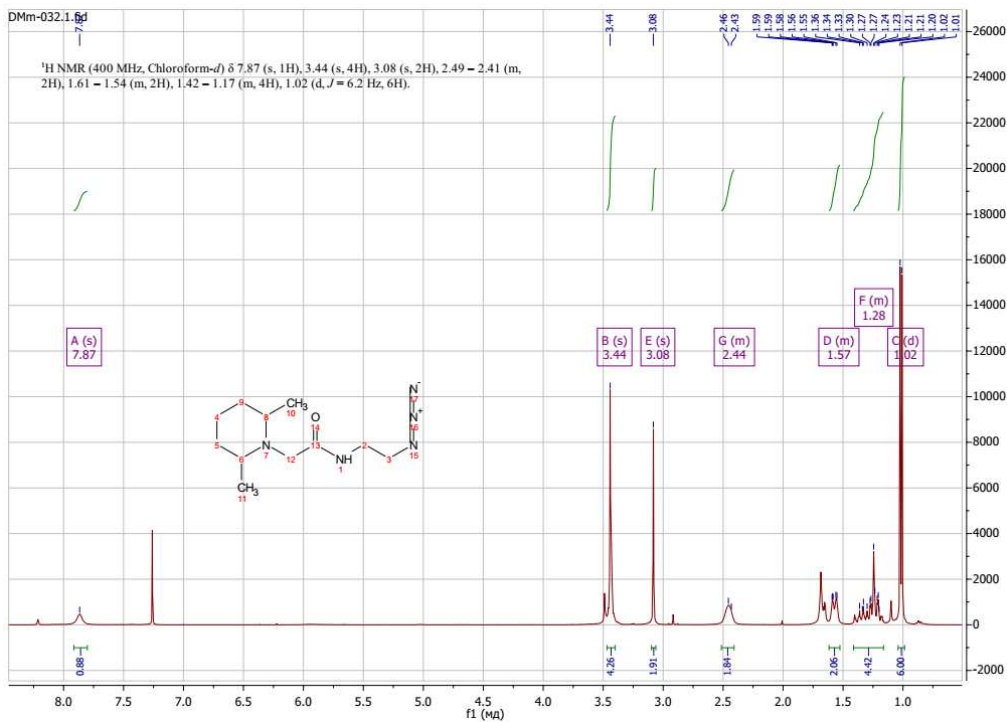
2-Azidoethan-1-amine hydrochloride (11)

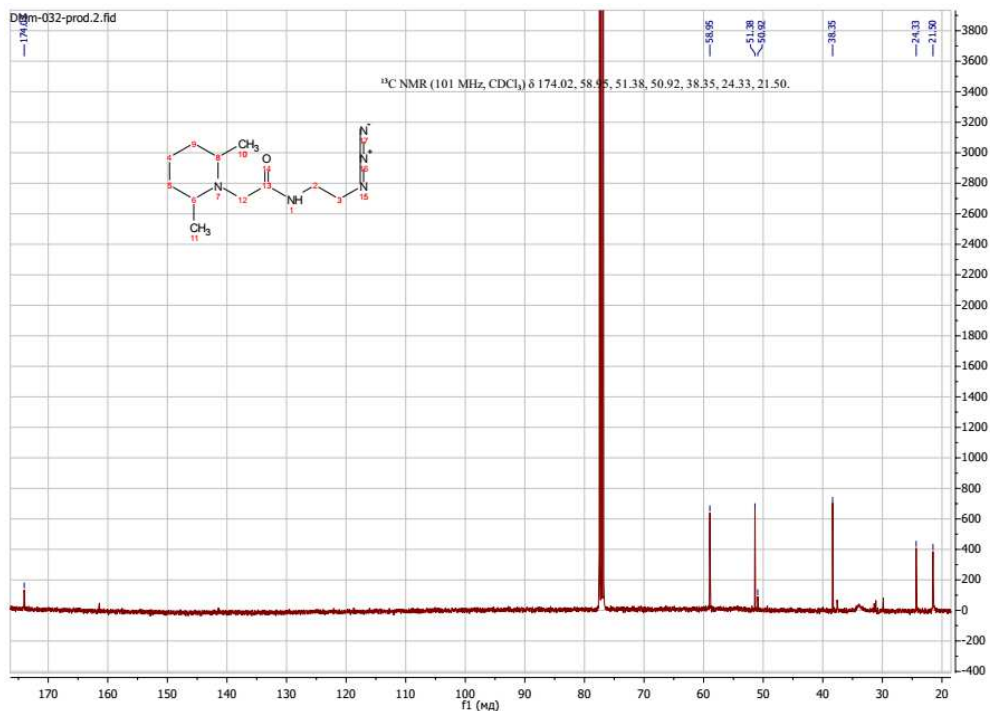


Positive Mode (100 m/z - 500 m/z)

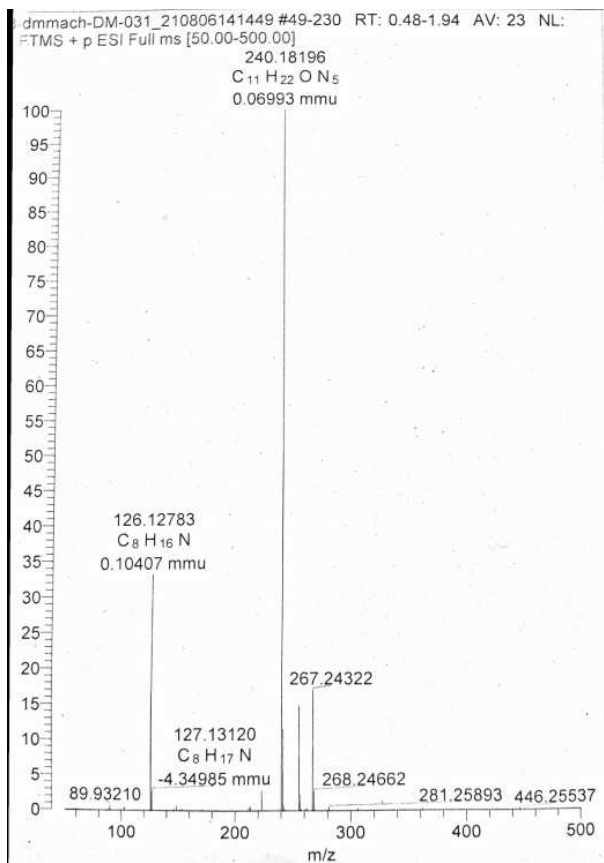
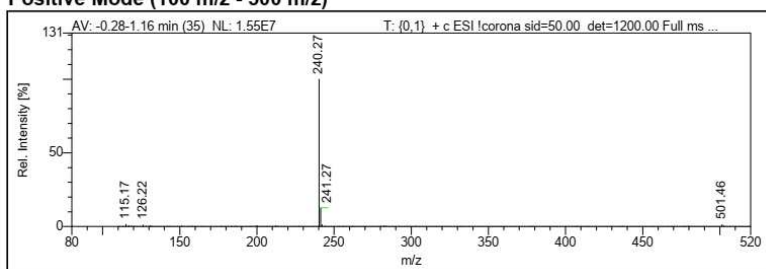


N-(2-azidoethyl)-2-(2,6-dimethylpiperidin-1-yl)acetamide (12)

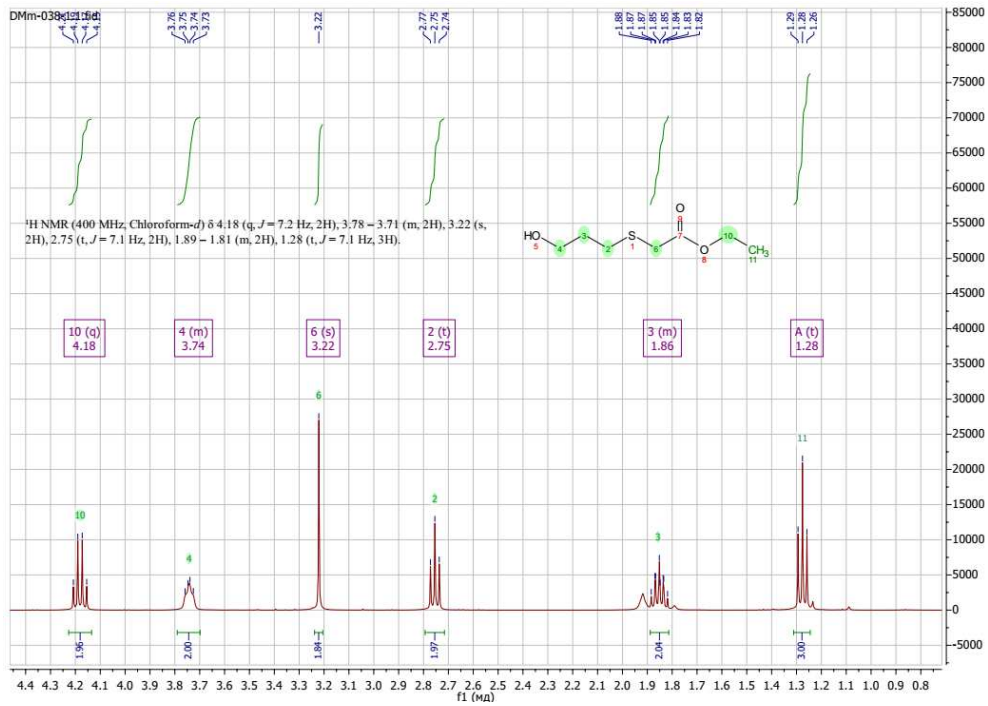
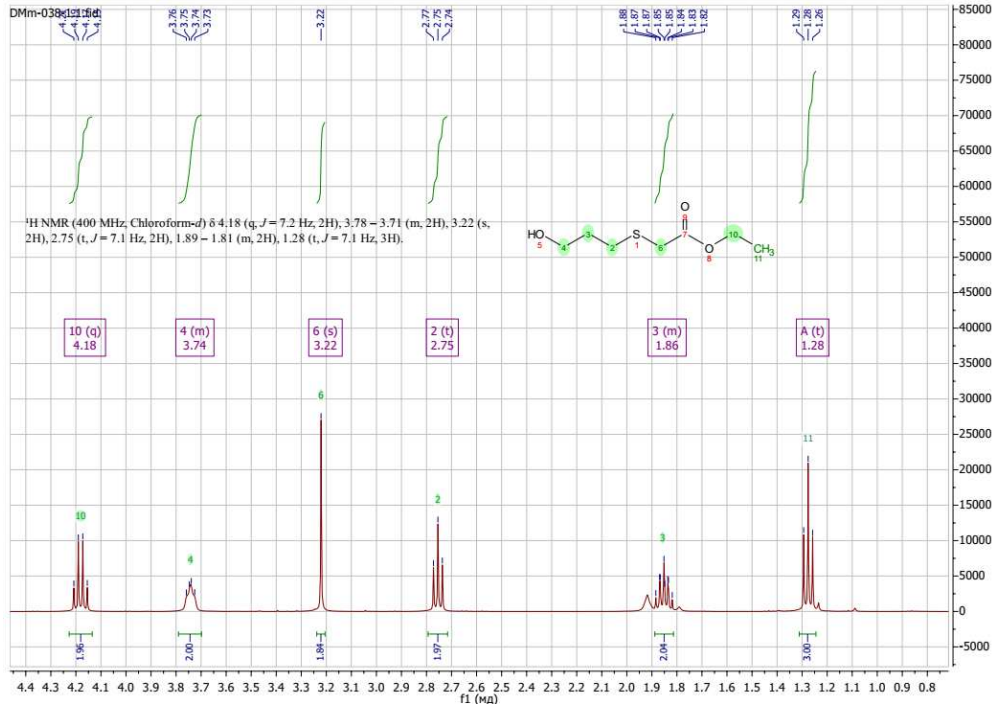


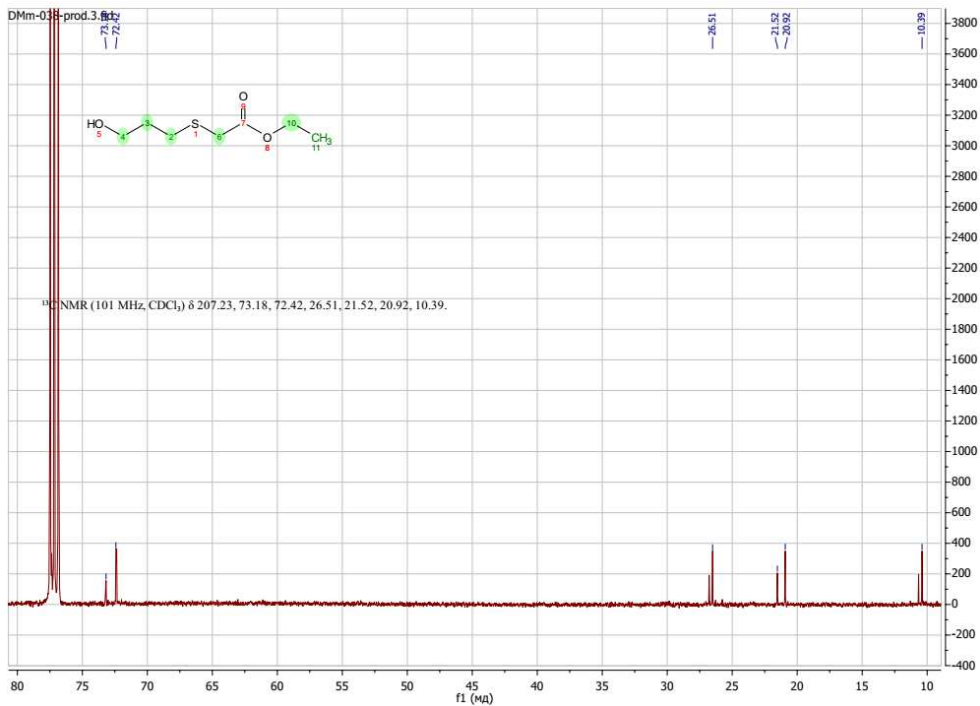


Positive Mode (100 m/z - 500 m/z)

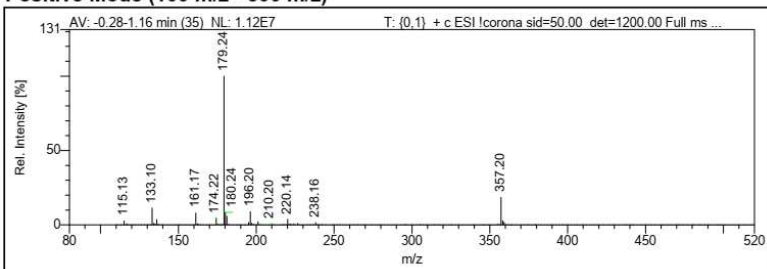


Ethyl 2-((3-hydroxypropyl)thio)acetate (12)

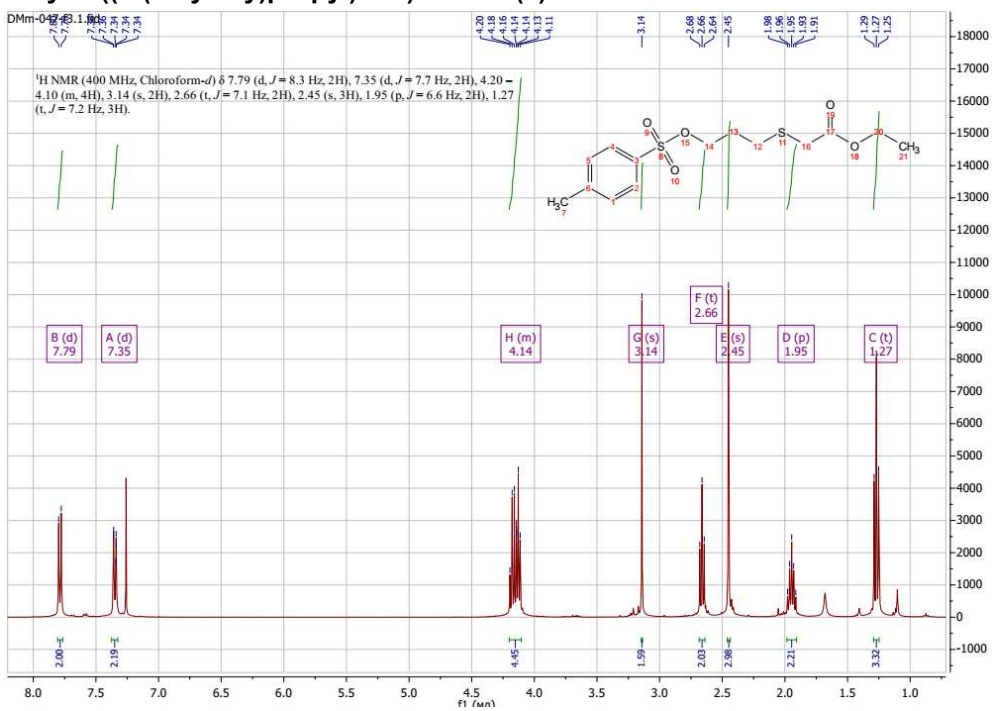


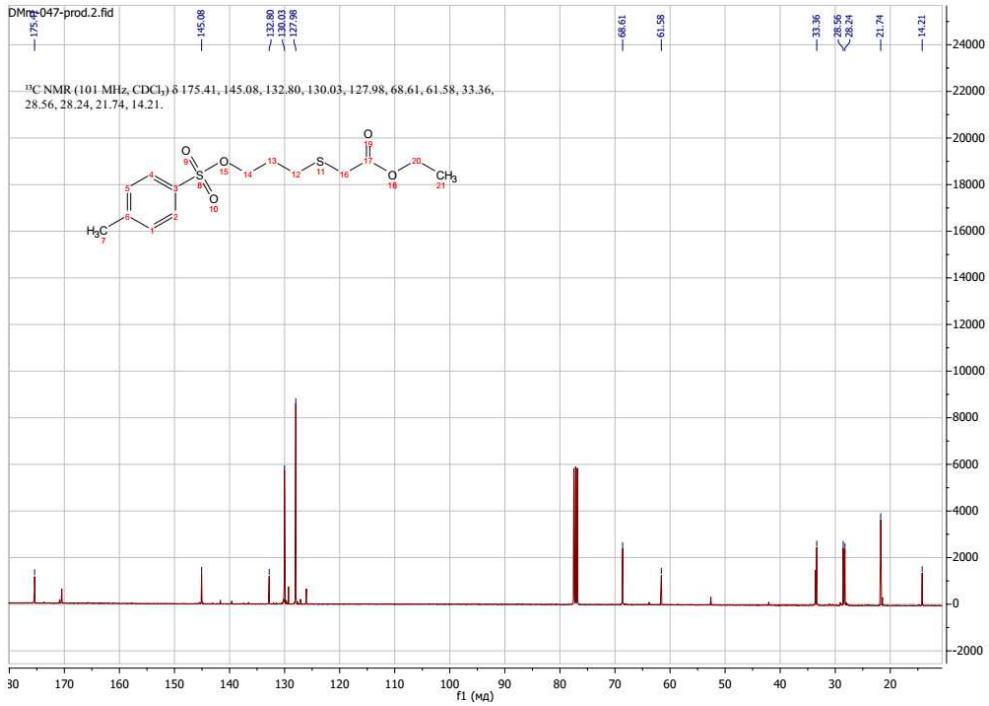


Positive Mode (100 m/z - 500 m/z)

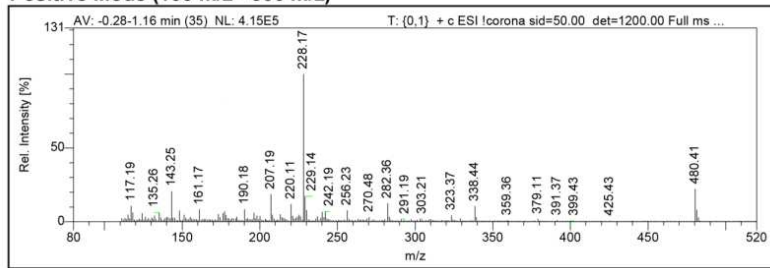


Ethyl 2-((3-(tosyloxy)propyl)thio)acetate (2)

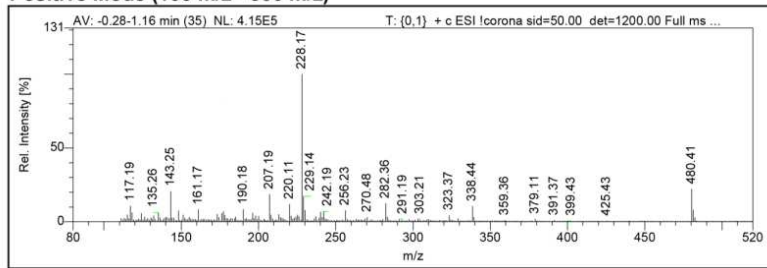




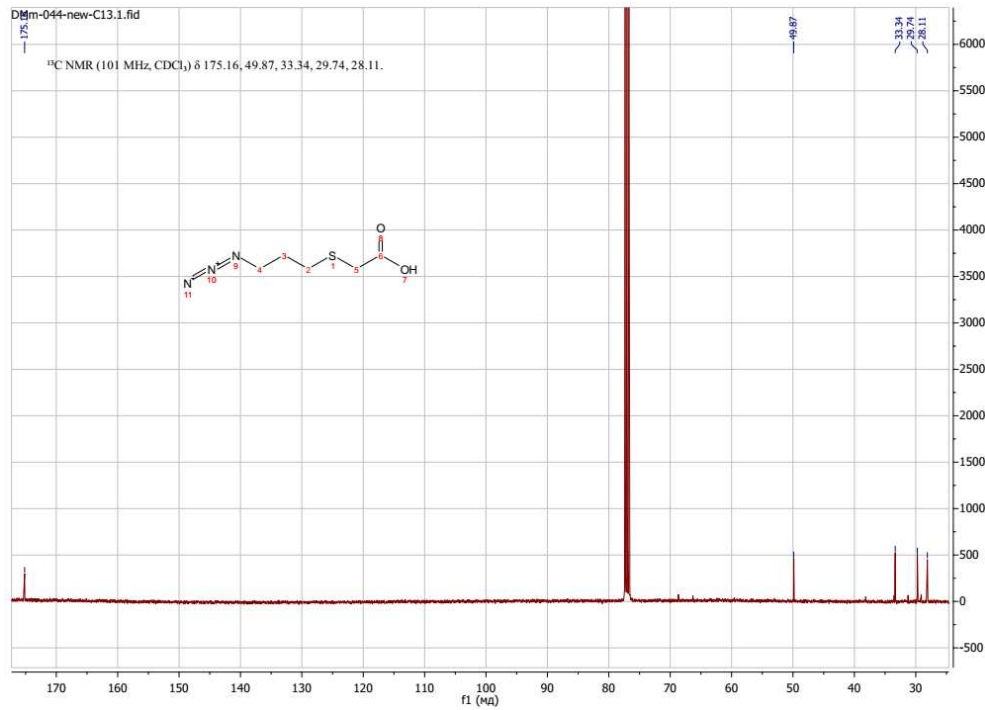
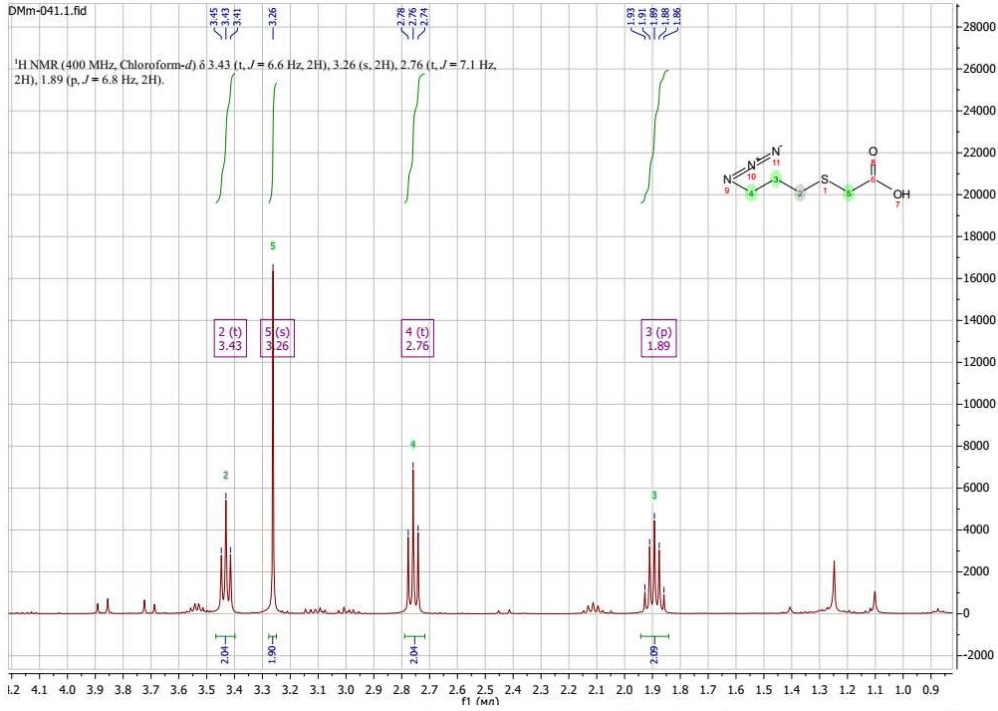
Positive Mode (100 m/z - 500 m/z)



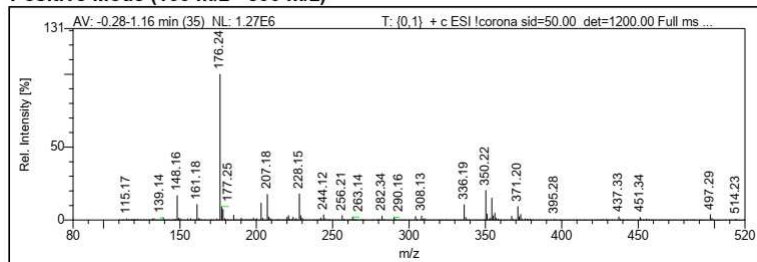
Positive Mode (100 m/z - 500 m/z)



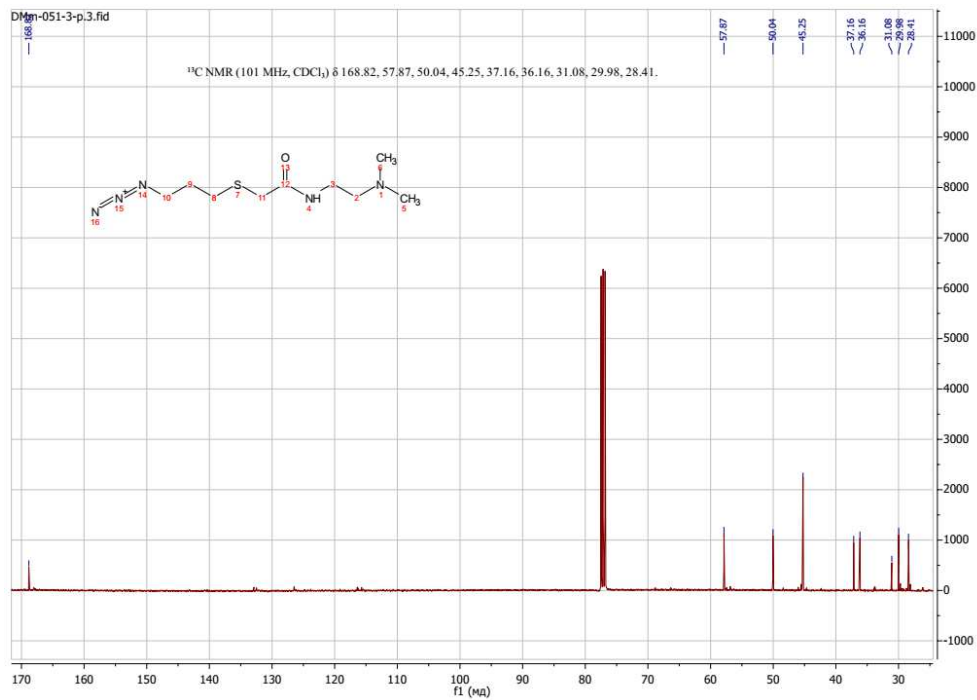
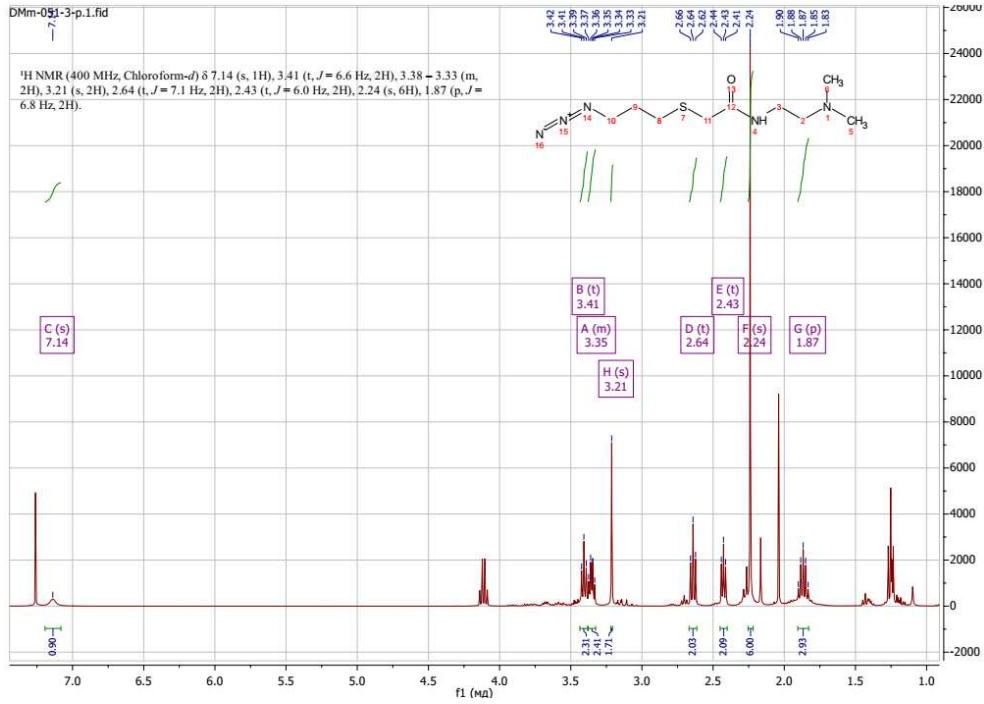
2-((3-azidopropyl)thio)acetic acid (3)



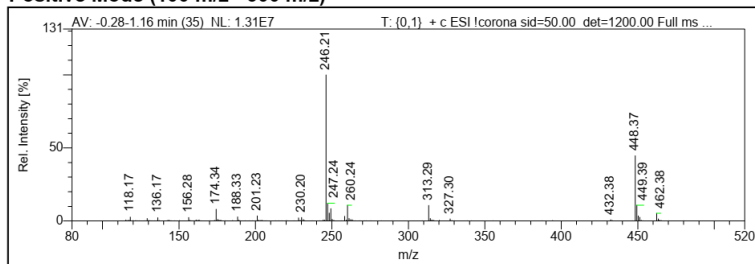
Positive Mode (100 m/z - 500 m/z)



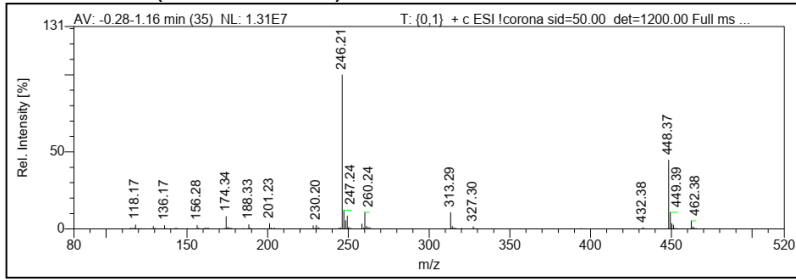
2-((3-Azidopropyl)thio)-N-(2-(dimethylamino)ethyl)acetamide (4)



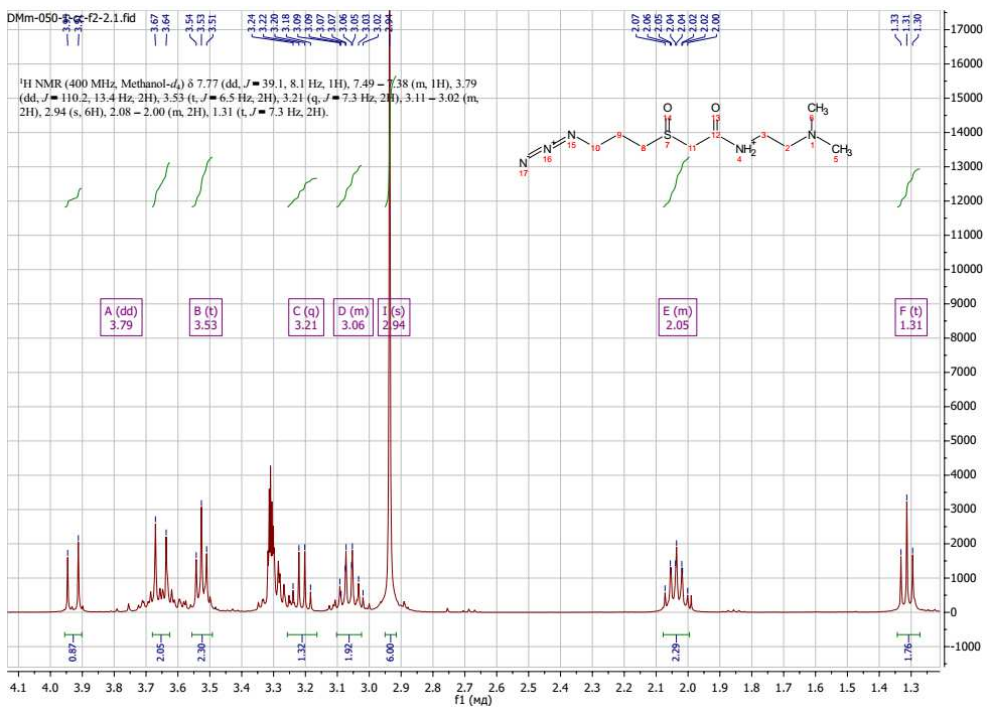
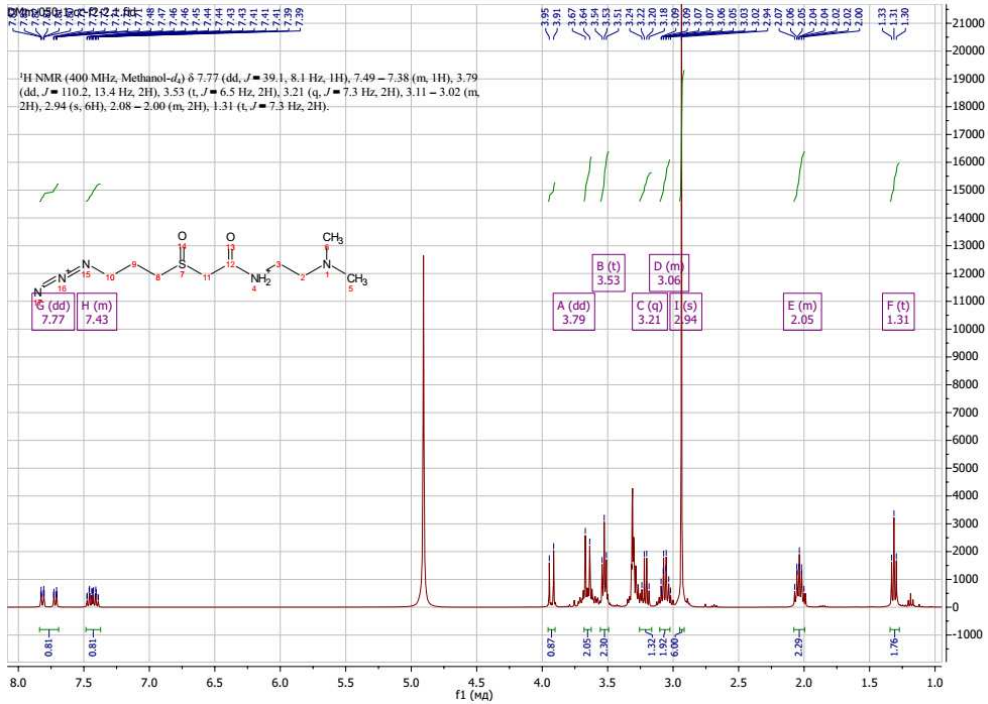
Positive Mode (100 m/z - 500 m/z)



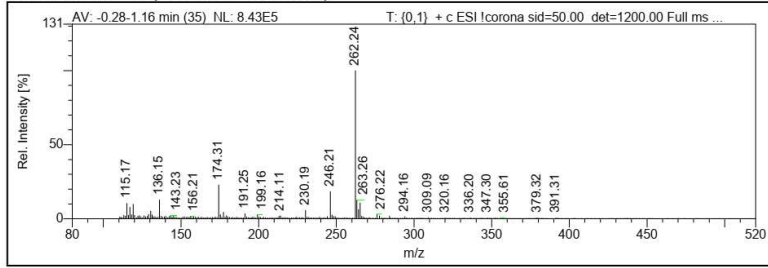
Positive Mode (100 m/z - 500 m/z)



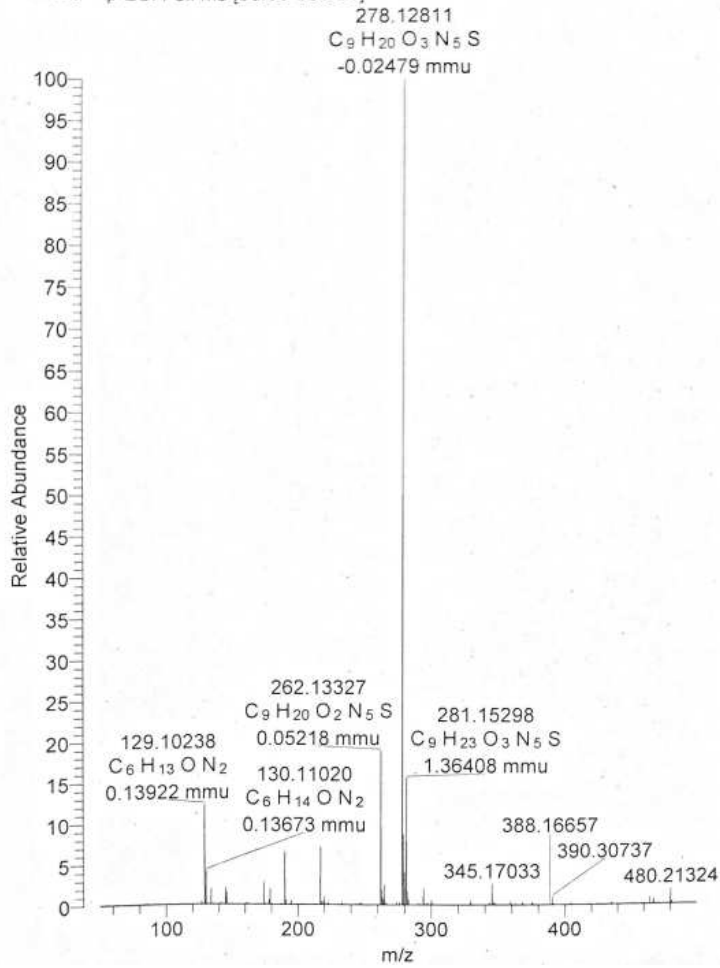
2-((3-Azidopropyl)sulfinyl)-N-(2-(dimethylamino)ethyl)acetamide (14)



Positive Mode (100 m/z - 500 m/z)



09-dmmach-DM-067 #49-227 RT: 0.56-1.97 AV: 22 NL: 1.92E6
 F: FTMS + p ESI Full ms [50.00-500.00]



8.2. Supplementary information for “Chemical Proteomics Reveals Protein Tyrosination Extends Beyond the Alpha-Tubulins in Human Cells”

Makarov, D.; Kielkowski, P. Chemical Proteomics Reveals Protein Tyrosination Extends Beyond the Alpha-Tubulins in Human Cells**. ChemBioChem 2022, 23 (23), e202200414. <https://doi.org/10.1002/cbic.202200414>.

ChemBioChem

Supporting Information

Chemical Proteomics Reveals Protein Tyrosination Extends Beyond the Alpha-Tubulins in Human Cells**

Dmytro Makarov and Pavel Kielkowski*

Table of Contents

Supplementary Figures	3
Supplementary Tables.....	11
Organic synthesis	13
Synthesis of (<i>tert</i> -butoxycarbonyl)-L-tyrosine (2) ^[1]	13
Synthesis of prop-2-yn-1-yl (<i>S</i>)-2-amino-3-(4-(prop-2-yn-1-yloxy)phenyl)propanoate (4) ^[1]	13
Synthesis of (<i>S</i>)-2-amino-3-(4-(prop-2-yn-1-yloxy)phenyl)propanoic acid (Tyr-O-Alk, 6) ^[3]	14
Synthesis of ONBY	14
Synthesis of <i>tert</i> -butyl L-tyrosinate (7) ^[4]	14
Synthesis of <i>tert</i> -butyl (<i>tert</i> -butoxycarbonyl)-L-tyrosinate (8).....	15
Synthesis of <i>tert</i> -butyl (<i>S</i>)-2-((<i>tert</i> -butoxycarbonyl)amino)-3-(4-((2-nitrobenzyl)oxy)phenyl)propanoate (9)	15
Synthesis of (<i>S</i>)-2-amino-3-(4-((2-nitrobenzyl)oxy)phenyl)propanoic acid (10)	16
Biochemistry	17
Cell lines	17
SH-SY5Y cell line	17
iNGNs cell line	17
Cells treatment and harvesting	18
Lysates preparation	18
Protein concentration measurement	18
SP2E workflow large scale.....	18
In-gel analysis of the enriched proteins.....	19
Sample preparation for MS analysis.....	19
SP2E workflow small scale	20
In-gel analysis.....	20
Western blot.....	20
Whole proteome samples preparation	21
Enrichments with trifunctional linker (5/6-TAMRA-N ₃ -biotin).....	21
Tubulin fraction isolation.....	21
Fluorescence microscopy.....	22
Cytotoxicity measurement.....	23
Competition experiment.....	23
CHX inhibition experiment.....	23

MS measurement.....	23
Quantification and statistical analysis.....	24
NMR Spectra.....	26
References	30

Supplementary Figures

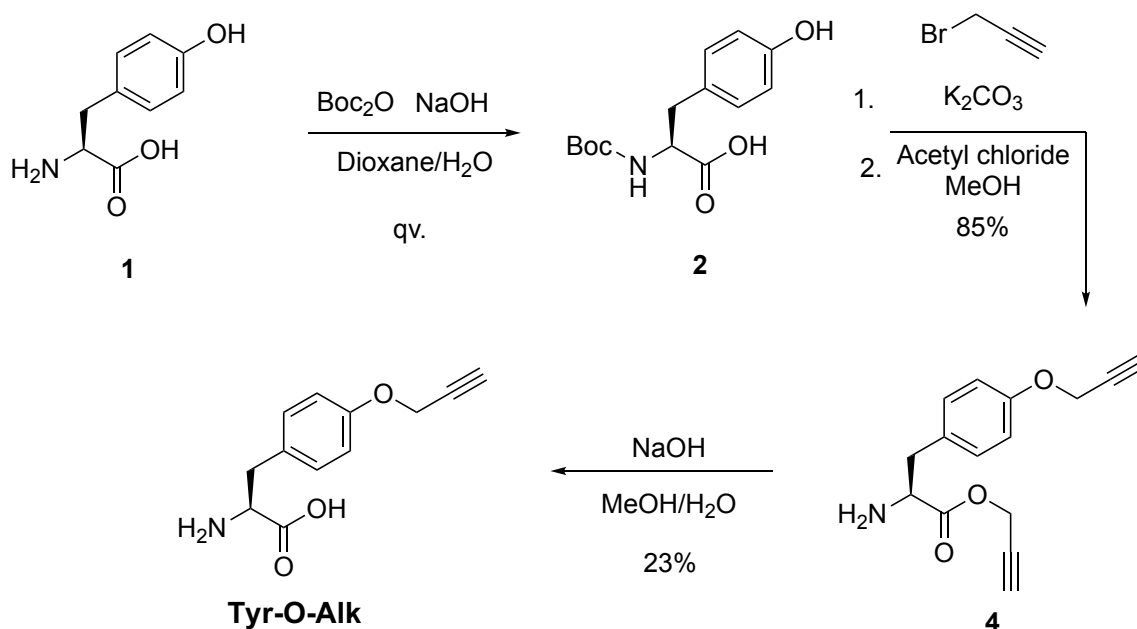


Figure S1. Synthesis of the **Tyr-O-Alk** probe. The three-step synthesis starts with L-tyrosine **1** to Boc-protected L-tyrosine **2**, which enters nucleophilic substitution reaction with subsequent deprotection of Boc group. The ester hydrolysis of the compound **4** results in the desired probe.

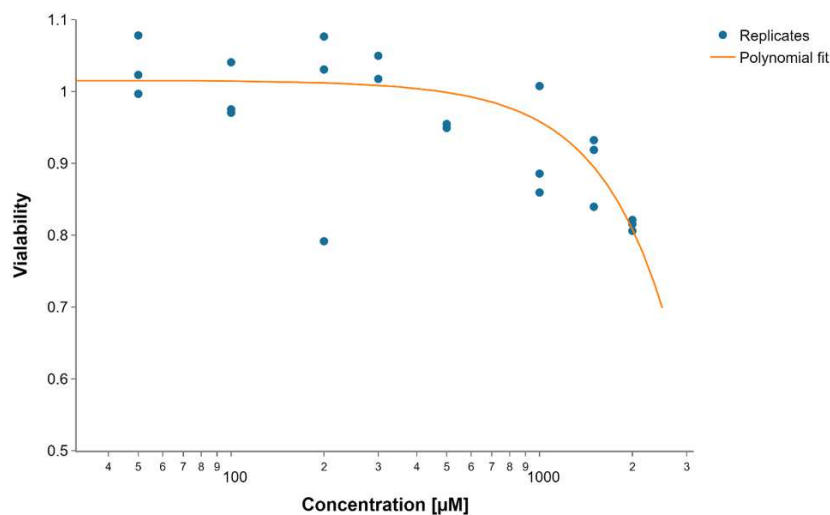


Figure S2. **Tyr-O-Alk** MTT cytotoxicity evaluation in SH-SY5Y cells. The final concentration of the probe is plotted on x-axis in \log_{10} -scale; y-axis represents viability. Viability of the control group was set to 1.

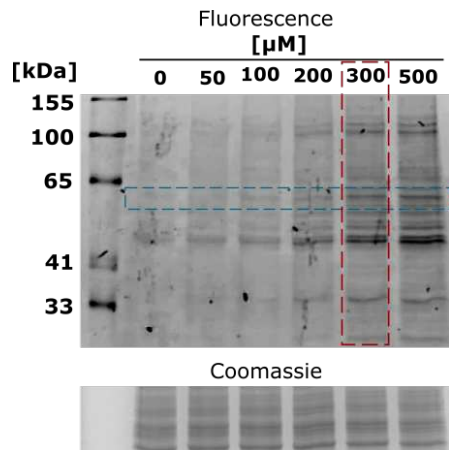


Figure S3. In-gel fluorescence analysis of dose-dependent labelling in SH-SY5Y cells with **Tyr-O-Alk** probe. Probe concentration of 0.3 mM was used within the study.

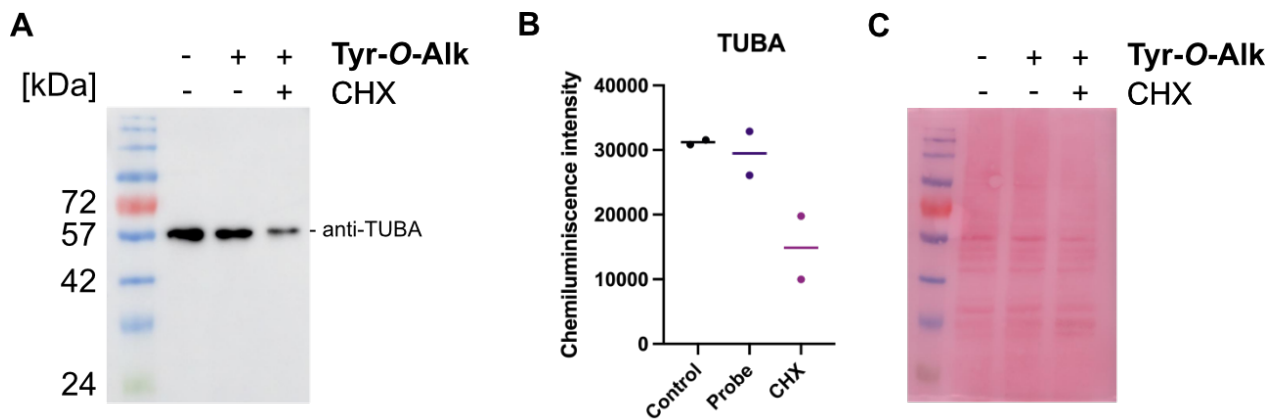


Figure S4. The quantification of α -tubulin levels by western blot after CHX treatment of SH-SY5Y cells. **A)** The representative western blot using the anti-TUBA antibody. **B)** Plot showing the changes in TUBA after probe and CHX treatment. The line shows median. **C)** Ponceau S staining for protein loading control.

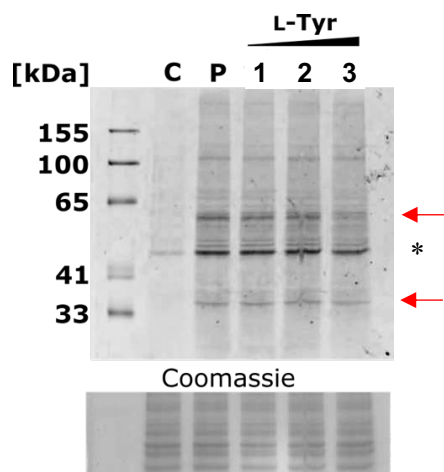


Figure S5. Competition experiment between natural L-tyrosine (**L-Tyr**) and the **Tyr-O-Alk** probe. Negative control (**C**): cells were treated with plain solvent. Positive control (**P**): cells were treated

with **Tyr-O-Alk** probe. Samples 1, 2 and 3 contain a mixture of **Tyr-O-Alk** and **L-Tyr** in following ratios 1:0.1; 1:1 and 1:10. The red arrows point to fluorescent band stemming from estimated tubulin (~50 kDa) and MAPRE1 (~30 kDa) labelling. A star marks an unspecific TAMRA-N₃ labelling.

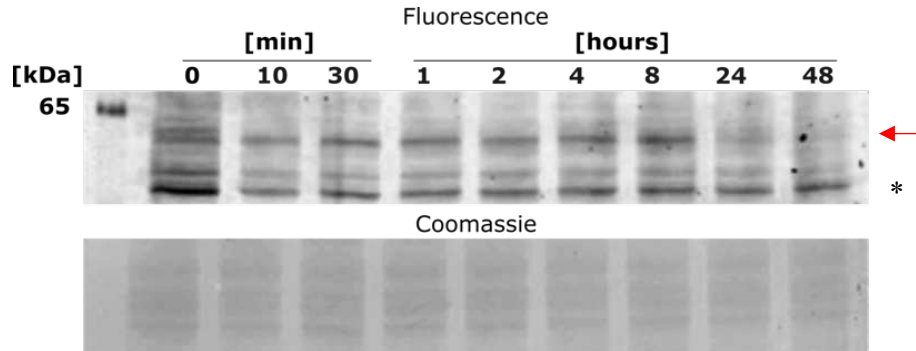


Figure S6. Turnover of the **Tyr-O-Alk** probe in SH-SY5Y cells. After one day of SH-SY5Y cells incubation with the **Tyr-O-Alk** probe, the medium was exchanged for the probe-free media. Cells were harvested at different time points after the media exchange. The red arrow points to a ~50 kDa band of the tubulins. An asterisk marks an unspecific TAMRA-N₃ labelling.

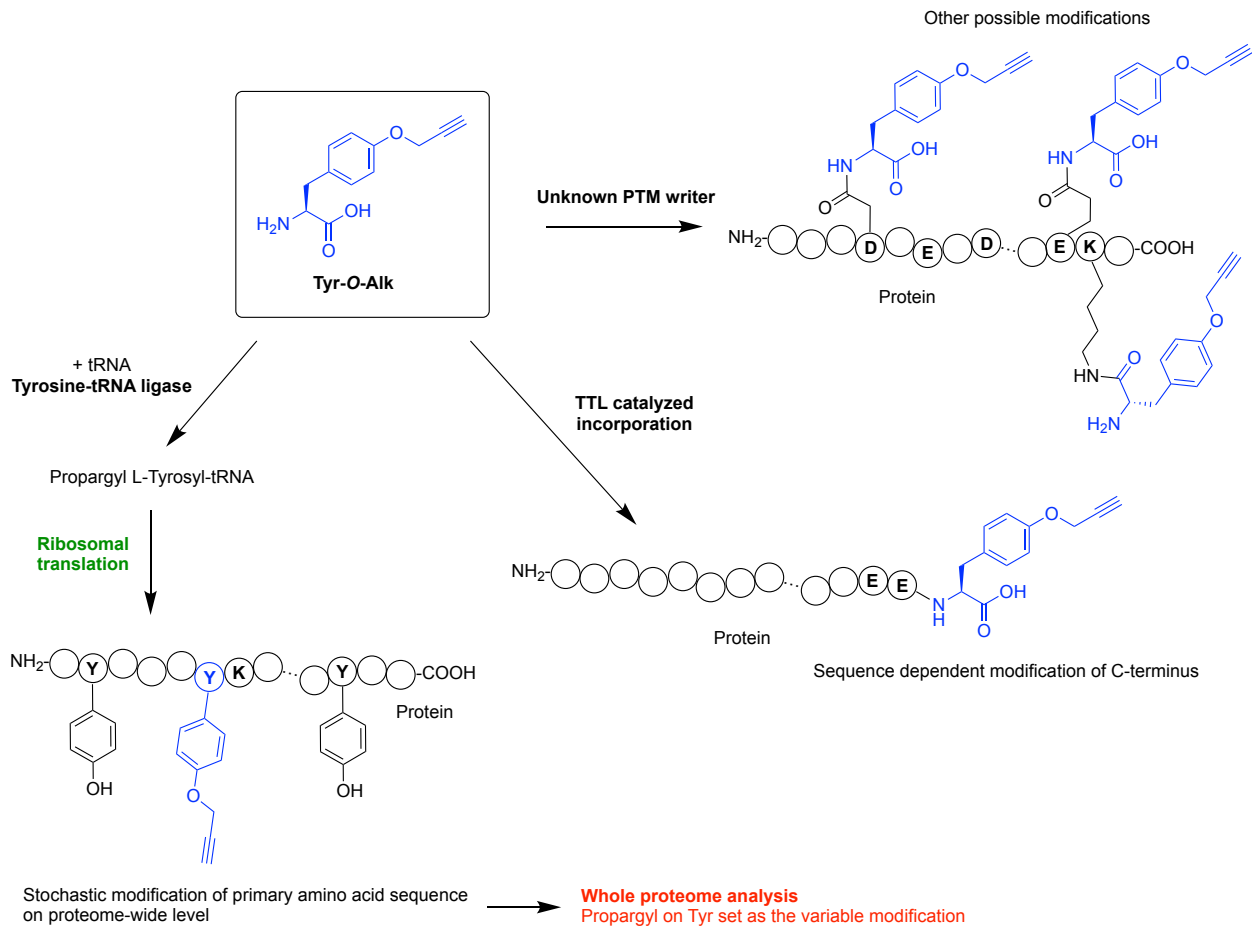


Figure S7. Visualization of possible **Tyr-O-Alk** probe incorporation into protein primary amino acid sequence and post-translational incorporation catalyzed by TTL or other PTM writers.

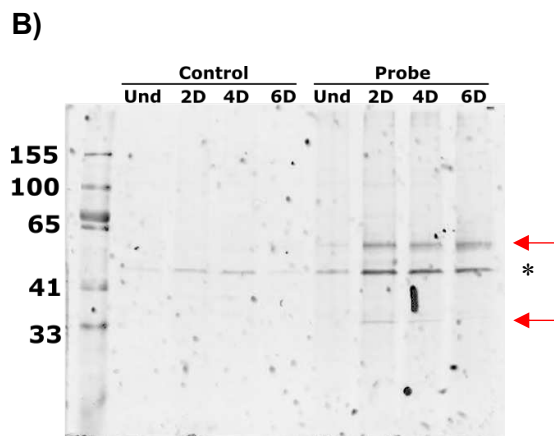
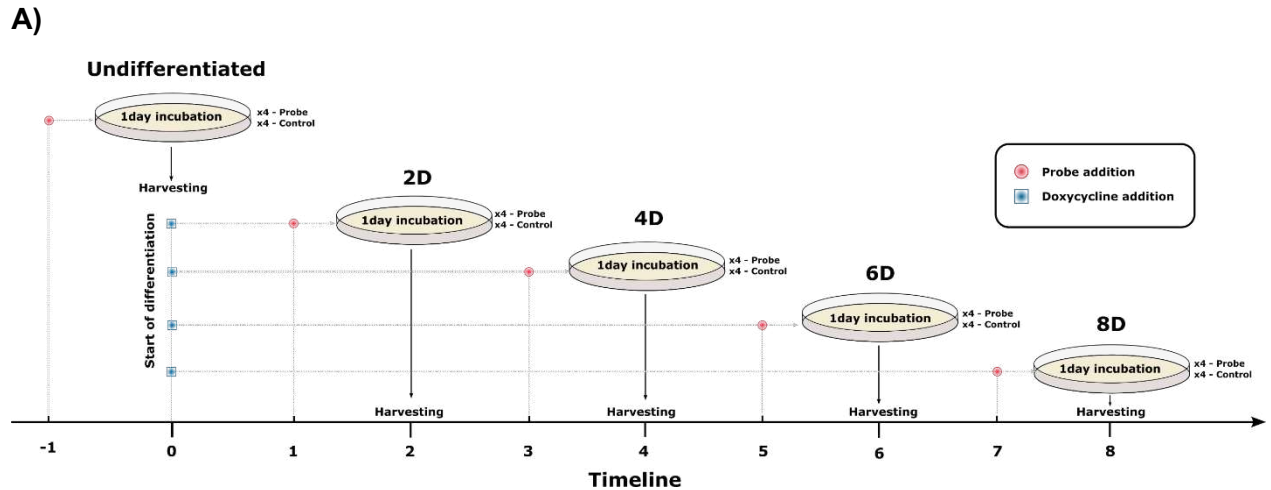


Figure S8. A) iNGNs probe treatment and harvesting scheme. **B)** In-gel fluorescence imaging from iNGNs cells upon the **Tyr-O-Alk** probe treatment during iNGNs differentiation. **Und**: undifferentiated iNGNs stem cells, **2D, 4D, 6D, 8D**: differentiated iNGNs cells after two, four, six and eight days after DOX addition. **Control (control)**: without addition of the **Tyr-O-Alk** probe, and probe-treated (**probe**) samples with the **Tyr-O-Alk** probe. The red arrows point to fluorescent band stemming from estimated tubulin (~50 kDa) and MAPRE1 (~30 kDa) labelling. A star marks an unspecific TAMRA-N₃ labelling.

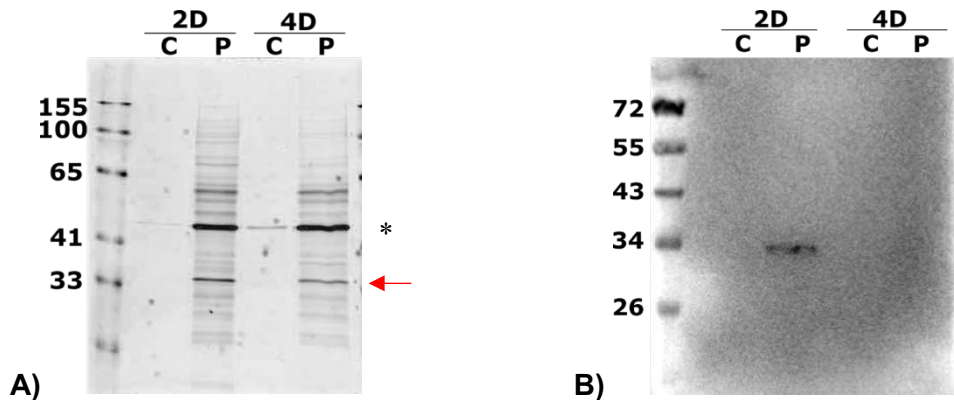


Figure S9. The SP2E enrichment of the **Tyr-O-Alk** probe treated iNGNs using the trifunctional linker (TAMRA-N₃-biotin). **A)** In-gel fluorescence after proteins elution from the streptavidin-coated

magnetic beads. **B)** Western blot with anti-MARPRE1 antibody. Differentiated iNGNs cells, two (2D) and four (4D) days after differentiation started. (C) – control set of cells without addition of the probe; (P) - probe-treated cells. The red arrow point to fluorescent band stemming from estimated MAPRE1 (~30 kDa) labelling. A star marks an unspecific TAMRA-N₃ labelling.

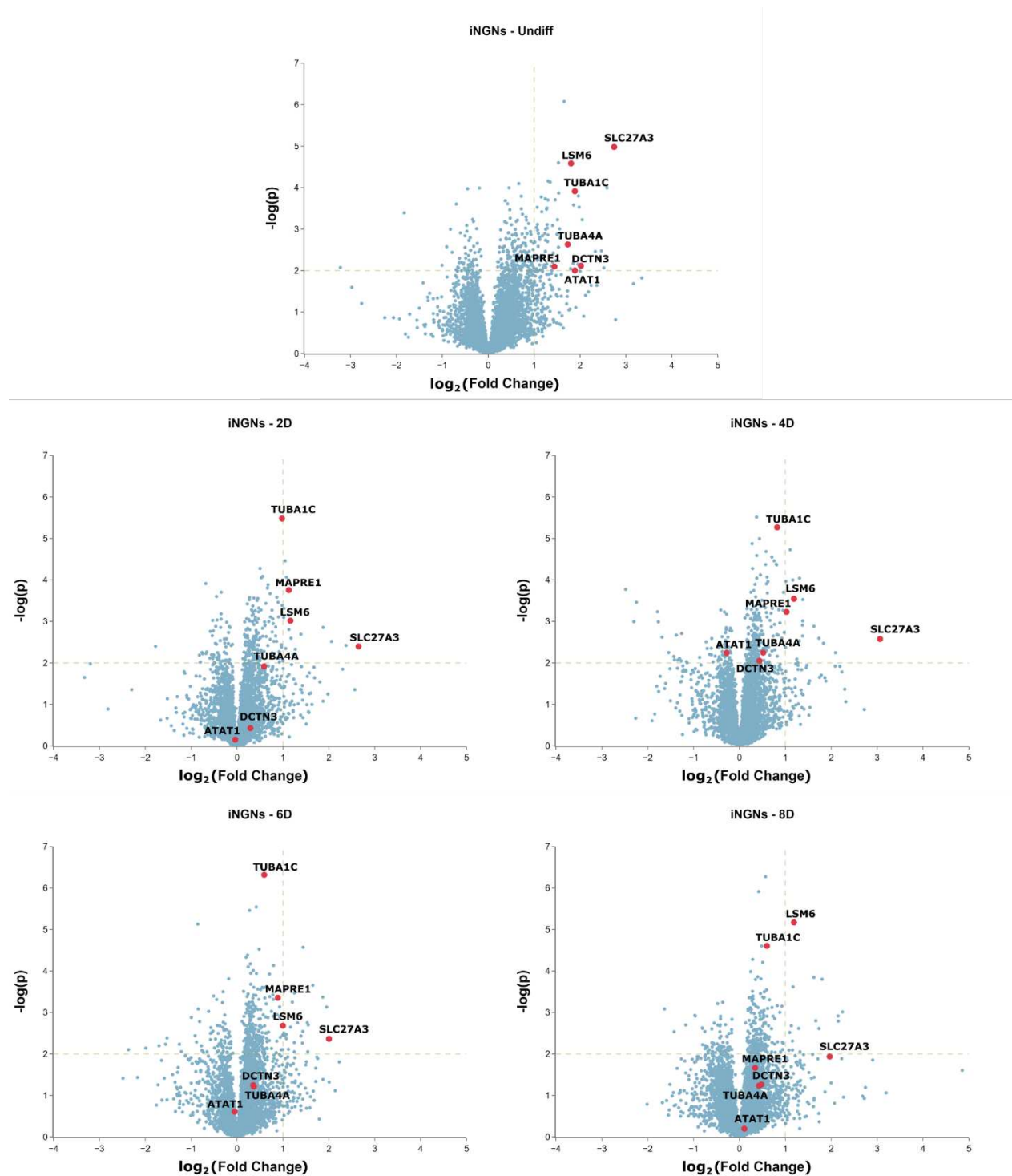


Figure S10. Volcano plots showing enrichment of tyrosinated proteins during iNGNs differentiation. The x-axis represents fold enrichment (probe – control) in \log_2 -scale. Vertical axis is a negative \log_{10} from p -value (statistical significance), $n = 4$. The red dots show α -tubulins and other proteins of interest which were enriched in at least two experiments (iNGNs and SH-SY5Y).

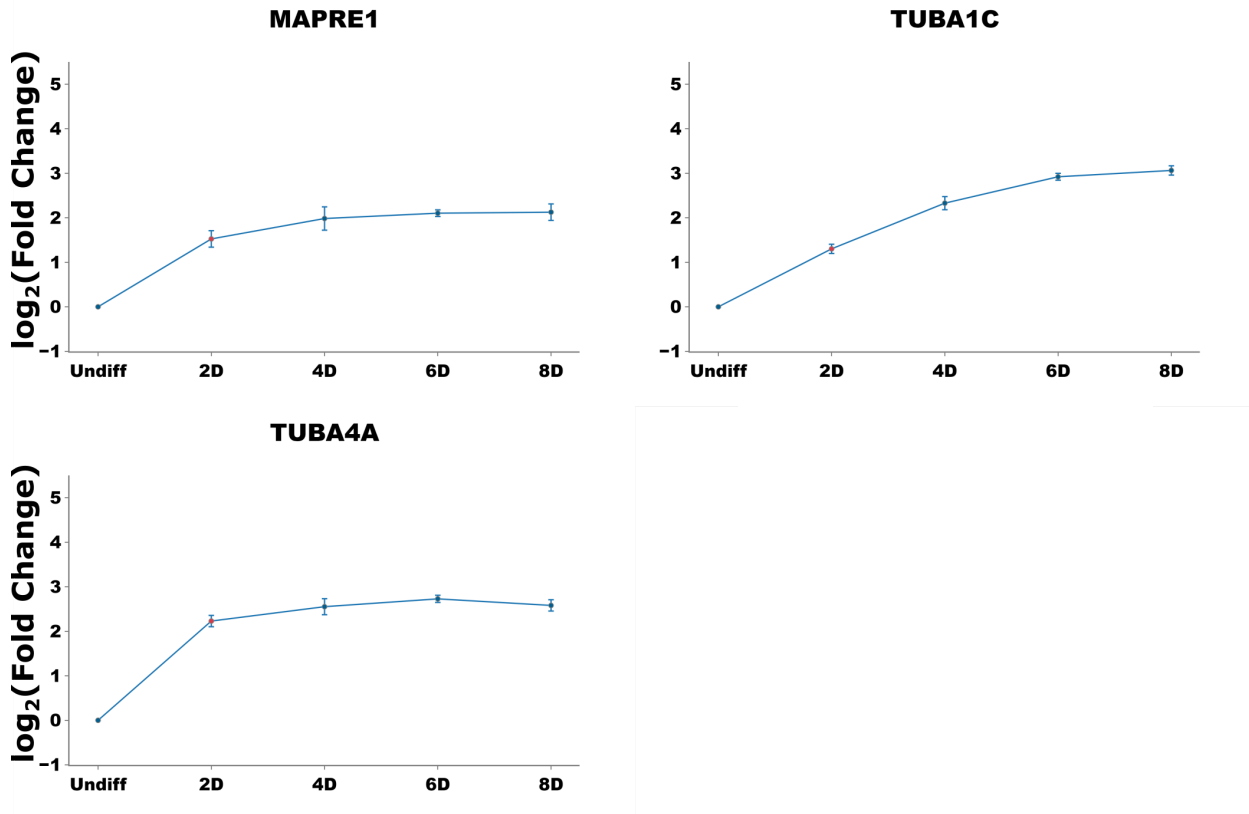


Figure S11. Whole proteome analysis of iNGNs differentiation – tyrosinated proteins. Graphs show protein expression changes during neuronal differentiation. Change of the protein expression is related to the first time point (undifferentiated iNGNs) and is represented in \log_2 -scale, $n = 4$. The whiskers show standard error of the mean (SEM).

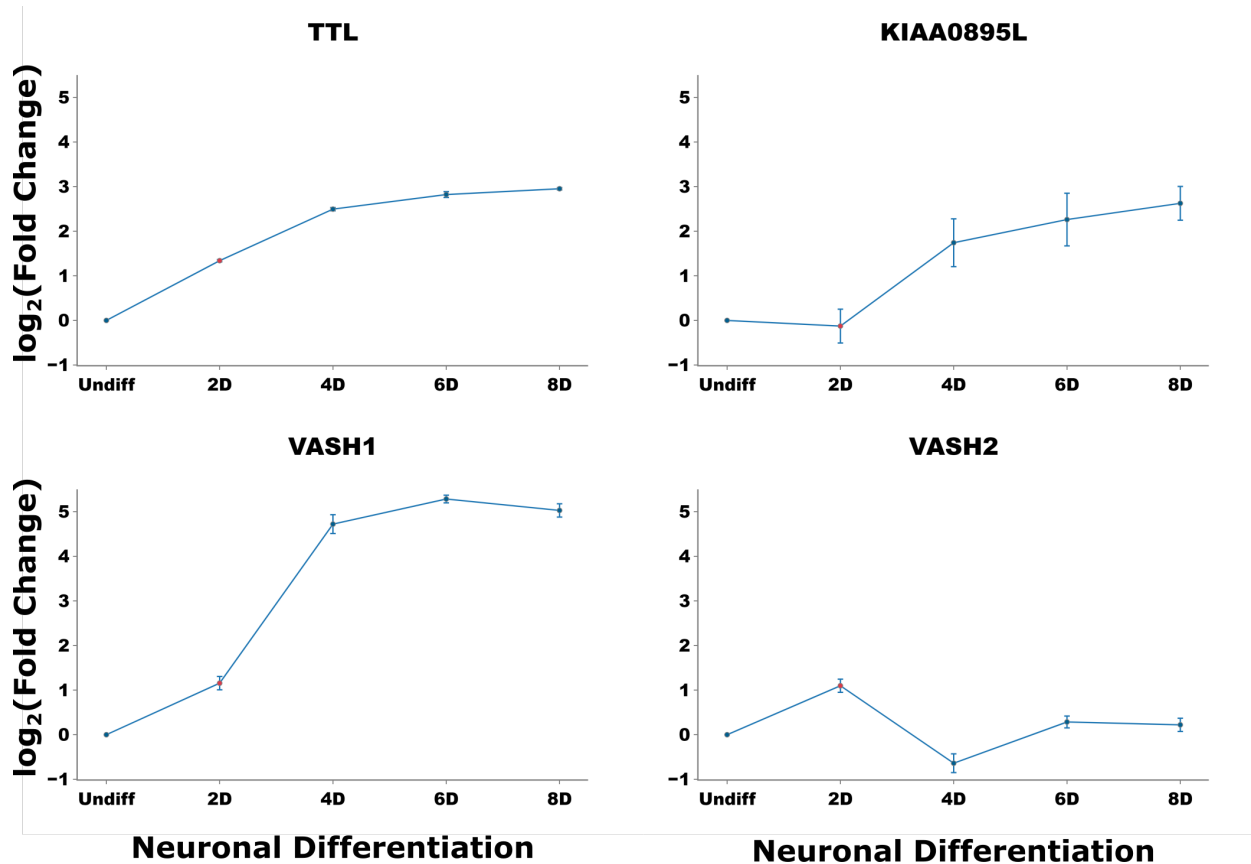


Figure S12. Whole proteome analysis of iNGNs differentiation – tyrosination modulators. Graphs show protein expression change of the key detyrosination-tyrosination cycle regulators. Change of the protein expression is related to the first time point (undifferentiated iNGNs) and is represented in a log₂-scale, $n = 4$. For VASH1 and KIAA0895L (MATCAP), no proteins were identified in undifferentiated iNGNs. The values in undifferentiated iNGNs were imputed with downshifted normal distribution. The whiskers show standard error of the mean (SEM).

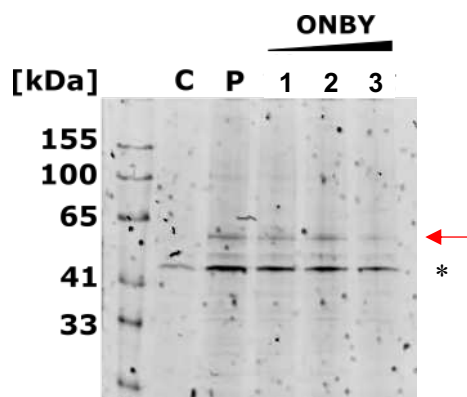


Figure S13. Competition experiment between *O*-(2-nitrobenzyl)-L-tyrosine (**ONBY**) and the **Tyr-O-Alk** probe in SH-SY5Y cells. Negative control (**C**): cells were treated with plain solvent. Positive control (**P**): cells were treated with **Tyr-O-Alk** probe. Samples 1, 2 and 3 contain a mixture of **Tyr-O-Alk** and **L-Tyr** in following ratios 1:0.1; 1:1 and 1:10. The red arrow point to fluorescent band

stemming from estimated tubulin (~50 kDa) labelling. A star marks an unspecific TAMRA-N₃ labelling.

Supplementary Tables

Table S1. List of SP2E-enriched peptides found in SH-SY5Y cells samples for specific proteins.

TUBA1C		
Unique	Peptide sequence	Precursor charge
yes	AVC(Acetyl)MLSNTTAVAEAWAR	3
yes	AVC(Acetyl)M(Carbamidomethyl)LSNTTAVAEAWAR	3
	AVFVDLEPTVIDEVR	3
	DVNAAIATIK	2
	EIIDLVLDLDR	2
	GHYTIGKEIIDLVLDLDR	3
	GHYTIGKEIIDLVLDLDRIR	3
	GHYTIGKEIIDLVLDLDRIR	4
	IHFPLATYAPVISA EK	3
	LDHKFDLMYAK	2
	NLDIERPTYTNLNR	3
	QLFHPEQLITGK	2
	QLFHPEQLITGKEDAANNYAR	4
	RNLDIERPTYTNLNR	3
	TIGGGDDSFNTFFSETGAGK	3
	VGINYQPPTVVPGGDLAK	3
	VGINYQPPTVVPGGDLAKVQR	3
	YMAC(Acetyl)C(Acetyl)LLYR	2
	YM(Carbamidomethyl)AC(Acetyl)C(Acetyl)LLYR	2
TUBA4A		
Unique	Peptide sequence	Precursor charge
	AVC(Acetyl)MLSNTTAIAEAWAR	3
	AVC(Acetyl)M(Carbamidomethyl)LSNTTAIAEAWAR	3
yes	AVFVDLEPTVIDEIR	3
	AYHEQLSVAEITNAC(Acetyl)FEPANQMVK	4
	AYHEQLSVAEITNAC(Acetyl)FEPANQM(Carbamidomethyl)VK	4
yes	EIIDPVLDR	2
MAPRE1		
Unique	Peptide sequence	Precursor charge
	FFDANYDGK	2
	KFFDANYDGK	2
yes	KPLTSSSAAPQRPISTQR	3
yes	LEHEYIQNFK	2
yes	QGQETAVAPSLVAPALNKPK	3
yes	QGQETAVAPSLVAPALNKPK	4
TUBGCP5		

Unique	Peptide sequence	Precursor charge
yes	LDPC(Carbamidomethyl)ISWK	2

Table S2. Number of peptides found with variable modification of propargyl group (38.0156 m/z shift) on a tyrosine amino acid. SH-SY5Y cells; whole proteome samples.

	Contr. 1	Contr. 2	Contr. 3	Contr. 4	Probe 1	Probe 2	Probe 3	Probe 4
Peptides with modification	44	39	38	49	25	30	43	34
Total peptides	39114	38677	38413	38220	35679	37870	37720	37896

Table S3. iNGNs growth factors treatment timeline after thawing a cryo-stock or splitting a maintenance plate

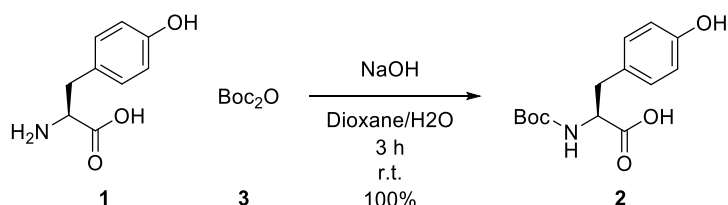
Thawing/splitting day	1 day	2 day	3 day	Change medium every 2 days until 80-90% confluency reached
E7 + Tz + TGF + FGF	E7 + TGF + FGF	skip	E7 + TGF + FGF	

Table S4. iNGNs differentiation timeline treatment

		2D		4D		Change medium every 2 days
Splitting day	1 day	2 day	3 day	4 day	5 day	
E7 + Tz + Dox	E7 + Dox	skip	E7 + Dox	E7/Neurobasal A = 1:1 + 2% NeuroBrew-21	Neurobasal A + 2% NeuroBrew-21	

Organic synthesis

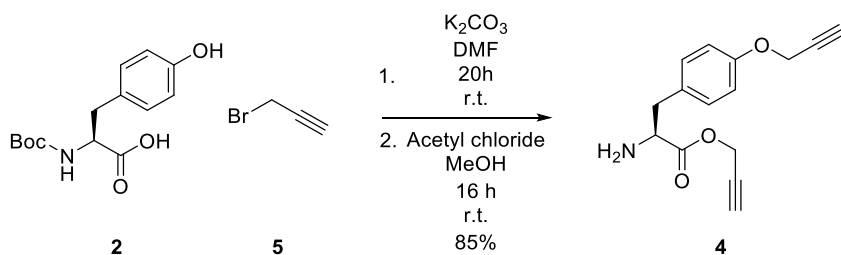
Synthesis of (*tert*-butoxycarbonyl)-L-tyrosine (**2**)^[1]



In a round-bottom flask, L-tyrosine (**1**) (11.04 mmol, 2.00 g) was dissolved in a mixture of dioxane/H₂O (100 mL) in a 2/1 ratio. Afterward, alongside the addition of 1M NaOH solution (25 mL), di-*tert*-butyl dicarbonate (**3**) (12.14 mmol, 2.65 g) was added to the reaction mixture. The solution was stirred for 3 h at r.t. The reaction mixture was pre-evaporated *in vacuo*, and pH was adjusted to 2 with 6M HCl. The acidified aqueous solution was extracted with EtOAc (3 × 50 mL). Collected organic fractions were washed with brine (1 × 50 mL) and dried under anhydrous MgSO₄. The organic solvent was evaporated *in vacuo*, and the residue was placed under high vacuum. Boc-tyrosine **2** was obtained as yellowish oily residue (3.10 g, 100%). The NMR spectra were in agreement with the literature.^[2]

¹H NMR (400 MHz, DMSO-*d*₆) δ 12.55 (s, 1H), 9.20 (s, 1H), 7.02 (d, *J* = 8.2 Hz, 2H), 6.65 (d, *J* = 8.5 Hz, 2H), 4.02 – 3.95 (m, 1H), 2.90 – 2.83 (m, 1H), 2.73 – 2.64 (m, 1H), 1.32 (s, 9H).

Synthesis of prop-2-yn-1-yl (*S*)-2-amino-3-(4-(prop-2-yn-1-yloxy)phenyl)propanoate (**4**)^[1]

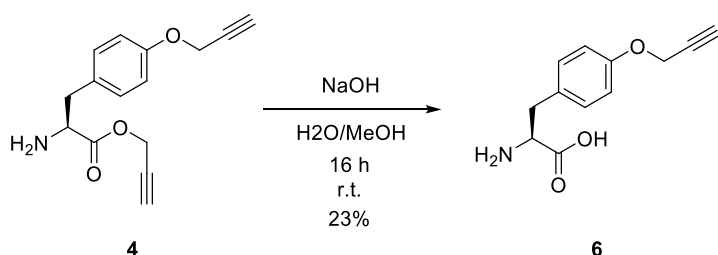


Under inert conditions, Boc-tyrosine **2** (5.33 mmol, 1.50 g) and K₂CO₃ (16.00 mmol, 2.21 g) were suspended in anhydrous DMF (40 mL). The RM was cooled in an ice bath before the dropwise addition of propargyl bromide (**5**). The resulted mixture was removed from the bath and stirred for 20 h at r.t. The RM was diluted with H₂O (50 mL), and the aqueous phase was extracted with EtOAc (3 × 40 mL). The combined organic phase was washed with H₂O (1 × 20 mL), brine (1 × 20 mL), and dried over anhydrous MgSO₄. The solvent was removed *in vacuo*, and the crude residue was used directly in the next step.

To the ice-cooled anhydrous MeOH (25 mL), acetyl chloride (2.20 mL) was slowly added. The obtained solution was then added to the crude product from the previous step, and the reaction mixture was stirred overnight at r.t. The organic phase was removed *in vacuo*, and the desired product was additionally dried on a vacuum line. Propargyl ester **4** (1.17 g, 85%) was obtained as a brown solid. The NMR spectra were in agreement with the literature.^[3]

¹H NMR (400 MHz, DMSO-*d*₆) δ 7.21 – 7.15 (m, 2H), 6.96 – 6.92 (m, 2H), 4.83 (d, *J* = 2.6 Hz, 2H), 4.78 (d, *J* = 2.4 Hz, 2H), 4.36 – 4.21 (m, 1H), 3.71 (t, *J* = 2.5 Hz, 1H), 3.59 (t, *J* = 2.4 Hz, 1H), 3.13 – 3.03 (m, 1H).

Synthesis of (S)-2-amino-3-(4-(prop-2-yn-1-yloxy)phenyl)propanoic acid (Tyr-O-Alk, **6**)^[3]

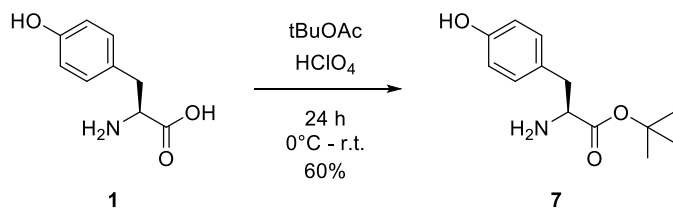


Propargyl ester **4** (4.56 mmol, 1.17 g) was dissolved in MeOH (10 mL), and 1M NaOH solution (20 mL) was added to the reaction flask. After the RM was stirred for 24 h at r.t., it was acidified with conc. HCl to pH 3 and left in the fridge overnight at 4°C. The precipitated product was filtered and dried on a vacuum line. Tyr-O-Alk (**6**) (0.23 g, 23%) was obtained as a brown solid. The NMR spectra were in agreement with the literature.^[3]

¹H NMR (400 MHz, DMSO-*d*₆) δ 7.19 (d, *J* = 8.6 Hz, 2H), 6.89 (d, *J* = 8.6 Hz, 2H), 4.75 (d, *J* = 2.4 Hz, 2H), 3.56 (t, *J* = 2.3 Hz, 1H), 3.32 (dd, *J* = 8.3, 4.3 Hz, 1H), 3.07 (dd, *J* = 14.4, 4.3 Hz, 1H), 2.78 (dd, *J* = 14.4, 8.3 Hz, 1H).

Synthesis of ONBY

Synthesis of *tert*-butyl L-tyrosinate (**7**)^[4]

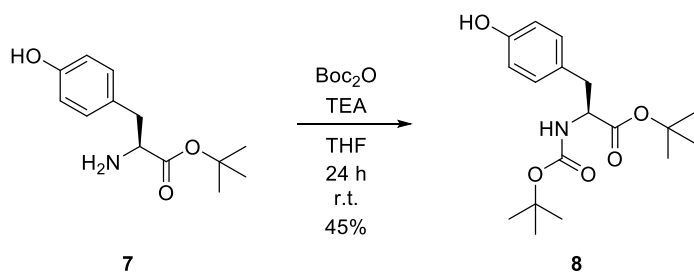


Under inert conditions, perchloric acid (70%, 0.29 mL, 8.28 mmol, 1.5 eq.) was added dropwise to a suspension of L-tyrosine **1** (1 g, 5.52 mmol, 1 eq.) in tBuOAc (14 mL) at 0°C, and the mixture was stirred overnight at r.t. The reaction mixture was then washed with H₂O (1 × 28 mL) and HCl (1 M, 1 × 14 mL). The combined aqueous phase was adjusted to pH 9 with concentrated K₂CO₃ solution and extracted with DCM (3 × 15 mL). The organic phase was dried over MgSO₄, and the

solvent was removed *in vacuo*. Ester **7** (0.79 g, 60%) was obtained as a white solid. Spectra were in agreement with the literature.^[5]

¹H NMR (400 MHz, Chloroform-*d*) δ 7.04 (d, J = 8.5 Hz, 2H), 6.68 (d, J = 8.5 Hz, 2H), 3.58 (dd, J = 7.8, 5.4 Hz, 1H), 2.99 (dd, J = 13.7, 5.4 Hz, 1H), 2.76 (dd, J = 13.7, 7.7 Hz, 1H), 1.45 (s, 9H).

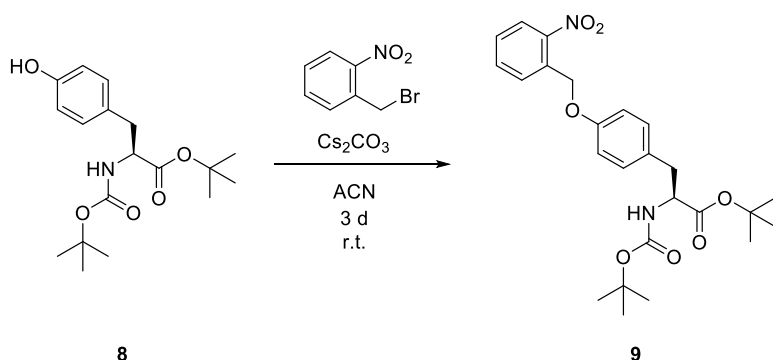
Synthesis of *tert*-butyl (*tert*-butoxycarbonyl)-L-tyrosinate (**8**)



Tyr-O-tBu **7** (780 mg, 3.29 mmol, 1 eq.), Boc-anhydride **3** (924 mg, 3.29 mmol, 1 eq.), and triethylamine (45 μL , 0.33 mmol, 0.1 eq.) were dissolved in THF (30 mL), and the reaction mixture was stirred for 24 h at r.t. THF was then removed *in vacuo*. The mixture was dissolved in ethyl acetate (15 mL), washed with water (3 \times 10 mL), and dried over MgSO_4 . Ethyl acetate was removed *in vacuo*, and the product was purified using ethyl acetate/DCM (9:1) mixture as eluent. Boc-protected ester **8** (497 mg, 45%) was obtained as a white solid. Spectra were in agreement with the literature.^[6]

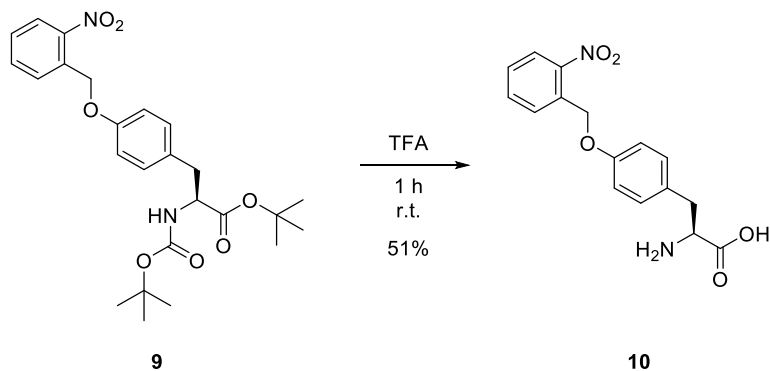
¹H NMR (400 MHz, DMSO-*d*₆) δ 9.20 (s, 1H), 7.00 (d, J = 8.5 Hz, 2H), 6.65 (d, J = 8.5 Hz, 2H), 3.95 – 3.88 (m, 1H), 2.83 – 2.66 (m, 2H), 1.34 (s, 18H).

Synthesis of *tert*-butyl (*S*)-2-((*tert*-butoxycarbonyl)amino)-3-(4-((2-nitrobenzyl)oxy)phenyl)propanoate (**9**)



In a round-bottomed flask, Boc-Tyr-OtBu **8** (0.2 g, 0.59 mmol), 2-nitrobenzyl bromide (0.13 g, 0.59 mmol), and Cs_2CO_3 (0.1 g, 0.30 mmol) were dissolved in ACN (5 mL). The reaction was stirred for 3 days at r.t. The reaction mixture was filtered, and the solvent was reduced *in vacuo*. The crude product **9** was used in the subsequent step without purification and isolation.

Synthesis of (S)-2-amino-3-(4-((2-nitrobenzyl)oxy)phenyl)propanoic acid (10)



The crude product from the previous step (0.28 g) was dissolved in TFA (5 mL), and the reaction mixture was mixed for 1 h at r.t. TFA was then co-evaporated with toluene *in vacuo*. Afterward, the residue was dissolved in MeOH (5 mL), and by-products were filtered off. Methanol was removed *in vacuo*, and the product was further purified by recrystallization. The solids were dissolved in 1 M NaOH, and pH was adjusted to 5 by adding 3 M HCl solution to recrystallize the product. The solution was left in the fridge overnight, and the crystals were then filtered and dried under high vacuum. The final product (96 mg, 51% yield after two reactions) was obtained as yellowish crystals. Spectra were in agreement with the literature.^[7]

¹H NMR (400 MHz, Methanol-*d*₄) δ 8.12 (dd, *J* = 8.2, 1.3 Hz, 1H), 7.84 (dd, *J* = 7.8, 1.2 Hz, 1H), 7.72 (td, *J* = 7.6, 1.3 Hz, 1H), 7.59 – 7.52 (m, 1H), 7.20 (d, *J* = 8.6 Hz, 2H), 6.91 (d, *J* = 8.6 Hz, 2H), 5.43 (s, 2H), 3.41 (dd, *J* = 8.0, 4.8 Hz, 1H), 3.04 (dd, *J* = 13.6, 4.7 Hz, 1H), 2.73 (dd, *J* = 13.6, 8.0 Hz, 1H).

¹³C NMR (101 MHz, MeOD) δ 181.78, 158.40, 148.99, 134.84, 134.75, 132.95, 131.62, 130.15, 129.76, 125.85, 115.87, 68.01, 59.01, 41.92.

MS (ESI⁺): *m/z* (%): 317.23 (100) [M+Na]⁺.

Biochemistry

Cell lines

SH-SY5Y cell line

The human neuroblastoma cell line SH-SY5Y (CRL-226) was cultivated in a high-glucose Dulbecco's Modified Eagle Medium (DMEM) that was further supplemented with 10% (v/v) heat-inactivated fetal bovine serum (FBS) and 2% (v/v) L-glutamine. Cells were maintained in cell culture dishes for adherent cells at 37°C under constant humidity and 5% CO₂ concentration.

iNGNs cell line

Before culturing the cell line, a Petri dish (p100) was coated with a Geltrex LDEV-free coating. Geltrex was added in a cold coating medium (1 eq. DMEM, 1 eq. F-12, 1% pen/strep) (10 mL) in 1/1000 dilution, mixed thoroughly, and poured directly into the dish. It was left in the incubator for at least 1 h before seeding the cells.

E7 medium preparation

For iNGN cells, an E7 medium was prepared. DMEM and F-12 were mixed in a 1:1 ratio, then the mixture was supplemented with L-Ala-L-Gln (2 mM), L-ascorbic acid 2-phosphate (64 mg/L), Na₂SO₃ (77.6 nM) and NaCl (11.2 mM). hHolo-transferrin (10 µg/mL) and hInsulin (20 µg/mL). The E7 medium was filtered through a 0.2 µm bottle filter and stored at 4°C.

Thawing and seeding of iNGN cells

Frozen cells were taken out from a nitrogen tank and placed on dry ice. Cells were thawed fast by placing into 37°C bath and transferred into 50 mL falcon. Depending on the volume of the cryostock, ten times excess of E7 medium without prewarming was added to the falcon slowly with mild agitation. Cells were subsequently pelletized by centrifuging at 200 rcf for 5 min, and the supernatant was removed. Afterward, cells were resuspended in 10 mL of prewarmed E7 media. Coating medium was removed from the prewarmed dish before transferring the cell suspension dropwise. Additional growth factors and ROCK inhibitor were added in specific concentrations: TGF-β (2 ng/mL), FGF-2-IS (20 ng/mL) and Thiazovivin (Tz) (2 µM). The next day, the medium was changed for the fresh E7 medium adding TGF-β (2 ng/mL) and FGF-2-IS (20 ng/mL), but without addition of Tz. The medium of the same composition as for the second day was changed every two days. See **Table S3**.

Splitting of undifferentiated iNGNs

Cells in a maintenance plate (p100) were washed once with PBS (5 mL) before adding TrypLE™ (1 mL) and placing the plate in the incubator for 7-10 min. Tz (2 µM) was added to the prewarmed E7 medium. Supplemented with Tz, E7 medium (5 mL) was added to the plate and pipetted against its walls to form a single-cell suspension. The suspension was then transferred to a 15 mL falcon and centrifuged at r.t. for 5 min at 200 rcf. The supernatant was sucked away, and the cells were suspended in a fresh prewarmed Tz-supplemented E7 medium. The volume of the medium was calculated in such a way as to reach the seeding density of 2 mil. cells for a p100 Petri dish. Before transferring the appropriate amount of cell suspension to the dish, the coating medium was discarded. Finally, cells were additionally supplemented with growth factors – TGF-β (2 ng/mL)

and FGF-2-IS (20 ng/mL). The next day, the medium was exchanged for an E7 medium with growth factors but without adding Tz. The medium with growth factors was exchanged every two days. The treatment scheme is represented in **Table S3**.

Seeding and culturing of differentiated iNGN cells

The seeding procedure was the same as for undifferentiated cells with minor differences. The seeding density for the differentiation was 3 mil. cells per p100 dish. After preparing the cell suspension in E7 medium containing Tz (2 μ M) as was previously described, Doxycyclin (Dox) (0.5 μ g/mL) was added instead of growth factors to initiate the differentiation. The next day, the medium was exchanged for fresh E7 without Tz but with the addition of Dox at the same concentration (0.5 μ g/mL). On day four after the splitting, the medium was exchanged for a mixture of E7 and Neurobasal A in a 1:1 ratio supplemented with 2% NeuroBrew-21. After that point, the medium was exchanged for the fresh one every two days. **Table S4** represents the treatment scheme.

Cells treatment and harvesting

SH-SY5Y or iNGN cells were treated with the stock solution of **Tyr-O-Alk** (H₂O:1M NaOH 2:1, 144 mM, sterile filtered), the final concentration in culture media was 0.3 mM. Unless otherwise stated, the cells were probe treated for 24 h. Using the same volume as for the probe-treated cells, we treated the control group with a plain solvent, the same as that used to prepare the probe stock solution.

For the cells harvesting, the medium was removed, and the cells were washed once with 5 mL of a phosphate-buffered saline solution (PBS). After removing PBS from a dish, cells were scraped with 1 mL of PBS, transferred to a 1.5 mL tube. To obtain the cell pellet, the cell suspension was centrifuged at 4°C at 100 rcf. Subsequently, the supernatant was carefully removed, and the cell pellet was stored at -80°C until further use.

Lysates preparation

To prepare a cell lysate, the cell pellet was reconstituted in 300 μ L of a lysis buffer (1% NP40, 0.2% SDS in 25 mM Hepes, 7.5 pH) by sonication with an ultrasonic tip in 1 s on/ 1 s off cycles at 20% intensity for 10 s of total time. The solution was clarified by centrifugation at 4°C at 14000 rcf for 15 min. The clear supernatant was then transferred to a new 1.5 mL tube and stored at -80°C until use.

Protein concentration measurement

Protein concentration measurement was performed with a Pierce™ BCA Protein Assay Kit (Thermo Scientific).

SP2E workflow large scale

The enrichment samples were prepared from the lysates so that each sample contained 400 μ g of proteins. Lysates were diluted to 200 μ L with lysis buffer (1% NP40, 0.2% SDS in 25 mM Hepes, 7.5 pH). For each sample, 2 μ L of Biotin-N₃ (10 mM in DMSO), 2 μ L of TCEP (100 mM in H₂O), and 0.24 μ L TBTA (83.5 mM in DMSO) were added, vortexed, spun down, and supplemented with 4 μ L of CuSO₄ (50 mM in H₂O) to initiate the reaction. The reaction mixture was incubated at r.t. while shaking at 450 rpm for 1.5 h.

Streptavidin-coated magnetic beads (50 μ L) were transferred to a new 1.5 mL tube and washed three times with 500 μ L 0.2% SDS in PBS, sequentially vortexing and spinning down. A 1:1 mixture of hydrophobic and hydrophilic carboxylate-coated magnetic beads (100 μ L) was transferred to a new 1.5 mL tube and washed three times with 500 μ L MS-grade H₂O, vortexed, and spun down.

After completion of the click reaction, the mixture was diluted with 200 μ L of 8 M Urea to a total volume of 400 μ L. The reaction mixture was placed on carboxylate-coated beads, diluted with 600 μ L of absolute ethanol, vortexed, and spun down. The suspension was incubated at r.t. while shaking at 950 rpm for 5 min. Afterward, the supernatant was discarded, and the beads were washed three times with 500 μ L of 80% ethanol in H₂O, vortexed, and spun down. After the last washing step, proteins were eluted from carboxylate-coated beads to streptavidin-coated beads. To elute the proteins, 300 μ L 0.2% SDS in PBS was added to the carboxylate-coated beads, vortexed, and incubated at 40°C while shaking at 950 rpm for 5 min, and the solution was transferred to dry streptavidin-coated beads. The elution step was repeated two more times.

The eluates were incubated on streptavidin-coated beads at r.t. while shaking at 950 rpm for 20 min. The supernatant was discarded, and the beads were washed three times with 500 μ L 1% NP-40 in PBS, twice with 500 μ L 6 M Urea in H₂O, and twice with 500 μ L MS-grade H₂O. After each round of washing, beads were vortexed and spun down.

At that point, proteins can be further processed for MS measurement or *in-gel* analysis.

In-gel analysis of the enriched proteins

After the last washing step, 20 μ L of MS-grade H₂O and 5 μ L of 5 \times SDS reducing Loading Buffer were added to the beads, vortexed, and spun down. The resulting suspension was incubated at 95°C while shaking at 950 rpm for 5 min. The supernatant was subsequently placed on an SDS-PAGE gel.

Sample preparation for MS analysis

After the last washing step, the beads were reconstituted in 80 μ L of ammonium bicarbonate buffer (125 mM in H₂O) (ABC buffer). For the suspension, 10 μ L of TCEP (100 mM) and 10 μ L of chloracetamide (400 mM) solutions were added, and samples were incubated at 95°C for 5 min. After cooling the samples, trypsin (0.5 μ g/ μ L) was added and incubated at 37°C overnight with agitation. The supernatant was transferred into a new 1.5 mL tube, and the beads were then washed with 100 μ L of ABC buffer (100 mM in H₂O) three times. All washings were combined with the supernatant, and the resulting mixture was supplemented with 2.5 μ L of formic acid. To desalt the samples, Sep-Pak C18 cartridges were used. The cartridge was flushed with 1 mL of ACN and 1 mL of ACN and FA mixture (80% + 0.5% in H₂O). Equilibration was performed three times with 1 mL FA (0.5% in H₂O). Afterward, the sample was loaded into the cartridge. The column was then washed three times with 1 mL of FA (0.5% in H₂O). Peptides were eluted with ACN and FA mixture (80% + 0.5% in H₂O) in two 250 μ L batches. The samples were dried in a SpeedVac.

Dry peptides were then reconstituted in 30 μ L FA (1% in H₂O), vortexed, and placed in a sonication bath for 15 min. Samples were afterward spun down and transferred into MS vials.

SP2E workflow small scale

Lysates containing 100 µg of proteins were diluted to 19 µL with lysis buffer (1% NP40, 0.2% SDS in 25 mM Hepes, 7.5 pH). For each sample, 0.2 µL Biotin-N₃ (10 mM in DMSO), 0.2 µL of TCEP (100 mM in H₂O), and 0.125 µL TBTA (16.7 mM in DMSO) was added, vortexed, spun down, and supplemented with 0.4 µL of CuSO₄ (50 mM in H₂O) to initiate the reaction. The reaction mixture was incubated at r.t. while shaking at 450 rpm for 1.5 h.

After completion of the click reaction, each sample was diluted with 60 µL of 8M urea. A 1:1 mixture of hydrophobic and hydrophilic carboxylate-coated magnetic beads (100 µL) was washed three times with 100 µL MS-grade H₂O, and the reaction mixture was placed on the beads, diluted with 100 µL of absolute ethanol and vortexed. The suspension was incubated at r.t. while shaking at 950 rpm for 5 min. Afterward, the supernatant was discarded, and the beads were washed three times with 150 µL of 80% ethanol in H₂O and once with 150 µL acetonitrile (LC-MS). Proteins were eluted separately by adding 60 µL of 0.2 % SDS in PBS. For this, beads were resuspended and incubated for 5 min at 40 ° C and 950 rpm. The supernatant was directly transferred onto 50 µL equilibrated streptavidin-coated magnetic beads (3 times prewashed with 100 µL 0.2% SDS in PBS). The elution step was repeated twice and the combined beads mixture was incubated at r.t. while shaking at 800 rpm for 1 h.

The supernatant was discarded, and the beads were washed three times with 150 µL 1% NP-40 in PBS, twice with 150 µL 6 M Urea in H₂O, and twice with 500 µL MS-grade H₂O. After each round of washing, the beads were incubated at r.t. while shaking at 800 rpm for 1 min. The rinsed beads mixtures were resuspended in 50 µL 50 mM TEAB, and the proteins were digested overnight at 37°C by adding 1.5 µL sequencing grade trypsin (0.5 mg/mL). The following day, the beads were washed twice with 20 µL of 50 mM TEAB buffer and twice with 20 µL 0.5% FA, and the wash fractions were collected and combined. The beads were incubated for 5 min at 40°C and 600 rpm for each washing step. The combined washed fractions were acidified by adding 0.9 µL formic acid (FA) and transferred to MS vials.

In-gel analysis

The resolution of proteins was made with the SDS-PAGE method using 10% acrylamide gels. Before loading onto the gel, a protein solution (20 µL) was mixed with 5 × SDS reducing loading buffer (5 µL) (10% (w/v) SDS, 50% (v/v) glycerol, 25% (v/v) β-mercaptoethanol, 0.5% (w/v) bromphenol blue, 315 mM Tris/HCl, pH 6.8) and placed in wells. As a reference, two types of protein markers were used: BenchMark™ Fluorescent Protein Standard (Invitrogen™), Color Prestained Protein Standard, Broad Range (10-250 kDa) (New England Biolabs GmbH). Afterward, the gel was scanned on Amersham Imager 680 (GE Healthcare).

Western blot

After separating the proteins on a gel, they were blotted on a PVDF membrane using a Semi-Dry Blotter (Bio-Rad). Before making a blotting sandwich, a thick blot paper was soaked in a blot buffer (48 mM Tris, 39 mM glycine, 0.0375% (m/v) SDS, 20% (v/v) methanol) for 5 min, and a membrane was incubated in methanol. After the blotting, the membrane was set in a blocking solution (0.5 g nonfat dried milk powder in 10 mL PBST (PBS + 0.5% Tween)) for 60 min to hide all nonspecific binding sites. The membrane was then placed in the primary antibody of interest solution and incubated at 4°C overnight. The next day, the membrane was washed 3 × 10 min with PBST

solution before incubation with the secondary HRP-linked antibody solution at r.t. for 1 h. The membrane was then washed with PBST 3 × 10 min. Before scanning the membrane on Amersham Imager 680 (GE Healthcare), it was wetted with the ECL substrate and the peroxide solution in a 1:1 ratio.

Whole proteome samples preparation

SH-SY cell lysates were prepared under standard conditions using the standard treatment and harvesting procedures. The volume of a lysate containing 100 µg of proteins was normalized to 400 µL with lysis buffer. A mixture of hydrophilic and hydrophobic carboxylate-coated magnetic beads was washed three times with 500 µL of MS-grade H₂O. The sample was added to the beads and thoroughly mixed. 600 µL of absolute EtOH was added, and the mixture was incubated at r.t. for 5 min with agitation. Subsequently, the beads were washed with EtOH (80% in H₂O) three times.

To cleave the proteins, on-beads digestion was performed. The procedure was identical to those which was used for MS-samples preparation. In brief, beads were reconstituted in ABC buffer alongside reducing and alkylating agent and boiled. After the samples were cooled down, trypsin was added and left overnight at 37°C. The supernatant was then placed in a new 1.5 mL tube, and the beads were washed several times with ABC buffer. After desalting the peptide mixture on a C18 column, samples were dried on a SpeedVac.

The dry peptides were reconstituted in 200 µL of FA (1% in H₂O) and transferred into MS vials.

Enrichments with trifunctional linker (5/6-TAMRA-N₃-biotin)

Lysates from iNGNs were prepared on the 2nd (2D) and 4th (4D) day after starting of the differentiation using standard protocols. Cells were treated with 0.3 mM of the probe and incubated for 1 day before harvesting. Protein concentration in the lysates was evaluated with Pierce™ BCA Protein Assay Kit. The large-scale SP2E protocol was implemented as a template for the preparation of the probes with minor differences. Instead of the biotin-N₃ probe, 5/6-TAMRA-N₃-biotin (trifunctional linker) probe underwent the click reaction with the same parameters as in the original SP2E protocol. After enrichment, proteins were eluted from the beads into separate 1.5 mL tube instead of being digested with trypsin. For the elution, 20 µL of H₂O and 5 µL of 5 × SDS reducing Loading Buffer were placed on beads, vortexed and incubated at 95°C at 850 rpm for 5 min. Afterward, samples were placed on a magnet rack and let to cool at r.t. Supernatants were further used for *in-gel* analysis. For WB analysis, rat anti-mapre1 (Abcam - ab53358) antibody was used at 2 µg/mL concentration. A goat anti-rat HRP-linked secondary antibody (Cell Signaling Technology - 7077S) was used in 1/1000 dilution.

Tubulin fraction isolation

SH-SY5Y cells were grown in a p150 Petri dish in DMEM under standard conditions and with the standard probe treatment scheme. Cell pellets were prepared with a standard protocol and placed in 1.3 mL Hepes/Pipes buffer (25 mM Hepes, 60 mM Pipes) without the addition of EGTA. The cell suspension was sonicated on ice with a microsonic tip at 50% intensity for 1 min in 10 s on/off cycles. The samples were then centrifuged at 20k rcf at 4°C for 1 h. The first pellet was kept to confirm the absence of tubulins. The supernatant was transferred to a new 1.5 mL tube and additional additives were added – MgCl₂ (3 mM final concentration), Taxol (50 µM final concentration), and GTP (2 mM final concentration). The samples were then incubated at 37°C

for 1 h. After incubation, the supernatants were placed on 0.2 mL sucrose cushion containing 20 μ M Taxol and 1.5 mM GTP, and the samples were ultracentrifuged at 150k rcf at 37°C for 2 h. After the centrifugation, MTs pellet was then resuspended in 0.25 mL of a click buffer (1% NP40, 0.2% SDS in 25 mM Hepes, 7.5 pH) and sonicated on ice with a microsonic tip at 20% intensity for 10 s in 1 s on/off cycles. The supernatant was additionally clarified by centrifugation at 10k rcf at 4°C for 10 m. Protein concentrations in the lysates from two fractions were evaluated with Pierce™ BCA Protein Assay Kit. Afterward, a click reaction was performed with a fraction containing cell debris (PI – first pellet), and MTs fraction (PII – second pellet). For the click reaction, 50 μ g of proteins in 100 μ L of total volume were prepared. To each sample, 1 μ L TAMRA-N₃ (10 mM in DMSO), 1 μ L of TCEP (100 mM in H₂O), and 0.12 μ L TBTA (83.5 mM in DMSO) was added, vortexed, spun down, and supplemented with 2 μ L of CuSO₄ (50 mM in H₂O) to initiate the reaction. The reaction mixture was incubated at r.t. while shaking at 450 rpm for 1.5 h. After the click reaction, proteins were precipitated in acetone ON. Next, they were centrifuged at 14k rcf at 4°C for 10 min. The pellets were then washed twice with cold methanol. After the last wash, pellets were reconstituted in 50 μ L H₂O. To the new tube, 10 μ L of the solution was transferred and mixed with 2 μ L of 5 \times SDS reducing Loading Buffer and incubated at 95°C for 5 min with agitation. The resulting mixture was loaded on a 10% acrylamide gel. Subsequently, proteins were blotted and stained with a rat anti-alpha-tubulin antibody (MA1-80017, Thermo Fisher) at 2 μ g/mL concentration.

Fluorescence microscopy

The SH-SY5Y neuroblastoma cell line was cultivated in slides - Nunc™ Lab-Tek™ II Chamber Slide™ System (Thermo Scientific™) to prepare samples for fluorescence microscopy. The seeding density for each well was $2 \cdot 10^4$ cells/mL, the medium volume for one well was 0.5 mL. After one day of cell growth, the cultivating medium was exchanged for the fresh medium containing the propargyl-tyrosine probe at a concentration of 0.2 mM. The cultivation medium was exchanged for the medium containing 1% DMSO in a control group. The next day, the cells were washed with 0.5 mL of PBS three times before the fixation step. Cells were incubated in 0.5 mL of 4% PFA for 15 min with gentle mixing to fix the cells. Then, cells were washed with 0.5 mL PBS three times before permeating in 0.5 mL 0.1% Triton X-100 in PBS for 15 min with gentle agitation. After the permeabilization, cells were washed three times with PBS. Blocking nonspecific binding sites was performed in 0.5 mL of 1% BSA in PBS solution for 1 h. Subsequently, the washing step was performed.

After preparing the cells for the click reaction, the Master Mix was prepared: CuSO₄ and TBTA solutions were mixed so that the final concentration after dilution was 1 mM and 5 μ M, respectively. To the solution, sodium ascorbate was added to reach the final concentration of 10 mM. The mixture was incubated at r.t. for 15 min. TAMRA-azide was added in 10 μ M final concentration. The cells were incubated with the resulting solution at r.t. for 1.5 h in the dark under mild agitation. Subsequently, cells were thoroughly washed with 0.5 mL of PBS for 15 min trice to remove all unbound TAMRA. Cells were incubated at 4°C overnight in a blocking solution treated with primary antibodies in 1/1000 dilution. Rabbit anti-MAP2 polyclonal antibody (PA5-110744, Thermo Fisher) and rat anti-tubulin monoclonal antibody (MA1-80017, Thermo Fisher) were used. After trice washing with PBS, cells were incubated with secondary fluorophore-labelled antibodies in 1/500 dilution at r.t. for 1 h (anti-Rabbit IgG (H+L) F(ab')₂ Fragment (Alexa Fluor (R) 488 conjugate) (4412S, Cell Signal) and anti-Rat IgG (H+L) Cross-Adsorbed Secondary Antibody

(Alexa Fluor 647) (A-21247, Thermo Fisher)). As the last step, anti-fade fluorescence mounting medium (Fluoroshield (ab104135, abcam)) was applied to the slides. Images were obtained on a Leica confocal microscope.

Cytotoxicity measurement

Cells were seeded in triplicates for each concentration in a transparent flat-bottomed 96-well plate at a density of 5000 cells per well in a total 100 μ L and left to settle down overnight. Next, the medium was exchanged for a fresh medium supplemented with the probe to reach concentrations in a range of 0 to 2000 μ M in a well, while the control samples were treated with a medium containing 1% DMSO. The cells were incubated with the probe for another 24 h. In each well, 20 μ L of 3-(4,5-dimethylthiazol-2-yl)-2,5-diphenyltetrazolium bromide (MTT) solution was added and incubated for 4 h. Subsequently, the medium was removed, and the cells were lysed by adding 200 μ L of DMSO. Absorbance was measured at 570 nm wavelength using 630 nm as a reference.

Competition experiment

The human neuroblastoma cell line SH-SY5Y was cultured under standard conditions in five dishes. The **Tyr-O-Alk** probe concentration was maintained at a constant concentration of 0.3 mM in all probe-treated plates. The competitor's concentration was changed in tenfold steps compared to the probe concentration of interest – 0.03 mM, 0.3 mM, and 3 mM. Two dishes were prepared as a control group, where one of them contained cells without any treatment (negative control), and another was treated only with the probe (0.3 mM) without the competitor (positive control). The incubation time was set to 1 day, after which the cells were harvested and processed under standard conditions as described above. Briefly, after collecting cells and measuring protein concentration, samples underwent a click reaction with TAMRA-azide, proteins were precipitated in acetone overnight and separated by SDS-Page. Gel images were taken by Amersham Imager.

CHX inhibition experiment

The human neuroblastoma cell line SH-SY5Y was cultured in three plates under standard conditions. One plate served as a negative control without any supplement. The second plate was treated only with the **Tyr-O-Alk** probe (0.3 mM). The experiment plate was first treated with cycloheximide (50 μ g/mL) 30 min prior addition of the **Tyr-O-Alk** probe (0.3 mM). After one day of incubation, cells were harvested and protein concentration was standardly measured. From each plate, 150 μ g of proteins in 150 μ L of buffer were then subjected to click reaction with TAMRA-azide under standard conditions as described above. After 1.5 h, 20 μ L of the reaction mixture was mixed with 5 μ L of 5 x SDS loading buffer, and proteins were separated by SDS-Page. The gels were imaged with an Amersham imager. The changes in TUBA were quantified from a western blot with the rat anti-tubulin monoclonal antibody (MA1-80017, Thermo Fisher).

MS measurement

MS measurements were performed on an Orbitrap Eclipse Tribrid Mass Spectrometer (Thermo Fisher Scientific) coupled to an UltiMate 3000 Nano-HPLC (Thermo Fisher Scientific) via an EASY-Spray source (Thermo Fisher Scientific) and FAIMS interface (Thermo Fisher Scientific). First, peptides were loaded on an Acclaim PepMap 100 μ -precolumn cartridge (5 μ m, 100 \AA , 300 μ m ID x 5 mm, Thermo Fisher Scientific). Then, peptides were separated at 40°C on a PicoTip

emitter (noncoated, 15 cm, 75 μm ID, 8 μm tip, New Objective) that was *in-house* packed with Reprosil-Pur 120 C18-AQ material (1.9 μm , 150 \AA , Dr. A. Maisch GmbH).

Buffer composition. Buffer A consist of MS-grade H_2O supplemented with 0.1% FA. Buffer B consists of acetonitrile supplemented with 0.1% FA.

Following LC gradient was used for the short acquisition method: 4% buffer B (minutes 0 - 5), 4% - 7% buffer B (minutes 5 - 6), 7% - 24.8% (minutes 6 - 36), 24.8% - 35.2% buffer B (minutes 36 - 41), 35.2% - 80% buffer B (minutes 41 - 41.1), 80% buffer B (minutes 41.1 - 46), 80% - 4% buffer B (minutes 46 - 46.1) then hold on 4% until minute 60. The flow rate was 0.3 $\mu\text{L}/\text{min}$.

Following LC gradient was used for the long acquisition method: 4% buffer B (minutes 0 - 5), 4% - 7% buffer B (minutes 5 - 6), 7% - 24.8% buffer B (minutes 6 - 105), 24.8% - 35.2% buffer B (minutes 105 - 126), 35.2% - 80% buffer B (minutes 126 - 126.1), 80% buffer B (minutes 126.1 - 131), 80% - 4% buffer B (minutes 130 - 130.1) then hold on 4% until minute 150. The flow rate was 0.3 $\mu\text{L}/\text{min}$.

Data-independent acquisition

The DIA duty cycle consisted of one MS1 scan followed by 30 MS2 scans with an isolation window of the 4 m/z range, overlapping with an adjacent window at the 2 m/z range. MS1 scan was conducted with Orbitrap at 60000 resolution power and a scan range of 200 - 1800 m/z with an adjusted RF lens at 30%. MS2 scans were conducted with Orbitrap at 30000 resolution power, RF lens was set to 30%. The precursor mass window was restricted to a 500 - 740 m/z range. HCD fragmentation was enabled as an activation method with a fixed collision energy of 35%. FAIMS was performed with one CV at -45V for both MS1 and MS2 scans during the duty cycle.

Data-dependent acquisition

For measurements of DDA-MS2 mode, the Orbitrap Eclipse Tribrid Mass Spectrometer was operated with the following settings: Polarity: positive; MS1 resolution: 240k; MS1 AGC target: standard; MS1 maximum injection time: 50 ms; MS1 scan range: m/z 375-1500; MS2 ion trap scan rate: rapid; MS2 AGC target: standard; MS2 maximum injection time: 35 ms; MS2 cycle time: 1.7 s; MS2 isolation window: m/z 1.2; HCD stepped normalised collision energy: 30%; intensity threshold: 1.0×10^4 counts; included charge states: 2-6; dynamic exclusion: 60 s. FAIMS was performed with two alternating CVs, including -50 V and -70 V.

Quantification and statistical analysis

Computational evaluation of DIA raw files

Raw files were converted in the first step with "MSConvertGUI" as a part of the "ProteoWizard" software package (<http://www.proteowizard.org/download.html>) to an output mzML format applying the "peakPicking" filter with "vendor msLevel=1", and the "Demultiplex" filter with parameters "Overlap Only" and "mass error" set to 10 ppm.

Standalone DIA-NN software under version 1.8.1 was used for protein identification and quantification.

First, a spectral library was predicted *in silico* by the software's deep learning-based spectra, RTs and IMs prediction using Uniprot *H. sapiens* decoyed FASTA (canonical and isoforms - May 2022). FASTA digest for library-free search/library generation option was enabled for this. Spectral

library prediction was performed in 4 batches of 10 samples each to decrease the computational load.

Second, all samples (40) were processed together without spectral library generation, with a match between runs (MBR) option and precursor FDR level set at 1%. Previously generated spectral libraries were implemented during the search by presenting the command ('--lib [file name]') into the command box.

DIA-NN search settings: Library generation was set to smart profiling, Quantification strategy - Robust LC. The mass accuracy and the scan window were set to 0 to allow the software to identify optimal conditions. The precursor m/z range was changed to 500-740 m/z to fit the measuring parameters.

Carbamidomethylation was set as a fixed modification, oxidation of methionine and N-term acetylation were set as variable modifications. On the contrary, the small-scale samples of the 96-well plate were calculated without carbamidomethylation as a fixed modification.

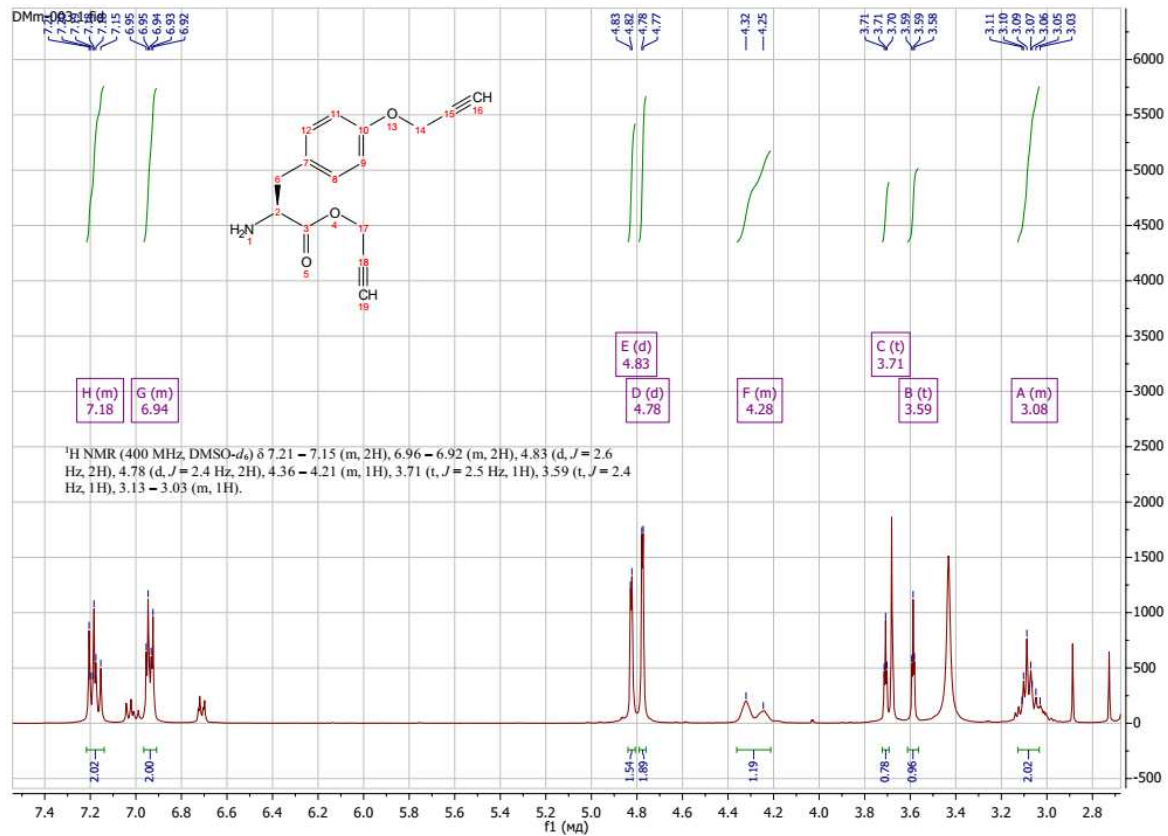
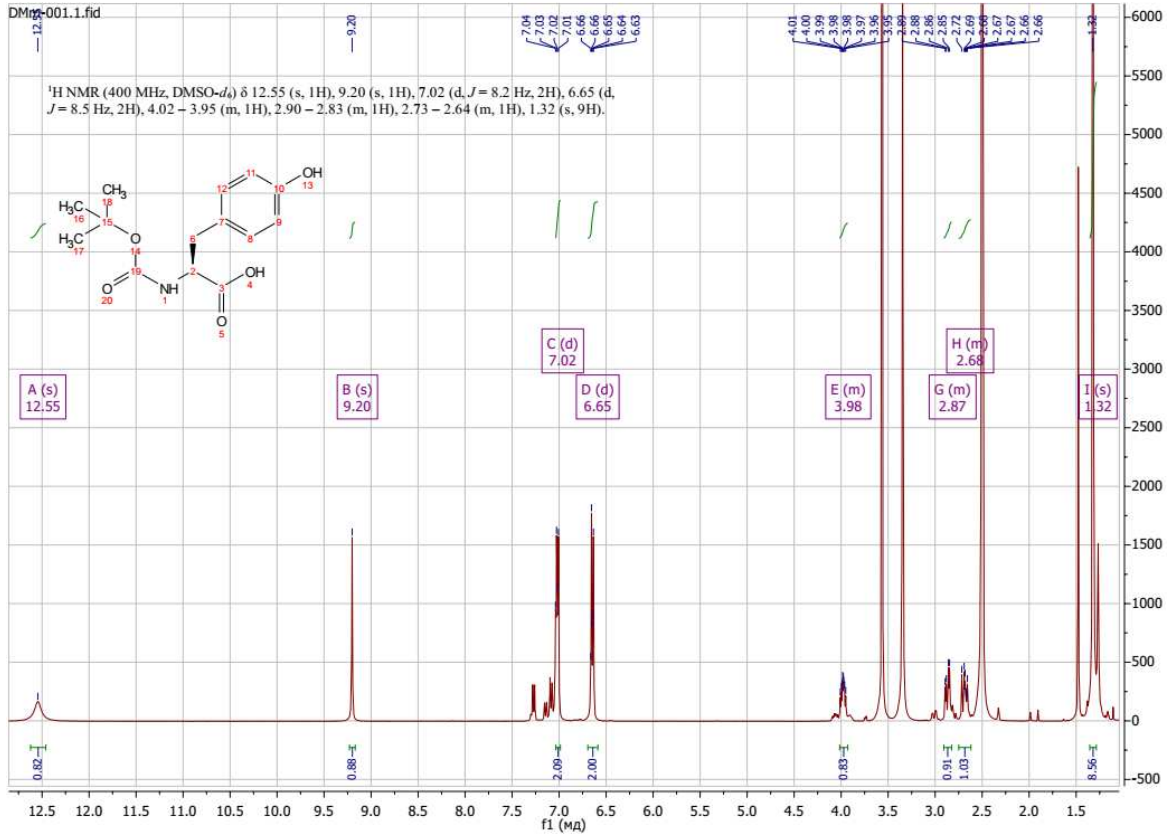
Statistical analysis of the DIA-NN result table "report.pg_matrix.csv" was done with Perseus 1.6.10.43.^[8] First, potential contaminants, as well as reverse peptides, were removed from the table. Then the LFQ intensities were log₂-transformed. Afterward, the rows corresponding to a time point were divided into two groups – Control and Probe-treated sample. Subsequently, the groups were filtered for at least three valid values out of four rows in at least one group, and the missing values were replaced from a normal distribution with a downshift of 1.8. The -log₁₀(p-values) were obtained by a two-sided one-sample Student's t-test over replicates with the initial significance level of p = 0.05. Fold change values, as well as p-values, were obtained for each time point.

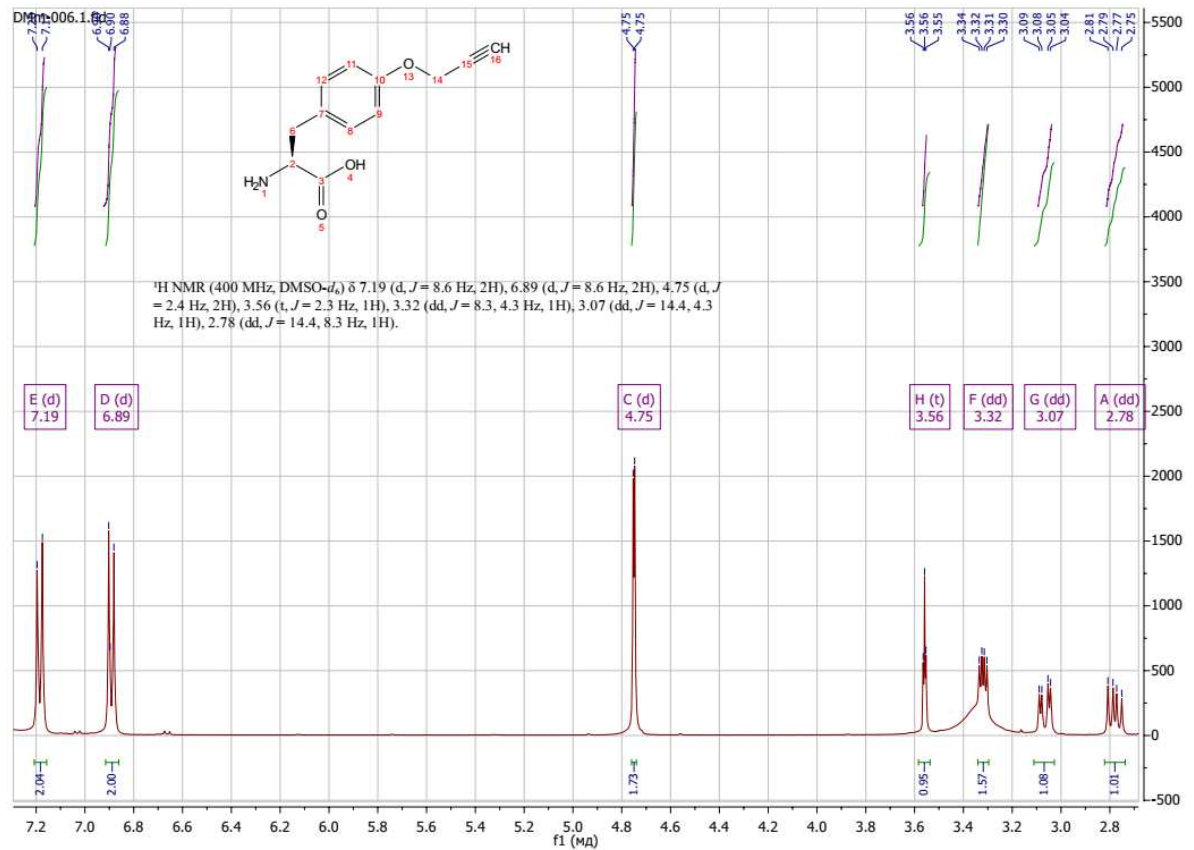
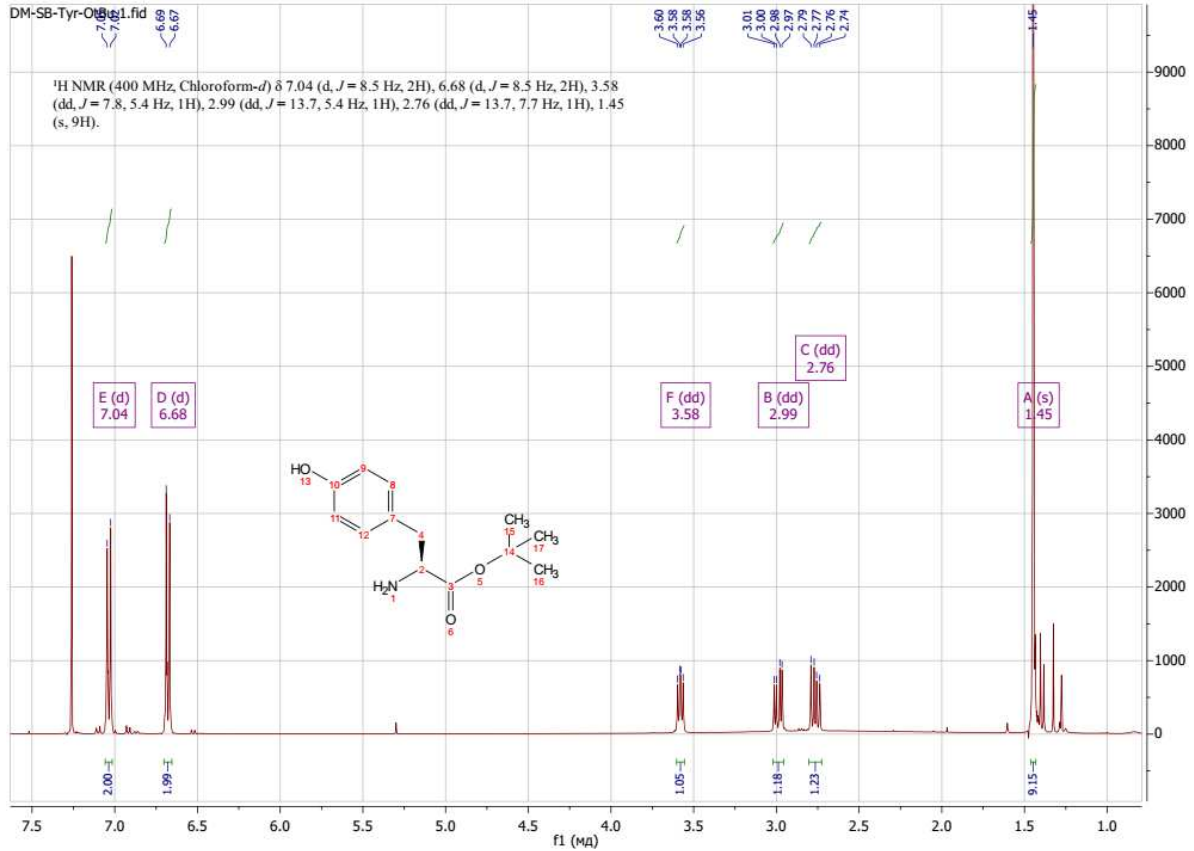
Computational evaluation of DDA raw files

Raw files were converted in the first step, with "MSConvertGUI" as a part of the "ProteoWizard" software package (<http://www.proteowizard.org/download.html>) to an output mzML format applying the "peakPicking" filter with "vendor msLevel=1". Converted files were further calculated with the proteomics pipeline FragPipe version 18.0 containing a search engine MSFragger version 3.5. Search settings were established: closed search approach with precursor mass tolerance in a range of -20 – 20 ppm and fragment mass tolerance 20 ppm. Carbamidomethylation was set as a fixed modification and methionine oxidation as well as N-terminal acetylation as a variable modification. As a variable modification, a mass delta of 38.0156 m/z was set corresponding to a propargyl modification, occurring on Y. False discovery rate determination was carried out using a decoy database and thresholds were set to 1% FDR both at a peptide-spectrum match and at protein levels.

Mass spectrometry-based proteomics data have been deposited at ProteomeXchange. The accession number is PXD037402.

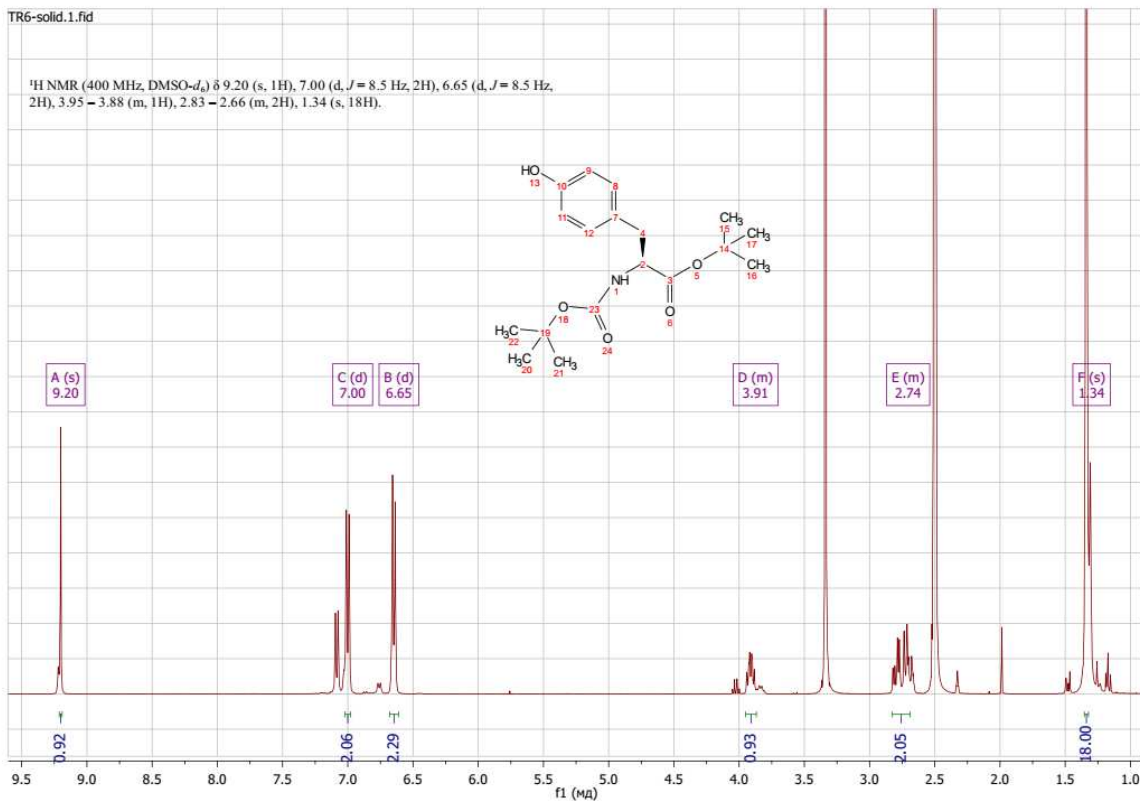
NMR Spectra





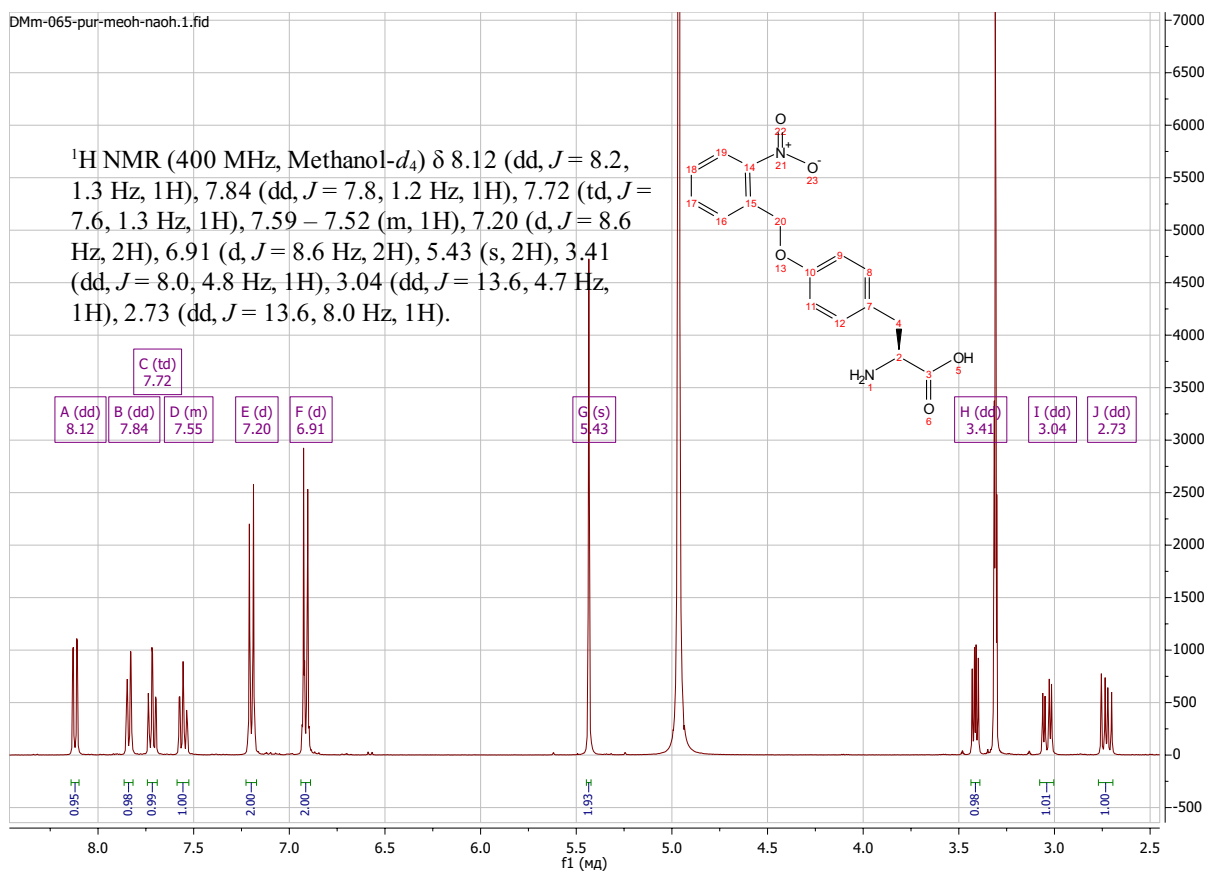
TR6-solid.1.fid

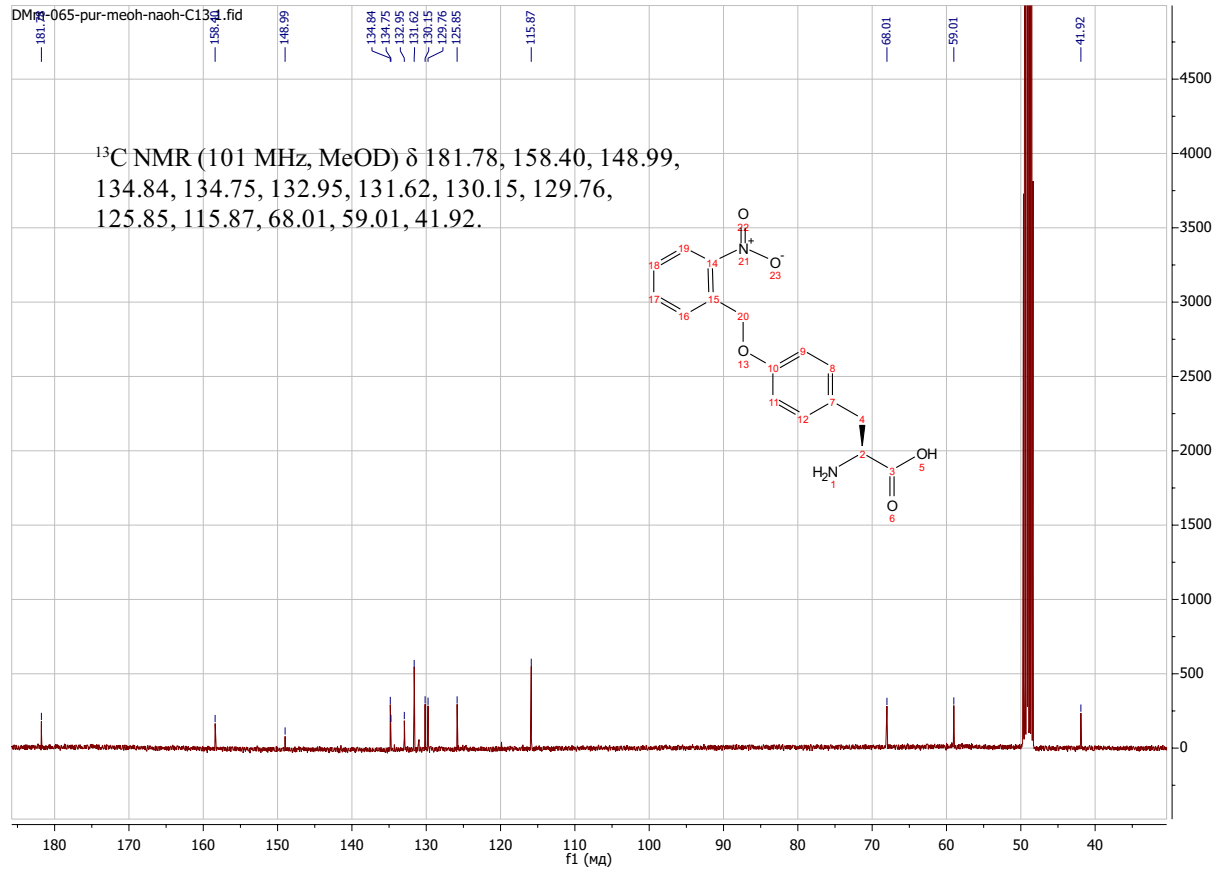
$^1\text{H NMR}$ (400 MHz, $\text{DMSO-}d_6$) δ 9.20 (s, 1H), 7.00 (d, $J = 8.5$ Hz, 2H), 6.65 (d, $J = 8.5$ Hz, 2H), 3.95 – 3.88 (m, 1H), 2.83 – 2.66 (m, 2H), 1.34 (s, 18H).



DMm-065-pur-meoh-naoh.1.fid

$^1\text{H NMR}$ (400 MHz, $\text{Methanol-}d_4$) δ 8.12 (dd, $J = 8.2$, 1.3 Hz, 1H), 7.84 (dd, $J = 7.8$, 1.2 Hz, 1H), 7.72 (td, $J = 7.6$, 1.3 Hz, 1H), 7.59 – 7.52 (m, 1H), 7.20 (d, $J = 8.6$ Hz, 2H), 6.91 (d, $J = 8.6$ Hz, 2H), 5.43 (s, 2H), 3.41 (dd, $J = 8.0$, 4.8 Hz, 1H), 3.04 (dd, $J = 13.6$, 4.7 Hz, 1H), 2.73 (dd, $J = 13.6$, 8.0 Hz, 1H).





References

- [1] N. A. Bindman, S. C. Bobeica, W. R. Liu, W. A. van der Donk, *J Am Chem Soc* **2015**, *137*, 6975–8.
- [2] M. Farhadpour, S. Maghari, H. Rezadoost, M. Bagheri, A. Ghassempour, *J Chromatogr* **2020**, *1621*, 461045.
- [3] Z. Zhang, L. Yin, Y. Xu, R. Tong, Y. Lu, J. Ren, J. Cheng, *Biomacromolecules* **2012**, *13*, 3456–3462.
- [4] K. Manna, H. M. Begam, K. Samanta, R. Jana, *Org Lett* **2020**, *22*, 7443–7449.
- [5] V. Rerat, G. Dive, A. A. Cordi, G. C. Tucker, R. Bareille, J. Amédée, L. Bordenave, J. Marchand-Brynaert, *J Med Chem* **2009**, *52*, 7029–43.
- [6] M. Trebacz, Y. Wang, L. Makotta, L. Henschke, M. Köhn, *J Org Chem* **2019**, *85*, 1712–1717.
- [7] S. Peuker, H. Andersson, E. Gustavsson, K. S. Maiti, R. Kania, A. Karim, S. Niebling, A. Pedersen, M. Erdelyi, S. Westenhoff, *J Am Chem Soc* **2016**, *138*, 2312–8.
- [8] S. Tyanova, T. Temu, P. Sinitcyn, A. Carlson, M. Y. Hein, T. Geiger, M. Mann, J. Cox, *Nat Methods* **2016**, *13*, 731–40.

8.3. Experimental section: Investigating Tubulin Dynamics Using Tyr-O-Alk Probes in TTL and SVBP Knockout Model Systems

Cell culture

Mice embryonic fibroblast (**MEF**) cell line was prepared from cryostocks using the standard protocol. The tube containing the frozen cells was defrosted by placing it into 37°C water bath. The content of the tube was transferred into 50 mL falcon and 10 mL of MEF medium (low glucose DMEM, 10% FBS, 1% PenStrep) was added. The cells were centrifuged at 250 × rcf for 5 min and the medium was removed. The cells were resubstituted in the fresh MEF medium (5mL) and the cell suspension was placed into p60 Petri dish. For the cell splitting, the standard protocol from Chapter 8.2 was used.

Cell harvesting and lysate preparation

The standard protocol from Chapter 8.2 was used.

BCA protein concentration evaluation

The standard protocol from Chapter 8.2 was used.

MS samples preparation

Standard protocol for a big-scale SP2E enrichment analysis from Chapter 8.2 was used.

MS measurement and data analysis

MS samples were measured using the DIA method described in Chapter 8.2.

8.4. Experimental section: Implementation of Tyr-O-Alk probe-based screening platform for identifying potential TTL inhibitors

Cell culture

Standard protocol for SH-SY5Y cells culturing described in Chapter 8.2 was used.

Harvesting and lysate preparation

The standard protocol from Chapter 8.2 was used.

Protein concentration

The standard protocol from Chapter 8.2 was used.

Click reaction

The final concentration of the proteins in the samples was adjusted at 1mg/mL. Lysates were diluted to 100 μ L with lysis buffer (1% NP40, 0.2% SDS in 25 mM Hepes, 7.5 pH). For each sample, 1 μ L of Tamra-N₃ (10 mM in DMSO), 3 μ L of TCEP (100 mM in H₂O), and 0.125 μ L TBTA (83.5 mM in DMSO) were added, vortexed, spun down, and supplemented with 2 μ L of CuSO₄ (50 mM in H₂O) to initiate the reaction. The reaction mixture was incubated at RT. while shaking at 650 rpm for 1.5 h in dark.

SDS-Page

Standard protocol for in-gel analysis from Chapter 8.2 was used.

WB

The standard protocol from Chapter 8.2 was used.

Anti- α -tubulin Antibody, tyrosinated, clone YL1/2 with catalog number MAB1864-I (Sigma-Aldrich) and anti-alpha tubulin antibody, non-tyrosinated with catalog number ABT170 (Sigma-Aldrich) were used for the analysis.

Normalization of the signals from SDS-Page and WB

For the intensity analysis, GelAnalyzer, ver 19.1 was used.⁹⁷ The pixel density of each fluorescent or WB band (PI_{band}) was measured and normalized to the overall band intensity from the Coomassie staining gel (PI_{ref}) or to GAPDH band to obtain normalized intensity value (PI_{norm}).

$$PI_{norm} = \frac{PI_{band}}{PI_{ref}}$$

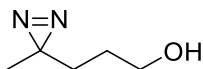
Where:

- PI_{band} – pixel intensity of the band representing protein of interest
- PI_{ref} – pixel intensity of the reference signal (Coomassie staining or GAPDH-signal)

8.5. Experimental section: Synthesis of modified tyrosine probe simultaneously derivatized with terminal alkyne and photocleavable diazirine probe for the study of tubulin PPIs

Synthesis

Synthesis of 3-(3-methyl-3*H*-diazirin-3-yl)propan-1-ol



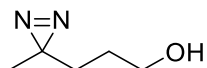
2

Under anhydrous conditions, the reaction flask containing the starting compound **1** (1.0 g, 9.8 mmol, 1 eq) was dissolved in anhydrous MeOH (10 mL) and cooled down on an ice bath. A methanolic solution of NH₃ (7N NH₃ in MeOH, 21 mL, 15 eq) was added to the mixture and incubated for 5 h. A separate flask containing hydroxylamine-*O*-sulfonic acid (HOSA) (1.4g, 12.7 mmol, 1.3 eq) in anhydrous MeOH (10 mL) was prepared under anhydrous conditions and cooled down on an ice bath. The solution of imine from the first RM was added to the HOSA solution dropwise. The RM was incubated at RT. overnight. To eliminate the excess of NH₃, N₂ gas was bubbled through the RM for 30 min. The formed solids were filtered off through the celite and the filter cake was washed with MeOH (3 × 10 mL). The combined fraction was concentrated *in vacuo* until half volume. The concentrated mixture was then treated with Et₃N (7 mL, 68.5 mmol, 7 eq) and cooled down for 30 min on ice. Molecular I₂ (3.5 g, 13.7 mmol, 1.4 eq) was added to the RM portion-wise at 0°C. The RM was stirred for 3 hours at RT. The RM was concentrated *in vacuo*, and the residue was extracted with Et₂O (3 × 30 mL). The combined organic phase was washed with HCl (1M in H₂O, 10 mL), a solution of Na₂S₂O₃ (10% in H₂O, 10 mL), and brine (10 mL). The organic phase was dried under MgSO₄ and evaporated *in vacuo*. The product was purified by silica gel column chromatography (DCM/MeOH = 95/5). The pale-yellow product **2** was obtained in low yield (70.0 mg, 6%)

NMR data agreed with the literature.⁹⁸

¹H NMR (500 MHz, Chloroform-*d*) δ 3.64 – 3.60 (m, 2H), 1.46 – 1.43 (m, 4H), 1.02 (s, 3H).

Synthesis of 3-(3-methyl-3H-diazirin-3-yl)propan-1-ol⁷⁸



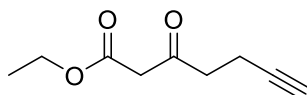
2

The model ketone **1** (0.4 g, 3.9 mmol, 1 eq.) was dissolved in dry MeOH (2 mL) under anhydrous conditions, then a methanolic solution of NH₃ (7N NH₃ in MeOH, 2.8 mL, 20 mmol, 10 eq.) was added dropwise into the solution. Before the dropwise addition to the RM, *t*-BuOCl (1.3 g, 11.8 mmol, 3 eq) was dissolved in *t*-BuOH (2 mL). The reaction mixture was stirred for 4 h at rt. The inert gas was then bubbled through the solution for 20 min to remove the excess of ammonia. The second portion of *t*-BuOCl (0.6 g, 5.8 mmol, 1.5 eq.) was dissolved in *t*-BuOH (2 mL) and added dropwise to the solution, and the RM was stirred for 30 min at RT. under anhydrous conditions. The RM was then concentrated *in vacuo*. The crude product was quenched with a solution of saturated aq. Na₂S₂O₃ (5 mL) and extracted with Et₂O (3 × 10 mL). The combined organic fractions were dried over MgSO₄ and concentrated *in vacuo*. The product was purified by silica gel column chromatography (Hex/EtOAc = 7/3). The product **2** was obtained in reasonable yield (0.12 g, 27%).

NMR data agreed with the literature.⁹⁸

¹H NMR (500 MHz, Chloroform-*d*) δ 3.65 – 3.59 (m, 2H), 1.47 – 1.43 (m, 4H), 1.02 (s, 3H).

Synthesis of ethyl 3-oxohept-6-ynoate⁹⁹



5

To a solution of DiPA (6.2 mL, 44.1 mmol, 2.3 eq) in dry THF (30 mL), *n*-BuLi (2.5M in Hex, 18 mL, 44.1 mmol, 2.3 eq.) was added dropwise at -78°C (dry ice-acetone bath) under anhydrous conditions, and the solution was stirred for 5 min. The -78°C bath was exchanged for an ice bath before the addition of acetoacetate. Acetoacetate (2.5 g, 2.45 mL, 19.2 mmol, 1 eq.) was added dropwise to the LDA solution. Then, the RM was stirred at 0°C for 30 min. Then, propargyl bromide was added (2.9 g, 2.1 mL, 19.2 mmol, 1 eq.), and the mixture was stirred for another 1 hour at 0°C. The reaction was quenched by pouring the RM into aq. NH₄Cl solution (1M, 40 mL) and mixing. Excess THF was evaporated *in vacuo* before extraction of the product with EtOAc (3 × 30 mL). The resulting organic fraction was dried under MgSO₄. The solvent was removed

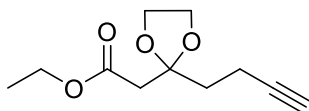
in vacuo. The product **5** was purified by silica gel column chromatography (Hex/EtOAc = 9/1). The product was obtained in reasonable yield (1.9 g, 58%).

NMR data agreed with the literature.⁹⁹

¹H NMR (500 MHz, Chloroform-*d*) δ 4.20 (q, $J = 7.1$ Hz, 2H), 3.46 (s, 2H), 2.81 (t, $J = 7.2$ Hz, 2H), 2.52 – 2.38 (m, 2H), 1.96 (t, $J = 2.7$ Hz, 1H), 1.28 (t, $J = 7.1$ Hz, 3H).

MS (ESI⁺): m/z (%): 169.16 (100) [M+H]⁺, 186.25 (40) [M+NH₄]⁺

Synthesis of ethyl 2-(2-(but-3-yn-1-yl)-1,3-dioxolan-2-yl)acetate⁹¹



6

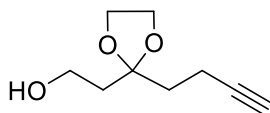
Propargyl **5** (0.83 g, 1 eq) was dissolved in dry DCM (20 mL), and TMS-protected ethan-1,2-diol (3.71 mL, 2 eq) was added to the reaction mixture under inert conditions. Trimethylsilyl triflate (0.18 mL, 0.2 eq) was carefully added to the RM. The RM was then incubated for 18 hours at rt. An aq. solution of NaHCO₃ (1M, 30 mL) was added to the RM, and mixed. After the separation of phases, the aqueous phase was extracted with Et₂O (3 × 20 mL). Organic phases were combined, dried, and concentrated *in vacuo*. The product was purified by silica gel column chromatography (Hex/EtOAc = 0-15%). The product **6** was obtained in almost quantitative yield (1 g, 96%)

NMR data agreed with the literature.⁹⁹

¹H NMR (500 MHz, Chloroform-*d*) δ 4.15 (q, $J = 7.1$ Hz, 2H), 4.07 – 3.91 (m, 4H), 2.65 (s, 2H), 2.36 – 2.25 (m, 2H), 2.20 – 2.04 (m, 2H), 1.93 (t, $J = 2.7$ Hz, 1H), 1.27 (t, $J = 7.1$ Hz, 3H).

MS (ESI⁺): m/z (%): 213.17 (100) [M+H]⁺.

Synthesis of 2-(2-(but-3-yn-1-yl)-1,3-dioxolan-2-yl)ethan-1-ol⁹⁹



7

To a stirred suspension of LiAlH₄ (6.6 mL, 1.4 eq, 1M in THF) in dry THF (20 mL) a solution of propargyl ester **6** (1.0 g, 4.7 mmol, 1 eq) premixed in dry THF (5 mL) was added dropwise at 0°C. The mixture was stirred for 30 min at 0°C and subsequently for 1.5 hours at rt. The reaction was

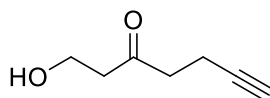
quenched with H₂O (50 mL) at 0°C and filtered. The filter cake was washed with Et₂O (3 × 50mL) and filtered. After phase separation, the organic phase was dried over MgSO₄, filtered and concentrated *in vacuo*. The crude product was purified by silica gel column chromatography (Hex/EtOAc = 7/3). The product **7** was obtained in almost quantitative yield (0.72 g, 90%).

NMR data agreed with the literature.⁹⁹

¹H NMR (500 MHz, Chloroform-*d*) δ 4.06 – 3.94 (m, 4H), 3.76 (q, *J* = 5.6 Hz, 2H), 2.63 (t, *J* = 5.7 Hz, 1H), 2.31 – 2.23 (m, 2H), 1.98 – 1.90 (m, 4H), 1.90 – 1.81 (m, 1H).

MS (ESI⁺): *m/z* (%): 171.19 (100) [M+H]⁺.

Synthesis of 1-hydroxyhept-6-yn-3-one⁷⁶



8

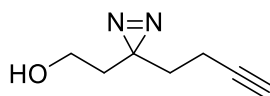
The propargyl ketal **7** (0.5 g, 2.9 mmol, 1.0 eq) was treated with *p*-TsOH × H₂O (0.2 g, 1 mmol, 0.35 eq.) in acetone (20 mL) mixed with H₂O (2 mL). The mixture was stirred at room temperature for 16 hours. The RM was concentrated *in vacuo* before the extraction with Et₂O (3 × 25 mL). The extract was washed with saturated aq. solution of NaHCO₃ (1 × 10 mL), water (1 × 10 mL), and brine (1 × 10 mL), and then dried over MgSO₄. The residue was purified by silica gel column chromatography (Hex/EtOAc = 7:3). The product **8** was obtained in reasonable yield (180.0 mg, 49%).

NMR data agreed with the literature.⁷⁶

¹H NMR (500 MHz, Chloroform-*d*) δ 3.87 (q, *J* = 5.6 Hz, 2H), 2.73 – 2.68 (m, 4H), 2.47 (td, *J* = 7.4, 7.3, 2.7 Hz, 2H), 2.33 (t, *J* = 6.3 Hz, 1H), 1.96 (t, *J* = 2.7 Hz, 1H).

MS (ESI⁺): *m/z* (%): 127.23 (100) [M+H]⁺.

Synthesis of 2-(3-(but-3-yn-1-yl)-3H-diazirin-3-yl)ethan-1-ol⁷⁸



9

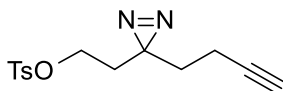
Propargyl-ketone **8** (0.24 g, 1.9 mmol, 1 eq.) was dissolved in dry MeOH (2 mL), then a methanolic solution of NH₃ (7N NH₃ in MeOH, 2.75 mL, 20 mmol, 10 eq.) was added dropwise into the RM.

Before the dropwise addition to the RM, *t*-BuOCl (0.640 g, 3 eq) was dissolved in *t*-BuOH (2 mL). The reaction mixture was stirred for 4 hours at rt. The inert gas was then bubbled through the solution for 20 min to remove the excess of ammonia. The second portion of *t*-BuOCl (0.320 g, 1.5 eq.) was dissolved in *t*-BuOH (2 mL) and added dropwise to the solution, and the RM was stirred for 30 min at rt. under anhydrous conditions. The RM was then concentrated *in vacuo*. The crude product was quenched with a solution of saturated aq. solution of Na₂S₂O₃ (5 mL) and extracted with Et₂O (3 × 10 mL). The combined organic fractions were dried over MgSO₄ and concentrated *in vacuo*. The residue was purified by silica gel column chromatography (Hex/EtOAc = 7/3). The product **9** was obtained in reasonable yield (0.12 g, 45%).

NMR data agreed with the literature⁷⁶

¹H NMR (500 MHz, Chloroform-*d*) δ 3.50 (q, *J* = 5.6 Hz, 2H), 2.07 – 2.03 (m, 2H), 2.00 (t, *J* = 2.6 Hz, 1H), 1.73 – 1.67 (m, 4H), 1.46 (t, *J* = 5.3 Hz, 1H).

Synthesis of 2-(3-(but-3-yn-1-yl)-3*H*-diazirin-3-yl)ethyl 4-methylbenzenesulfonate



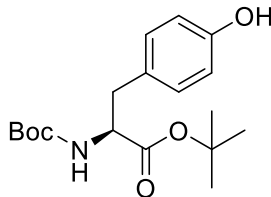
10

Propargyl diazirine **9** (0.12 g, 0.87 mmol, 1 eq.) was dissolved in DCM (5 mL), and the reaction mixture was cooled down at 0°C. *para*-Toluene sulfonyl chloride (0.2 g, 1.1 mmol, 1.2 eq.), triethylamine (0.17 mL, 1.4 eq.) and DMAP (10.00 mg, 0.1 eq.) were subsequently added to the RM. The RM was incubated for 18 hours allowing temperature to slowly increase to rt. After the completion of the reaction, the RM was washed with aq. NH₄Cl solution (1M, 1 × 10 mL), H₂O (1 × 10mL) and brine (1 × 5 mL). The combined organic phase was dried over MgSO₄. The product was then concentrated *in vacuo*. The product was purified by silica gel column chromatography (Hex/EtOAc = 7/3). The product **10** was obtained in reasonable yield (0.19 g, 73%).

¹H NMR (500 MHz, Chloroform-*d*) δ 7.81 (d, *J* = 8.3 Hz, 2H), 7.37 (d, *J* = 8.1 Hz, 2H), 3.90 (t, *J* = 6.4 Hz, 2H), 2.46 (s, 3H), 2.00 – 1.92 (m, 3H), 1.77 (t, *J* = 6.4 Hz, 2H), 1.61 (t, *J* = 7.4 Hz, 2H).

MS (ESI⁺): *m/z* (%): 293.20 (40) [M+H]⁺, 310.30 (100) [M+NH₄]⁺.

Synthesis of *tert*-butyl (*tert*-butoxycarbonyl)-L-tyrosinate⁹³



12

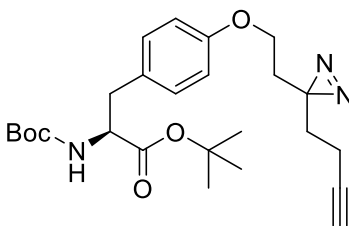
Boc-protected tyrosine **11** (2.0 g, 7.1 mmol, 1 eq.), BTEAC (1.6 g, 7.1 mmol, 1 eq.) and K₂CO₃ (25.5 g, 184.9 mmol, 26 eq.) was added to DMA (25 mL). After that, *t*-BuBr (46.7 g, 38.3 mL, 341.3 mmol, 48 eq.) was provided into RM. The reaction was incubated for 48 hours at 55°C. After cooling down, the RM was poured into H₂O (40 mL) and extracted with EtOAc (3 × 100 mL). The combined organic phase was dried with MgSO₄ and concentrated *in vacuo*. The crude product was purified by silica gel column chromatography (EtOAc/Hex = 10 – 50%). The product **12** was obtained as a yellowish viscous liquid in good yield (1.5 g, 61%).

NMR data agreed with the literature.⁹²

¹H NMR (500 MHz, Chloroform-*d*) δ 7.02 (d, *J* = 8.2 Hz, 2H), 6.75 (d, *J* = 8.5 Hz, 2H), 4.98 (d, *J* = 8.2 Hz, 1H), 4.39 (q, *J* = 6.7 Hz, 1H), 2.99 – 2.95 (m, 2H), 1.41 (d, *J* = 6.4 Hz, 18H).

MS (ESI⁺): *m/z* (%): 338.40 (100) [M+H]⁺.

Synthesis of *tert*-butyl (S)-3-(4-(2-(3-(but-3-yn-1-yl)-3H-diazirin-3-yl)ethoxy)phenyl)-2-((*tert*-butoxycarbonyl)amino)propanoate



13

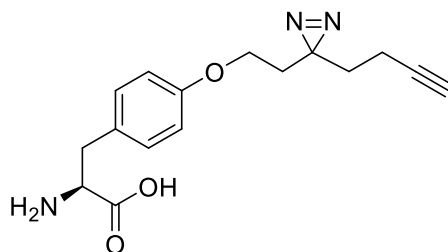
Boc-tyrosine *tert*-butyl ester **12** (0.22 g, 0.64 mmol, 1 eq.), tosyl-diazirine **10** (0.19 g, 0.64 mmol, 1 eq.) and Cs₂CO₃ (0.21 g, 0.64 mmol, 1 eq.) were added in one portion into DMF (5 mL). The RM was heated at 60°C for 18 hours. After completion of the reaction, DMF was evaporated *in vacuo*, and the crude product was dissolved in EtOAc (20 mL) and washed with H₂O (1 × 10 mL). The organic phase was concentrated *in vacuo*. The product was purified by silica gel column

chromatography (EtOAc/Hex = 0 – 20%). The product **13** was obtained in moderate yield (0.17 g, 60%).

^1H NMR (500 MHz, Chloroform-*d*) δ 7.07 (d, J = 8.6 Hz, 2H), 6.80 (d, J = 8.6 Hz, 2H), 4.96 (d, J = 8.2 Hz, 1H), 4.40 (q, J = 6.6 Hz, 1H), 3.80 (t, J = 6.2 Hz, 2H), 2.99 (t, J = 5.8 Hz, 1H), 2.07 (dd, J = 7.5, 2.5 Hz, 2H), 1.98 (t, J = 2.6 Hz, 1H), 1.87 (t, J = 6.2 Hz, 2H), 1.73 (t, J = 7.5 Hz, 2H), 1.42 (d, J = 4.5 Hz, 18H).

MS (ESI⁺): m/z (%): 458.46 (100) [M+H]⁺, 915.70 (80) [2M+H]⁺.

Synthesis of (S)-2-amino-3-(4-(2-(3-(but-3-yn-1-yl)-3H-diazirin-3-yl)ethoxy)-phenyl)propanoic acid



14

Protected tyrosine diazirine **13** (170.0 mg, 1 eq.) was dissolved in aq. TFA (90%, 3 mL) and incubated for 3 hours at rt. After the completion of the reaction, TFA was co-evaporated with toluene (5 times). The crude product was dissolved in aq. ACN (40%, 3 mL), and purified by reversed-phase chromatography on a C-18 column (ACN/H₂O = 20 – 80%). The desired product **14** was obtained in moderate yield (30.0 mg, 27%).

^1H NMR (800 MHz, DMSO-*d*₆) δ 7.16 (d, J = 8.6 Hz, 2H), 6.83 (d, J = 8.6 Hz, 2H), 3.76 (t, J = 6.0 Hz, 2H), 3.31 (dd, J = 8.3, 4.5 Hz, 1H), 3.05 (dd, J = 14.4, 4.5 Hz, 1H), 2.84 (t, J = 2.7 Hz, 1H), 2.78 (dd, J = 14.4, 8.3 Hz, 1H), 2.03 (td, J = 7.4, 2.7 Hz, 2H), 1.86 (t, J = 6.0 Hz, 2H), 1.65 (t, J = 7.4 Hz, 2H).

^{13}C NMR (201 MHz, DMSO) δ 169.13, 156.86, 130.39, 129.80, 114.31, 83.21, 71.82, 62.31, 55.66, 36.07, 31.83, 31.81, 27.08, 12.65.

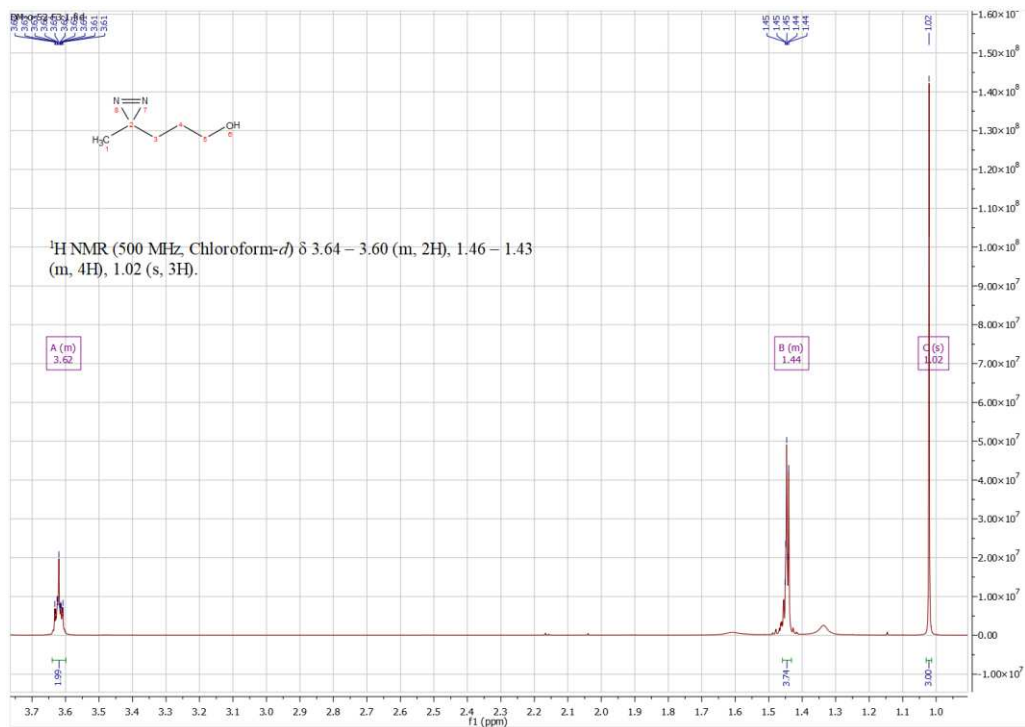
MS (ESI⁺): m/z (%): 302.28 (100) [M+H]⁺

HR-MS(ESI⁺): calculated for C₁₆H₂₀N₃O₃⁺ 301.15047, found 302.14974 (-0.17369 ppm)

HR-MS(ESI⁻): calculated for C₁₆H₁₈N₃O₃⁺ 300.13482, found 300.13478 (-0.5878 ppm)

Analytical section

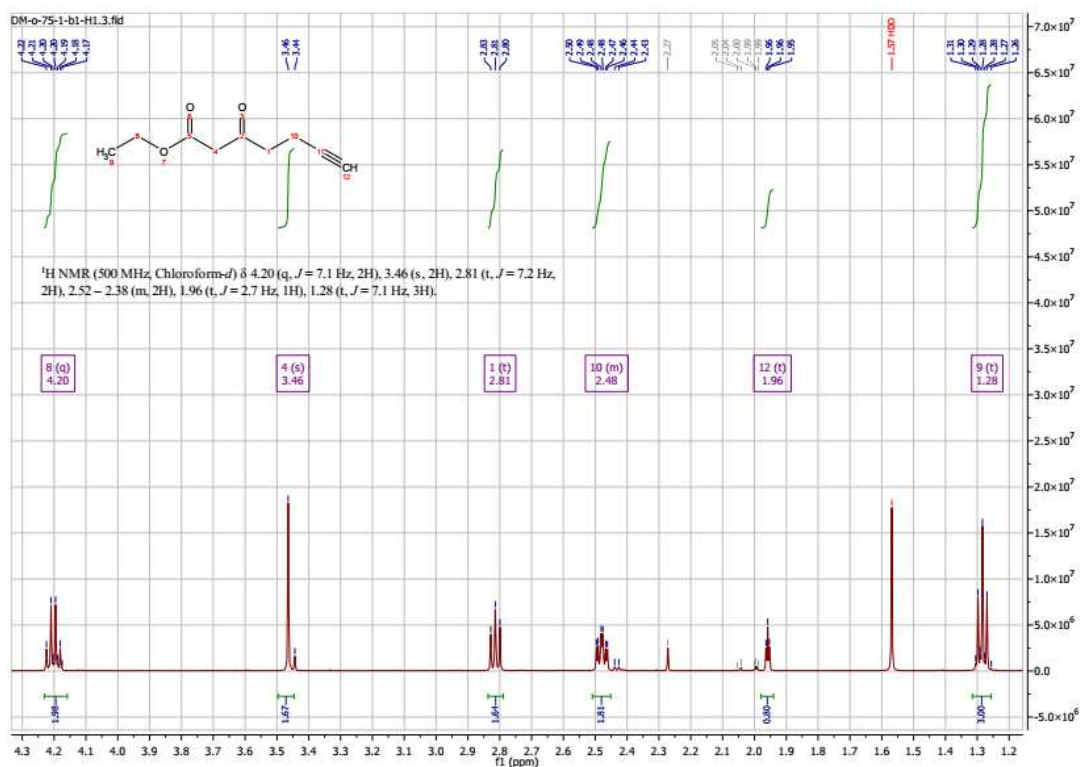
Synthesis of 3-(3-methyl-3*H*-diazirin-3-yl)propan-1-ol (**2**) under standard HOSA conditions



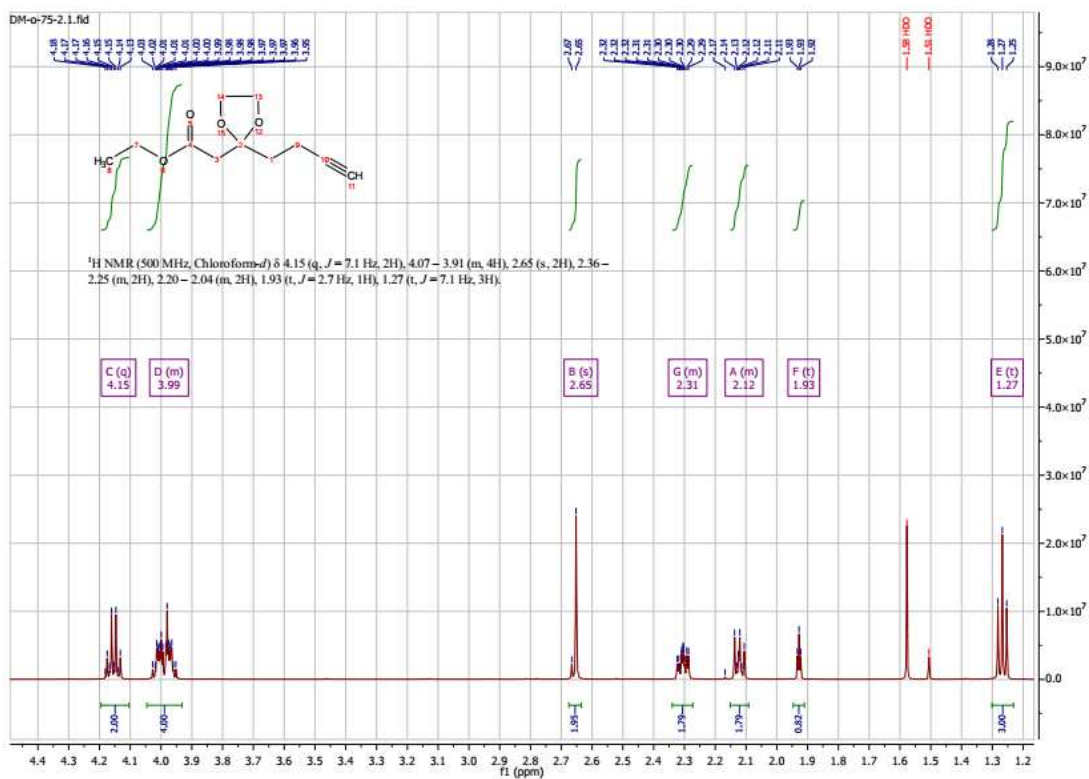
Synthesis of 3-(3-methyl-3*H*-diazirin-3-yl)propan-1-ol (**2**) under *t*-BuOCl conditions



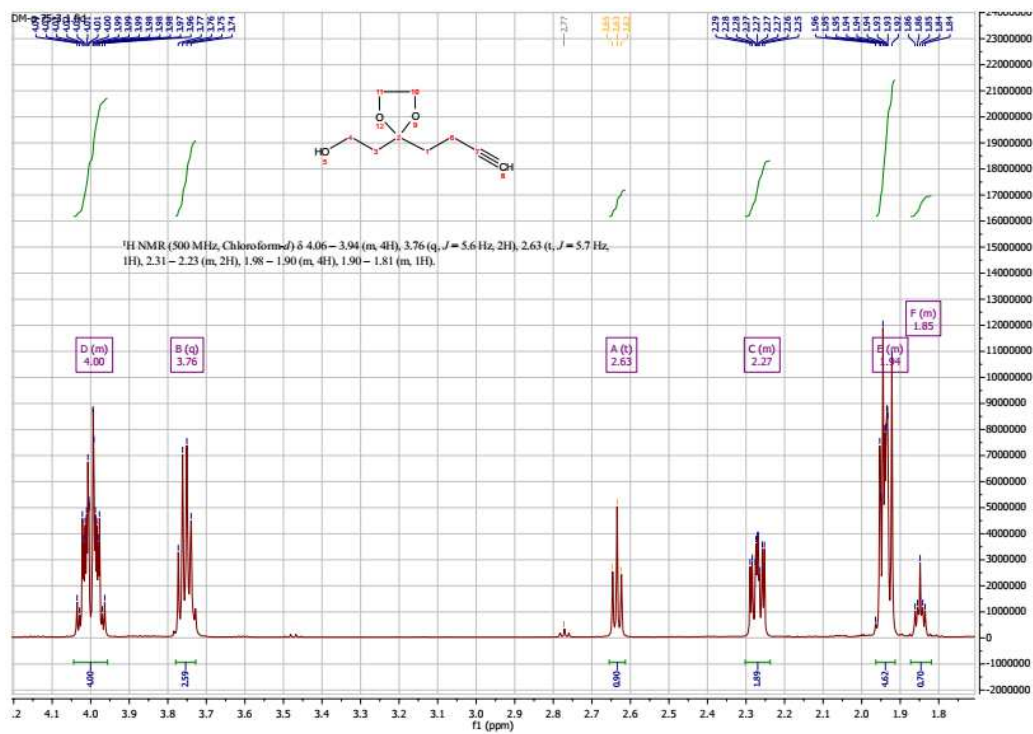
Synthesis of ethyl 3-oxohept-6-ynoate (5)



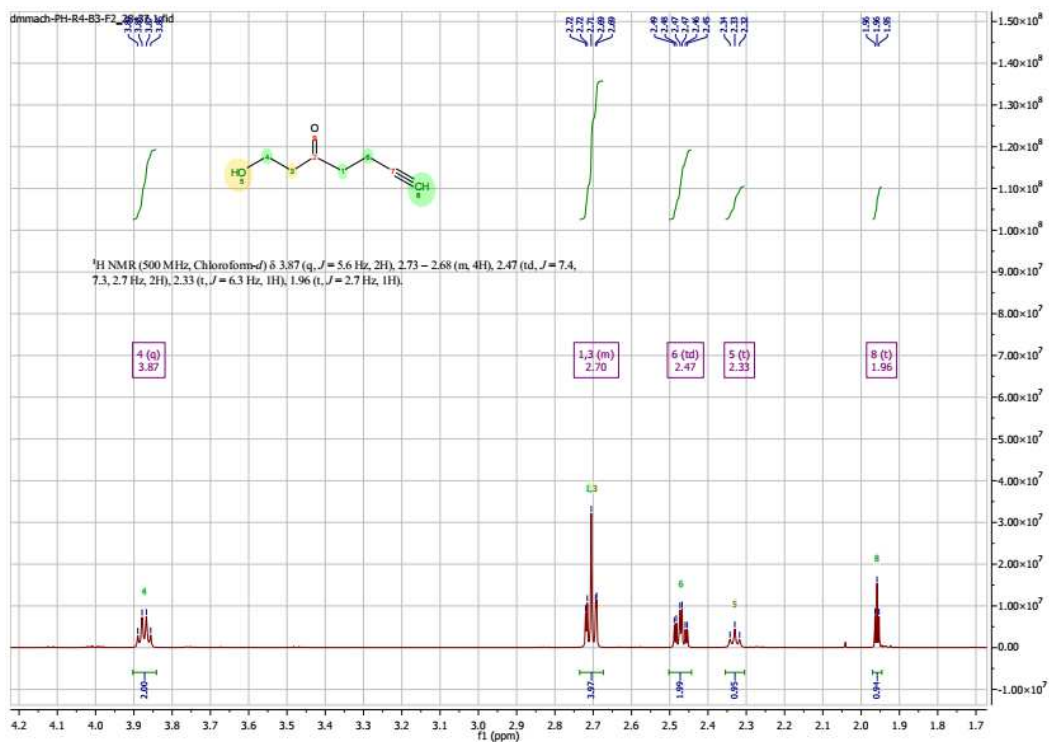
Synthesis of ethyl 2-(2-(but-3-yn-1-yl)-1,3-dioxolan-2-yl)acetate (6)



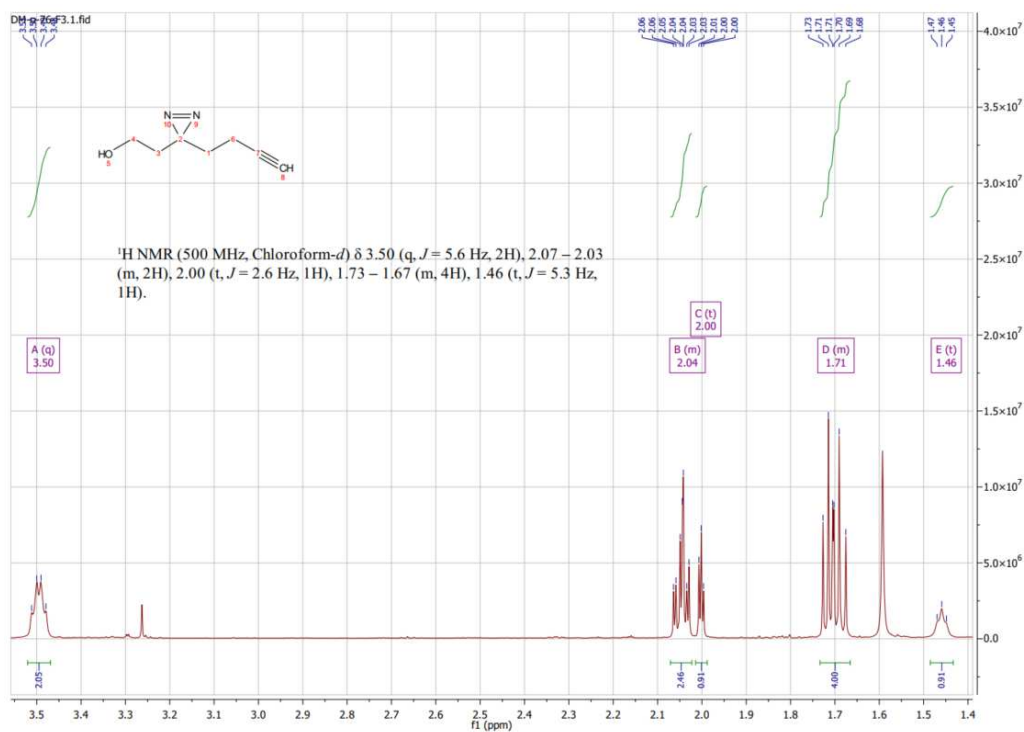
Synthesis of 2-(2-(but-3-yn-1-yl)-1,3-dioxolan-2-yl)ethan-1-ol (7)



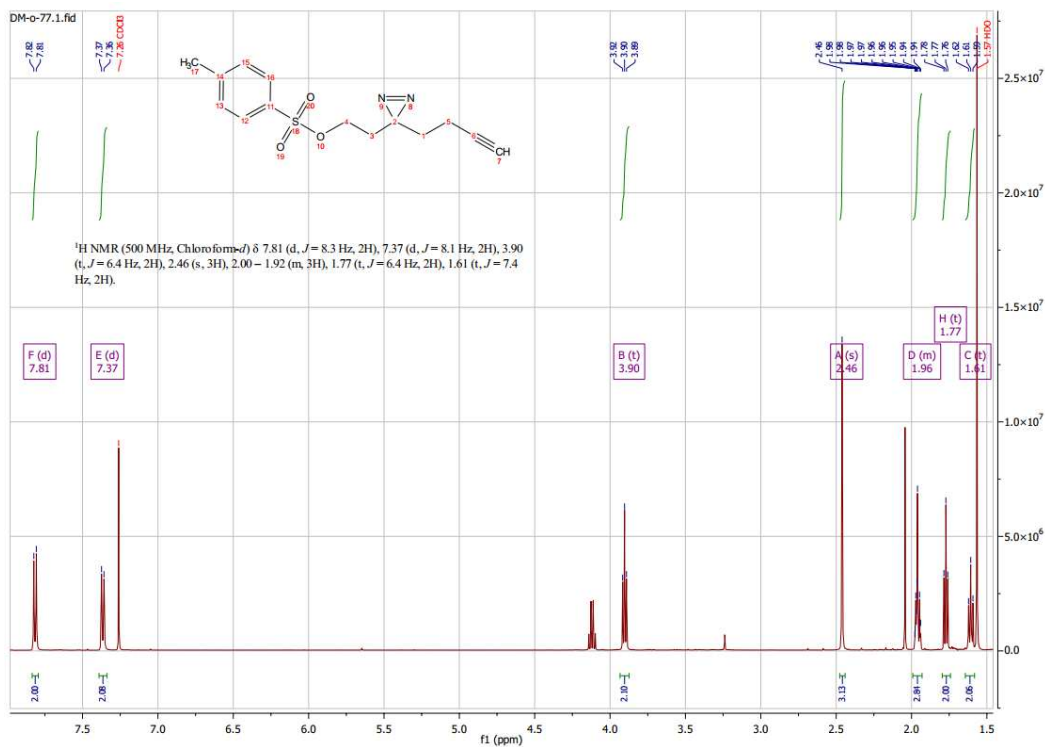
Synthesis of 1-hydroxyhept-6-yn-3-one (8)



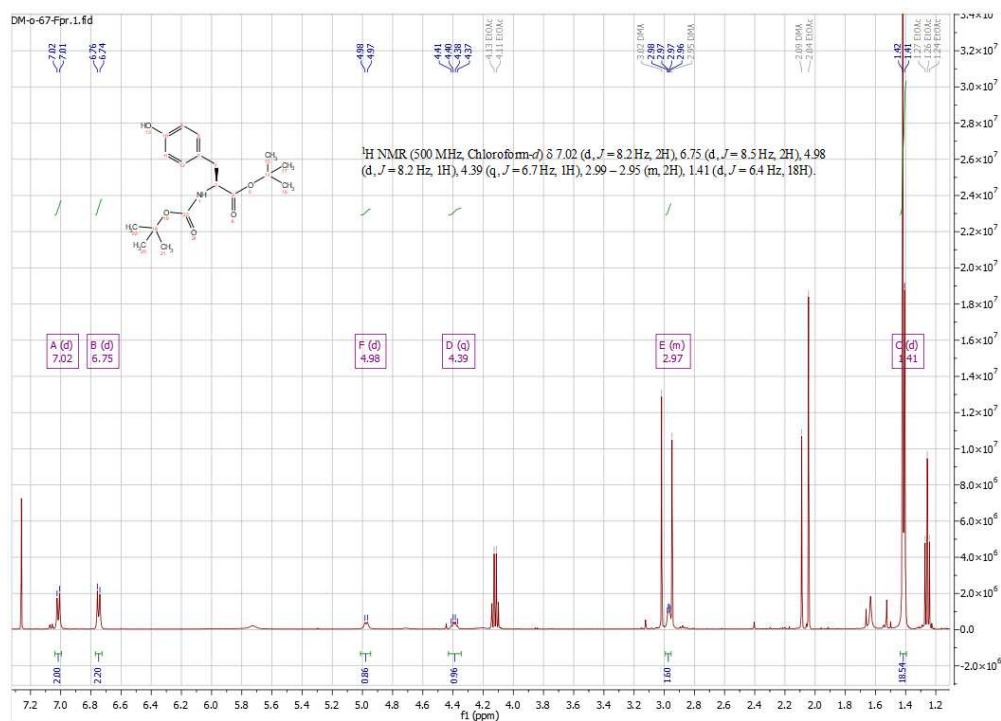
Synthesis of 2-(3-(but-3-yn-1-yl)-3H-diazirin-3-yl)ethan-1-ol (**9**)



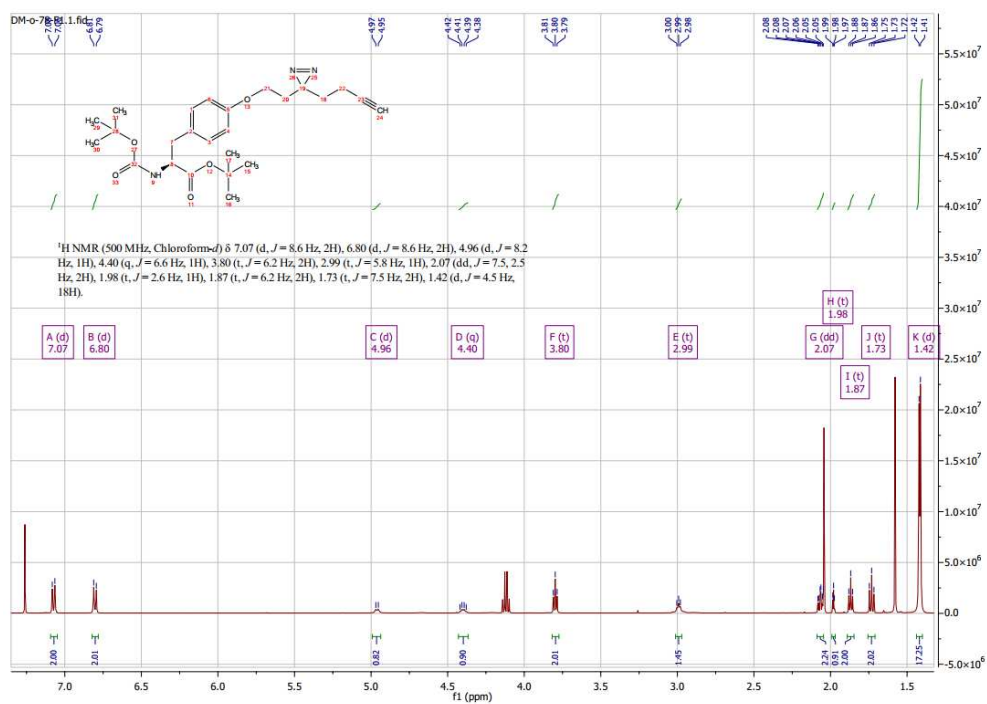
Synthesis of 2-(3-(but-3-yn-1-yl)-3H-diazirin-3-yl)ethyl 4-methylbenzenesulfonate (**10**)



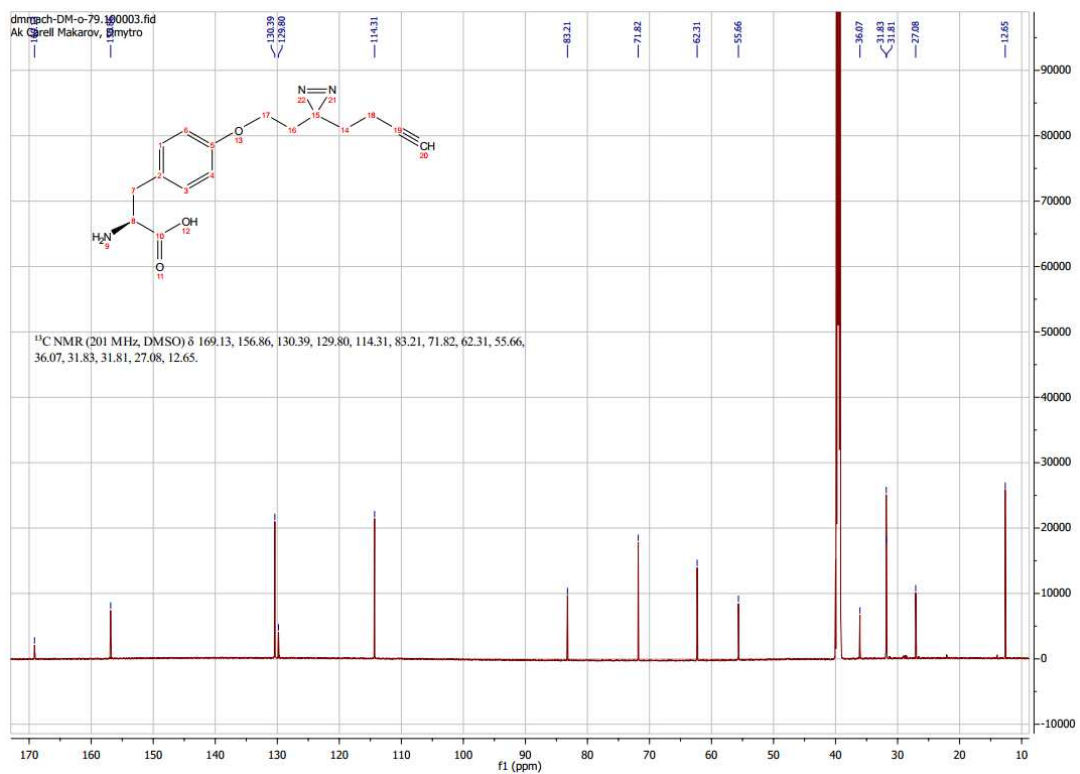
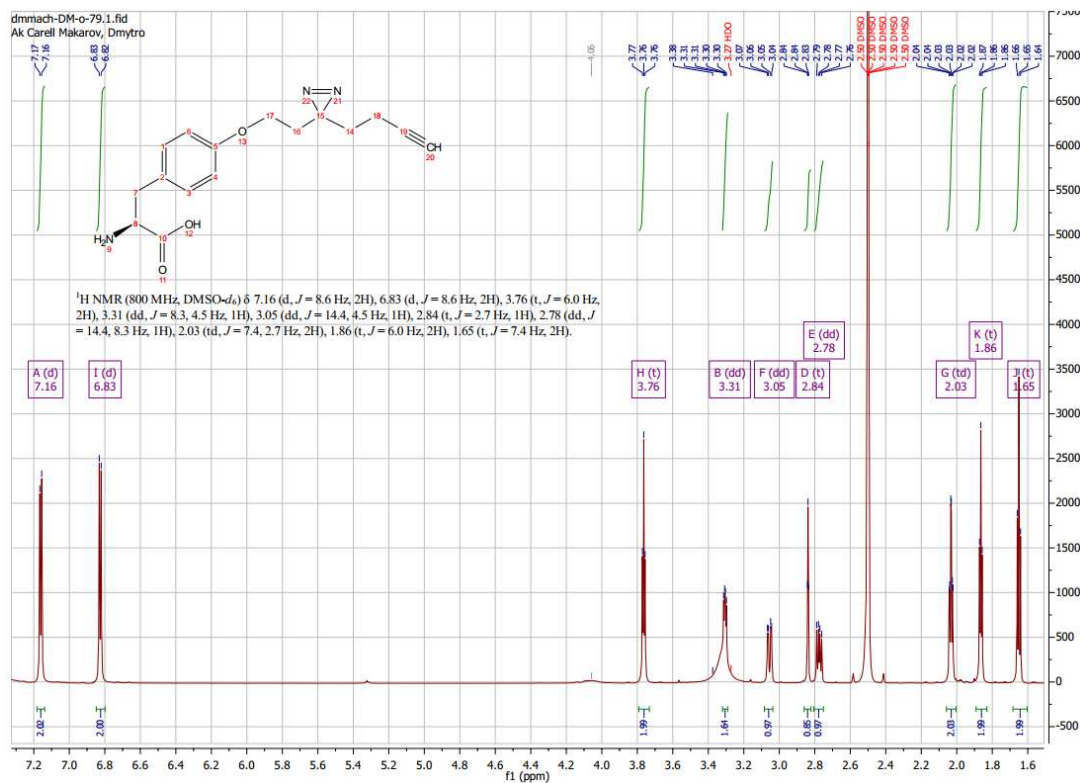
Synthesis of *tert*-butyl (*tert*-butoxycarbonyl)-L-tyrosinate (**12**)



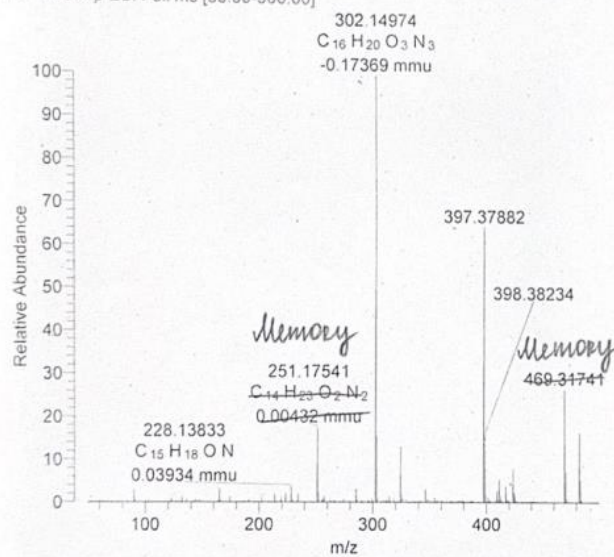
Synthesis of *tert*-butyl (S)-3-(4-(2-(3-(but-3-yn-1-yl)-3*H*-diazirin-3-yl)ethoxy)phenyl)-2-((*tert*-butoxycarbonyl)amino)propanoate (**13**)



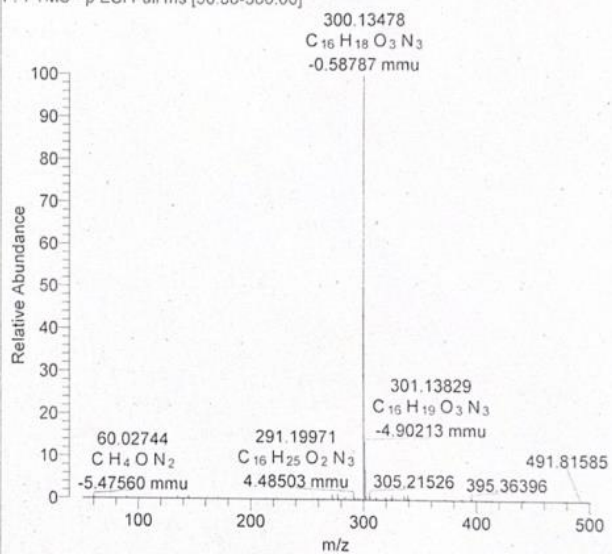
Synthesis of (S)-2-amino-3-(4-(2-(3-(but-3-yn-1-yl)-3H-diazirin-3-yl)ethoxy)phenyl)propanoic acid (14)



08-dmmach-DM-o-79 #38-189 RT: 0.51-1.95 AV: 19 NL: 1.41E6
F: FTMS + p ESI Full ms [50.00-500.00]



08-dmmach-DM-o-79 #38-187 RT: 0.55-1.90 AV: 18 NL: 6.33E6
F: FTMS - p ESI Full ms [50.00-500.00]



8.6. Experimental section: Decoding α -tubulin protein-protein interactions using photo-cleavable tyrosine probe

Cell culture

Standard protocol for SH-SY5Y cells culturing described in Chapter 8.2 was used.

Treatment scheme

cells were cultivated under 4 different conditions. Conditions were labeled as “Control”, “Probe UV-“, “Probe UV+”, and “Background control”. “Control” cells were treated with a blank solution without the probe for 24 hours. “Probe UV-“ condition cells were treated with the tyrosine-diazirine probe for 24 hours without subsequent photo-crosslinking reaction. “Probe UV+” cells were treated with the tyrosine-diazirine probe for 24 hours. The medium then was changed to a fresh one without the tyrosine-diazirine probe and cells were incubated for another 3 hours. Subsequently, the photo-crosslinking reaction was performed. “Background control” cells were grown under standard conditions and were treated with the tyrosine-diazirine probe 3 hours before the harvesting. Four biological replicates for each condition were collected. The final concentration of the tyrosine-diazirine probe was 0.3 mM in each treated plate.

UV-induced cross-linking and harvesting of cells

Cells were washed once with PBS (10 mL). After that, fresh PBS (10 mL) was added to the dish. “Probe UV+” and “Background control” cells were exposed to a 365 nm UV diode for 5 min before harvesting.

Harvesting and lysate preparation

The standard protocol from Chapter 8.2 was used.

Protein concentration measurement

The standard protocol from Chapter 8.2 was used.

Protein enrichment and MS sample preparation

A Large-scale SP2E protocol from Chapter 8.2 was implemented for the enrichment analysis with optimized click conditions aiming to reduce the background reactivity of the click reaction. Click reaction was conducted under the following conditions.

Samples for the enrichment protocol were prepared from the lysates so that each sample contained 400 µg of proteins. Lysates were diluted to 200 µL with lysis buffer (1% NP40, 0.2% SDS in 25 mM Hepes, 7.5 pH). For each sample, 2 µL of Biotin-N₃ (10 mM in DMSO), 6 µL of TCEP (100 mM in H₂O), and 0.24 µL TBTA (83.5 mM in DMSO) were added, vortexed, spun down, and supplemented with 4 µL of CuSO₄ (50 mM in H₂O) to initiate the reaction. The reaction mixture was incubated at RT. while shaking at 650 rpm for 1.5 h.

Later steps from the SP2E protocol remained unchanged.

MS measurement and data analysis

Samples were measured with DIA method and analyzed with DIA-NN software as described in the chapter 8.2.

GO term analysis

GO term analysis of upregulated proteins (226) in BG-control samples from the first experiment.

Data is obtained from VP [BG-control / Probe UV-] – see **Figure 32**

Table 1. GO Cellular Compartment. BG-control samples were obtained after the first experiment. A set of 226 hits was analyzed.

GO cellular component complete	Reflist (20592)	Found	Fold Enrichment	raw P-value	FDR
muscle thin filament tropomyosin (GO:0005862)	4	3	69.88	4.01E-05	1.60E-03
endosome to plasma membrane transport vesicle (GO:0070381)	3	2	62.12	1.10E-03	2.93E-02
sarcoplasmic reticulum lumen (GO:0033018)	10	3	27.95	3.12E-04	9.60E-03
spindle pole centrosome (GO:0031616)	15	3	18.64	8.57E-04	2.35E-02
striated muscle thin filament (GO:0005865)	23	4	16.2	1.79E-04	5.78E-03
smooth endoplasmic reticulum (GO:0005790)	31	5	15.03	3.72E-05	1.52E-03
myofilament (GO:0036379)	27	4	13.8	3.11E-04	9.71E-03
COPII-coated ER to Golgi transport vesicle (GO:0030134)	93	10	10.02	1.48E-07	7.80E-06
endoplasmic reticulum-Golgi intermediate compartment membrane (GO:0033116)	81	8	9.2	4.81E-06	2.13E-04
endoplasmic reticulum-Golgi intermediate compartment (GO:0005793)	134	13	9.04	6.10E-09	4.35E-07
endoplasmic reticulum lumen (GO:0005788)	314	29	8.61	5.59E-18	2.79E-15
azurophil granule membrane (GO:0035577)	58	5	8.03	5.50E-04	1.59E-02
azurophil granule (GO:0042582)	154	12	7.26	2.21E-07	1.08E-05
primary lysosome (GO:0005766)	154	12	7.26	2.21E-07	1.05E-05
vacuolar lumen (GO:0005775)	178	13	6.81	1.38E-07	7.48E-06
lysosomal lumen (GO:0043202)	99	7	6.59	1.38E-04	4.54E-03
azurophil granule lumen (GO:0035578)	90	6	6.21	5.61E-04	1.60E-02
sarcoplasmic reticulum (GO:0016529)	76	5	6.13	1.72E-03	4.09E-02

organelle envelope lumen (GO:0031970)	92	6	6.08	6.26E-04	1.74E-02
endoplasmic reticulum protein-containing complex (GO:0140534)	127	7	5.14	5.81E-04	1.64E-02
melanosome (GO:0042470)	113	6	4.95	1.72E-03	4.18E-02
pigment granule (GO:0048770)	113	6	4.95	1.72E-03	4.13E-02
coated vesicle (GO:0030135)	321	14	4.06	1.49E-05	6.35E-04
secretory granule lumen (GO:0034774)	321	13	3.77	6.27E-05	2.37E-03
cytoplasmic vesicle lumen (GO:0060205)	326	13	3.72	7.29E-05	2.65E-03
vesicle lumen (GO:0031983)	327	13	3.7	7.51E-05	2.68E-03
lytic vacuole (GO:0000323)	758	30	3.69	1.39E-09	1.21E-07
lysosome (GO:0005764)	758	30	3.69	1.39E-09	1.16E-07
endoplasmic reticulum (GO:0005783)	2065	78	3.52	1.14E-23	1.14E-20
vacuole (GO:0005773)	855	32	3.49	1.40E-09	1.12E-07
myofibril (GO:0030016)	241	9	3.48	1.46E-03	3.70E-02
contractile fiber (GO:0043292)	251	9	3.34	1.91E-03	4.50E-02
nuclear outer membrane-endoplasmic reticulum membrane network (GO:0042175)	1229	42	3.18	3.99E-11	4.20E-09
lytic vacuole membrane (GO:0098852)	443	15	3.15	1.21E-04	4.17E-03
lysosomal membrane (GO:0005765)	443	15	3.15	1.21E-04	4.10E-03
endoplasmic reticulum subcompartment (GO:0098827)	1212	41	3.15	9.61E-11	9.61E-09
endoplasmic reticulum membrane (GO:0005789)	1206	40	3.09	2.98E-10	2.84E-08
secretory granule (GO:0030141)	905	30	3.09	6.66E-08	4.16E-06
extracellular exosome (GO:0070062)	2102	69	3.06	1.71E-17	6.84E-15
extracellular vesicle (GO:1903561)	2126	69	3.02	3.05E-17	1.02E-14
extracellular organelle (GO:0043230)	2127	69	3.02	3.12E-17	8.92E-15
extracellular membrane-bounded organelle (GO:0065010)	2127	69	3.02	3.12E-17	7.81E-15
organelle inner membrane (GO:0019866)	559	18	3	4.76E-05	1.86E-03
mitochondrial inner membrane (GO:0005743)	501	16	2.98	1.38E-04	4.60E-03
transport vesicle (GO:0030133)	439	14	2.97	3.66E-04	1.09E-02
organelle subcompartment (GO:0031984)	1536	48	2.91	2.55E-11	2.83E-09
vacuolar membrane (GO:0005774)	487	15	2.87	3.24E-04	9.83E-03
secretory vesicle (GO:0099503)	1084	33	2.84	9.55E-08	5.30E-06
Golgi membrane (GO:0000139)	679	20	2.74	6.01E-05	2.31E-03
mitochondrial matrix (GO:0005759)	499	14	2.61	1.23E-03	3.23E-02
perinuclear region of cytoplasm (GO:0048471)	749	21	2.61	7.74E-05	2.72E-03
nuclear envelope (GO:0005635)	500	14	2.61	1.25E-03	3.24E-02
mitochondrial envelope (GO:0005740)	823	23	2.6	3.66E-05	1.52E-03
envelope (GO:0031975)	1292	36	2.6	1.95E-07	9.98E-06
organelle envelope (GO:0031967)	1292	36	2.6	1.95E-07	9.73E-06
Golgi apparatus (GO:0005794)	1639	43	2.44	6.15E-08	3.97E-06
endomembrane system (GO:0012505)	4801	120	2.33	8.20E-23	5.47E-20
extracellular space (GO:0005615)	3330	82	2.29	7.57E-14	1.01E-11
mitochondrial membrane (GO:0031966)	775	19	2.28	1.03E-03	2.78E-02
vesicle (GO:0031982)	4008	98	2.28	7.84E-17	1.74E-14

cytoplasmic vesicle (GO:0031410)	2535	61	2.24	1.10E-09	9.97E-08
intracellular vesicle (GO:0097708)	2541	61	2.24	1.88E-09	1.44E-07
mitochondrion (GO:0005739)	1689	40	2.21	3.17E-06	1.44E-04
organelle membrane (GO:0031090)	3780	85	2.1	3.29E-12	3.86E-10
extracellular region (GO:0005576)	4303	96	2.08	6.60E-14	9.42E-12
endosome (GO:0005768)	1072	23	2	1.99E-03	4.62E-02
cytoplasmic vesicle membrane (GO:0030659)	1241	26	1.95	1.52E-03	3.81E-02
vesicle membrane (GO:0012506)	1255	26	1.93	1.63E-03	4.02E-02
supramolecular complex (GO:0099080)	1434	29	1.88	1.25E-03	3.21E-02
bounding membrane of organelle (GO:0098588)	2212	44	1.85	7.05E-05	2.61E-03
cytosol (GO:0005829)	5536	101	1.7	2.74E-09	2.03E-07
organelle lumen (GO:0043233)	5655	98	1.61	9.01E-08	5.46E-06
intracellular organelle lumen (GO:0070013)	5655	98	1.61	9.01E-08	5.30E-06
membrane-enclosed lumen (GO:0031974)	5655	98	1.61	9.01E-08	5.15E-06
cytoplasm (GO:0005737)	12184	201	1.54	8.29E-26	1.66E-22
intracellular membrane-bounded organelle (GO:0043231)	12185	185	1.41	8.78E-15	1.46E-12
intracellular organelle (GO:0043229)	13320	196	1.37	7.04E-16	1.28E-13
membrane-bounded organelle (GO:0043227)	13258	191	1.34	3.10E-13	3.87E-11
membrane (GO:0016020)	9970	143	1.34	1.34E-06	6.23E-05
organelle (GO:0043226)	14116	200	1.32	1.40E-14	2.15E-12
intracellular anatomical structure (GO:0005622)	14968	208	1.29	6.62E-16	1.32E-13
cellular_component (GO:0005575)	18923	221	1.09	1.35E-08	9.31E-07
cellular anatomical entity (GO:0110165)	18778	218	1.08	5.84E-06	2.54E-04

GO term analysis of proteins downregulated in UV-irradiated samples (204) from the second experiment (Probe UV+). Data is obtained from VP [Probe UV+ / Probe UV-] – see **Figure 37**

Table 2. GO Cellular Compartments. Downregulated proteins from Probe UV+ conditions were obtained after the second experiment. A set of 204 hits was analyzed

Term	Name	Count	%	PValue	Fold Enrichment	FDR
GO:0005829	cytosol	161	78.5	2.0E-55	3.0	4.2E-53
GO:0070062	extracellular exosome	84	41.0	1.6E-29	3.9	1.8E-27
GO:0005737	cytoplasm	128	62.4	3.2E-26	2.3	2.3E-24
GO:0034774	secretory granule lumen	10	4.9	1.9E-06	8.9	1.0E-04
GO:0005925	focal adhesion	16	7.8	2.2E-05	3.8	9.4E-04
GO:1904813	ficolin-1-rich granule lumen	8	3.9	2.1E-04	6.6	7.6E-03
GO:0005634	nucleus	81	39.5	8.1E-04	1.4	2.4E-02
GO:0005968	Rab-protein geranylgeranyltransferase complex	3	1.5	9.1E-04	61.9	2.4E-02
GO:0005938	cell cortex	8	3.9	1.8E-03	4.6	4.4E-02
GO:0035578	azurophil granule lumen	5	2.4	1.2E-02	5.7	2.5E-01
GO:0005739	mitochondrion	24	11.7	1.4E-02	1.7	2.8E-01

GO:0001726	ruffle	5	2.4	1.6E-02	5.2	2.8E-01
GO:0005654	nucleoplasm	53	25.9	1.7E-02	1.3	2.8E-01
GO:0002102	podosome	3	1.5	3.8E-02	9.7	5.1E-01
GO:0030027	lamellipodium	6	2.9	4.0E-02	3.2	5.1E-01
GO:0005874	microtubule	8	3.9	4.2E-02	2.5	5.1E-01
GO:0015630	microtubule cytoskeleton	6	2.9	4.2E-02	3.1	5.1E-01
GO:0005856	cytoskeleton	11	5.4	4.4E-02	2.0	5.1E-01
GO:0015629	actin cytoskeleton	7	3.4	4.5E-02	2.7	5.1E-01
GO:0005875	microtubule associated complex	3	1.5	4.7E-02	8.6	5.1E-01
GO:0072686	mitotic spindle	5	2.4	5.2E-02	3.6	5.3E-01

GO term analysis of proteins upregulated in UV-irradiated samples after background subtraction (235) from the second experiment (Probe UV+). Data is obtained from VP [Probe UV+ / Probe UV-] – see **Figure 39**

Table 3. GO Cellular Compartments. Upregulated proteins from Probe UV+ conditions were obtained after the second experiment, and after subtracting the background. A set of 235 hits was analyzed

Term	Term Name	Hits Count	% of total	PValue	Fold Enrichment	FDR
GO:0005789	endoplasmic reticulum membrane	58	24.36975	3.15E-22	4.520876748	1.12E-19
GO:0005743	mitochondrial inner membrane	34	14.28571	1.64E-16	6.072857192	2.92E-14
GO:0005739	mitochondrion	57	23.94958	3.37E-16	3.430694022	4.00E-14
GO:0016020	membrane	90	37.81513	1.22E-13	2.159682852	1.08E-11
GO:0005783	endoplasmic reticulum	43	18.06723	2.52E-11	3.229027096	1.79E-09
GO:0030176	integral component of endoplasmic reticulum membrane	15	6.302521	2.27E-10	10.25988869	1.35E-08
GO:0005759	mitochondrial matrix	21	8.823529	4.02E-08	4.563881521	2.04E-06
GO:0016021	integral component of membrane	95	39.91597	2.36E-06	1.536069097	1.05E-04
GO:0005635	nuclear envelope	13	5.462185	4.76E-06	5.488304094	1.88E-04
GO:0005637	nuclear inner membrane	9	3.781513	8.86E-06	8.726542688	3.15E-04
GO:0042645	mitochondrial nucleoid	7	2.941176	1.60E-05	12.8676104	4.86E-04
GO:0005654	nucleoplasm	74	31.09244	1.64E-05	1.601911963	4.86E-04
GO:0031966	mitochondrial membrane	10	4.201681	1.39E-04	5.190296631	0.003795
GO:0005741	mitochondrial outer membrane	11	4.621849	1.79E-04	4.49345125	0.004553
GO:0031965	nuclear membrane	12	5.042017	2.09E-04	4.025933509	0.00497
GO:0000139	Golgi membrane	20	8.403361	3.36E-04	2.553836259	0.007469
GO:0098826	endoplasmic reticulum tubular network membrane	3	1.260504	0.00124	52.94102564	0.025966
GO:0030054	cell junction	10	4.201681	0.001494	3.738772997	0.029553
GO:0030056	hemidesmosome	3	1.260504	0.002565	37.81501832	0.048066
GO:0005761	mitochondrial ribosome	4	1.680672	0.002716	14.11760684	0.048347